Engineering polymeric biomaterials to treat kidney diseases and leverage boronic acid chemistry for drug delivery

Alexander Prossnitz

A dissertation

submitted in partial fulfillment of the

requirements for the degree of

Doctor of Philosophy

University of Washington

2022

Reading Committee:

Suzie H. Pun, Chair

Alshakim Nelson

Daniel Ratner

Patrick Stayton

Program Authorized to Offer Degree:

Bioengineering

University of Washington

Abstract

Engineering polymeric biomaterials to treat kidney diseases and leverage boronic acid chemistry for drug delivery

Alexander Prossnitz

Chair of the Supervisory Committee:

Suzie H. Pun

Department of Bioengineering

Polymer drug delivery vehicles are diverse and powerful tools to modulate biodistrubution, cellular uptake, and dosing of therapeutics. As our understanding of the biological barriers improves, the challenges facing the field of precision nanomedicine have become more nuanced requiring *specific* engineering design. On the other hand, the therapeutic landscape is rapidly evolving to compass a wide range of biologic drugs, in addition to traditional small molecules. As the definition of a therapeutic continues to expand, drug delivery vehicles must be *versatile* using simple techniques to achieve a broad range of functionality. This work highlights achievements both in improving the understanding of biological barriers, and engineering conjugation techniques to load a variety of therapeutic cargo. First, a brief overview of polymeric nanomaterial drug delivery systems, therapeutic drug cargo, biological barriers, and synthesis techniques are reviewed (Chapter 1). With these design criteria in mind, a panel of anionic polymers was synthesized and screened to optimize passive targeting to kidneys (Chapter 2). We further investigated these anionic polymers by synthesizing novel boronic ester-based polymer-drug conjugates of polyphenolic drugs to specifically treat fibrotic tubular epithelial cells (Chapter 3). While these unimer systems are effective for drug delivery to the tubular epithelial cells of the kidney, we developed a more generalized boronic ester drug delivery approach by encapsulating polyphenolic drugs into micellular nanoparticles and tuning drug release with neighboring tertiary amines (Chapter 4). Finally, we demonstrate the diverse utility of these boronic acid copolymers for enhanced intracellular delivery of peptides, proteins, and nucleic acids (Chapter 5). The work concludes with a summary of major findings and suggestions for future projects (Chapter 6).

Table of Contents

Chapter 1: Polymeric drug delivery vehicles: cargo, design, and synthesis 1

1.1. Overview of Polymer Nanomaterial Drug Delivery and Synthetic Techniques 2

1.1.1. Therapeutic Cargo 2

1.1.2. Peptide Drugs 3

1.1.3. Protein Therapeutics 4

1.1.4. Nucleic Acid Gene Therapies 5

1.2. Nanomaterials for Drug Delivery 6

1.2.1. Polymeric Nanomaterials 7

1.2.1.1. Polymer Structures and Chemical Compositions 9

1.3. Biological Barriers 13

1.3.1. Biodistribution 14

1.3.2. Cellular Internalization 16

1.4. Controlled Polymerization* 19

1.4.1. Reversible Deactivation Radical Polymerization (RDRP) 20

1.4.2. Atom Transfer Radical Polymerization (ATRP) 21

1.4.3. Ring Opening Polymerization (ROP) 23

1.4.4. Ring Opening Metathesis Polymerization (ROMP) 25

1.4.5. Reverse Addition Fragmentation Chain Transfer (RAFT) 26

References 28

Chapter 2: Glomerular disease augments kidney accumulation of synthetic anionic polymers 41

Abstract 41

2.1 Introduction 42
2.2 Results 44
2.2.1 Polymer panel synthesis and characterization 44
2.2.2 Biodistribution of LMW polymers in normal mice 46
2.2.3 Biodistribution of HMW and LMW polymers in normal and experimental FSGS mice 48
2.2.4 In vitro characterization of polymers in proximal tubule cells 49
2.3 Discussion 50
2.4 Conclusions 55
2.5 Concise methods 56
2.5.1 Materials 56
2.5.2 Polymer synthesis and characterization 57
2.5.3 Polymer deprotection and fluorescent labeling 58
2.5.4 Polymer biodistribution studies 59
2.5.5 Tissue processing and imaging 60
2.5.6 Urine albumin and creatinine quantification 60
2.5.7 HK-2 cell culture and polymer characterization 60
2.6 References 61

Chapter 3: Targeted delivery of polymer-drug conjugates to tubular epithelia to prevent progression of kidney disease 66

Abstract 66
3.1. Introduction 67
3.2. Results and Discussion 71
3.2.1. Efficacy determination of EGCG *in vitro* 71
3.2.2. Anionic polymer synthesis 74

3.2.3. Boronic acid conjugation 77
3.2.4. EGCG conjugation 81
3.3. Conclusions 83
3.4. Future Work 83
3.4.1. EMT prevention *in vitro* 83
3.4.2. FSGS rescue *in vivo* 85
3.5. Experimental 86
3.5.1. Materials 86
3.5.2. Instrumentation 87
3.5.3. Methods 87
References: 92
Chapter 4: Modulating boronic ester stability in block copolymer micelles via the neighbor effect of copolymerized tertiary amines for controlled release of polyphenolic drugs 96
Abstract 96
4.1 Introduction 97
4.2 Results and Discussion 99
4.2.1 Polymer Synthesis and micelle characterization 99
4.2.2 Determination of catechol affinity of polymeric boronic acids via ^{19}F NMR 101
4.2.3 Drug loading optimization of DB micelles with EGCG, Quercetin, and EA 102
4.2.4 pH sensitive micelle disassembly 104
4.2.5 Optimization of tertiary amine content in DB block copolymers 105
4.2.6 Prevention of radical scavenging due to high binding affinity DB polymer 105
4.2.7 Increased catechol affinity enhances polyphenol stability 106
4.2.8 Monomer ratio dependent drug release kinetics 108

4.3 Conclusions 109
4.4 References 111
4.5 Supporting Information 117
4.5.1 Materials 117
4.5.2 Instrumentation 117
4.5.3 Methods 119
4.5.3.1 DMA macroCTA synthesis 119
4.5.3.2 DMA chain extension with APBA 119
4.5.3.3 DBEAA monomer synthesis 120
4.5.3.4 DMA chain extension with APBA and DBEAA 120
4.5.3.5 Pinacol protection of APBA containing copolymers 121
4.5.3.6 Micelle formulation 121
4.5.3.7 Drug loading measurements 121
4.5.3.8 Transparency 123
4.5.3.9 Micelle disassembly 123
4.5.3.10 Boronic ester equilibrium determination with ^{19}F NMR 123
4.5.3.11 Radical scavenging activity 125
4.5.3.12 Forced degradation of EA 125
4.5.3.13 Drug release: dialysis method 125
4.5.4 Supporting Figures 127
Chapter 5: Boronic acid copolymers for intracellular delivery of proteins, peptides, and nucleic acids 140
Abstract 140
5.1 Introduction 141
5.1.1 Intracellular delivery of biologics for gene therapy 141
5.2 Results and Discussion 144

5.2.1 Cytocompatibility of BA and DB micelles 144
5.2.2 BA copolymer Synthesis 145
5.2.3 Cellular Internalization 146
5.2.4 Effect of micelle surface charge on cellular internalization 148
5.2.5 BA – protein nanocomplex formation and characterization 150
5.2.6 Protein and peptide encapsulation efficiency 151
5.2.7 Intracellular protein delivery 154
5.2.8 Linear cationic and lipophilic boronic acid polymers for gene delivery to T-cells 155
5.2.9 Boronic acid polyplex cellular internalization 158
5.3 Conclusions 161
5.4 Experimental 162
5.4.1 Instruments 162
5.4.2 Methods 163
5.4.2.1 Viability Assay 163
5.4.2.2 Rhodamine Acrylamide (RHEAA) synthesis 163
5.4.2.3 DMA macroCTA synthesis 164
5.4.2.4 DMA chain extension with APBA 165
5.4.2.5 Cationic Copolymer Synthesis 165
5.4.2.6 Micelle formulation and protein encapsulation 166
5.4.2.7 Polyplex formulation 166
5.4.2.8 Cell Culture 166
5.4.2.9 Neutral polymer internalization 167
5.4.2.10 Cationic Micelle Toxicity and Uptake 167
5.4.2.11 Protein Delivery 168
5.4.2.12 Polyplex Uptake and transfection efficiency 168
References: 169
Chapter 6: Summary of major findings and suggestions for future work 174

6.1 Major Findings 174
6.1.1 Anionic polymers for passive targeting of glomerular disease 174
6.1.2 Anionic boronic ester-based polymer-drug conjugates for reversal of EMT 175
6.1.3 Utilizing the neighbor effect of tertiary amines for control of polyphenolic drug release from boronic esters 175
6.1.4 Boronic acid copolymers for intracellular delivery of proteins, peptides and nucleic acids 176
6.2 Recommendations for Future Work 176
6.2.1 Exploring architecture effects of polycations for gene delivery to T cells 176
6.2.2 Effects of polymer dispersity on gene delivery 178
6.2.3 DNA-Aptamer modification in organic solvents 179

List of Figures

Figure 1.1 Overview of biological barriers that nanomaterials must overcome and various therapeutic opportunities that are enabled by successfully navigating these barriers. 8

Figure 1.2 Schematic overview of polymerization mechanisms for ATRP, RAFT, ROP and ROMP. 20

Figure 2.1 Schematics of polymer synthesis and composition. 45

Figure 2.2 Organ distribution of low molecular weight (23 - 27 kDa) polymers in normal mice. 47

Figure 2.3 Kidney distribution of low molecular weight (23e27 kDa) polymers in normal mice. 48

Figure 2.4 Organ distribution of polymers in normal and experimental FSGS mice. 51

Figure 2.5 *In vitro* LMW 1:4 polymer characterization.....53

Figure 3.1 Overview of kidney structure and organization. 68

Figure 3.2 Acute kidney injury (AKI) induces tubular cell death and damage. 70

Figure 3.3 Determination of IC_{50} value of EGCG in HK-2 cells after 48 h exposure. 72

Figure 3.4 Quantification of vimentin expression after induction of EMT with TGFβ. 73

Figure 3.5 Treatment with EGCG decreases vimentin and Twist1 expression in a dose dependent manner. 74

Figure 3.6 Scheme for RAFT polymerization of highly anionic polymer for TEC targeting.75

Figure 3.7 ^{1}H NMR spectra showing the complete deprotection of tBuMA 76

Figure 3.8 SEC chromatogram for MOB 2 polymer 77

Figure 3.9 Post polymerization modification of methacrylic acid containing anionic polymer 78

Figure 3.10 ^{1}H NMR spectra of anionic polymers after various conjugation reactions with amino PBAs. 79

Figure 3.11 Conjugation of fluorescent Cy5 amine to MOB polymer. 80

Figure 3.12 ^{1}H NMR spectra of EGCG, MOB polymer, and purified EGCG-MOB polymer-drug conjugate..... 81

Figure 3.13 A) ^{1}H NMR spectra of the aromatic region of EGCG B) Annotated protons for MOB polymer EGCG conjugate..... 82

Figure 4.1 A) Synthesis scheme for diblock copolymers BA and DB using sequential RAFT polymerization. B) Comparison of SEC chromatograms of DMA mCTA and chain extended APBA copolymer after pinacol protection of the boronic acid. C) Comparison of SEC chromatograms of DMA mCTA and chain extended APBAcoDBEAA copolymer after pinacol protection of the boronic acid. D) DLS determination of micelle size after nanoprecipitation of BA and DB diblock copolymers. 100

Figure 4.2 A) Equilibrium of F-Cat and DB polymer complex at various boronic acid to catechol ratios measured by ^{19}F NMR and normalized to free F-Cat signal. B) Schematic depicting higher binding affinity and quantitative binding of catechols to DB polymer compared to the mixture of bound and unbound catechols in the presence of BA polymer and CPBA. Percent of F-Cat bound to boronic acid and converted to boronic ester as a function of boronic acid to catechol ratio for DB polymer, BA polymer, and CPBA... 102

Figure 4.3 A) Representation of complexing polyphenolic drugs Quercetin, EA and EGCG with the boronic acids in the DB polymer. B) Determination of micelle size in PBS after nanoprecipitation of each polymer drug conjugate loaded with 10% weight drug. C) UV-Vis spectra for each polymer drug micelle at 10%, 20%, 30%, 40% and 50% weight drug. D) Comparison of normalized absorbance intensity at the wavelength

characteristic to the polymer drug conjugate (EGCG, 312 nm), (Quercetin, 400 nm), and (EA, 400 nm) at various weight percentages. E) Transparency of micelle solutions at various weight percentages. F) Diameter of soluble micelles at various weight percentages.....104

Figure 4.4 A) Scheme of pH dependent transition in ionization state of DB polymer. B) Determination of micelle stability between pH 5.5 and 11 for BA and DB polymers. The increased fluorescence of solvatochromic dye Nile Red indicates the presence of micelles. C) Depiction of DPPH assay for determining antioxidant potential. D) Comparison of radical scavenging activity of EA, polymers, and polymer-drug conjugates at 10% weight drug in methanol. E) Comparison of radical scavenging activity of EGCG, polymers, and polymer-drug conjugates at 10% weight drug in methanol. F) UV-Vis of free EA at 425 nm as a function of increased NaOH concentration and drug oxidation. G) UV-Vis of BA-EA conjugate at 425 nm as a function of increased NaOH concentration and drug oxidation. H) UV-Vis of DB-EA conjugate at 425 nm as a function of increased NaOH concentration and drug oxidation. I) Percent oxidation of EA in solution, BA micelles or DB micelles at various NaOH concentrations. EC_{50} values were determined by normalization and nonlinear curve fitting.....107

Figure 4.5 A) Formulation of 20% by weight Q micelles with BA polymer, DB polymer or an equal mix of BA and DB polymer. B) Percent drug release determined by dialysis of BA, a 1:1 mix of BA and DB, and DB micelles over 24 hours at pH 7.4. C) Percent drug release determined by dialysis of BA, a 1:1 mix of BA and DB, and DB micelles over 24 hours at pH 4.5.....109

Figure 5.1 MTS viability assay measuring cytotoxicity of micelle doses over 24h. 145

Figure 5.2 A) Fluorescence intensity histograms of cellular internalization of rhodamine labeled BA micelles in NIH 3T3 cells. B) Viability and internalization percentages of NIH 3T3 cells treated with rhodamine labeled BA micelles 147

Figure 5.3 A) Structure of DR polymers including DMA, DMPA, RHEA, and APBA. B) DLS histograms of micelle sizes, with diameters for each micelle DR0 (59.3 nm), DDR5 (102 nm), and DDR10 (71.2 nm).....149

Figure 5.4 A) Fluorescence intensity histograms of PC-12 cells after 1 h incubation with cationic BA micelles. B) Percentages of cells that internalized BA micelles based on rhodamine fluorescence. C) Acute toxicity of cationic BA micelles to neuronal cell line after 1 h exposure, determined by Zombie Violet live/dead staining. 150

Figure 5.5 Dynamic Light Scattering (DLS) measurement of the nanocomplex composed of BA copolymers and BSA.....151

Figure 5.6 Encapsulation efficiency of labeled BSA in BA copolymer nanocomplex at neutral pH, resulting in a nanocomplex with 76% encapsulation efficiency.....152

Figure 5.7 Comparison of encapsulated and free labeled BSA in BA-BSA nanocomplex formulations at pH 6.8 and 7.4.....152

Figure 5.8 Encapsulation efficiency of labeled melittin in BA-melittin nanocomplex at equal mass loading of peptide and polymer. 153

Figure 5.9 Median FITC signal from fluorescently labeled BSA in HeLa cells. 154

Figure 5.10 Structures of the monomers used for the synthesis of linear cationic boronic acid polymers for nonviral gene delivery. 155

Figure 5.11 Conversion of acrylamide polymerizations with various DMPA content.....156

Figure 5.12 SEC of DD50 polymer in 150 mM Acetate buffer (pH 4.4).. 157

Figure 5.13 Flow cytometry analysis of Jurkat cells treated with polyplexes.. 160

Figure 5.14 ^{1}H NMR Spectrum of RHEAA ($CDCl_3$) 164

List of Tables

Table 2.1 Summary of p(OEGMA-co-MAA) copolymers. 46

Table 3.1 Efficiency of coupling reactions between amino phenyl boronic acids and carboxylic acid polymers. 79

Table 4.1 Degree of polymerization and molecular weight of polymers synthesized by RAFT polymerization 101

Table 5.1 Degrees of polymerization of monomers in the DR polymers and relative fluorescence intensity ratios. 148

Table 5.2 Compositions of cationic BA polymers used for nucleic acid delivery to T cells. 158

Acknowledgements

To my advisor **Dr. Suzie Pun**, whose work ethic, professionalism, and kindness continually inspires and leaves her students awestruck. A Ph.D. has many challenges, and I can confidently say every single one was made easier by your steadfast support. I have grown so much as a scientist, collaborator, and person under your mentorship, and I will truly miss being a part of the wonderful team you have assembled at UW.

To my committee members, **Patrick Stayton**, **Daniel Ratner,** and **Alshakim Nelson**, thank you for volunteering your time and expertise to improve my scientific endeavors and also connecting me with the UW community in the form of your students, postdocs, and research scientists.

To my Bioengineering cohort, I couldn't imagine better colleagues to have during this amazing journey. **Meilyn Sylvestre**, your passion and aptitude for connecting people established communities on and off campus that were instrumental in all of my successes and that I will cherish long after I graduate. **Ian Cardle**, your unwavering loyalty to both your friends and scientific excellence, inspires me on a regular basis. **Jamie Hernandez**, my fellow southwesterner, your creativity has been a constant source of joy from the bigfoot mug in my kitchen to the homemade turkeys, pickles, and pizzas you've kindly shared. **Sara Keller**, whose endless patience is matched only by her epic endurance, your support enabled me to push my personal limits far beyond what I would have ever thought possible.

To my lab mates and mentors, the best part of my Ph.D. was sharing a space with a remarkable collection of brilliant, caring, and inspiring individuals. **Gary Liu**, there are no words that could do justice to the myriad of concepts I have learned from you over the years, and I feel so lucky to have had you as a role model from the first time I set foot the UW campus. **Bob Lamm**, who was never too busy to help (even when he definitely was) and taught me how to take apart and reassemble the everything in the lab. **Daniel Lee,** your meticulous approach to life and science, as well as your willingness to share feedback, enabled me to improve technically and organizationally as a chemist in ways that I appreciate every time I step into the lab. **David Peeler,** both inside and outside of the lab, your spirit is a force of nature, empowering you and those around you to tackle even the most daunting challenges. **Trey Pichon**, your endless enthusiasm for understanding how the world works is infectious, and I am a better person and scientist after every one of our conversations. **Ben Nguyen**, your constant search for optimization has made me rethink so many protocols I just took at face value, and I will continue to use your tips and tricks as long as I am in a wet lab.

To my friends, whose council and love of adventure were vital to my survival not just in graduate school, but during a global pandemic. **Jordan Fonseca**, I have learned so much about self-reflection, perseverance, and communication from your actions and our conversations. Your commitment to your friends, family, and your values has been a source of inspiration for over ten years, and I feel so lucky that we ended up at the same grad school. **Jeremy Hartse**, from the moment we first met virtually up until this very day, your sense of adventure and passion for our shared hobbies has brought endless fun and excitement into my life. Regardless of my stress or anxiety, I could always count on you to brighten my mood, and your ability to find fun, even during quarantine, undoubtably saved my sanity. **Ross**

Bretherton, as a scientist, expedition partner, and confidant, you truly are a polymath. Your expertise has guided me, both literally and figuratively, through some of the most difficult terrain of my life. And last but certainly not least, to all of my **friends** in Seattle, thank you for enriching my life through countless evenings at breweries, afternoons at the climbing gym, weekends in the mountains, or even just a simple walk on the Ave.

To my partner, **Samantha Tetef**, you have filled my life with relentless optimism and boundless curiosity, and. I am thankful every day for your unconditional love, roaring laugh, and incredible insight.

Chapter 1

Polymeric drug delivery vehicles: cargo, design, and synthesis

Abstract

As the complexity of biomedical therapeutics continues to increase, the demands for smart drug delivery vehicles to precisely regulate biodistribution, cellular uptake, and drug dosing grow more stringent. The rise of biologics, recently with mRNA vaccines and historically with monoclonal antibodies, is taking the pharmaceutical industry by storm. These new therapeutics necessitate nanomaterial vehicles that can strike a balance between versatility and specificity. The field of nanomedicine failed to deliver on early promises because the heterogeneity of biological barriers was underestimated. However, with advances in controlled polymerization techniques, polymeric materials can meet these increasingly complex requirements due to unprecedented customization on both the molecular and macroscopic levels. In this new era of precision polymer nanomedicine, each aspect of the carrier is tuned independently of the associated cargo, and by optimizing size, morphology, solubility, charge, pKa, hydrolysis, enzyme degradation, and a host of other material properties, new therapeutics utilizing unstable small molecules or cell impermeable biologics are quickly becoming a reality.

1.1 Overview of Polymer Nanomaterial Drug Delivery and Synthetic Techniques

1.1.1 Therapeutic Cargo

The landscape of biomedical therapeutics has changed dramatically over the past couple decades. Where once synthetic small molecules dominated the scene, now treatments encompassing a broad range of biologics and even cellular therapies are continuing to gain popularity. From 1989 to 2012 the number of biotechnology products increased from 13 to 210.[1] As recently as 2019, biologics already composed 25% of the global pharmaceutical market and this fraction is projected to increase over the coming years.[2] The rise of biologics, specifically, peptide, protein and nucleic acid, therapeutics can be attributed to improved manufacturing practices and discoveries in basic biology.[3–5] However, while these novel approaches provide access to previously undruggable targets they suffer many of the same drawbacks as traditional small molecule therapeutics: poor stability, short circulation half-lives, off target toxicity, and inadequate accumulation in the tissue or cell of interest.[6–13] Many promising drug candidates for cancers or infectious diseases fail to improve patient outcomes due to one or more of these shortcomings listed above.[14] For example, the small molecules, bromodomain and extra-terminal motif protein inhibitors (BETis) are a potent class of cancer therapeutics that decrease expression of key proteins (e.g. c-MYC) but caused severe toxic side effects, resulting in termination of clinical trials.[15–17] In this case, the combination of systemic delivery and the high concentrations required for appropriate dosing to the cancer tissue caused catastrophic side effects. This story is well worn in the field of cancer research but similar examples can be found in the world of infection disease. Particularly in the developing world where adherence can be poor and logistical obstacles push small molecule stability to the limit, even drugs that show efficacy in clinical trials can

fail to solve human health challenges.[18,19] For example, highly active antiretroviral therapy (HAART), a combination of multiple small molecule nucleoside reverse transcriptase inhibitors, has a high success rate of reducing HIV/AIDS viral load. Unfortunately, only 33% of individuals who are prescribed HAART use the medication as indicated.[20] One of the main causes of this poor adherence is the complexity and frequency with which these drugs must be consumed.[21] With these examples of the challenges still facing small molecules in mind, the hurdles facing the successful translation of biologics are daunting indeed.

1.1.2 Peptide Drugs

Peptides, proteins, and nucleic acids are susceptible to the shortcomings of their small molecule counterparts, but also possess unique biologic challenges. Peptides are arguably the first class of biologics to be isolated and used medically with the first case of a therapeutic peptide treatment being insulin in 1922. However, it was not until the early 2000s that multiple peptide therapeutics would translate to the clinic. Advances in synthetic techniques, high throughput screening, and a growing library of naturally occurring peptides have led to the stead rise of peptide drug approvals.[22] Currently 80 peptide drugs are available to treat cardiovascular, reproductive, gastrointestinal, central nervous system, metabolic, hormonal, and oncologic diseases.[23,24] While there is much to be excited about in the field of peptide therapeutics, a major limitation is the need to inject these drugs directly into the blood stream to avoid the first pass metabolism.[25] Moreover, the rapid degradation, short half-life, and poor membrane permeability of peptides means that these injections must be frequent.[26]

1.1.3 Protein Therapeutics

Peptide and protein therapeutics have significant overlap, but for the purpose of this discussion, proteins will be defined as macromolecules containing 50 or more amino acids. As a result of these size differences, peptides and proteins having different manufacturing practices, biodistribution, and molecular targets. Currently, over 100 protein drugs are on the market and can be broadly classified into three categories enzymes/regulatory proteins, antibodies, and foreign proteins.[27] Several successes in enzyme replacement, administering a functional protein to treat individuals that are deficient or abnormal in expression of specific protein, include gaucher's disease, severe combined immunodeficiency (adenosine deaminase deficiency), and cystic fibrosis, or delivering proteins to repair genetic diseases.[28–31] The second category, consisting mainly of monoclonal antibodies, has been used for blocking receptors important to cancer proliferation (bevacizumab, cetuximab, trastuzumab) or arthritis (adalimumab, infliximab, rituximab).[27] Additionally, antibodies can mark cells for destruction, or stimulate signaling pathways. Monoclonal antibodies have been developed against entire cell types, specific signaling pathways or even secreted small molecules. Isolation of viral or bacterial proteins for use as vaccines has been effective for preventing hepatitis B and human papillomavirus infections.[32,33] Lastly, ribonucleoproteins (RNPs) for gene editing hold tremendous promise for treating a wide range of genetic diseases, but translation has been hindered by the need to delivery proteins and nucleic acids simultaneously.[34–36] Overall, protein drugs have enormous therapeutic potential in large part due to their highly specific macromolecular organization. This structural complexity comes with a cost, as many of these drugs are unstable at ambient temperature, must be directly injected, and have limited cellular permeability.[27,37] While stability and administration issues

limit access to protein therapeutics, the inability of protein drugs to enter the cytosol leaves the entire world of intracellular machinery as “undruggable” targets.

1.1.4 Nucleic Acid Gene Therapies

Taking one step back from peptide and protein drugs, nucleic acids offer a different approach for replacing malfunctioning proteins and augmenting signaling pathways. Nucleic acid therapies are composed of DNA or RNA, with the purpose of either eliciting protein expression or suppressing it.[11,38] Plasmids and minicircles are double stranded DNA molecules that upon entering the nucleus can cause protein expression for long periods of time, up to months or years. The RNA analog, mRNA, is single stranded and when present in the cytosol the nucleic acid is translated into the protein of interest. While the end result of these DNA and RNA therapies is similar, the duration of protein expression (months vs. days) and the intracellular compartment (nucleus vs. cytosol) required for activity are different.[39–41] The applications for this category of therapeutic span from inherited genetic diseases like muscular dystrophy and cystic fibrosis, to acquired health issues such as cardiovascular diseases, neurological diseases, improper wound healing and cancer.[42–50] Additionally, delivery of mRNA that encodes for foreign proteins, for example viruses, has recently gained attention due to the coronavirus pandemic. Both short development times and large-scale production of the Moderna and Pfizer mRNA vaccines are a direct result of the unique advantages afforded by nucleic acid vaccines.[51,52] The second class of nucleic acid therapeutics, target intracellular mRNA expression resulting in either degradation or alternative splicing. siRNA or antisense oligonucleotides (ASOs) can form duplexes with single stranded mRNA in the cytosol causing degradation by RNA-induced silencing complex (RISC) or RNase H respectively. Splice switching oligonucleotides can restore

correct production of proteins in rare diseases by sterically hindering cellular splicing machinery. This inhibition redirects the RNA to a different processing pathway allowing the proper splice variants to be made. The aforementioned gene therapies are the most common approaches, but over the past decade there have been several other therapeutics developed using nucleic acids. For further discussions of these topics the reader is referred to these excellent reviews.[10,41] Similarly to protein and peptide therapeutics, nucleic acids have exquisite biological specificity and provide opportunities to reprogram malfunctioning cells. Unfortunately, clinical success of nucleic acid therapies has been limited due to extremely poor stability (half life of seconds to minutes) and, again, poor intracellular uptake.[40,53,54] Significant progress had been made to modify nucleic acids chemically to increase their serum stability, such as 2' methylation, phosphorothioate linkages, and modification of the 3' and 5' ends, however long circulating nucleic acids can cause toxic side effects and trigger adverse immune responses. [5,55]

1.2 Nanomaterials for Drug Delivery

Despite the diversity of mechanistic approaches undertaken by state-of-the-art biomedical therapeutics, ranging from small molecules and peptides all the way to proteins and nucleic acids, universally, target specific delivery remains a major barrier to clinical translation. To realize the full potential of these various therapies it is necessary to design drug delivery systems that decouple biodistribution, stability, and intracellular uptake from the properties of the active drug itself (Figure 1.1). The field of nanomedicine has promised to overcome these challenges consistently over the past 50 years, however the early success of liposomal formulations oversimplified the barriers to personalized precision

nanomedicine.[56] For example, the discovery the enhanced permeation and retention (EPR) effect in animal models, which postulated that nanoparticles (NPs) of a specific size would passively accumulate in the leaky vasculature of tumors; led to a flurry of exciting NP based cancer therapies. Upon further study and several failed clinical trials the extent of EPR in human subjects is still hotly debated 30 years after its initial documentation.[57,58] This example highlights the difficulties in studying basic biological interactions with NPs. Unfortunately, the picture is complicated even further by the constantly changing landscape of human health. Specifically, one of the initial successes of nanomedicine was the development of "stealthy" drug delivery vehicles. These NPs contained a hydrophilic coating of polyethylene glycol (PEG) that prevented protein adsorption to the particle surface, resulting in these particles avoiding the mononuclear phagocytic system (MPS).[59,60] The MPS is the main pathway by which NPs are cleared from the blood stream, and for most therapeutics would be considered off target accumulation.[61] Inclusion of PEG (known as PEGylation) shows significant advantages in biodistribution and circulation time especially for protein therapeutics, but unfortunately the ubiquitous use of PEG in commercial products has lead to as much as 72% of the population producing anti-PEG antibodies.[62] The evolution of PEG from a biologically inert polymer to an immunogen highlights that biological barriers to nanomedicine are not static, but ever evolving. As the understanding of nanomaterial interactions with the human body grows, it is clear that NPs are not the one-size fits all, silver bullet that was once promised.

1.2.1 Polymeric Nanomaterials

While the field of nanomedicine has suffered setbacks over the past 20 years, the continued development of precision synthesis techniques has led to an unprecedented level of

molecular control.[63,64] Along with improved understanding of the biological mechanisms that compose the barriers to therapeutics, this molecular control allows for rational design and engineering of nanomaterials. Specially, improved polymerization reactions (section 1.3) enable scientists to synthesize materials with various chemical compositions, architectures, and drug cargoes.[65–68] Acknowledging the complexity of the barriers to drug delivery, precision polymeric nanomedicine aims to leverage synthetic simplicity and versatility to rationally design materials to overcome disease specific biological barriers.

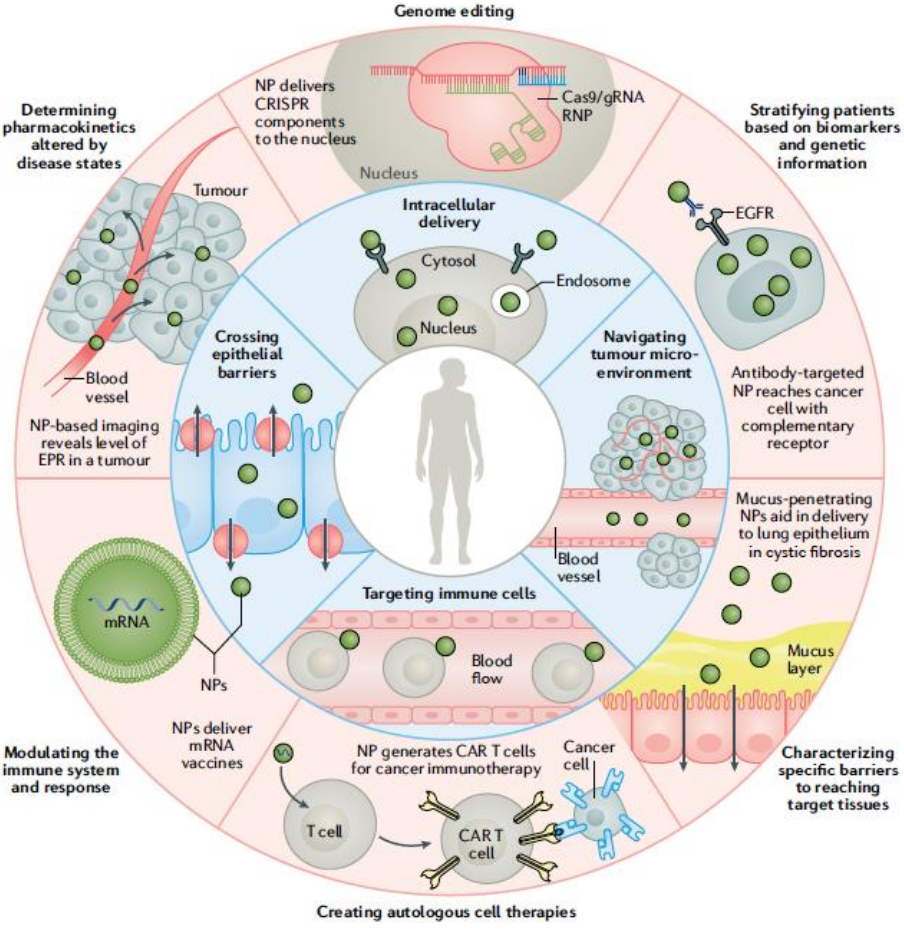

Figure 1.1 Overview of biological barriers that nanomaterials must overcome and various therapeutic opportunities that are enabled by successfully navigating these barriers. The main barriers described are navigating the vasculature, extravasation into the target tissue, and cellular uptake. Figure adapted from Mitchell *et al.* [21]

1.2.1.1 Polymer Structures and Chemical Compositions

Architectures

Polymeric nanomaterials are unique in their versatility because the chemical techniques used to synthesize them allow for finely tuned control of both architecture and chemcial functionality. With regards to architecture, polymeric nanomaterials can be classified into two main groups, unimers and self-assembled structures. Unimers encompass a broad range of water-soluble single molecule polymers. Linear polymers between 5,000 and 40,000 Da have long circulation times, dispersities near one, and relatively small hydrodynamic radii (~5-15 nm).[69,70] These polymers have various backbone chemistries ranging from biodegradable polyesters and polyamides to biointert polyolefins. Single unimers were used as early as the 1950s to deliver small molecules and are commonly used today to improve the biodistribution of protein drugs.[71–73] In addition to linear unimers, branched single polymer nanoparticles such as bottle-brushes, stars, or dendrimers can have similar backbone compositions, but approach sizes of 10-100 nm, at masses between 100,000 to 10,000,000 Da.[17,63,74] The dispersity of these materials varies depending on the synthetic approach, but can be as low as one in the case of dendrimers. Increasing polymer size can prevent rapid clearance of therapeutics by the renal system and can increase uptake in specific cell types such as macrophages.[75] Just considering unimers, the potential to modulate nanomaterial size across orders of magnitude while maintaining a consisting chemical composition makes polymeric materials an attractive option for precision medicine. Self-assembled polymers can adopt a variety of morphologies but for drug delivery the most common are micelles, polymersomes, and solid nanoparticles.[26,73,75] These structures are held together by the hydrophobic forces exerted by aliphatic or aromatic groups in multiblock copolymers. Micelles contain two major regions, a hydrophobic core and a hydrophilic

corona. As such simple structures, there are very few design limitations to micelle compositions.[76] These materials have been used to deliver hydrophobic drugs via encapsulation, peptides via conjugation or nucleic acids via electrostatic complexation to name a few.[77–81] The size and stability of micelles is highly dependent on the hydrophobicity and the molecular weight of the polymers that compose them. The dependence of the structural properties of micelles on molecular composition enables precise tuning of size and stability. Polymersomes are similar to liposomes in that they have a bilayer of hyphophobic material that encapsulates a hydrophilic core. Both hydrophilic and hydrophobic cargo can be efficiently encapsulated in polymersomes, but engineering a stable bilayer structure requires specific formulation conditions and polymers.[82] Lastly, solid polymer nanoparticles, most often composed of poly-lactic-*co*-glycolic acid (PLGA), have been used to non-covalently encapsulate a broad range of therapeutics. Unfortunately, these PLGA particles rely exclusively on hydrolysis for drug release, which severely limits the control of drug pharmacokinetics. [83] Overall, polymer nanomaterials can take on a broad range of structures enabling precise engineering of the delivery vehicle to the application.

Polymer Solubility

The chemical versatility of polymeric nanomaterials allows scientists to control bulk properties (charge, solubility, and biodegradation) and specific drug/targeting group conjugation. More importantly, these properties can all be modulated *in vivo* in response to biological stimuli, such as pH, heat, reactive oxygen species (ROS), or enzymes.[84–86] Polymeric nanomaterials for drug delivery must inherently be hydrophilic, but the exact nature of this hydrophilicity can vary dramatically. Polymers containing PEG, poly(dimethylacrylamide) (pDMA), hydroxyproypl methacrylamide HPMA), glycydiyl monomethacrylate (GmMA) or various sugars moieties are all neutrally charged. These

materials are not all encompassing but they do cover the functional groups that impart neutral hydrophilic properties: ethers, amides, and hydroxyls. Charged hydrophilic polymers can be cationic (containing tertiary amines), anionic (containing carboxylic acids) or zwitterionic (most often quaternary amines, sulfates, or phosphates). The biological implications of these various hydrophilic functional groups will be covered in section (Chapter 2). Polymer solubility can be modulated by contrasting hydrophilic components with hydrophobic aliphatic or aromatic groups. The choice of hydrophobic group can dramatically affect the stability of self-assembled structures but can also impact drug loading, such as the pi-pi stacking of aromatic rings.[87–89] For example, inclusion of highly hydrophilic mannose methacrylates in copolymers with extremely hydrophobic small molecule drug monomers can dramatically increase drug solubility. [90]

Stimuli Responsive Chemistry

However, more important than the ability to tailor a static set of chemical characteristics, many polymeric drug delivery vehicles take advantage of stimuli responsive technologies. Changes in pH, temperature, reducing environment, or the presence of enzymes can impact polymer solubility and stability.[86] For example, inclusion of tertiary amines with pKas near 6 in the hydrophobic block of polymeric micelles, results in a stable hydrophobic core at neutral pH and dissolution of the micelles due to the formation of positively charged tertiary amines under acidic conditions.[91,92] For temperature dependent responses, polymer lower critical solution temperature (LCST) or upper critical solution temperature (USCT) can be leveraged. Polymers that exhibit LCST behavior under biologically relevant conditions, are highly soluble at room temperature, but begin to aggregate and crash out of solution at temperatures around 37 °C. Polymers with USCTs are the opposite, exhibiting hydrophilic properties at higher temperatures but aggregating a lower temperatures.[93] The most well

know thermally responsive polymer is poly-N-isopropyl acrylamide (NIPAAm), which displays LCST behavior around body temperature.[94] Interestingly, PEG also has a LCST near 70-100 °C depending on the molecular weight. With regards to reducing conditions, polymeric micelles that contain disulfides or thioether crosslinks are stable during circulation, but upon entering the cytosol, are degraded due to the presence of glutathione (GSH).[95–99] Polymers containing amide or ester bonds in the backbone can also be enzymatically degraded either nonspecifically over time, or quickly in response to specific enzymes with the use of peptide motifs. [100–102] One of the most exciting applications of these stimuli responsive technologies is the development of size switchable NPs that remain large during circulation, but fall apart into smaller structures in tumors to increase tissue penetration. [103]

Linker Chemistry

While modulating the macroscopic properties of drug delivery vehicles is fundamental to improving biodistrubtion and targeting, the ability to tune drug release kinetics via covalent linker chemistry is key to the success of polymer therapeutics. The most common covalent drug linkage is an ester, which hydrolyzes over time in aqueous media. Importantly, the stability of the ester bond formed between the polymer and the drug can be finely tuned. For example, phenolic esters cleave rapidly (complete release in hours) whereas aliphatic esters can have half-lives between days and months. [17,90] Another common category of cleavable linkers is pH sensitive bonds. For example, hydradzones, aconityl and acetal functional groups are all stable at neutral pH but degrade under acidic conditions.[86] Additionally, while disulfide and thioethers were previously mentioned as crosslinking groups, these functionalities are common used as intracellularly cleavable bonds for peptides containing cysteine residues.[92] Additionally, borrowing from the design of antibody drug conjugates, polymeric materials with enzyme cleavable linkers can easily be

synthesized.[100,102] These materials show promise as cancer therapeutics due to the increased expression of cathepsin B and matrix metalloproteinases, which result in selective release of the drug payload in tumors. These various stimuli responsive linker technologies have been used extensively to deliver small molecule therapeutics. Recently more interest has developed in applying these techniques to biologics, particularly for the development of polymer protein conjugates. [86]

Active Targeting

For therapeutic cargo, drug release, or breaking of covalent bonds, is vital to efficacy. In contrast, stable conjugation of targeting moieties to polymeric nanomaterials improves both tissue and cellular specific accumulation. Polymeric materials have been actively targeted to cells or tissues with a broad range of molecules including, sugars, aptamers, peptides, antibodies, proteins, and small molecules.[104–106] The ease and diversity of conjugation approaches, including post-polymerization modification and polymerization of functional monomers, has made actively targeted polymeric materials successful for treating cancer, improving hemostasis, and curing bacterial infections. [90,100,107,108]

1.3 Biological Barriers

With the variety of surface chemistries, sizes, drug release profiles, and stimuli responsive techniques available to polymer chemists, developing tailor made nanomaterials to solve specific therapeutic challenges has been the major focus of the field. Polymeric nanomaterials are positioned to apply the lessons learned from the nanoparticle field at large over the past 50 years, including recent data regarding the EPR effect and antiPEG antibodies, to dramatically improve delivery of biologics, vaccines, and the treatment of

infectious diseases.[13,75,109,110] The key aspects for improving current therapies are biodistribtion and cellular internalization. Biodistribution has several components, including circulation, stability, tissue accumulation, and clearance. Cellular uptake requires internalization of the nanomaterial and release of the cargo. General strategies for customization of biodistribution and cellular internalization will be discussed in following section.

1.3.1 Biodistribution

Due to the systemic nature of nanomaterial therapies, interactions during circulation and with structures in the clearance organs dominate tissue level accumulation. After injection, NPs are immediately diluted by orders of magnitude, subjected to shear forces, and bombarded with serum proteins. A clear advantage of single molecule (unimeric) nanomaterials is that there is minimal change in overall stability upon dilution. By contrast, self-assembled structures, particularly micelles, are held together by hydrophobic interactions, the strength of which interactions are concentration dependent. The stability of micelles is described by the critical micelle concentration (CMC). Below a micelle's CMC there is no longer sufficient hydrophobic force to hold the structure together and the polymer dissolves into single unimers.[88] The CMC of micelles is effected by both the hydrophilic and hydrophobic block and commonly values around 0.01 mg / mL prove to be stable *in vivo*. [92] If the micellular assembly does not have a sufficiently low CMC, the micelle can be physically or chemically crosslinked.[111,112] Once stable NPs are in circulation, the materials will experience shear forces as a result of fluid flow through blood vessels.[113] These forces can be leveraged to control distribution of materials within the vasculature by tuning the aspect ratio of the NPs. Shapes such as rods and ellipsoids with high aspect ratios will tumble towards vessel walls

increasing the likelihood of extravasation.[114] Spherical particles do not experience this flow induced rolling and remain in circulation longer. If a NP remains in the blood for an extended period of time, interactions between the surface of the material and serum proteins will cause the formation of a protein corona. [115,116] Both the accumulation of specific proteins and the folding state of those proteins is highly influenced by the surface chemistry.[117] NPs with neutral and hydrophilic surfaces (PEG, zwitterions, or hydroxyls) show the least tendency to accumulate a protein corona. Conversely, charged or hydrophobic surfaces tend to aggregate and denature proteins on their surfaces.[76] While this protein corona can result in uptake and clearance, reducing circulation half-life, for certain applications these surface proteins may act as targeting groups or therapeutics.[118] Moreover, there is growing appreciation for impact of adhered protein structure on overall biodistribution. [119]

The other major barriers to effective tissue targeting of NPs are the renal system and mononuclear phagocytic system (MPS).[120,121] The renal system is composed of a blood filter (called the glomerular basement membrane) that rapidly removes nanomaterials with sizes below 10 nm.[122] Additionally, materials with anionic charge accumulate passively in the tubules of the kidneys.[123] To avoid the renal system most therapeutic NPs have hydrodynamic diameters of 20-100 nm and neutral surface charges. The MPS is a multi-organ system predominately composed of phagocytic cells in the liver (Kupffer cells) and spleen (splenic macrophages).[124,125] Non-specific internalization of nanomaterials in response to the protein coronas discussed earlier can result in over 95% of NPs accumulating in the liver and spleen.[120] Materials with positive surface charges have the greatest affinity for cells in the MPS, while neutrally charged hydrophilic surfaces (due to less protein adsorption) have the longest circulation times.[126,127]

The versatile nature of polymeric NPs makes it easy to design materials that avoid

these adverse interactions during circulation. In addition to avoiding off target effects, polymeric nanomaterials can also take advantage of a variety disease induced changes to the tissue microenvironment to increase specific accumulation. As previously discussed, the EPR effect was long thought to be the prime example of harnessing leaky vasculature to increase drug delivery to tumors.[57,58] While the effectiveness of this approach has been debated, in animal models it remains a good example of size dependent biodistrubtion. Interestingly, size can also impact uptake into phagocytic cells with dendritic cells preferentially internalizing 50 nm NPs and macrophages internalizing predominantly micrometer-sized particles.[26,128] Additionally, NPs can also leverage the acidic environment created by tumors and the wound healing process for triggered morphology chances.[103] This approach has also been utilized to take advantage of the elevated temperatures at wound sites, using thermoresponsive polymers.[73] Overall, polymeric nanomaterials can be designed to avoid clearance after injection and passively accumulate in tissues of interest.

1.3.2 Cellular Internalization

Polymeric nanoparticles primarily enter cells through energy-mediated endocytosis. Endocytosis can be mediated by nonspecific charge interactions between NPs and cell membranes, or specific receptor ligand interactions. There are five main endocytotic mechanisms: clathrin-coated pit mediated (CME), fast endophilin-mediated (FEME), clatharin-independent carrier (CLIC) / glycosylphosphatidylinositol-anchored protein enriched early endocytic compartment (GEEC), macropinocytosis, and phagocytosis. CME, FEME, and CLIC/GEEC can internalize particles with diameters between 30 - 200 nm.[129] If the NPs are below 30 nm, some evidence suggests that the cell membrane will not effectively wrap around the particle.[130] For these small NPs receptor ligand interactions determine the

route of uptake. For example, transferrin is internalized by CME, dopamine and acetylcholine by FEME, and hyaluronic acid by CLIC/GEEC.[131–133] Larger particles (greater than 200 nm) are only internalized by macropinocytosis and phagocytosis.[129] Not all cell types can perform macrophinocytosis and phagocytosis, so uptake of large particles occurs most often in macrophages and dendritic cells.[134,135] Interestingly, in cultured cell lines macropinocytosis is often upregulated due to the presence of growth factors.[136] While there is still much to be understood about the various endocytotic pathways, numerous reports indicate that 50 nm diameter materials have the most internalization.[75]

Once nanoparticles enter the cell via one of the previously discussed pathways, they will most often enter early endosomes (via a Rab5/EEA1-dependent pathway).[137] While it is possible for these early endosomes to be recycled back to the cell surface, the majority of reports show that early endosomes containing nanoparticles progress to late endosomes and eventually lysosomes.[129] Especially, for the biologic drugs discussed in previous sections, the harsh conditions of the lysosome (low pH, ROS, nucleases, and proteases) will result in degradation.[138] It is imperative that the therapeutic cargo escapes the endosome before the lysosome is fully formed to deliver intact cargo to the correct intracellular compartment. The main strategies for endosomal escape are the proton sponge effect, anionic membrane destabilization, and pore formation.[26] The proton sponge effect has been observed when amine-containing polymers become protonated under the increasingly acidic conditions of the endosome. The influx of hydrogen ions is followed by chloride ions, which dramatically increases the osmotic pressure. When the osmotic pressure reaches a critical threshold, the endosomal compartment bursts, releasing its contents into the cyotosol.[139] The proton sponge effect has been used to great effect to deliver nucleic acids into the cyotosol.[140] Despite some success, the proton sponge effect remains controversial with several mechanistic studies

being unable to confirm the proposed effects of buffering and increased pressure.[141,142] The second approach to endosomal escape, anionic membrane destabilization, takes advantage of the pKa of carboxylic acids. At neutral conditions polyanions are hydrophilic and do not interact with lipid membranes. However, below the pKa of the carboxylic acid groups, the polyanion loses its negative charge and becomes hydrophobic. Specific hydrophobic copolymers have shown pH dependent membrane lytic activity and have been used to escape endosomes.[143,144] The last approach for endosomal escape, pore formation, is inspired by the pH-triggered display of lytic proteins by viruses. By sequestering membrane lytic peptides into the cores of tertiary amine containing micelles, only upon acidification of endosome does the micelle disassemble and release the peptide. One of the most active peptides for pore formation that results in endosomal escape is melittin, the main component in honeybee venom.[92,145,146] In summary, both the processes of cellular internalization and endosomal escape are critical to the development of successful therapeutics. Unfortunately, while there are many examples of polymeric nanomaterials that accomplish both of these tasks, the underlying mechanisms responsible for these successes remain obscure.[76,147]

1.4 Controlled Polymerization*

A polymerization has three distinct steps: initiation, propagation and termination. In a controlled polymerization, initiation is rapid, propagation is slow (by comparison), and termination events are extremely minimal or nonexistent. These criteria can best be met under chain growth, the mechanism by which individual monomers are added to the growing polymer chain one at a time. The polymerization techniques covered in this section, atom transfer radical polymerization (ATRP), reverse addition fragmentation chain transfer polymerization (RAFT), ring-opening polymerization (ROP), and ring opening metathesis polymerization (ROMP) proceed by chain growth mechanisms and exhibit "living characteristics" (Figure 1.2). Criteria used to characterize the control of a polymerization (and the "livingness) are low dispersity ($Đ < 1.2$), predictable molecular weight, and chain end fidelity. Furthermore, while it is difficult to perform a textbook "living" polymerization (requiring a total absence of termination events) these techniques have the aforementioned "living characteristics". The potential for these polymerizations to yield precise molecular weight distributions with unique properties holds great promise for therapeutic biomedical applications. The advantages and drawbacks of ATRP, RAFT, ROP and ROMP for controlled synthesis of polymers will be highlighted.

*Adapted with permission from Lee, Daniel C., Lamm, Robert J., **Prossnitz, Alexander N.**, *et al.* Dual Polymerizations: untapped potential for biomaterials. *Advanced healthcare materials*, 8, (2019). Copyright 2019 Wiley.

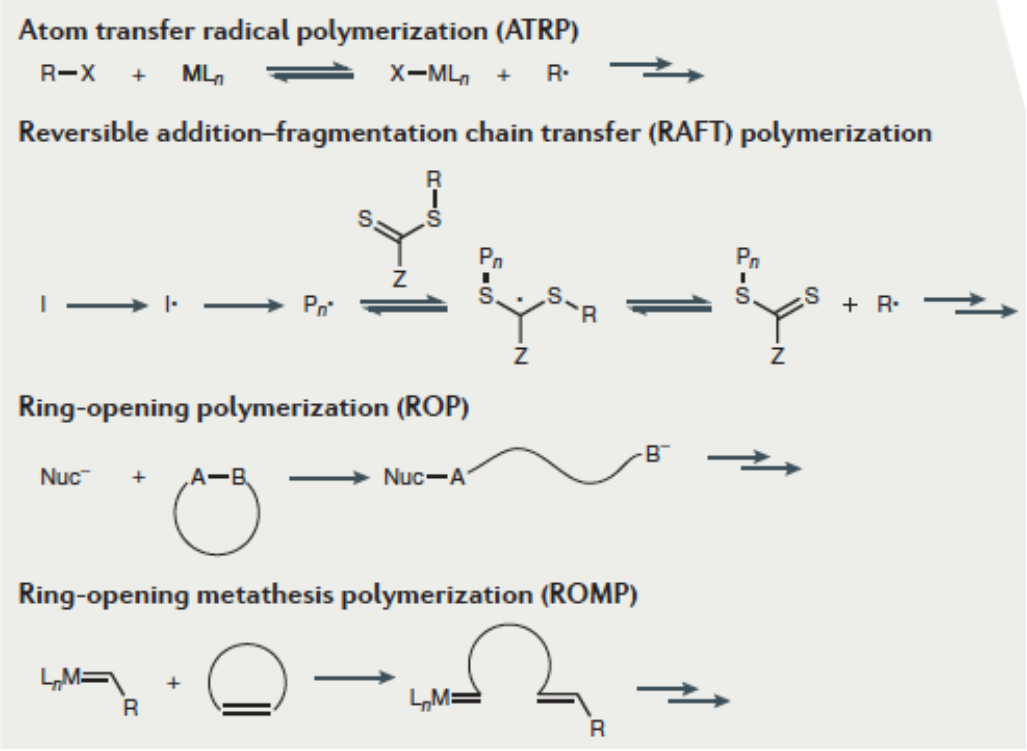

Figure 1.2 Schematic overview of polymerization mechanisms for ATRP, RAFT, ROP and ROMP. Double arrows indicate propagation. Figure adapted from Lutz *et al.* (Section 1.2 [9])

1.4.1 Reversible Deactivation Radical Polymerization (RDRP)

RDRP techniques seek to obtain control over radical polymerizations by dramatically reducing the concentration of free radicals. After initiation of a radical polymerization, growing polymer chains will have an active chain end consisting of a free radical. These radical chain ends are highly reactive, causing irreversible termination reactions (disproportionation and chain end coupling). Irreversible termination reactions result in polymers with broad dispersities, unpredictable molecular weights, and loss of chain end functionality. Two mechanistically distinct approaches, reversible deactivation and degenerative transfer, have been developed to reduce the free radical concentration, limiting termination reactions and resulting in a controlled polymerization. During reversible deactivation the active radical chain end reacts reversibly to form a covalent bond, causing in

deactivation. With regards to degenerative transfer, the active radical on the chain end is relocated to a dormant polymer chain (one that was previously deactivated by the same mechanism). However, these low concentrations of radicals can be quickly scavenged by atmospheric oxygen, halting polymer propagation. This obstacle can be easily overcome by performing the reactions under inert atmosphere by purging, sparging, or utilizing a glove box. This review will address ATRP and RAFT, two of the most widely used RDRP techniques for bioapplications and block copolymers.

Chain Transfer

In addition to termination events, reactions between the active chain end and the polymer backbone, called chain transfer, can scramble a polymer's sequence and increase dispersity. While chain transfer is present in all polymerizations, it impacts ROP and ROMP more than ATRP and RAFT, because in both ring-opening systems, the polymer backbone contains the same reactive functionality as the monomer (esters and amides in ROP and olefins in ROMP).

1.4.2 Atom Transfer Radical Polymerization (ATRP)

A reversible deactivation radical polymerization (RDRP) technique pioneered by Krzysztof Matyjaszewski in 1994, ATRP utilizes a transition metal complex to both activate and deactivate the growing polymer chain.[148] This radical polymerization is commonly used in bioapplications for the highly controlled synthesis of polymethacrylates and polyacrylates, but can tolerate a host of polar vinyl monomers if only moderate control is necessary. While it is feasible to perform aqueous ATRP, challenges such as high rates of activation (increasing radical concentration), ionic interactions between charged monomers and the transition metal complex, and catalyst degradation via disproportionation make it a daunting

task.[149,150] Polymers synthesized with ATRP will generally have aliphatic backbones linked to functional groups via ester bonds. Due to solvent restrictions, many ATRP monomers exhibit hydrophobic moieties, but ethylene glycol, hydroxyl, and tertiary amine containing monomers can be polymerized under these conditions with reasonable success. Overall, ATRP is a robust technique for the synthesis of polar and hydrophobic polyacrylates and polymethacrylates.[151]

In the initiation step of ATRP, a halogen is abstracted from the alkyl halide initiator by a low oxidation state transition metal (most often Cu(I)X, where X is Br or Cl). This reaction generates a radical (a process referred to as activation) that will polymerize vinyl monomers. However, the growing polymer chain is rapidly deactivated by the reverse reaction. This mechanism is an example of RDRP by reversible deactivation. This activation and deactivation results in an equilibrium, which under ideal circumstances greatly favors the deactivated species. In early applications of ATRP, the use of Cu(I) alone to catalyze the polymerization meant that this equilibrium was not established until after the start of the reaction. This initial burst of radicals, created before the deactivating equilibrium is established, led to irreversible termination events. This observation highlights the importance of maintaining a low Cu(I) to Cu(II) ratio throughout the polymerization.

Advances over the past 20 years have focused on both reducing the necessary amount of Cu(I) and increasing the ratio of Cu(II) to Cu(I) to improve control. These advances include: reverse ATRP, activators regenerated by electron transfer (AGET) ATRP, initiators for continuous activator regeneration (ICAR) ATRP, and supplemental activators and reducing agents (SARA) ATRP. Additionally, ATRP can be externally controlled with the use of electrochemical potential (eATRP), light (photoATRP) and ultrasound (mechanoATRP).[151,152] For example, in reverse ATRP, Cu(II) can be added to the reaction

instead of Cu(I) and a radical initiator can be used to slowly convert the Cu(II) into the active Cu(I). In eATRP an applied potential induces an electrochemical one-electron transfer to reduce the copper resulting in the active species.

1.4.3 Ring Opening Polymerization (ROP)

By far the oldest approach mentioned in this review, (the first recorded ROP of N-carboxyanhydrides (NCA) was performed in 1906), this technique has the greatest variety of unique synthetic approaches. Specifically, ROP constitutes a large category of nucleophilic ring opening propagation reactions of cyclic electrophilic monomers. For the sake of simplicity and due to their applicability to medicine, only ROP of lactones, lactides and NCAs will be discussed. First the various types of ROP (anionic, cationic, organometalic, and enzyme catalyzed) will be discussed and then these approaches will be analyzed in the context of each monomer. The key advantage of these polyesters and polyamides is their biodegradability. These materials are commonly used in the core of biocompatible self-assembled structures since high molecular weight polyesters and polyamides can be quite hydrophobic, particularly with regards to block copolymers in aqueous solvents.

Ionic polymerizations of ring-strained monomers can be either cationic or anionic. The cationic polymerization is catalyzed by the presence of an acid and anionic polymerization is catalyzed by the addition of base.[153,154] While both techniques were originally developed with strong acid (ex. trifluoromethanesulfonic acid) and strong base (ex. potassium tert-butoxide and butyllithium), recent advances have enabled the use of milder reagents.[153] Specifically, cationic polymerization has been conducted using diphenyl phosphate with various alcohols as the initiators.[155] The milder analog of anionic polymerization is known as nucleophilic ROP. Nucleophiles such as amines, phosphines, and

N-heterocyclic carbenes (NHCs) can polymerize cyclic monomers.[156] Generally anionic and nucleophilic ROP provide significantly more control over a broader range of molecular weights compared cationic ROP.

Organometallic catalysis of ROP will be addressed with regards to lactones and NHCs following this brief introduction. The use of transition metal complexes to accelerate ROP has enabled mass production of polylactic acid and polyglycolic acid. Mechanistically, these catalysts coordinate to the esters present in the cyclic monomers and act as Lewis acids, activating the monomers for nucleophilic attack and polymer propagation.[153,157,158]

Lastly, the formation of polyesters can be catalyzed enzymatically by lipases. These enzymes actively hydrolyze lactones and lactides, forming an acyl enzyme intermediate. These enzyme-activated monomers are subsequently cleaved from the enzyme by water. This process produces a hydroxycarboxylic acid, which can act as an initiator. This initiator attacks additional enzyme-activated monomers, forming a polymeric hydroxycarboxylic acid. Again, this initiator (now polymeric) can continue to attack enzyme-actived monomers, resulting in propagation.[159]

Lactones and lactides are structurally similar, and as such, the mechanism and reaction considerations are comparable. Industrially, polyesters are synthesized with the organometallic catalyst tin(II) octanoate and an alcohol initiator by coordination insertion polymerization. While this ROP strategy is fast (minutes to hours) and easy to use, due to its high reactivity, the resulting polymers also have high dispersity, of about 2, because of intra and intermolecular transesterification reactions.[153] Anionic and nucleophilic ROP of lactones and lactides provides much tighter control over dispersity at the cost of usability and scale. It is possible to perform cationic ROP to synthesize polyesters but to date it remains the least common technique.[153]

Poly(NHCs) are predominately synthesized by one of two nucleophilic ROP mechanisms: amine or activated monomer. In the amine ROP of NHC, the base performs a nucleophilic attack on the anhydride, breaking the ring. The resulting carbamic acid undergoes decarboxylation, yielding another primary amine to continue propagation. In the activated monomer mechanism, a base deprotonates the nitrogen in the NHC, rendering it nucleophilic, causing propagation. Interestingly, transition metal catalysts containing cobalt, nickel, and platinum have shown efficiency at performing ROP of NHCs. However, further discussion of those mechanisms is beyond the scope of this discussion.[154,157,158]

Overall, there is a vast amount of literature exploring the various techniques for performing ROP. For the purpose of synthesizing block copolymers using lactides, lactones or NHCs, nucleophilic ROP affords the greatest control and simplicity.

1.4.4 Ring Opening Metathesis Polymerization (ROMP)

ROMP is unique to the other approaches mentioned in this discussion because it is a combination of a ROP and olefin polymerization. Metathesis polymerization of ring-strained olefins began in the 1960s making use of ill-defined catalysts (aluminum, titanium, tantalum) and well defined catalysts (tungsten and molybdenum), but it was not until the 1990s with the discovery of ruthenium-based catalysts that ROMP became feasible for bioapplications.[160,161] Until the ruthenium-based system (known as Grubbs catalyst), ROMP had poor functional group tolerability and was highly moisture sensitive. Importantly, not only can Grubbs catalyst polymerize functional (containing aldehyde, ketone or alcohol) ring-strained olefins but also it can do so in protic media and aqueous solvents.[161,160] This unprecedented stability facilitated the widespread adoption of ROMP. The ring-strained olefin, norbornene, is the most common ROMP monomer due to its controlled polymerization kinetics and wide

variety of functional analogs. ROMP has been used to synthesize a variety of bioactive polymers containing peptides, nucleic acids, and small molecules. The mechanism of chain growth that occurs during ROMP remains largely unaffected by the size of the monomers, even large bioactive functionalities.[161] In the context of comb, brush, and bottle-brush polymers, Grubbs catalyst enables grafting densities of close to 100% and can be achieved with side chains up to 7,000 Da.[162] To summarize, ROMP is a highly versatile technique to prepare polymers with unsaturated backbones and broad bioactive functionality.

Mechanistically, ROMP proceeds with an active chain end and is mainly driven by the enthalpic release of ring-strain from the cyclic monomers. Polymerization begins once one of the two ligands bound to the ruthenium catalyst dissociates, allowing coordination of the catalyst to the olefin containing monomer. This monomer then undergoes a [2+2]-cycloaddition, resulting in an unstable four-membered transition state and a subsequent cycloreversion. This process yields a metal alkylidene complex consisting of the ring-opened monomer and the active Grubbs catalyst. Due to the high chain end fidelity, these polymerizations must be terminated by the addition of a quenching agent. Most often, vinyl ethers are used as the quenching agent because the resulting metal-alkylidene renders the ruthenium catalyst metathesis inactive and displaces it from the chain end.[161,160]

1.4.5 Reverse Addition Fragmentation Chain Transfer (RAFT)

Similar to ATRP, RAFT is an RDRP technique used for the polymerization of vinyl monomers. RAFT was first reported by the CSIRO group in 1998.[163] While initial studies focused on elucidating the RAFT mechanism, more recent work has been targeted at expanding usability (both for laboratory and commercial settings) and expanding applications. Since RAFT is a fully organic system (no metal) it is highly customizable. By

combining various chain transfer agents (CTAs) and radical initiators, RAFT can be biocompatible, performed in aqueous or organic solvents, and is not affected by the presence of charges or ions. For example, RAFT polymerizations have been done directly on the surface of living cells and in complex aqueous solvents (including, beer, wine, and liquor).[164,165] This broad compatibility translates directly to the monomer scope of this technique, which includes methacrylates, acrylates, methacrylamides, acrylamides, vinyl esters, and vinyl amides.[166] In short, RAFT is a powerful and versatile tool for the synthesis of most vinyl monomers.

RAFT maintains a low concentration of propagating species by degenerative transfer, (radicals are moved from a propagating polymer to a dormant polymer). This fundamentally different mechanism begins with the generation of free radicals (by thermal, redox, or photoinitiation).[166] These radicals react quickly with CTAs that sequester the radicals for a short time before fragmenting. Upon fragmentation (also a radical producing process), monomers will start to polymerize. However, because the CTA is much more reactive towards radicals than the monomer, before a second monomer can be added to the growing chain, the CTA will trap and transfer the radical to a different monomer. As a result, during an ideal RAFT polymerization, about one monomer is added per addition/fragmentation cycle. Therefore, each polymer chain grows at approximately the same rate, producing polymers with low dispersity.[166,167] To achieve ideal RAFT polymerization conditions, the initiator to CTA ratio can be decreased (decreasing the number of active chain ends) and an optimal CTA for the given monomer can be selected (there are many published guides for this selection).[166] It is also important to note that as a result of the degenerative transfer mechanism, the degree of polymerization of the polymer is determined by the CTA to monomer ratio not the monomer to initiator ratio.

References

(1) None Listed. Biotech Products in Big Pharma Clinical Pipelines Have Grown Dramatically. *Tufts CSDD Impact Report*. 2013, pp 1–15.

(2) Muttenthaler, M.; King, G. F.; Adams, D. J.; Alewood, P. F. Trends in Peptide Drug Discovery. *Nat Rev Drug Discov* **2021**, *20* (4), 309–325. https://doi.org/10.1038/s41573-020-00135-8.

(3) Goeddel, D. V.; Kleid, D. G.; Bolivar, F.; Heyneker, H. L.; Yansura, D. G.; Crea, R.; Hirose, T.; Kraszewski, A.; Itakura, K.; Riggs, A. D. Expression in Escherichia Coli of Chemically Synthesized Genes for Human Insulin. *Proc Natl Acad Sci U S A* **1979**, *76* (1), 106–110.

(4) Zaykov, A. N.; Mayer, J. P.; DiMarchi, R. D. Pursuit of a Perfect Insulin. *Nat Rev Drug Discov* **2016**, *15* (6), 425–439. https://doi.org/10.1038/nrd.2015.36.

(5) *Antisense Drug Technology: Principles, Strategies, and Applications*, 2nd ed.; Crooke, S. T., Ed.; CRC Press: Boca Raton, 2008.

(6) Adessi, C.; Soto, C. Converting a Peptide into a Drug: Strategies to Improve Stability and Bioavailability. *Curr Med Chem* **2002**, *9* (9), 963–978. https://doi.org/10.2174/0929867024606731.

(7) Albarran, B.; Hoffman, A. S.; Stayton, P. S. Efficient Intracellular Delivery of a Pro-Apoptotic Peptide With A PH-Responsive Carrier. *React Funct Polym* **2011**, *71* (3), 261–265. https://doi.org/10.1016/j.reactfunctpolym.2010.09.008.

(8) Craik, D. J.; Fairlie, D. P.; Liras, S.; Price, D. The Future of Peptide-Based Drugs. *Chemical Biology & Drug Design* **2013**, *81* (1), 136–147. https://doi.org/10.1111/cbdd.12055.

(9) Nestor, J. J. The Medicinal Chemistry of Peptides. *Curr Med Chem* **2009**, *16* (33), 4399–4418. https://doi.org/10.2174/092986709789712907.

(10) Kole, R.; Krainer, A. R.; Altman, S. RNA Therapeutics: Beyond RNA Interference and Antisense Oligonucleotides. *Nat Rev Drug Discov* **2012**, *11* (2), 125–140. https://doi.org/10.1038/nrd3625.

(11) Pack, D. W.; Hoffman, A. S.; Pun, S.; Stayton, P. S. Design and Development of Polymers for Gene Delivery. *Nat Rev Drug Discov* **2005**, *4* (7), 581–593. https://doi.org/10.1038/nrd1775.

(12) van Haasteren, J.; Li, J.; Scheideler, O. J.; Murthy, N.; Schaffer, D. V. The Delivery Challenge: Fulfilling the Promise of Therapeutic Genome Editing. *Nat Biotechnol* **2020**, *38* (7), 845–855. https://doi.org/10.1038/s41587-020-0565-5.

(13) Mitragotri, S.; Burke, P. A.; Langer, R. Overcoming the Challenges in Administering Biopharmaceuticals: Formulation and Delivery Strategies. *Nat Rev Drug Discov* **2014**, *13* (9), 655–672. https://doi.org/10.1038/nrd4363.

(14) Rosenblum, D.; Joshi, N.; Tao, W.; Karp, J. M.; Peer, D. Progress and Challenges towards Targeted Delivery of Cancer Therapeutics. *Nat Commun* **2018**, *9* (1), 1410. https://doi.org/10.1038/s41467-018-03705-y.

(15) Alqahtani, A.; Choucair, K.; Ashraf, M.; Hammouda, D. M.; Alloghbi, A.; Khan, T.; Senzer, N.; Nemunaitis, J. Bromodomain and Extra-Terminal Motif Inhibitors: A Review of Preclinical and Clinical Advances in Cancer Therapy. *Future Science OA* **2019**, *5* (3), FSO372. https://doi.org/10.4155/fsoa-2018-0115.

(16) Amorim, S.; Stathis, A.; Gleeson, M.; Iyengar, S.; Magarotto, V.; Leleu, X.; Morschhauser, F.; Karlin, L.; Broussais, F.; Rezai, K.; Herait, P.; Kahatt, C.; Lokiec,

F.; Salles, G.; Facon, T.; Palumbo, A.; Cunningham, D.; Zucca, E.; Thieblemont, C. Bromodomain Inhibitor OTX015 in Patients with Lymphoma or Multiple Myeloma: A Dose-Escalation, Open-Label, Pharmacokinetic, Phase 1 Study. *The Lancet Haematology* **2016**, *3* (4), e196–e204. https://doi.org/10.1016/S2352-3026(16)00021-1.

(17) Vohidov, F.; Andersen, J. N.; Economides, K. D.; Shipitsin, M. V.; Burenkova, O.; Ackley, J. C.; Vangamudi, B.; Nguyen, H. V.-T.; Gallagher, N. M.; Shieh, P.; Golder, M. R.; Liu, J.; Dahlberg, W. K.; Ehrlich, D. J. C.; Kim, J.; Kristufek, S. L.; Huh, S. J.; Neenan, A. M.; Baddour, J.; Paramasivan, S.; de Stanchina, E.; Kc, G.; Turnquist, D. J.; Saucier-Sawyer, J. K.; Kopesky, P. W.; Brady, S. W.; Jessel, M. J.; Reiter, L. A.; Chickering, D. E.; Johnson, J. A.; Blume-Jensen, P. Design of BET Inhibitor Bottlebrush Prodrugs with Superior Efficacy and Devoid of Systemic Toxicities. *J. Am. Chem. Soc.* **2021**, *143* (12), 4714–4724. https://doi.org/10.1021/jacs.1c00312.

(18) Fries, C. N.; Curvino, E. J.; Chen, J.-L.; Permar, S. R.; Fouda, G. G.; Collier, J. H. Advances in Nanomaterial Vaccine Strategies to Address Infectious Diseases Impacting Global Health. *Nat. Nanotechnol.* **2021**, *16* (4), 1–14. https://doi.org/10.1038/s41565-020-0739-9.

(19) Kirtane, A. R.; Verma, M.; Karandikar, P.; Furin, J.; Langer, R.; Traverso, G. Nanotechnology Approaches for Global Infectious Diseases. *Nat. Nanotechnol.* **2021**, *16* (4), 369–384. https://doi.org/10.1038/s41565-021-00866-8.

(20) Bedell, S. E.; Jabbour, S.; Goldberg, R.; Glaser, H.; Gobble, S.; Young-Xu, Y.; Graboys, T. B.; Ravid, S. Discrepancies in the Use of Medications: Their Extent and Predictors in an Outpatient Practice. *Arch Intern Med* **2000**, *160* (14), 2129. https://doi.org/10.1001/archinte.160.14.2129.

(21) Martin, L. R.; Williams, S. L.; Haskard, K. B.; DiMatteo, M. R. The Challenge of Patient Adherence. *Ther Clin Risk Manag* **2005**, *1* (3), 189–199.

(22) Muttenthaler, M.; King, G. F.; Adams, D. J.; Alewood, P. F. Trends in Peptide Drug Discovery. *Nat Rev Drug Discov* **2021**, *20* (4), 309–325. https://doi.org/10.1038/s41573-020-00135-8.

(23) Fosgerau, K.; Hoffmann, T. Peptide Therapeutics: Current Status and Future Directions. *Drug Discovery Today* **2015**, *20* (1), 122–128. https://doi.org/10.1016/j.drudis.2014.10.003.

(24) Lau, J. L.; Dunn, M. K. Therapeutic Peptides: Historical Perspectives, Current Development Trends, and Future Directions. *Bioorganic & Medicinal Chemistry* **2018**, *26* (10), 2700–2707. https://doi.org/10.1016/j.bmc.2017.06.052.

(25) Mitragotri, S.; Burke, P. A.; Langer, R. Overcoming the Challenges in Administering Biopharmaceuticals: Formulation and Delivery Strategies. *Nat Rev Drug Discov* **2014**, *13* (9), 655–672. https://doi.org/10.1038/nrd4363.

(26) Lv, S.; Sylvestre, M.; Prossnitz, A. N.; Yang, L. F.; Pun, S. H. Design of Polymeric Carriers for Intracellular Peptide Delivery in Oncology Applications. *Chem. Rev.* **2021**, acs.chemrev.0c00963. https://doi.org/10.1021/acs.chemrev.0c00963.

(27) Leader, B.; Baca, Q. J.; Golan, D. E. Protein Therapeutics: A Summary and Pharmacological Classification. *Nat Rev Drug Discov* **2008**, *7* (1), 21–39. https://doi.org/10.1038/nrd2399.

(28) Morales, L. E. Gaucher's Disease: A Review. *Ann Pharmacother* **1996**, *30* (4), 381–388. https://doi.org/10.1177/106002809603000411.

(29) Slaff, J.; Jacobson, D.; Tillman, C. R.; Curington, C.; Toskes, P. Protease-Specific Suppression of Pancreatic Exocrine Secretion. *Gastroenterology* **1984**, *87* (1), 44–52.

(30) Hershfield, M. S.; Buckley, R. H.; Greenberg, M. L.; Melton, A. L.; Schiff, R.; Hatem, C.; Kurtzberg, J.; Markert, M. L.; Kobayashi, R. H.; Kobayashi, A. L.; Abuchowski, A. Treatment of Adenosine Deaminase Deficiency with Polyethylene Glycol–Modified Adenosine Deaminase. *N Engl J Med* **1987**, *316* (10), 589–596. https://doi.org/10.1056/NEJM198703053161005.

(31) Wei, T.; Cheng, Q.; Farbiak, L.; Anderson, D. G.; Langer, R.; Siegwart, D. J. Delivery of Tissue-Targeted Scalpels: Opportunities and Challenges for *In Vivo* CRISPR/Cas-Based Genome Editing. *ACS Nano* **2020**, *14* (8), 9243–9262. https://doi.org/10.1021/acsnano.0c04707.

(32) Shi, L.; Sings, H. L.; Bryan, J. T.; Wang, B.; Wang, Y.; Mach, H.; Kosinski, M.; Washabaugh, M. W.; Sitrin, R.; Barr, E. GARDASIL®: Prophylactic Human Papillomavirus Vaccine Development – From Bench Top to Bed-Side. *Clinical Pharmacology & Therapeutics* **2007**, *81* (2), 259–264. https://doi.org/10.1038/sj.clpt.6100055.

(33) Szmuness, W.; Stevens, C. E.; Harley, E. J.; Zang, E. A.; Oleszko, W. R.; William, D. C.; Sadovsky, R.; Morrison, J. M.; Kellner, A. Hepatitis B Vaccine: Demonstration of Efficacy in a Controlled Clinical Trial in a High-Risk Population in the United States. *N Engl J Med* **1980**, *303* (15), 833–841. https://doi.org/10.1056/NEJM198010093031501.

(34) Rosenblum, D.; Gutkin, A.; Dammes, N.; Peer, D. Progress and Challenges towards CRISPR/Cas Clinical Translation. *Advanced Drug Delivery Reviews* **2020**, *154–155*, 176–186. https://doi.org/10.1016/j.addr.2020.07.004.

(35) van Haasteren, J.; Li, J.; Scheideler, O. J.; Murthy, N.; Schaffer, D. V. The Delivery Challenge: Fulfilling the Promise of Therapeutic Genome Editing. *Nat Biotechnol* **2020**, *38* (7), 845–855. https://doi.org/10.1038/s41587-020-0565-5.

(36) Behr, M.; Zhou, J.; Xu, B.; Zhang, H. In Vivo Delivery of CRISPR-Cas9 Therapeutics: Progress and Challenges. *Acta Pharmaceutica Sinica B* **2021**, *11* (8), 2150–2171. https://doi.org/10.1016/j.apsb.2021.05.020.

(37) Mitragotri, S.; Burke, P. A.; Langer, R. Overcoming the Challenges in Administering Biopharmaceuticals: Formulation and Delivery Strategies. *Nat Rev Drug Discov* **2014**, *13* (9), 655–672. https://doi.org/10.1038/nrd4363.

(38) Roberts, T. C.; Langer, R.; Wood, M. J. A. Advances in Oligonucleotide Drug Delivery. *Nat Rev Drug Discov* **2020**, *19* (10), 673–694. https://doi.org/10.1038/s41573-020-0075-7.

(39) Sahin, U.; Karikó, K.; Türeci, Ö. MRNA-Based Therapeutics — Developing a New Class of Drugs. *Nature Reviews Drug Discovery* **2014**, *13* (10), 759–780. https://doi.org/10.1038/nrd4278.

(40) Hill, A. B.; Chen, M.; Chen, C.-K.; Pfeifer, B. A.; Jones, C. H. Overcoming Gene-Delivery Hurdles: Physiological Considerations for Nonviral Vectors. *Trends Biotechnol* **2016**, *34* (2), 91–105. https://doi.org/10.1016/j.tibtech.2015.11.004.

(41) Lostalé-Seijo, I.; Montenegro, J. Synthetic Materials at the Forefront of Gene Delivery. *Nat Rev Chem* **2018**, *2* (10), 258–277. https://doi.org/10.1038/s41570-018-0039-1.

(42) Heyde, M.; Partridge, K. A.; Oreffo, R. O. C.; Howdle, S. M.; Shakesheff, K. M.; Garnett, M. C. Gene Therapy Used for Tissue Engineering Applications. *J Pharm Pharmacol* **2007**, *59* (3), 329–350. https://doi.org/10.1211/jpp.59.3.0002.

(43) Burton, E. A.; Glorioso, J. C.; Fink, D. J. Gene Therapy Progress and Prospects: Parkinson's Disease. *Gene Therapy* **2003**, *10* (20), 1721–1727. https://doi.org/10.1038/sj.gt.3302116.
(44) McNeish, I. A.; Bell, S. J.; Lemoine, N. R. Gene Therapy Progress and Prospects: Cancer Gene Therapy Using Tumour Suppressor Genes. *Gene Therapy* **2004**, *11* (6), 497–503. https://doi.org/10.1038/sj.gt.3302238.
(45) Bunnell, B. A.; Morgan, R. A. Gene Therapy for Infectious Diseases. *Clin Microbiol Rev* **1998**, *11* (1), 42–56.
(46) Alisky, J. M.; Davidson, B. L. Gene Therapy for Amyotrophic Lateral Sclerosis and Other Motor Neuron Diseases. *Hum Gene Ther* **2000**, *11* (17), 2315–2329. https://doi.org/10.1089/104303400750038435.
(47) Dzau, V. J.; Beatt, K.; Pompilio, G.; Smith, K. Current Perceptions of Cardiovascular Gene Therapy. *The American Journal of Cardiology* **2003**, *92* (9, Supplement 2), 18–23. https://doi.org/10.1016/S0002-9149(03)00964-0.
(48) Vile, R. G.; Russell, S. J.; Lemoine, N. R. Cancer Gene Therapy: Hard Lessons and New Courses. *Gene Therapy* **2000**, *7* (1), 2–8. https://doi.org/10.1038/sj.gt.3301084.
(49) Ferrari, S.; Geddes, D. M.; Alton, E. W. F. W. Barriers to and New Approaches for Gene Therapy and Gene Delivery in Cystic Fibrosis. *Adv Drug Deliv Rev* **2002**, *54* (11), 1373–1393. https://doi.org/10.1016/s0169-409x(02)00145-x.
(50) van Deutekom, J. C. T.; van Ommen, G.-J. B. Advances in Duchenne Muscular Dystrophy Gene Therapy. *Nat Rev Genet* **2003**, *4* (10), 774–783. https://doi.org/10.1038/nrg1180.
(51) Verbeke, R.; Lentacker, I.; De Smedt, S. C.; Dewitte, H. The Dawn of MRNA Vaccines: The COVID-19 Case. *Journal of Controlled Release* **2021**, *333*, 511–520. https://doi.org/10.1016/j.jconrel.2021.03.043.
(52) Ball, P. The Lightning-Fast Quest for COVID Vaccines — and What It Means for Other Diseases. *Nature* **2020**, *589* (7840), 16–18. https://doi.org/10.1038/d41586-020-03626-1.
(53) Tsui, N. B. Y.; Ng, E. K. O.; Lo, Y. M. D. Stability of Endogenous and Added RNA in Blood Specimens, Serum, and Plasma. *Clin Chem* **2002**, *48* (10), 1647–1653.
(54) Thierry, A. R.; Rabinovich, P.; Peng, B.; Mahan, L. C.; Bryant, J. L.; Gallo, R. C. Characterization of Liposome-Mediated Gene Delivery: Expression, Stability and Pharmacokinetics of Plasmid DNA. *Gene Therapy* **1997**, *4* (3), 226–237. https://doi.org/10.1038/sj.gt.3300350.
(55) Krieg, A. M. Therapeutic Potential of Toll-like Receptor 9 Activation. *Nature Reviews Drug Discovery* **2006**, *5* (6), 471–484. https://doi.org/10.1038/nrd2059.
(56) Hua, S.; de Matos, M. B. C.; Metselaar, J. M.; Storm, G. Current Trends and Challenges in the Clinical Translation of Nanoparticulate Nanomedicines: Pathways for Translational Development and Commercialization. *Front. Pharmacol.* **2018**, *9*. https://doi.org/10.3389/fphar.2018.00790.
(57) Price, L. S. L.; Stern, S. T.; Deal, A. M.; Kabanov, A. V.; Zamboni, W. C. A Reanalysis of Nanoparticle Tumor Delivery Using Classical Pharmacokinetic Metrics. *Sci. Adv.* **2020**, *6* (29), eaay9249. https://doi.org/10.1126/sciadv.aay9249.
(58) Challenging Paradigms in Tumour Drug Delivery. *Nature Materials* **2020**, *19* (5), 477–477. https://doi.org/10.1038/s41563-020-0676-x.
(59) Harris, J. M.; Chess, R. B. Effect of Pegylation on Pharmaceuticals. *Nature Reviews Drug Discovery* **2003**, *2* (3), 214–221. https://doi.org/10.1038/nrd1033.

(60) Veronese, F. M.; Pasut, G. PEGylation, Successful Approach to Drug Delivery. *Drug Discovery Today* **2005**, *10* (21), 1451–1458. https://doi.org/10.1016/S1359-6446(05)03575-0.
(61) Gustafson, H. H.; Holt-Casper, D.; Grainger, D. W.; Ghandehari, H. Nanoparticle Uptake: The Phagocyte Problem. *Nano Today* **2015**, *10* (4), 487–510. https://doi.org/10.1016/j.nantod.2015.06.006.
(62) Freire Haddad, H.; Burke, J. A.; Scott, E. A.; Ameer, G. A. Clinical Relevance of Pre-Existing and Treatment-Induced Anti-Poly(Ethylene Glycol) Antibodies. *Regen. Eng. Transl. Med.* **2021**. https://doi.org/10.1007/s40883-021-00198-y.
(63) Kakkar, A.; Traverso, G.; Farokhzad, O. C.; Weissleder, R.; Langer, R. Evolution of Macromolecular Complexity in Drug Delivery Systems. *Nat Rev Chem* **2017**, *1* (8), 0063. https://doi.org/10.1038/s41570-017-0063.
(64) Lutz, J.-F.; Lehn, J.-M.; Meijer, E. W.; Matyjaszewski, K. From Precision Polymers to Complex Materials and Systems. *Nat Rev Mater* **2016**, *1* (5), 16024. https://doi.org/10.1038/natrevmats.2016.24.
(65) Perrier, S. *50th Anniversary Perspective*: RAFT Polymerization—A User Guide. *Macromolecules* **2017**, *50* (19), 7433–7447. https://doi.org/10.1021/acs.macromol.7b00767.
(66) Boyer, C.; Corrigan, N. A.; Jung, K.; Nguyen, D.; Nguyen, T.-K.; Adnan, N. N. M.; Oliver, S.; Shanmugam, S.; Yeow, J. Copper-Mediated Living Radical Polymerization (Atom Transfer Radical Polymerization and Copper(0) Mediated Polymerization): From Fundamentals to Bioapplications. *Chem. Rev.* **2016**, *116* (4), 1803–1949. https://doi.org/10.1021/acs.chemrev.5b00396.
(67) Bielawski, C. W.; Grubbs, R. H. Living Ring-Opening Metathesis Polymerization. *Progress in Polymer Science* **2007**, *32* (1), 1–29. https://doi.org/10.1016/j.progpolymsci.2006.08.006.
(68) Corrigan, N.; Jung, K.; Moad, G.; Hawker, C. J.; Matyjaszewski, K.; Boyer, C. Reversible-Deactivation Radical Polymerization (Controlled/Living Radical Polymerization): From Discovery to Materials Design and Applications. *Progress in Polymer Science* **2020**, *111*, 101311. https://doi.org/10.1016/j.progpolymsci.2020.101311.
(69) Stirland, D. L.; Nichols, J. W.; Miura, S.; Bae, Y. H. Mind the Gap: A Survey of How Cancer Drug Carriers Are Susceptible to the Gap between Research and Practice. *J Control Release* **2013**, *172* (3), 1045–1064. https://doi.org/10.1016/j.jconrel.2013.09.026.
(70) Duncan, R. The Dawning Era of Polymer Therapeutics. *Nature Reviews Drug Discovery* **2003**, *2* (5), 347–360. https://doi.org/10.1038/nrd1088.
(71) Duncan, R.; Spreafico, F. Polymer Conjugates. Pharmacokinetic Considerations for Design and Development. *Clin Pharmacokinet* **1994**, *27* (4), 290–306. https://doi.org/10.2165/00003088-199427040-00004.
(72) Seymour, L. W.; Ferry, D. R.; Anderson, D.; Hesslewood, S.; Julyan, P. J.; Poyner, R.; Doran, J.; Young, A. M.; Burtles, S.; Kerr, D. J.; Cancer Research Campaign Phase I/II Clinical Trials committee. Hepatic Drug Targeting: Phase I Evaluation of Polymer-Bound Doxorubicin. *J Clin Oncol* **2002**, *20* (6), 1668–1676. https://doi.org/10.1200/JCO.2002.20.6.1668.

(73) Ekladious, I.; Colson, Y. L.; Grinstaff, M. W. Polymer–Drug Conjugate Therapeutics: Advances, Insights and Prospects. *Nat Rev Drug Discov* **2019**, *18* (4), 273–294. https://doi.org/10.1038/s41573-018-0005-0.

(74) Das, D.; Srinivasan, S.; Brown, F. D.; Su, F. Y.; Burrell, A. L.; Kollman, J. M.; Postma, A.; Ratner, D. M.; Stayton, P. S.; Convertine, A. J. Radiant Star Nanoparticle Prodrugs for the Treatment of Intracellular Alveolar Infections. *Polym. Chem.* **2018**, *9* (16), 2134–2146. https://doi.org/10.1039/C8PY00202A.

(75) Mitchell, M. J.; Billingsley, M. M.; Haley, R. M.; Wechsler, M. E.; Peppas, N. A.; Langer, R. Engineering Precision Nanoparticles for Drug Delivery. *Nat Rev Drug Discov* **2021**, *20* (2), 101–124. https://doi.org/10.1038/s41573-020-0090-8.

(76) Mitchell, M. J.; Billingsley, M. M.; Haley, R. M.; Wechsler, M. E.; Peppas, N. A.; Langer, R. Engineering Precision Nanoparticles for Drug Delivery. *Nat Rev Drug Discov* **2021**, *20* (2), 101–124. https://doi.org/10.1038/s41573-020-0090-8.

(77) Lv, S.; Sylvestre, M.; Prossnitz, A. N.; Yang, L. F.; Pun, S. H. Design of Polymeric Carriers for Intracellular Peptide Delivery in Oncology Applications. *Chem. Rev.* **2021**, acs.chemrev.0c00963. https://doi.org/10.1021/acs.chemrev.0c00963.

(78) Du, F.; Qiao, B.; Nguyen, T. D.; Vincent, M. P.; Bobbala, S.; Yi, S.; Lescott, C.; Dravid, V. P.; Olvera de la Cruz, M.; Scott, E. A. Homopolymer Self-Assembly of Poly(Propylene Sulfone) Hydrogels via Dynamic Noncovalent Sulfone–Sulfone Bonding. *Nature Communications* **2020**, *11* (1), 4896. https://doi.org/10.1038/s41467-020-18657-5.

(79) Zhang, L.; Beatty, A.; Lu, L.; Abdalrahman, A.; Makris, T. M.; Wang, G.; Wang, Q. Microfluidic-Assisted Polymer-Protein Assembly to Fabricate Homogeneous Functionalnanoparticles. *Materials Science and Engineering: C* **2020**, *111*, 110768. https://doi.org/10.1016/j.msec.2020.110768.

(80) Strand, M. S.; Krasnick, B. A.; Pan, H.; Zhang, X.; Bi, Y.; Brooks, C.; Wetzel, C.; Sankpal, N.; Fleming, T.; Goedegebuure, S. P.; DeNardo, D. G.; Gillanders, W. E.; Hawkins, W. G.; Wickline, S. A.; Fields, R. C. Precision Delivery of RAS-Inhibiting SiRNA to KRAS Driven Cancer via Peptide-Based Nanoparticles. *Oncotarget* **2019**, *10* (46), 4761–4775. https://doi.org/10.18632/oncotarget.27109.

(81) Jose, S.; Cinu, T. A.; Sebastian, R.; Shoja, M. H.; Aleykutty, N. A.; Durazzo, A.; Lucarini, M.; Santini, A.; Souto, E. B. Transferrin-Conjugated Docetaxel–PLGA Nanoparticles for Tumor Targeting: Influence on MCF-7 Cell Cycle. *Polymers (Basel)* **2019**, *11* (11). https://doi.org/10.3390/polym11111905.

(82) Rideau, E.; Dimova, R.; Schwille, P.; Wurm, F. R.; Landfester, K. Liposomes and Polymersomes: A Comparative Review towards Cell Mimicking. *Chem. Soc. Rev.* **2018**, *47* (23), 8572–8610. https://doi.org/10.1039/C8CS00162F.

(83) Rezvantalab, S.; Drude, N. I.; Moraveji, M. K.; Güvener, N.; Koons, E. K.; Shi, Y.; Lammers, T.; Kiessling, F. PLGA-Based Nanoparticles in Cancer Treatment. *Front. Pharmacol.* **2018**, *9*. https://doi.org/10.3389/fphar.2018.01260.

(84) Colson, Y. L.; Grinstaff, M. W. Biologically Responsive Polymeric Nanoparticles for Drug Delivery. *Advanced Materials* **2012**, *24* (28), 3878–3886. https://doi.org/10.1002/adma.201200420.

(85) Zhang, Y.; Yin, Q.; Yin, L.; Ma, L.; Tang, L.; Cheng, J. Chain-Shattering Polymeric Therapeutics with On-Demand Drug-Release Capability. *Angewandte Chemie International Edition* **2013**, *52* (25), 6435–6439. https://doi.org/10.1002/anie.201300497.

(86) Ekladious, I.; Colson, Y. L.; Grinstaff, M. W. Polymer–Drug Conjugate Therapeutics: Advances, Insights and Prospects. *Nat Rev Drug Discov* **2019**, *18* (4), 273–294. https://doi.org/10.1038/s41573-018-0005-0.
(87) Attwood, D.; Elworthy, P. H.; Kayne, S. B. Membrane Osmometry of Aqueous Micellar Solutions of Pure Nonionic and Ionic Surfactants. *J. Phys. Chem.* **1970**, *74* (19), 3529–3534. https://doi.org/10.1021/j100713a016.
(88) Lu, Y.; Zhang, E.; Yang, J.; Cao, Z. Strategies to Improve Micelle Stability for Drug Delivery. *Nano Res* **2018**, *11* (10), 4985–4998. https://doi.org/10.1007/s12274-018-2152-3.
(89) Dong, X.; Guo, X.; Liu, G.; Fan, A.; Wang, Z.; Zhao, Y. When Self-Assembly Meets Topology: An Enhanced Micelle Stability. *Chem. Commun.* **2017**, *53* (27), 3822–3825. https://doi.org/10.1039/C7CC00914C.
(90) Das, D.; Chen, J.; Srinivasan, S.; Kelly, A. M.; Lee, B.; Son, H.-N.; Radella, F.; West, T. E.; Ratner, D. M.; Convertine, A. J.; Skerrett, S. J.; Stayton, P. S. Synthetic Macromolecular Antibiotic Platform for Inhalable Therapy against Aerosolized Intracellular Alveolar Infections. *Mol. Pharmaceutics* **2017**, *14* (6), 1988–1997. https://doi.org/10.1021/acs.molpharmaceut.7b00093.
(91) Li, S.; Luo, M.; Wang, Z.; Feng, Q.; Wilhelm, J.; Wang, X.; Li, W.; Wang, J.; Cholka, A.; Fu, Y.; Sumer, B. D.; Yu, H.; Gao, J. Prolonged Activation of Innate Immune Pathways by a Polyvalent STING Agonist. *Nature Biomedical Engineering* **2021**, 1–12. https://doi.org/10.1038/s41551-020-00675-9.
(92) Cheng, Y.; Yumul, R. C.; Pun, S. H. Virus-Inspired Polymer for Efficient in Vitro and in Vivo Gene Delivery. *Angew Chem Int Ed Engl* **2016**, *55* (39), 12013–12017. https://doi.org/10.1002/anie.201605958.
(93) Gandhi, A.; Paul, A.; Sen, S. O.; Sen, K. K. Studies on Thermoresponsive Polymers: Phase Behaviour, Drug Delivery and Biomedical Applications. *Asian Journal of Pharmaceutical Sciences* **2015**, *10* (2), 99–107. https://doi.org/10.1016/j.ajps.2014.08.010.
(94) De, P.; Li, M.; Gondi, S. R.; Sumerlin, B. S. Temperature-Regulated Activity of Responsive Polymer−Protein Conjugates Prepared by Grafting-from via RAFT Polymerization. *J. Am. Chem. Soc.* **2008**, *130* (34), 11288–11289. https://doi.org/10.1021/ja804495v.
(95) Hu, X.; Liu, G.; Li, Y.; Wang, X.; Liu, S. Cell-Penetrating Hyperbranched Polyprodrug Amphiphiles for Synergistic Reductive Milieu-Triggered Drug Release and Enhanced Magnetic Resonance Signals. *J. Am. Chem. Soc.* **2015**, *137* (1), 362–368. https://doi.org/10.1021/ja5105848.
(96) Mishra, M. K.; Beaty, C. A.; Lesniak, W. G.; Kambhampati, S. P.; Zhang, F.; Wilson, M. A.; Blue, M. E.; Troncoso, J. C.; Kannan, S.; Johnston, M. V.; Baumgartner, W. A.; Kannan, R. M. Dendrimer Brain Uptake and Targeted Therapy for Brain Injury in a Large Animal Model of Hypothermic Circulatory Arrest. *ACS Nano* **2014**, *8* (3), 2134–2147. https://doi.org/10.1021/nn404872e.
(97) Dubikovskaya, E. A.; Thorne, S. H.; Pillow, T. H.; Contag, C. H.; Wender, P. A. Overcoming Multidrug Resistance of Small-Molecule Therapeutics through Conjugation with Releasable Octaarginine Transporters. *PNAS* **2008**, *105* (34), 12128–12133. https://doi.org/10.1073/pnas.0805374105.
(98) Luo, C.; Sun, J.; Liu, D.; Sun, B.; Miao, L.; Musetti, S.; Li, J.; Han, X.; Du, Y.; Li, L.; Huang, L.; He, Z. Self-Assembled Redox Dual-Responsive Prodrug-Nanosystem

Formed by Single Thioether-Bridged Paclitaxel-Fatty Acid Conjugate for Cancer Chemotherapy. *Nano Lett.* **2016**, *16* (9), 5401–5408. https://doi.org/10.1021/acs.nanolett.6b01632.

(99) Yoo, D.; Magsam, A. W.; Kelly, A. M.; Stayton, P. S.; Kievit, F. M.; Convertine, A. J. Core-Cross-Linked Nanoparticles Reduce Neuroinflammation and Improve Outcome in a Mouse Model of Traumatic Brain Injury. *ACS Nano* **2017**, *11* (9), 8600–8611. https://doi.org/10.1021/acsnano.7b03426.

(100) Chavas, T. E. J.; Su, F.-Y.; Srinivasan, S.; Roy, D.; Lee, B.; Lovelace-Macon, L.; Rerolle, G. F.; Limqueco, E.; Skerrett, S. J.; Ratner, D. M.; West, T. E.; Stayton, P. S. A Macrophage-Targeted Platform for Extending Drug Dosing with Polymer Prodrugs for Pulmonary Infection Prophylaxis. *Journal of Controlled Release* **2021**, *330*, 284–292. https://doi.org/10.1016/j.jconrel.2020.11.031.

(101) Badeau, B. A.; Comerford, M. P.; Arakawa, C. K.; Shadish, J. A.; DeForest, C. A. Engineered Modular Biomaterial Logic Gates for Environmentally Triggered Therapeutic Delivery. *Nat Chem* **2018**, *10* (3), 251–258. https://doi.org/10.1038/nchem.2917.

(102) Kern, H. B.; Srinivasan, S.; Convertine, A. J.; Hockenbery, D.; Press, O. W.; Stayton, P. S. Enzyme-Cleavable Polymeric Micelles for the Intracellular Delivery of Proapoptotic Peptides. *Mol. Pharmaceutics* **2017**, *14* (5), 1450–1459. https://doi.org/10.1021/acs.molpharmaceut.6b01178.

(103) Li, H.-J.; Du, J.-Z.; Liu, J.; Du, X.-J.; Shen, S.; Zhu, Y.-H.; Wang, X.; Ye, X.; Nie, S.; Wang, J. Smart Superstructures with Ultrahigh PH-Sensitivity for Targeting Acidic Tumor Microenvironment: Instantaneous Size Switching and Improved Tumor Penetration. *ACS Nano* **2016**, *10* (7), 6753–6761. https://doi.org/10.1021/acsnano.6b02326.

(104) Srinivasarao, M.; Low, P. S. Ligand-Targeted Drug Delivery. *Chem. Rev.* **2017**, *117* (19), 12133–12164. https://doi.org/10.1021/acs.chemrev.7b00013.

(105) Yao, V. J.; D'Angelo, S.; Butler, K. S.; Theron, C.; Smith, T. L.; Marchiò, S.; Gelovani, J. G.; Sidman, R. L.; Dobroff, A. S.; Brinker, C. J.; Bradbury, A. R. M.; Arap, W.; Pasqualini, R. Ligand-Targeted Theranostic Nanomedicines against Cancer. *Journal of Controlled Release* **2016**, *240*, 267–286. https://doi.org/10.1016/j.jconrel.2016.01.002.

(106) Xu, H.; Ma, H.; Yang, P.; Zhang, X.; Wu, X.; Yin, W.; Wang, H.; Xu, D. Targeted Polymer-Drug Conjugates: Current Progress and Future Perspective. *Colloids Surf B Biointerfaces* **2015**, *136*, 729–734. https://doi.org/10.1016/j.colsurfb.2015.10.001.

(107) Luo, Y.; Prestwich, G. D. Cancer-Targeted Polymeric Drugs. *Curr Cancer Drug Targets* **2002**, *2* (3), 209–226. https://doi.org/10.2174/1568009023333836.

(108) Chan, L. W.; Wang, X.; Wei, H.; Pozzo, L. D.; White, N. J.; Pun, S. H. A Synthetic Fibrin Cross-Linking Polymer for Modulating Clot Properties and Inducing Hemostasis. *Science Translational Medicine* **2015**, *7* (277), 277ra29-277ra29. https://doi.org/10.1126/scitranslmed.3010383.

(109) Kirtane, A. R.; Verma, M.; Karandikar, P.; Furin, J.; Langer, R.; Traverso, G. Nanotechnology Approaches for Global Infectious Diseases. *Nat. Nanotechnol.* **2021**, *16* (4), 369–384. https://doi.org/10.1038/s41565-021-00866-8.

(110) Fries, C. N.; Curvino, E. J.; Chen, J.-L.; Permar, S. R.; Fouda, G. G.; Collier, J. H. Advances in Nanomaterial Vaccine Strategies to Address Infectious Diseases

Impacting Global Health. *Nat. Nanotechnol.* **2021**, *16* (4), 1–14. https://doi.org/10.1038/s41565-020-0739-9.
(111) Tanaka, R.; Arai, K.; Matsuno, J.; Soejima, M.; Lee, J. H.; Takahashi, R.; Sakurai, K.; Fujii, S. Furry Nanoparticles: Synthesis and Characterization of Nanoemulsion-Mediated Core Crosslinked Nanoparticles and Their Robust Stability in Vivo. *Polym. Chem.* **2020**, *11* (27), 4408–4416. https://doi.org/10.1039/D0PY00610F.
(112) Palanikumar, L.; Al-Hosani, S.; Kalmouni, M.; Nguyen, V. P.; Ali, L.; Pasricha, R.; Barrera, F. N.; Magzoub, M. PH-Responsive High Stability Polymeric Nanoparticles for Targeted Delivery of Anticancer Therapeutics. *Communications Biology* **2020**, *3* (1), 1–17. https://doi.org/10.1038/s42003-020-0817-4.
(113) Khor, S. Y.; Vu, M. N.; Pilkington, E. H.; Johnston, A. P. R.; Whittaker, M. R.; Quinn, J. F.; Truong, N. P.; Davis, T. P. Elucidating the Influences of Size, Surface Chemistry, and Dynamic Flow on Cellular Association of Nanoparticles Made by Polymerization-Induced Self-Assembly. *Small* **2018**, *14* (34), e1801702. https://doi.org/10.1002/smll.201801702.
(114) Da Silva-Candal, A.; Brown, T.; Krishnan, V.; Lopez-Loureiro, I.; Ávila-Gómez, P.; Pusuluri, A.; Pérez-Díaz, A.; Correa-Paz, C.; Hervella, P.; Castillo, J.; Mitragotri, S.; Campos, F. Shape Effect in Active Targeting of Nanoparticles to Inflamed Cerebral Endothelium under Static and Flow Conditions. *J Control Release* **2019**, *309*, 94–105. https://doi.org/10.1016/j.jconrel.2019.07.026.
(115) Cox, A.; Andreozzi, P.; Dal Magro, R.; Fiordaliso, F.; Corbelli, A.; Talamini, L.; Chinello, C.; Raimondo, F.; Magni, F.; Tringali, M.; Krol, S.; Jacob Silva, P.; Stellacci, F.; Masserini, M.; Re, F. Evolution of Nanoparticle Protein Corona across the Blood–Brain Barrier. *ACS Nano* **2018**, *12* (7), 7292–7300. https://doi.org/10.1021/acsnano.8b03500.
(116) Tenzer, S.; Docter, D.; Kuharev, J.; Musyanovych, A.; Fetz, V.; Hecht, R.; Schlenk, F.; Fischer, D.; Kiouptsi, K.; Reinhardt, C.; Landfester, K.; Schild, H.; Maskos, M.; Knauer, S. K.; Stauber, R. H. Rapid Formation of Plasma Protein Corona Critically Affects Nanoparticle Pathophysiology. *Nature Nanotechnology* **2013**, *8* (10), 772–781. https://doi.org/10.1038/nnano.2013.181.
(117) Vincent, M. P.; Bobbala, S.; Karabin, N. B.; Frey, M.; Liu, Y.; Navidzadeh, J. O.; Stack, T.; Scott, E. A. Surface Chemistry-Mediated Modulation of Adsorbed Albumin Folding State Specifies Nanocarrier Clearance by Distinct Macrophage Subsets. *Nat Commun* **2021**, *12* (1), 648. https://doi.org/10.1038/s41467-020-20886-7.
(118) Scheetz, L.; Park, K. S.; Li, Q.; Lowenstein, P. R.; Castro, M. G.; Schwendeman, A.; Moon, J. J. Engineering Patient-Specific Cancer Immunotherapies. *Nature Biomedical Engineering* **2019**, *3* (10), 768–782. https://doi.org/10.1038/s41551-019-0436-x.
(119) Park, S. J. Protein–Nanoparticle Interaction: Corona Formation and Conformational Changes in Proteins on Nanoparticles. *Int J Nanomedicine* **2020**, *15*, 5783–5802. https://doi.org/10.2147/IJN.S254808.
(120) Gustafson, H. H.; Holt-Casper, D.; Grainger, D. W.; Ghandehari, H. Nanoparticle Uptake: The Phagocyte Problem. *Nano Today* **2015**, *10* (4), 487–510. https://doi.org/10.1016/j.nantod.2015.06.006.
(121) Mitchell, M. J.; Billingsley, M. M.; Haley, R. M.; Wechsler, M. E.; Peppas, N. A.; Langer, R. Engineering Precision Nanoparticles for Drug Delivery. *Nat Rev Drug Discov* **2021**, *20* (2), 101–124. https://doi.org/10.1038/s41573-020-0090-8.

(122) Hoshyar, N.; Gray, S.; Han, H.; Bao, G. The Effect of Nanoparticle Size on in Vivo Pharmacokinetics and Cellular Interaction. *Nanomedicine (Lond)* **2016**, *11* (6), 673–692. https://doi.org/10.2217/nnm.16.5.
(123) Liu, G. W.; Prossnitz, A. N.; Eng, D. G.; Cheng, Y.; Subrahmanyam, N.; Pippin, J. W.; Lamm, R. J.; Ngambenjawong, C.; Ghandehari, H.; Shankland, S. J.; Pun, S. H. Glomerular Disease Augments Kidney Accumulation of Synthetic Anionic Polymers. *Biomaterials* **2018**, *178*, 317–325. https://doi.org/10.1016/j.biomaterials.2018.06.001.
(124) Mortimer, G. M.; Butcher, N. J.; Musumeci, A. W.; Deng, Z. J.; Martin, D. J.; Minchin, R. F. Cryptic Epitopes of Albumin Determine Mononuclear Phagocyte System Clearance of Nanomaterials. *ACS Nano* **2014**, *8* (4), 3357–3366. https://doi.org/10.1021/nn405830g.
(125) Briley-Saebo, K.; Bjørnerud, A.; Grant, D.; Ahlstrom, H.; Berg, T.; Kindberg, G. M. Hepatic Cellular Distribution and Degradation of Iron Oxide Nanoparticles Following Single Intravenous Injection in Rats: Implications for Magnetic Resonance Imaging. *Cell Tissue Res* **2004**, *316* (3), 315–323. https://doi.org/10.1007/s00441-004-0884-8.
(126) Kou, L.; Bhutia, Y. D.; Yao, Q.; He, Z.; Sun, J.; Ganapathy, V. Transporter-Guided Delivery of Nanoparticles to Improve Drug Permeation across Cellular Barriers and Drug Exposure to Selective Cell Types. *Front Pharmacol* **2018**, *9*, 27. https://doi.org/10.3389/fphar.2018.00027.
(127) Blanco, E.; Shen, H.; Ferrari, M. Principles of Nanoparticle Design for Overcoming Biological Barriers to Drug Delivery. *Nature Biotechnology* **2015**, *33* (9), 941–951. https://doi.org/10.1038/nbt.3330.
(128) Fifis, T.; Gamvrellis, A.; Crimeen-Irwin, B.; Pietersz, G. A.; Li, J.; Mottram, P. L.; McKenzie, I. F. C.; Plebanski, M. Size-Dependent Immunogenicity: Therapeutic and Protective Properties of Nano-Vaccines against Tumors. *The Journal of Immunology* **2004**, *173* (5), 3148–3154. https://doi.org/10.4049/jimmunol.173.5.3148.
(129) Rennick, J. J.; Johnston, A. P. R.; Parton, R. G. Key Principles and Methods for Studying the Endocytosis of Biological and Nanoparticle Therapeutics. *Nat. Nanotechnol.* **2021**, *16* (3), 266–276. https://doi.org/10.1038/s41565-021-00858-8.
(130) Hoshyar, N.; Gray, S.; Han, H.; Bao, G. The Effect of Nanoparticle Size on in Vivo Pharmacokinetics and Cellular Interaction. *Nanomedicine (Lond)* **2016**, *11* (6), 673–692. https://doi.org/10.2217/nnm.16.5.
(131) Ehrlich, M.; Boll, W.; Van Oijen, A.; Hariharan, R.; Chandran, K.; Nibert, M. L.; Kirchhausen, T. Endocytosis by Random Initiation and Stabilization of Clathrin-Coated Pits. *Cell* **2004**, *118* (5), 591–605. https://doi.org/10.1016/j.cell.2004.08.017.
(132) Boucrot, E.; Ferreira, A. P. A.; Almeida-Souza, L.; Debard, S.; Vallis, Y.; Howard, G.; Bertot, L.; Sauvonnet, N.; McMahon, H. T. Endophilin Marks and Controls a Clathrin-Independent Endocytic Pathway. *Nature* **2015**, *517* (7535), 460–465. https://doi.org/10.1038/nature14067.
(133) Sathe, M.; Muthukrishnan, G.; Rae, J.; Disanza, A.; Thattai, M.; Scita, G.; Parton, R. G.; Mayor, S. Small GTPases and BAR Domain Proteins Regulate Branched Actin Polymerisation for Clathrin and Dynamin-Independent Endocytosis. *Nature Communications* **2018**, *9* (1), 1835. https://doi.org/10.1038/s41467-018-03955-w.
(134) Kerr, M. C.; Teasdale, R. D. Defining Macropinocytosis. *Traffic* **2009**, *10* (4), 364–371. https://doi.org/10.1111/j.1600-0854.2009.00878.x.

(135) Lim, J. J.; Grinstein, S.; Roth, Z. Diversity and Versatility of Phagocytosis: Roles in Innate Immunity, Tissue Remodeling, and Homeostasis. *Front. Cell. Infect. Microbiol.* **2017**, *7*. https://doi.org/10.3389/fcimb.2017.00191.
(136) Palm, W. Metabolic Functions of Macropinocytosis. *Philos Trans R Soc Lond B Biol Sci* **2019**, *374* (1765), 20180285. https://doi.org/10.1098/rstb.2018.0285.
(137) Jovic, M.; Sharma, M.; Rahajeng, J.; Caplan, S. The Early Endosome: A Busy Sorting Station for Proteins at the Crossroads. *Histol Histopathol* **2010**, *25* (1), 99–112.
(138) Behzadi, S.; Serpooshan, V.; Tao, W.; Hamaly, M. A.; Alkawareek, M. Y.; Dreaden, E. C.; Brown, D.; Alkilany, A. M.; Farokhzad, O. C.; Mahmoudi, M. Cellular Uptake of Nanoparticles: Journey Inside the Cell. *Chem Soc Rev* **2017**, *46* (14), 4218–4244. https://doi.org/10.1039/c6cs00636a.
(139) Duchardt, F.; Fotin-Mleczek, M.; Schwarz, H.; Fischer, R.; Brock, R. A Comprehensive Model for the Cellular Uptake of Cationic Cell-Penetrating Peptides. *Traffic* **2007**, *8* (7), 848–866. https://doi.org/10.1111/j.1600-0854.2007.00572.x.
(140) Bus, T.; Traeger, A.; Schubert, U. S. The Great Escape: How Cationic Polyplexes Overcome the Endosomal Barrier. *J. Mater. Chem. B* **2018**, *6* (43), 6904–6918. https://doi.org/10.1039/C8TB00967H.
(141) Vermeulen, L. M. P.; De Smedt, S. C.; Remaut, K.; Braeckmans, K. The Proton Sponge Hypothesis: Fable or Fact? *European Journal of Pharmaceutics and Biopharmaceutics* **2018**, *129*, 184–190. https://doi.org/10.1016/j.ejpb.2018.05.034.
(142) Benjaminsen, R. V.; Mattebjerg, M. A.; Henriksen, J. R.; Moghimi, S. M.; Andresen, T. L. The Possible "Proton Sponge " Effect of Polyethylenimine (PEI) Does Not Include Change in Lysosomal PH. *Molecular Therapy* **2013**, *21* (1), 149–157. https://doi.org/10.1038/mt.2012.185.
(143) Murthy, N.; Robichaud, J. R.; Tirrell, D. A.; Stayton, P. S.; Hoffman, A. S. The Design and Synthesis of Polymers for Eukaryotic Membrane Disruption. *Journal of Controlled Release* **1999**, *61* (1), 137–143. https://doi.org/10.1016/S0168-3659(99)00114-5.
(144) Yessine, M.-A.; Lafleur, M.; Meier, C.; Petereit, H.-U.; Leroux, J.-C. Characterization of the Membrane-Destabilizing Properties of Different PH-Sensitive Methacrylic Acid Copolymers. *Biochimica et Biophysica Acta (BBA) - Biomembranes* **2003**, *1613* (1), 28–38. https://doi.org/10.1016/S0005-2736(03)00137-8.
(145) Peeler, D. J.; Thai, S. N.; Cheng, Y.; Horner, P. J.; Sellers, D. L.; Pun, S. H. PH-Sensitive Polymer Micelles Provide Selective and Potentiated Lytic Capacity to Venom Peptides for Effective Intracellular Delivery. *Biomaterials* **2019**, *192*, 235–244. https://doi.org/10.1016/j.biomaterials.2018.11.004.
(146) Sylvestre, M.; Lv, S.; Yang, L. F.; Luera, N.; Peeler, D. J.; Chen, B.-M.; Roffler, S. R.; Pun, S. H. Replacement of L-Amino Acid Peptides with D-Amino Acid Peptides Mitigates Anti-PEG Antibody Generation against Polymer-Peptide Conjugates in Mice. *Journal of Controlled Release* **2021**, *331*, 142–153. https://doi.org/10.1016/j.jconrel.2021.01.015.
(147) Rennick, J. J.; Johnston, A. P. R.; Parton, R. G. Key Principles and Methods for Studying the Endocytosis of Biological and Nanoparticle Therapeutics. *Nat. Nanotechnol.* **2021**, *16* (3), 266–276. https://doi.org/10.1038/s41565-021-00858-8.
(148) Wang, J. S.; Matyjaszewski, K. Controlled/"Living" Radical Polymerization. Atom Transfer Radical Polymerization in the Presence of Transition-Metal Complexes. *Journal of the American Chemical Society* **1995**, *117* (20), 5614–5615. https://doi.org/10.1021/ja00125a035.

(149) Fantin, M.; Isse, A. A.; Gennaro, A.; Matyjaszewski, K. Understanding the Fundamentals of Aqueous ATRP and Defining Conditions for Better Control. *Macromolecules* **2015**, *48* (19), 6862–6875. https://doi.org/10.1021/acs.macromol.5b01454.
(150) Fantin, M.; Isse, A. A.; Venzo, A.; Gennaro, A.; Matyjaszewski, K. Atom Transfer Radical Polymerization of Methacrylic Acid: A Won Challenge. *Journal of the American Chemical Society* **2016**, *138* (23), 7216–7219. https://doi.org/10.1021/jacs.6b01935.
(151) Boyer, C.; Corrigan, N. A.; Jung, K.; Nguyen, D.; Nguyen, T. K.; Adnan, N. N. M.; Oliver, S.; Shanmugam, S.; Yeow, J. Copper-Mediated Living Radical Polymerization (Atom Transfer Radical Polymerization and Copper(0) Mediated Polymerization): From Fundamentals to Bioapplications. *Chemical Reviews* **2016**, *116* (4), 1803–1949. https://doi.org/10.1021/acs.chemrev.5b00396.
(152) Pan, X.; Fantin, M.; Yuan, F.; Matyjaszewski, K. Externally Controlled Atom Transfer Radical Polymerization. *Chemical Society Reviews* **2018**. https://doi.org/10.1039/C8CS00259B.
(153) Dechy-cabaret, O.; Martin-vaca, B.; Bourissou, D.; Dechy-cabaret, O.; Martin-vaca, B.; Bourissou, D. Controlled Ring-Opening Polymerization of Lactide and Glycolide Controlled Ring-Opening Polymerization of Lactide and Glycolide. **2004**, *104* (October), 6147–6176. https://doi.org/10.1021/cr040002s.
(154) Hadjichristidis, N.; Iatrou, H.; Pitsikalis, M.; Sakellariou, G. Synthesis of Well-Defined Polypeptide-Based Materials via the Ring-Opening Polymerization of r -Amino Acid N -Carboxyanhydrides. *Chemical reviews* **2009**, *109*, 5528–5578. https://doi.org/10.1021/cr900049t.
(155) Makiguchi, K.; Satoh, T.; Kakuchi, T. Diphenyl Phosphate as an Efficient Cationic Organocatalyst for Controlled/Living Ring-Opening Polymerization of δ-Valerolactone and ε-Caprolactone. *Macromolecules* **2011**, *44* (7), 1999–2005. https://doi.org/10.1021/ma200043x.
(156) Kamber, N. E.; Jeong, W.; Waymouth, R. M.; Pratt, R. C.; Lohmeijer, B. G. G.; Hedrick, J. L. Organocatalytic Ring-Opening Polymerization. *Chemical Reviews* **2007**, *107* (12), 5813–5840. https://doi.org/10.1021/cr068415b.
(157) Kricheldorf, H. R. Polypeptides and 100 Years of Chemistry of α-Amino Acid N-Carboxyanhydrides. *Angewandte Chemie - International Edition* **2006**, *45* (35), 5752–5784. https://doi.org/10.1002/anie.200600693.
(158) Cheng, J.; Deming, T. J. Synthesis of Polypeptides by Ring-Opening Polymerization of α-Amino Acid N-Carboxyanhydrides BT - Peptide-Based Materials; Deming, T., Ed.; Springer Berlin Heidelberg: Berlin, Heidelberg, 2012; pp 1–26. https://doi.org/10.1007/128_2011_173.
(159) Kobayashi, S.; Kobayashi, S.; Uyama, H.; Uyama, H.; Kimura, S.; Kimura, S. Enzymatic Polymerization. *Chemical Reviews* **2001**, *101* (12), 3793–3818. https://doi.org/10.1021/cr990121l.
(160) Bielawski, C. W.; Grubbs, R. H. Living Ring-Opening Metathesis Polymerization. *Progress in Polymer Science (Oxford)* **2007**, *32* (1), 1–29. https://doi.org/10.1016/j.progpolymsci.2006.08.006.
(161) W., B. C.; H., G. R. Living Ring-Opening Metathesis Polymerization. In *Controlled and Living Polymerizations*; Wiley-Blackwell, 2010; pp 297–342. https://doi.org/10.1002/9783527629091.ch6.

(162) Verduzco, R.; Li, X.; Pesek, S. L.; Stein, G. E. Structure, Function, Self-Assembly, and Applications of Bottlebrush Copolymers. *Chem. Soc. Rev.* **2015**, *44* (8), 2405–2420. https://doi.org/10.1039/C4CS00329B.
(163) Chiefari, J.; Chong, Y. K. B.; Ercole, F.; Krstina, J.; Jeffery, J.; Le, T. P. T.; Mayadunne, R. T. A.; Meijs, G. F.; Moad, C. L.; Moad, G.; Rizzardo, E.; Thang, S. H. Living Free-Radical Polymerization by Reversible Addition - Fragmentation Chain Transfer : The RAFT Process We Wish to Report a New Living Free-Radical Polymer-Ization of Exceptional Effectiveness and Versatility . 1 The Living Character Is Conferred By. *Macromolecules* **1998**, *31* (16), 5559–5562. https://doi.org/S0024-9297(98)00495-1.
(164) Schneiderman, D. K.; Ting, J. M.; Purchel, A. A.; Miranda, R.; Tirrell, M. V.; Reineke, T. M.; Rowan, S. J. Open-to-Air RAFT Polymerization in Complex Solvents: From Whisky to Fermentation Broth. *ACS Macro Letters* **2018**, 406–411. https://doi.org/10.1021/acsmacrolett.8b00069.
(165) Niu, J.; Lunn, D. J.; Pusuluri, A.; Yoo, J. I.; O'Malley, M. A.; Mitragotri, S.; Soh, H. T.; Hawker, C. J. Engineering Live Cell Surfaces with Functional Polymers via Cytocompatible Controlled Radical Polymerization. *Nature Chemistry* **2017**, *9* (6), 537–545. https://doi.org/10.1038/nchem.2713.
(166) Perrier, S. 50th Anniversary Perspective: RAFT Polymerization - A User Guide. *Macromolecules* **2017**, *50* (19), 7433–7447. https://doi.org/10.1021/acs.macromol.7b00767.
(167) Boyer, C.; Bulmus, V.; Davis, T. P.; Ladmiral, V.; Liu, J.; Perrier, S. Bioapplications of RAFT Polymerization. *Chemical Reviews* **2009**, *109* (11), 5402–5436. https://doi.org/10.1021/cr9001403.

Chapter 2

Glomerular disease augments kidney accumulation of synthetic anionic polymers

Gary W. Liu*, **Alexander N. Prossnitz***, Diana G. Eng, Yilong Cheng, Nithya Subrahmanyam, Jeffrey W. Pippin, Robert J. Lamm, Chayanon Ngambenjawong, Hamidreza Ghandehari, Stuart J. Shankland, Suzie H. Pun

Abstract

Polymeric drug carriers can alter the pharmacokinetics of their drug cargoes, thereby improving drug therapeutic index and reducing side effects. Understanding and controlling polymer properties that drive tissue-specific accumulation is critical in engineering targeted drug delivery systems. For kidney disease applications, targeted drug delivery to renal cells that reside beyond the charge- and size-selective glomerular filtration barrier could have clinical potential. However, there are limited reports on polymer properties that might enhance kidney accumulation. Here, we studied the effects of molecular weight and charge on the *in vivo* kidney accumulation of polymers in health and disease. We synthesized a panel of well-defined polymers by atom transfer radical polymerization to answer several questions. First, the biodistribution of low molecular weight (23-27 kDa) polymers composed of various ratios of neutral:anionic monomers (1:0, 1:1, 1:4) in normal mice was determined. Then, highly anionic (1:4 monomer ratio) low molecular and high molecular weight (47 kDa) polymers were tested in both normal and experimental focal segmental glomerulosclerosis (FSGS) mice, a model that results in loss of glomerular filtration selectivity. Through these

Adapted with permission from Liu, G.W. **Prossnitz, A. N.** *et al.* Glomerular disease augments kidney accumulation of synthetic anionic polymers. *Biomaterials* 178, 317-325 (2018).

studies, we observed that kidney-specific polymer accumulation increases with anionic monomer content, but not molecular weight; experimental FSGS increases kidney accumulation of anionic polymers; and anionic polymers accumulate predominantly in proximal tubule cells, with some distribution in kidney glomeruli. These findings can be applied to the design of polymeric drug carriers to enhance or mitigate kidney accumulation.

2.1 Introduction

Polymeric carriers have been applied in drug delivery to improve circulation time, alter biodistribution, reduce metabolism, and facilitate cellular internalization of drug cargo [1-5]. The pharmacokinetics of polymeric carriers and their cargo depend on polymer properties including molecular weight, dispersity, charge, functionalization, and self-assembled size and shape [6-9]. Studies investigating polymer structure and resulting biodistribution have mainly focused on exploiting the enhanced permeability and retention effect for cancer applications [10-12]. However, polymeric carriers for kidney diseases remain relatively understudied despite the clinical potential of such technologies. For example, targeted drug delivery to glomerular podocytes could improve the standard of therapy for common glomerular diseases such as minimal change disease and focal segmental glomerulosclerosis (FSGS), and drug delivery to tubular epithelial cells may be strategic for acute kidney injury and polycystic kidney disease treatment [13,14]. The major challenge is that these cell populations reside beyond the multi-layered glomerular filtration barrier, which comprises the innermost endothelial cells, a middle glomerular basement membrane, and the outer podocytes.

Given that the glomerular filtration barrier is both size- and charge-selective, these two parameters are likely critical when designing drug carriers to target cells past the barrier.

Nanoparticle studies by the Davis group have revealed that gold nanoparticles of size ~75 nm target the kidney mesangium [15], and polycation- siRNA polymeric nanoparticles accumulate and disassemble in the anionic glomerular basement membrane [16]. However, the polymer physical properties required to cross this barrier for kidney targeting applications remain to be critically defined. Kamada et al. observed that hydrolyzed poly(vinylpyrrolidone-*co*-dimethyl maleic anhydride) copolymers of molecular weight approximately 10 kDa were anionic and distributed in kidneys up to 4 days after administration, with uptake primarily in proximal tubule cells [17]. Similarly, Borgman et al. reported that *N*-(2-hydroxypropyl)methacrylamide (HPMA) copolymers, functionalized with cyclo(RGDfK) targeting peptides and anionic penta-carboxylic acid residues, distributed preferentially in the kidneys compared to the designed target, tumors, and were retained up to 10 days after administration [18]. Recently, Bruni et al. reported on a panel of poly-ε-capro-lactone and poly(ethylene glycol) methyl ether methacrylate star co-polymers (10-27 kDa), which exhibited evidence of kidney clearance *in vivo* [19]. While these reports have revealed in broad strokes that polymers with anionic charge and molecular weight less than 50 kDa accumulate in the kidneys, a rigorous evaluation of the individual and combined effects of polymer molecular weight and charge has yet to be reported.

Advances in controlled radical polymerization techniques haveenabled polymer synthesis with precise control over molecular weight, dispersity, architecture, and chemical composition [20]. In this work, we used atom transfer radical polymerization (ATRP) to synthesize a panel of polymers to examine the effect of anionic charge density and molecular weight on kidney accumulation and distribution in mice. We first tested the effect of charge using a panel of low molecular weight (LMW) polymers, and then examined the effect of molecular weight in normal mice and mice with experimental FSGS, a model that results in

loss of filtration size-selectivity and proteinuria [21]. Here, we report that highly anionic, LMW polymers preferentially accumulate in the kidneys and are internalized into proximal tubule cells. Conditions of experimental FSGS enhance accumulation of anionic LMW polymers.

2.2 Results

2.2.1 Polymer panel synthesis and characterization

We synthesized a panel of copolymers with varying ratios of anionic and neutral monomers by ATRP, with different degrees of polymerization (Table 1). Importantly, this approach yields well-defined polymers with tailored anion densities and molecular weights while keeping other properties constant. The hydrophilic, small molecular weight (~300 Da) monomer oligo(ethylene glycol) methyl ether methacrylate (OEGMA) was selected, as OEGMA-based polymers have been shown to exhibit favorable circulation times, low protein-binding properties, and reduced immunogenicity due to shorter ethylene glycol repeats [22-25]. The second monomer, *tert*-butyl methacrylate (tBuMA), yields methacrylic acids (MAA, anionic in charge) after deprotection. The monomer tBuMA was selected as an alternative to direct MAA polymerization, as MAA is insoluble in many organic solvents. Organic ATRP presents several advantages over aqueous ATRP, and results in polymerizations with less synthetic complexity and higher quality materials.

By varying the ratio of the two monomers and the polymeri-

zation time, p(OEGMA-*co*-MAA) copolymers with defined OEGMA:MAA ratios and molecular weights were synthesized (Table 1 and Fig. 1). Polymers with fixed molecular weight but varying anionic MAA content (0%, 50%, and 80%) were prepared to test the effect

of charge on biodistribution. Two target molecular weight ranges were synthesized: low molecular weight (LMW) polymers of 20e25 kDa, and high molecular weight (HMW) polymers of 45e50 kDa. These two molecular weight regimes, which are either below or approximately at the renal filtration cutoff of ~50 kDa [26], respectively, were utilized to investigate the effect polymer molecular weight on kidney distribution. For biodistribution and tissue distribution analyses, polymers were fluorescently labeled with Cy3 fluorophore via a stable thioether bond by reduction of the disulfide bond of the pyridyl disulfide-terminated ATRP initiator and subsequent reaction with Cy3-maleimide (Fig. 1).

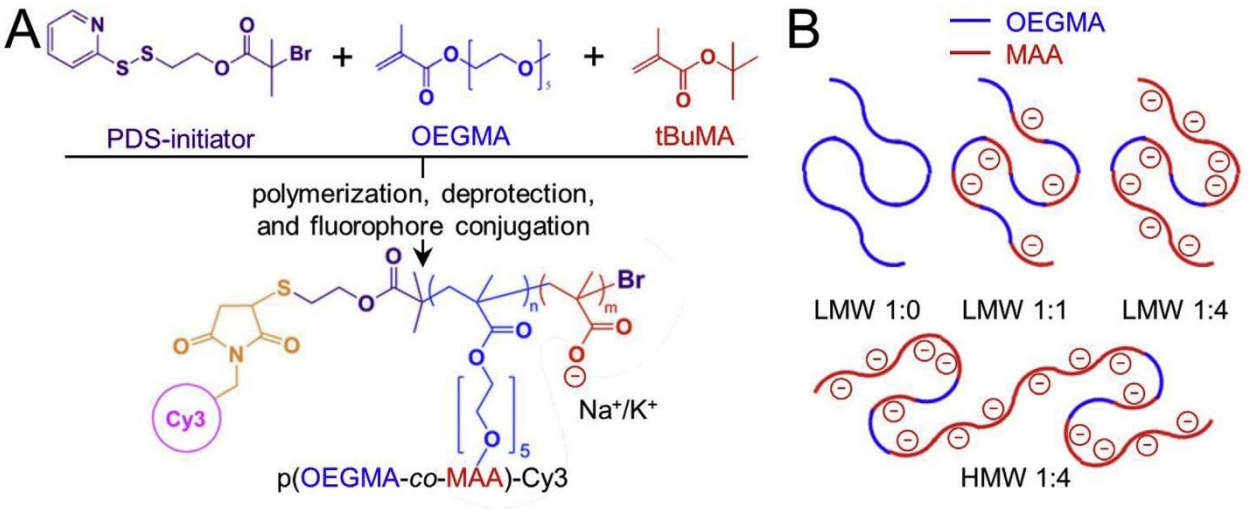

Figure 2.1 Schematics of polymer synthesis and composition. A. Concise synthesis scheme of polymers. Polymerization was performed with a pyridyl disulfide (PDS)-terminated ATRP initiator and OEGMA and tBuMA monomers. Deprotection and fluorophore conjugation of polymers yield p(OEGMA-co-MAA)-Cy3. B. Cartoon schematic of the tested polymers. Polymers were named based on molecular weight and monomer composition. LMW, low molecular weight; HMW, high molecular weight; 1:0, polymer comprising 100% OEGMA monomer; 1:1, polymer comprising 50%/50% of OEGMA and MAA, respectively; 1:4, polymer comprising 20%/80% of OEGMA and MAA, respectively. Blue lines represent OEGMA monomer, and red lines represent MAA monomer.

LMW polymers ranged in number average molecular weight (M_n) from 23 to 27 kDa, and HMW polymers had M_n of 47 kDa, as determined by gel permeation chromatography (GPC). All polymers exhibited dispersity ($Đ$) < 1.5. Within a molecular weight regime, the MAA

monomer fraction during polymerization was varied at 0%, 50%, and 80%, resulting in polymer OEGMA:MAA ratios of 1:0 (homopolymer pOEGMA), 1:1, and 1:4, respectively. Monomer ratios within the copolymers, as determined by ^{1}H nuclear magnetic resonance spectroscopy (NMR), were in good agreement with the feed ratios and suggest similar reactivity of the two co-monomers under the polymerization conditions used (Table 1 and Fig. S1).

2.2.2 Biodistribution of LMW polymers in normal mice

The effect of polymer charge on kidney accumulation was first determined by evaluating the biodistribution of LMW 1:0, 1:1, and 1:4 copolymers 7 days post intravenous injection. This time point is significantly past the circulation half-life of similarly sized polymers (generally $t_{1/2}$ < 24 h) [27,28] and was intentionally selected to measure organ accumulation. Fluorescence intensities of the three polymers prior to injection were comparable (Fig. S2). Polymer distribution to major organs (heart, lungs, liver, spleen, kidneys) was determined by whole organ fluorescence imaging after perfusion.

Table 2.1 Summary of p(OEGMA-co-MAA) copolymers. Number average molecular weight (M_n) and dispersity (Đ) values were determined by gel permeation chromatography. Polymer compositions were determined by ^{1}H

Polymer	Composition	OEGMA:tBuMA feed ratios	OEGMA:tBuMA measured ratios	M_n (Da)	Đ
LMW 1:0	p(OEGMA$_{76}$)-PDS	100:0	N/A	23,000	1.125
LMW 1:1	p(OEGMA$_{70}$-co-MAA$_{70}$)-PDS	50:50	1:1.1	27,000	1.140
LMW 1:4	p(OEGMA$_{39}$-co-MAA$_{157}$)-PDS	20:80	1:3.5	25,000	1.370
HMW 1:4	p(OEGMA$_{74}$-co-MAA$_{296}$)-PDS	20:80	1:5.4	47,000	1.400

The LMW polymers exhibited a statistically significant increasing linear trend (p-value < 0.0001) in both kidney and liver fluorescence trending with MAA content (anionic charge), with LMW 1:4 > 1:1 > 1:0 (Fig. 2A and B). Preferential kidney accumulation was quantified by normalizing the fluorescent signal in the kidneys by that in the liver. LMW 1:4 exhibited

the greatest kidney/ liver fluorescence ratio compared to other treatments (Fig. 2C). The distribution of labeled polymers in the kidney was determined by confocal microscopy. Fluorescence was primarily detected in the kidney cortex, intracellularly in proximal tubule cells as identified by morphology and proximity to glomeruli structures (Fig. 3). LMW 1:4 copolymers exhibited the most fluorescent staining as well as deposition in kidney glomeruli. In further confirmation of the role of anionic charge on kidney accumulation, *N*-(2-hydroxypropyl) methacrylamide (HPMA) copolymers modified with anionic diethylenetriaminepentaacetic acid chelator (DTPA) exhibited greater kidney/liver fluorescence compared to HPMA control polymers (Fig. S3).

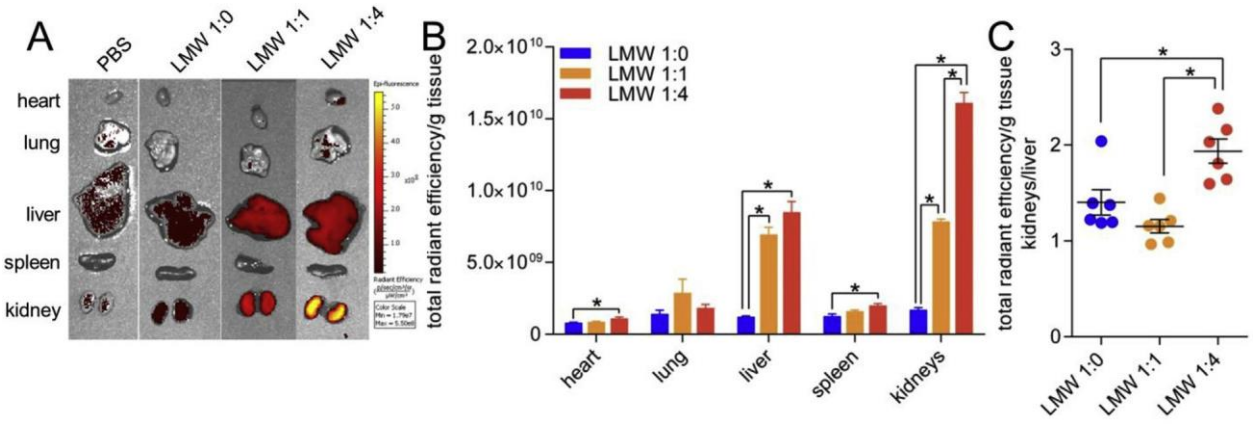

Figure 2.2 Organ distribution of low molecular weight (23 - 27 kDa) polymers in normal mice. A. Representative fluorescent images of major organs 7 days after intravenous administration of PBS or fluorescent polymers. B. Region of interest quantification of tissue fluorescence normalized by tissue weight. All treatments were n = 6. C. Kidney/liver normalized fluorescent signal ratio. Statistical analysis was performed using a one-way ANOVA with post-hoc Tukey's multiple comparisons test, and a post-hoc linear trend test. Bars represent means ± SEM. *p-value < 0.05.

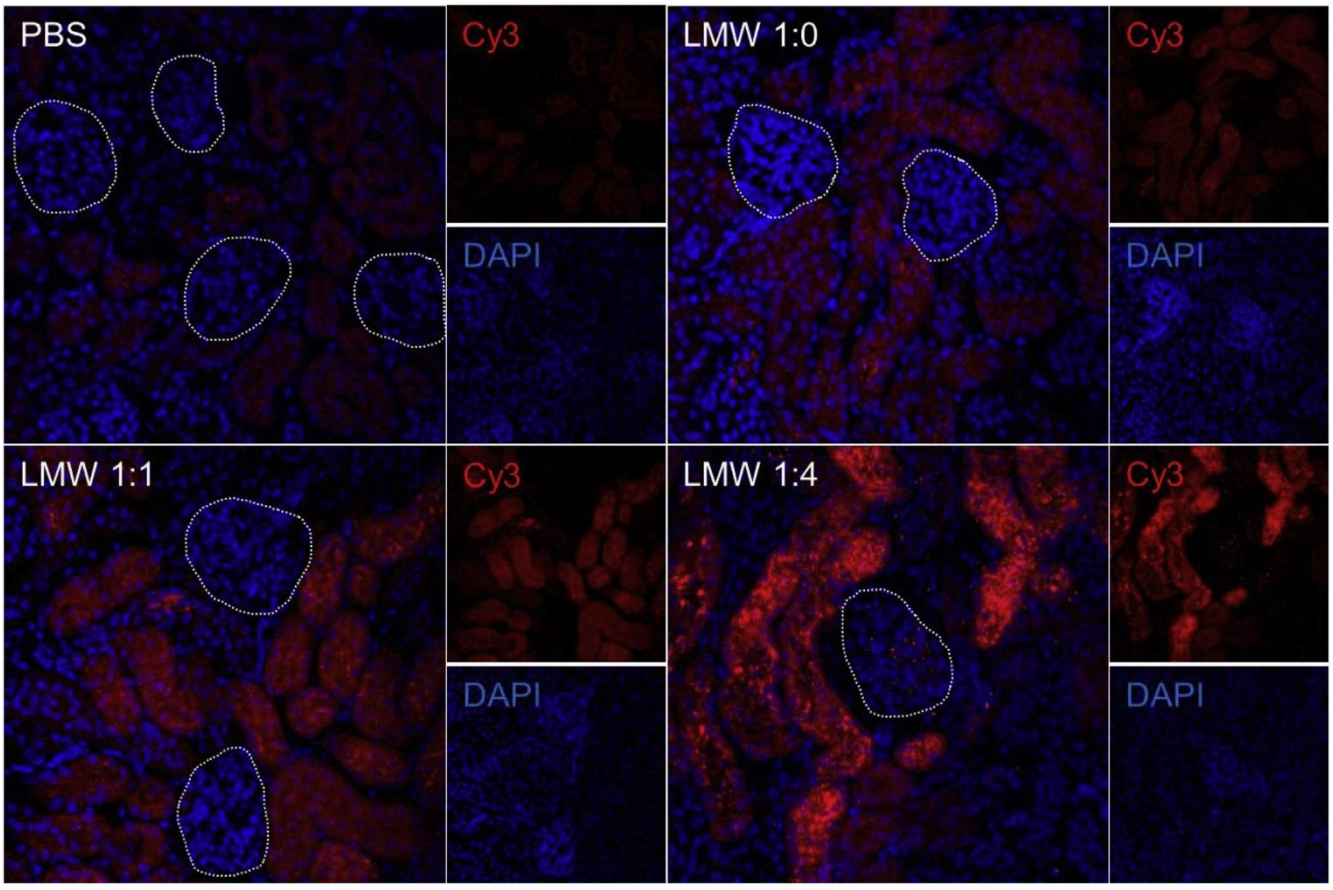

Figure 2.3 Kidney distribution of low molecular weight (23e27 kDa) polymers in normal mice. Representative fluorescent images of kidneys 7 days after intravenous administration of PBS or fluorescent polymers obtained by confocal microscopy. Kidney glomeruli are denoted by dashed white lines. Blue, DAPI; red, Cy3-labeled polymers. Individual DAPI and Cy3 channels are shown to the right of their respective images.

2.2.3 Biodistribution of HMW and LMW polymers in normal and experimental FSGS mice

We hypothesized that glomerular kidney disease may alter the polymer accumulation in this organ due to loss of filtration selectivity. As highly anionic LMW 1:4 (80% MAA content) copolymers exhibited the most fluorescence in the kidneys, HMW 1:4 (M_n = 47 kDa) and LMW 1:4 (M_n = 25 kDa) copolymers were tested to determine the effect of molecular weight on biodistribution in normal mice and mice with experimental FSGS. To induce FSGS, a cytotoxic anti-podocyte antibody that causes podocyte loss was administered to mice

[21]. Damage to glomeruli and disruption of the glomerular filtration barrier was confirmed histologically (Fig. S4) and by proteinuria, which peaked on day 7 (Fig. 4A) and persisted up to day 14. Polymers were injected on day 7 at peak proteinuria, and polymer distribution assessed 7 days post-polymer administration (Fig. 4A).

In normal animals, LMW 1:4 copolymers exhibited greater fluorescence in the kidneys than HMW 1:4 copolymers (Fig. 4B and C). Experimental FSGS increased kidney and liver fluorescence of LMW 1:4 copolymers, but not HMW 1:4 copolymers (Fig. 4C). Generally, LMW 1:4 copolymers exhibited greater kidney/liver fluorescence ratios compared to HMW 1:4 polymers in normal and experimental FSGS conditions (Fig. 4D). Kidney tissue distribution patterns were similar to the initial LMW polymer panel, with no remarkable differences noted in mice with experimental FSGS (data not shown).

2.2.4 In vitro characterization of polymers in proximal tubule cells

The LMW 1:4 polymer was then characterized for internalization, cytotoxicity, and uptake mechanism using an immortalized human proximal tubule cell line, HK-2, which exhibits key features of primary proximal tubule cells [29]. By confocal microscopy, polymer-treated cells exhibited punctate polymer fluorescence within the cell body (Fig. 5A). Treatment of HK-2 cells with 1 mM polymer for up to 7 days did not cause significant differences in viability compared to untreated cells, as determined by MTS/PMS assay (Fig. 5B). To investigate the mechanism of polymer internalization, polymer uptake was measured after incubation in either 37 ^{o} C or 4 ^{o} C using flow cytometry, as reduced temperature is known to effectively inhibit active endocytosis [17,30]. Incubation of cells on ice (4 ^{o} C) significantly reduced polymer fluorescence (*p*- value < 0.0001) compared to cells maintained at 37 ^{o} C (Fig. 5C).

Moreover, in a competition uptake experiment with anionic dextran sulfate (500 kDa), incubation of polymer in an excess of dextran sulfate significantly reduced polymer fluorescence intensity to ~46% compared to control (p-value < 0.0001, Fig. 5D).

2.3 Discussion

In engineering intravenous polymeric drug carriers for targeted drug delivery applications, careful consideration of polymer properties must be taken to understand and control "passive targeting" effects, inadvertent or intentional [20]. Ideally, materials are designed with properties that enhance accumulation at target tissue, and avoid characteristics that enhance accumulation in off-target tissues. This is especially true when considering the kidneys, which filter up to 180 liters of blood per day, and are a major clearance organ with intimate contact with the circulatory system. However, polymer design guidelines to either enhance or avoid kidney targeting have been limited.

Here, we systematically interrogated the effect of polymer anionic charge density and molecular weight, as well as glomerular filtration barrier integrity, on polymer accumulation in the kidneys. Polymers were synthesized by living radical polymerization to control composition and molecular weight. By using a pyridyl disulfide-terminated initiator, polymer chains were fluorescently labeled with a single Cy3-maleimide resulting in ~1:1 dye:polymer ratio, enabling direct comparison of fluorescent signals for the polymers tested. Thioether linkages have been reported in a variety of *in vivo* applications, including cellular nanoparticle "backpack" conjugation [31] and antibody-drug conjugates [32]. Whole-organ fluorescence imaging was selected due to ease of fluorophore conjugation and throughput. While this

method presents limitations to accurate quantification due to tissue light-scattering [33,34], it still provides a semi-quantitative means of evaluating biodistribution.

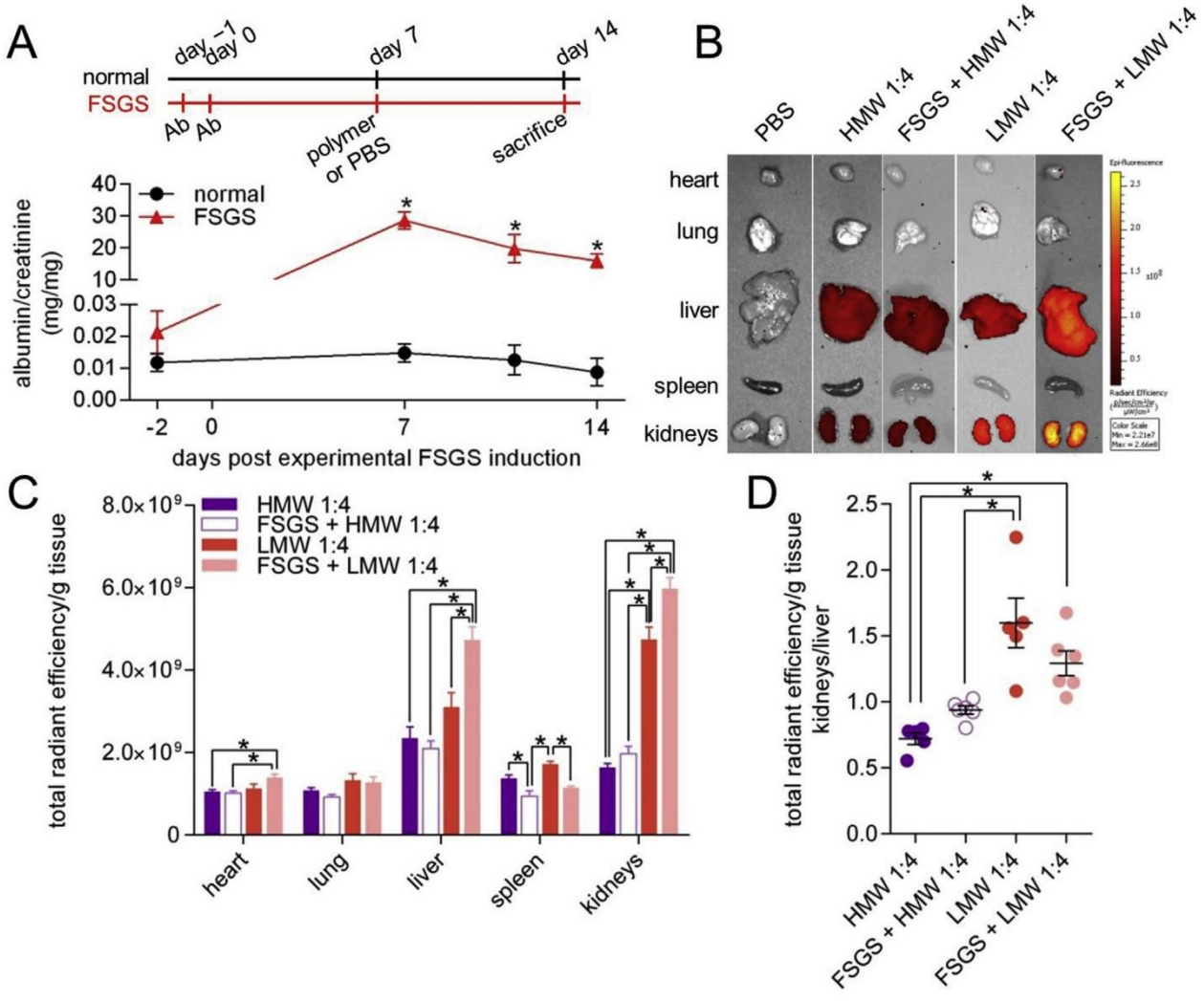

Figure 2.4 Organ distribution of polymers in normal and experimental FSGS mice. A. Top: treatment schedule of normal and experimental FSGS mice. FSGS mice were administered a cytotoxic anti-podocyte antibody on days 1 and 0. Both normal and FSGS mice were administered PBS or fluorescent polymers on day 7 and sacrificed on day 14 for analysis. Bottom: urine albumin/creatinine ratios of animals administered the cytotoxic anti-podocyte antibody (red, FSGS, n = 5) or not (black, normal, n = 4). All mice were administered PBS on day 7. Statistical analysis was performed using a two-tailed Student's t-test compared to normal animals. B. Representative fluorescent images of major organs analyzed on day 14. C. Region of interest quantification of tissue fluorescence normalized by tissue weight. All antibody treatments were n = 6; otherwise n = 5. D. Kidney/liver normalized fluorescent signal ratio. Statistical analysis was performed using a one-way ANOVA with post-hoc Tukey's multiple comparisons test. Bars represent means ± SEM. *p-value < 0.05.

In an initial panel, polymers with fixed molecular weights (23-27 kDa), but varying anionic charge, were examined in normal mice. Cationic polymers were not tested due to the toxicity of these materials [35]. The molecular weights were well below the renal filtration cutoff of 50 kDa, allowing passage of these polymers through the glomerular filtration barrier via filtration. A polymer with M_n 25 kDa and high (80%) anionic monomer content localized the most in the kidneys, and was internalized specifically in proximal tubule cells. This was a surprising result, as both the glomerular endothelial cells and the glomerular basement membrane of the filtration barrier are highly negatively charged due to glycocalyx and anionic heparan sulfate proteoglycans, respectively, and presumably repel the polymers [36]. Other uptake mechanisms, such as secretion and reabsorption, may also result in polymer uptake. Moreover, HPMA polymers containing anionic DTPA also exhibited kidney-specific accumulation, indicating that the observed biodistribution is not unique to MAA monomer and likely generalizable to other anionic monomers.

We utilized a cytotoxic anti-podocyte antibody to induce experimental FSGS. This antibody method is well-reported and specifically causes apoptosis of glomerular podocytes [21,37-47], leading to albuminuria, a clinical signature of a dysfunctional glomerular filtration barrier and loss of size-selective filtration [48]. This model was used to test the effects of polymer molecular weight with fixed anionic charge density (80%). Experimental FSGS increased the kidney fluorescence of LMW 1:4 polymer (25 kDa) but not HMW 1:4 polymer (47 kDa), providing some evidence that LMW 1:4 polymer kidney distribution is driven partly by filtration while HMW 1:4 is not. Moreover, these findings suggest that there is an optimal molecular weight for kidney delivery applications.

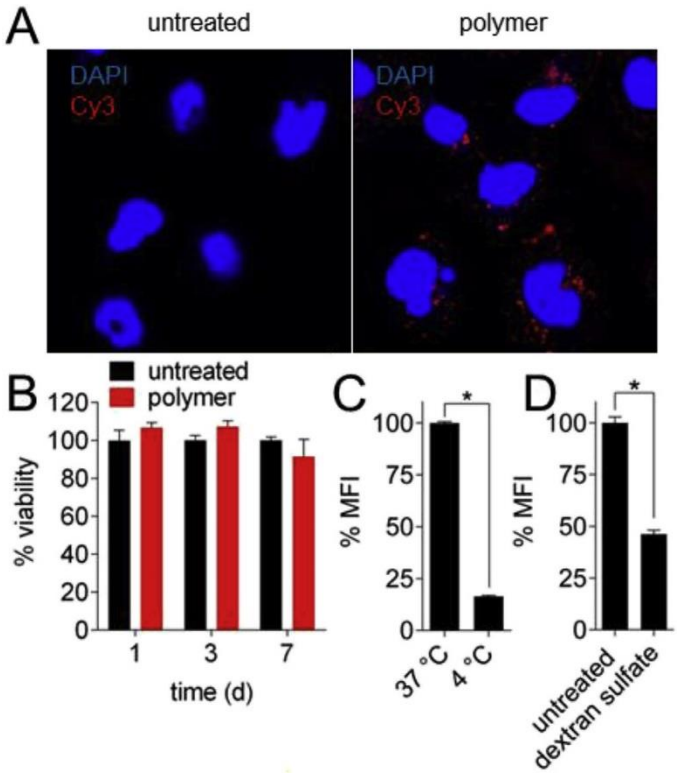

Figure 2.5 *In vitro* LMW 1:4 polymer characterization. A. Representative fluorescent images of HK-2 cells after incubation with fluorescent polymer. Cells were incubated with polymers for 2 h prior to imaging. Blue, DAPI; red, Cy3-labeled polymers. B. HK- 2 cell viability after polymer treatment at various days (n = 5). C. Polymer uptake, measured by mean fluorescence intensity (MFI), after 1 h incubation with polymer at 37 or 4 ºC (n = 4). D. Polymer uptake, measured by mean fluorescence intensity (MFI), after 1 h incubation with polymer in media or in the presence of dextran sulfate (n = 3). Bars represent means ± SEM. Statistical analysis was performed using a two- tailed Student's t-test. *p-value < 0.05.

Our observation that experimental FSGS enhanced LMW 1:4 polymer distribution suggests that disease conditions resulting in loss of filtration size-selectivity may be exploited to enhance material targeting to the kidneys, similar to the enhanced permeability and retention effect observed in animal models of tumors [20].

These two size regimes, low-molecular weight (~25 kDa) and high-molecular weight (~50 kDa), were selected to test the kidney distribution behavior of polymers below and near the

filtration cutoff for linear polymers (~50 kDa). Many reports have shown that circulation half-life increases significantly for linear polymers of size ~50 kDa compared to those of size 20 kDa [49,50], indicating that the filtration cutoff is near 50 kDa. Our study corroborates these findings. Given that the polymer backbones studied here are non-degradable and the clinical importance of eliminating nondegradable materials [51], we therefore studied these molecular weights as an intrinsic control point for elimination rate.

The immortalized human proximal tubule cell line, HK-2, was used to study polymer features *in vitro*, as these cells exhibit similar phenotype, function, and toxicity responses compared to primary cells [29]. LMW 1:4 polymers were internalized into punctate structures as early as 2 h after polymer treatment, and polymer treatment (1 mM) did not inflict significant toxicity, even at extended exposure times (7 d). Notably, this concentration and timescale is significantly higher and longer than what would be encountered *in vivo*, as the injected polymer concentration (40 mM) should be rapidly diluted and cleared after intravenous injection and tissue distribution. In subsequent experiments, polymer internalization was found to be significantly reduced at 4 ^{o} C and in the presence of excess anionic dextran sulfate, a known competitor of scavenger receptors, indicating that uptake is driven primarily by active endocytosis and/or non-specific scavenger receptors [17,52]. Proximal tubule reabsorption of macromolecules such as albumin and IgG is well-reported, with multi-ligand scavenger receptors megalin and cubilin responsible for uptake [53,54]. Indeed, various studies have shown that knockdown of megalin and/or cubilin results in reduced kidney uptake of synthetic peptides [55], albumin [56], and nanoparticles [57]. These receptors may mediate uptake of the polymers in the kidneys. Polymer uptake correlating with increasing anionic charge was also observed for the liver, albeit to a lesser

degree compared to the kidneys. Liver endothelial and Kupffer cells express scavenger receptors SR-AI and SR-AII that broadly recognize polyanionic ligands [58-60]. These non-specific scavenger receptors may mediate liver uptake of the polymers studied in this work.

While the polymers studied here did not exhibit significant podocyte uptake in the context of glomerular disease, these findings may still be useful for glomerular disease applications. As these polymers seem to be filtered, functionalization of these polymers with ligands that recognize podocyte receptors may enable cellular binding and internalization as these polymers travel through the glomerular filtration barrier. Moreover, targeted drug delivery to proximal tubule cells during glomerular disease may improve renal health. Proteinuria causes tubular cell atrophy and fibrosis due to protein overload, which contributes to worsening chronic kidney disease [61]. Therefore, delivery of pro-survival molecules may be a strategic method of halting tubular necrosis.

2.4 Conclusions

By examining a panel of synthetic polymers, we have determined that polymers with molecular weight ~25 kDa and high anionic monomer content are taken up in kidney proximal tubule cells up to 1 week after injection, with enhanced accumulation observed in conditions of loss of glomerular filtration barrier integrity. These guidelines may inform the development of improved polymeric materials for a variety of applications. For chemotherapeutics such as cisplatin that inflict serious renal toxicity [62], polymeric drug carriers should potentially avoid high anionic monomer content to mitigate uptake into proximal tubule cells. In kidney diseases such as polycystic kidney disease where tubule cells

are principally afflicted [63], anionic polymeric drug carriers may be considered to improve the therapeutic profile of drugs.

2.5 Concise methods

2.5.1 Materials

Poly(ethylene glycol) methyl ether methacrylate monomer (average molecular weight = 300 Da, OEGMA), *N*,*N*'-dicyclohexylcarbodiimide (DCC), 2,2-bipyridyl (BPY), 2-mercaptoethanol, copper (I) bromide, 4-dimethylaminopyridine (DMAP), and *N*,*N*,*N*',*N*'',*N*''-pentamethyldiethylenetriamine (PMDETA) were purchased from Sigma-Aldrich. 2,2-dipyridyl disulfide and *tert*-butylmethacrylate monomer (tBuMA) were purchased from TCI America. a-bromoisobutyric acid was purchased from Fluka. OEGMA and tBuMA were passed through a basic alumina column to remove inhibitors before polymerization. Cy3-maleimide was purchased from Lumiprobe.

2.5.2 Polymer synthesis and characterization

A pyridyl disulfide-terminated ATRP initiator was synthesized as previously described [64]. The initiator was purified by column chromatography, and purity was confirmed by ^{1}H NMR. In a typical polymerization, the ATRP initiator, ligand (PMDETA or BPY), and monomers (OEGMA and tBuMA) were dissolved in solvent and added to a round-bottom flask. The solution was purged with Ar gas for 10 min. After, solid CuBr was rapidly added, and the solution was purged again. The following reaction conditions were carried out for each polymer (mole ratios): (*i*) LMW 1:4 and HMW 1:4, initiator:PMDETA:OEGMA:tBuMA:Cu(I) ¼ 1:1:40:160:1, [monomer] = 3 M, in anisole, 60 ^{o}C for 4 or 8 h, respectively; (*ii*) LMW 1:1, initiator:PMDETA:OEGMA:tBuMA:Cu(I) = 1:1:400:400:1, [monomer] = 2 M, in methyl ethyl ketone, room temperature for 2 h; (*iii*) LMW 1:0, initiator:BPY:OEGMA:tBuMA:Cu(I) = 1:1.2:667:0:1, [monomer] = 2 M, in ethanol, 50 ^{o}C for 6 h. HMW and LMW 1:4 polymers were precipitated into cold hexanes; LMW 1:1 and LMW PEG polymers were precipitated in cold ether. Polymers were collected by centrifugation and vacuum-dried for at least 24 h, and characterized for molecular weight and dispersity (*Đ*) via gel permeation chromatography (GPC) as previously described [65]. Purity and monomer ratios in the statistical copolymers were assessed with ^{1}H NMR. The integrated signals of the terminal methyl groups of the OEGMA (3 protons) and the *tert*-butyl groups of the tBuMA (9 protons) were compared.

For the synthesis of the HPMA copolymers, the co-monomers *N*- (2-hydroxypropyl) methacrylamide (HPMA) [66], *N*-meth- acryloylaminopropyl-2-amino-3-(isothiourea-phenyl)propyl-cyclohexane-1,2-diamine-*N*-*N*,*N',N'',N''*-pentaacetic acid (APMA-CHX-A^{00}-DTPA)[67], and 5-[3-(methacryloylaminopropyl) thioureidyl] rhodamine (APMA-rhodamine) were synthesized using established methods. APMA-rhodamine was adapted from the synthesis of APMA-FITC [68], substituting rhodamine-isothiocyanate instead of fluorescein-isothiocyanate. Copolymerization was performed using free radical copolymerization, using azobisisobutyronitrile (AIBN) as an initiator. The reaction was carried out in a nitrogen-purged sealed glass ampule for 24 h and 50 ^{o}C. For the control copolymer, the following feed ratio in mole percent was used: HPMA:APMA-CHX-A$''$-DTPA:APMA-rhodamine (98:0:2). For the DTPA-containing (anionic) copolymer the following ratio was used: HPMA:APMA-CHX-A$''$-DTPA:APMA-rhodamine (88:10:2). Initiator concentration was 5 mg of initiator per 100 mg total monomers in both syntheses, in 500 mL of MeOH. Copolymers were purified through dialysis against dH_2O and lyophilized. Copolymers were characterized for molecular weight and dispersity using size exclusion chromatography. Co-monomer content was measured using UV-Vis spectroscopy. For the control copolymer, rhodamine fluorescent label content was determined to be 0.156 mmol/g. For the anionic copolymer, rhodamine content was determined to be 0.863 mmol/g and DTPA monomer content was found to be 0.598 mmol/g.

2.5.3 Polymer deprotection and fluorescent labeling

Polymers containing tBuMA were deprotected in trifluoroacetic acid, to remove the *tert*-butyl groups and reveal carboxylic acids, for 2 h with stirring. After, polymers were

precipitated in cold ether, collected by centrifugation, and vacuum-dried overnight. Polymers were then dissolved in molecular-grade H_2O pH 8, dialyzed against dH_2O for 24 h, and lyophilized. The deprotected polymers were prepared for dye conjugation by reducing the disulfide bond present in the initiator. Polymers were dissolved in PBS-EDTA, purged with Ar for 10 min, and a 1000-fold molar-excess of dithiothretriol (DTT) was added. The reaction was left overnight. Polymers were desalted using a PD-10 desalting column (GE), dissolved in a 2:1 PBS-EDTA:DMSO solution, purged, and a 5 molar-excess of Cy3-maleimide dye (Lumiprobe) dissolved in *N*,*N*-dimethylformamide was added. After 24 h, labeled polymers were dialyzed against dH_2O for 1.5 wk.

2.5.4 Polymer biodistribution studies

All animal experiments were executed in compliance with the University of Washington IACUC guidelines. For the initial LMW polymer biodistribution study, polymers (4 nmol) dissolved in PBS were injected in 7-week old mice via retro-orbital route. After 7 d, animals ¼ were sacrificed, perfused with PBS, and major organs (heart, lungs, liver, spleen, and kidneys) were harvested. Organ fluorescence was quantified by a Xenogen IVIS using ex/em 535/ 580 nm. Regions of interest were drawn across each organ for quantification, and total radiant efficiencies were normalized by organ weight. Statistical analyses were performed using GraphPad Prism and R software. Experimental FSGS was induced in 9-week old male BALB/c mice (Jackson Laboratory) via two intraperitoneal injections (10 mg/20 g mouse) of a cytotoxic anti-podocyte antibody 24 h apart. HMW and LMW polymers (4 nmol) were injected as above on day 7 after disease induction, and animals were sacrificed for organ fluorescence quantification on day 14 as described above.

2.5.5 Tissue processing and imaging

Kidney tissues were fixed in 4% PFA, washed with PBS, and incubated overnight with 30% sucrose/PBS at 4 °C. Tissues were then embedded in OCT and frozen in an ethanol/dry ice bath. After cryosectioning, tissues were stained with DAPI and mounted with Fluoromount-G (SouthernBiotech). Confocal images were taken as previously reported [37]. Images were captured using a Leica TCS SPE II laser scanning confocal microscope (Solms, Germany) with a HCX PL APO 40 /1.30 oil objective, at 1024 1024 pixel format with 8-bit intensity resolution. Sets of 8 serial images werecollected at 2-mm step size. The acquisition wavelengths were: DAPI excitation 405 nm, emission 380-468 nm; Cy3 excitation 561 nm, emission 576-644 nm. Masson's trichrome and silver staining were performed using standard methods. Images were collected at 600 x magnification.

2.5.6 Urine albumin and creatinine quantification

Spot urines were collected on various days before and throughout experimental FSGS induction. Urine albumin content was quantified by radial immunodiffusion as previously described [69], and creatinine quantified using a creatinine assay kit (Cayman Chemical).

2.5.7 HK-2 cell culture and polymer characterization

The human proximal tubule cell line HK-2 was cultured in K-SFM (ThermoFisher Scientific) and maintained as described by ATCC. For confocal imaging of polymer uptake, HK-2 cells were seeded on bovine collagen I (Corning)-coated glass coverslips in a 24-well plate at 4 10^4 cells/well. After overnight incubation, media was replaced with fresh media or polymer

dissolved in media to 1 mM for 2 h. After, cells were washed three times with PBS, and then fixed and stained with DAPI using standard methods. Confocal images were collected as described above.

For viability studies, HK-2 cells were plated in a 96-well plate at 5 x 10^3 cells/well. After overnight incubation, media was replaced

with fresh media or polymer dissolved in media to 1 mM. After 1, 3, or 7 d treatment, cells were washed with PBS, and viability was assayed by MTS/PMS (Promega) according to manufacturer instructions.

HK-2 cells were plated in a 24-well plate at 3 - 4 x 10^4 cells/well for uptake characterization studies and tested after overnight incubation. To test the effects of temperature on uptake, media was replaced with polymer dissolved in media to 1 mM, and cells were incubated for 1 h at 37 ^{o}C or on ice (4 ^{o}C). Cells were then washed 3 x with PBS, lifted with trypsin, resuspended in 1% BSA/PBS, and analyzed by flow cytometry. For competition studies, cells were first incubated with 1 mg/mL dextran sulfate (Sigma-Aldrich) in media for 30 min, and then incubated with 1 mM polymer in the presence of 1 mg/mL dextran sulfate for 2 h. Cells were then processed for flow cytometry as described above. Flow cytometry was performed using an Attune NxT Flow Cytometer (ThermoFisher Scientific). At least 1 x 10^4 cells were analyzed by FlowJo software, using mean fluorescence intensity as a measure of polymer uptake.

2.6 References

[1] R. Duncan, The dawning era of polymer therapeutics, Nat. Rev. Drug Discov. 2 (2003) 347-360.

[2] N. Larson, H. Ghandehari, Polymeric conjugates for drug delivery, Chem. Mater. 24 (2012) 840-853.

[3] R. Tong, J. Cheng, Anticancer polymeric nanomedicines, Polym. Rev. 47 (2007) 345-381.
[4] D.W. Pack, A.S. Hoffman, S. Pun, P.S. Stayton, Design and development of polymers for gene delivery, Nat. Rev. Drug Discov. 4 (2005) 581-593.
[5] M.E. Davis, Z.G. Chen, D.M. Shin, Nanoparticle therapeutics: an emerging treatment modality for cancer, Nat. Rev. Drug Discov. 7 (2008) 771-782.
[6] F.M. Veronese, et al., PEG-doxorubicin conjugates: influence of polymer structure on drug release, in vitro cytotoxicity, biodistribution, and antitumor activity, Bioconjugate Chem. 16 (2005) 775-784.
[7] F. Alexis, E. Pridgen, L.K. Molnar, O.C. Farokhzad, Factors affecting the clearance and biodistribution of polymeric nanoparticles, Mol. Pharm. 5 (2008) 505-515.
[8] C. He, Y. Hu, L. Yin, C. Tang, C. Yin, Effects of particle size and surface charge on cellular uptake and biodistribution of polymeric nanoparticles, Biomaterials 31 (2010) 3657-3666.
[9] M. Imran ul-haq, B.F. Lai, R. Chapanian, J.N. Kizhakkedathu, Influence of architecture of high molecular weight linear and branched polyglycerols on their biocompatibility and biodistribution, Biomaterials 33 (2012) 9135-9147.
[10] M. Thanou, R. Duncan, Polymer-protein and polymer-drug conjugates in cancer therapy, Curr. Opin. Invest. Drugs 4 (2003) 701-709.
[11] Y. Matsumura, H. Maeda, A new concept for macromolecular therapeutics in cancer chemotherapy: mechanism of tumoritropic accumulation of proteins and the antitumor agent smancs, Canc. Res. 46 (1986) 6387-6392.
[12] M.E. Fox, F.C. Szoka, J.M. Frechet, Soluble polymer carriers for the treatment of cancer: the importance of molecular architecture, Acc. Chem. Res. 42 (2009) 1141-1151.
[13] R.M. Williams, E.A. Jaimes, D.A. Heller, Nanomedicines for kidney diseases, Kidney Int. 90 (2016) 740-745.
[14] N. Kamaly, J.C. He, D.A. Ausiello, O.C. Farokhzad, Nanomedicines for renal disease: current status and future applications, Nat. Rev. Nephrol. 12 (2016) 738-753.
[15] C.H. Choi, J.E. Zuckerman, P. Webster, M.E. Davis, Targeting kidney mesangium by nanoparticles of defined size, Proc. Natl. Acad. Sci. U. S. A. 108 (2011) 6656-6661.
[16] J.E. Zuckerman, C.H. Choi, H. Han, M.E. Davis, Polycation-siRNA nanoparticles can disassemble at the kidney glomerular basement membrane, Proc. Natl. Acad. Sci. U. S. A. 109 (2012) 3137-3142.
[17] H. Kamada, et al., Synthesis of a poly(vinylpyrrolidone-co-dimethyl maleic anhydride) co-polymer and its application for renal drug targeting, Nat. Biotechnol. 21 (2003) 399-404.
[18] M.P. Borgman, et al., Tumor-targeted HPMA copolymer-(RGDfK)-(CHX-A'-DTPA) conjugates show increased kidney accumulation, J. Contr. Release 132 (2008) 193-199.
[19] R. Bruni, et al., Ultrasmall polymeric nanocarriers for drug delivery to podocytes in kidney glomerulus, J. Contr. Release 255 (2017) 94-107.
[20] C.E. Wang, P.S. Stayton, S.H. Pun, A.J. Convertine, Polymer nanostructures synthesized by controlled living polymerization for tumor-targeted drug delivery, J. Contr. Release 219 (2015) 345-354.
[21] D.G. Eng, et al., Glomerular parietal epithelial cells contribute to adult podocyte regeneration in experimental focal segmental glomerulosclerosis, Kidney Int. 88 (2015) 999-1012.

[22] H. Ma, J. Hyun, P. Stiller, A. Chilkoti, Non-fouling" oligo(ethylene glycol)-functionalized polymer brushes synthesized by surface-initiated atom transfer radical polymerization, Adv. Mater. 16 (2004) 338-341.
[23] S. Bhattacharjee, et al., Site-specific zwitterionic polymer conjugates of a protein have long plasma circulation, Chembiochem 16 (2015) 2451-2455.
[24] J.-F. Lutz, Polymerization of oligo(ethylene glycol) (meth)acrylates: toward new generations of smart biocompatible materials, J. Polym. Sci. Polym. Chem. 46 (2008) 3459-3470.
[25] Y. Qi, et al., A brush-polymer conjugate of exendin-4 reduces blood glucose for up to five days and eliminates poly(ethylene glycol) antigenicity, Nat Biomed Eng 1 (2016).
[26] A. Ruggiero, et al., Paradoxical glomerular filtration of carbon nanotubes, Proc. Natl. Acad. Sci. U. S. A. 107 (2010) 12369-12374.
[27] N. Nasongkla, et al., Dependence of pharmacokinetics and biodistribution on polymer architecture: effect of cyclic versus linear polymers, J. Am. Chem. Soc. 131 (2009) 3842-3843.
[28] A. Lewis, Y. Tang, S. Brocchini, J.W. Choi, A. Godwin, Poly(2-methacryloyloxyethyl phosphorylcholine) for protein conjugation, Bioconjugate Chem. 19 (2008) 2144-2155.
[29] M.J. Ryan, et al., HK-2: an immortalized proximal tubule epithelial cell line from normal adult human kidney, Kidney Int. 45 (1994) 48-57.
[30] K.L. Goldenthal, I. Pastan, M.C. Willingham, Initial steps in receptor-mediated endocytosis. The influence of temperature on the shape and distribution of plasma membrane clathrin-coated pits in cultured mammalian cells, Exp. Cell Res. 152 (1984) 558-564.
[31] M.T. Stephan, J.J. Moon, S.H. Um, A. Bershteyn, D.J. Irvine, Therapeutic cell engineering with surface-conjugated synthetic nanoparticles, Nat. Med. 16 (2010) 1035-1041.
[32] R.P. Lyon, D.L. Meyer, J.R. Setter, P.D. Senter, Conjugation of anticancer drugs through endogenous monoclonal antibody cysteine residues, Methods Enzymol. 502 (2012) 123-138.
[33] Y. Liu, Y.-c. Tseng, L. Huang, Biodistribution studies of nanoparticles using fluorescence imaging: a qualitative or quantitative method? Pharmaceut. Res. 29 (2012) 3273-3277.
[34] E. Tasciotti, et al., Near-infrared imaging method for the in vivo assessment of the biodistribution of nanoporous silicon particles, Mol. Imag. 10 (2011), 7290.2011.00011.
[35] H. Lv, S. Zhang, B. Wang, S. Cui, J. Yan, Toxicity of cationic lipids and cationic polymers in gene delivery, J. Contr. Release 114 (2006) 100-109.
[36] J.H. Miner, The glomerular basement membrane, Exp. Cell Res. 318 (2012) 973-978.
[37] D.G. Eng, et al., Detection of renin lineage cell transdifferentiation to podocytes in the kidney glomerulus with dual lineage tracing, Kidney Int. (2018).
[38] N.V. Kaverina, et al., WT1 is necessary for the proliferation and migration of cells of renin lineage following kidney podocyte depletion, Stem Cell Reports 9 (2017) 1152-1166.
[39] N.V. Kaverina, D.G. Eng, R.R. Schneider, J.W. Pippin, S.J. Shankland, Partial podocyte replenishment in experimental FSGS derives from nonpodocyte sources, Am. J. Physiol. Ren. Physiol. 310 (2016) F1397-F1413.

[40] N.V. Kaverina, et al., Tracking the stochastic fate of cells of the renin lineage after podocyte depletion using multicolor reporters and intravital imaging, PLoS One 12 (2017) -0173891.
[41] J. Lichtnekert, et al., Renin-angiotensin-aldosterone system inhibition increases podocyte derivation from cells of renin lineage, J. Am. Soc. Nephrol. 27 (2016) 3611-3627.
[42] T. Ohse, et al., De novo expression of podocyte proteins in parietal epithelial cells during experimental glomerular disease, Am. J. Physiol. Ren. Physiol. 298 (2010) F702-F711.
[43] J.W. Pippin, et al., Cells of renin lineage are adult pluripotent progenitors in experimental glomerular disease, Am. J. Physiol. Ren. Physiol. 309 (2015) F341-F358.
[44] R.R. Schneider, et al., Compound effects of aging and experimental FSGS on glomerular epithelial cells, Aging (Albany NY) 9 (2017) 524-546.
[45] J. Zhang, et al., Podocyte repopulation by renal progenitor cells following glucocorticoids treatment in experimental FSGS, Am. J. Physiol. Ren. Physiol. 304 (2013) F1375-F1389.
[46] J. Zhang, et al., Retinoids augment the expression of podocyte proteins by glomerular parietal epithelial cells in experimental glomerular disease, Nephron Exp. Nephrol. 121 (2012) 23-37.
[47] S.S. Roeder, et al., Activated ERK1/2 increases CD44 in glomerular parietal epithelial cells leading to matrix expansion, Kidney Int. 91 (2017) 896-913.
[48] J.A. Jefferson, C.E. Alpers, S.J. Shankland, Podocyte biology for the bedside, Am. J. Kidney Dis. 58 (2011) 835-845.
[49] P. Caliceti, F.M. Veronese, Pharmacokinetic and biodistribution properties of poly(ethylene glycol)-protein conjugates, Adv. Drug Deliv. Rev. 55 (2003) 1261-1277.
[50] L.W. Seymour, R. Duncan, J. Strohalm, J. Kopecek, Effect of molecular weight (Mw) of N (2-hydroxypropyl)methacrylamide copolymers on body distribution and rate of excretion after subcutaneous, intraperitoneal, and intravenous administration to rats, J. Biomed. Mater. Res. 21 (1987) 1341-1358.
[51] H.H. Gustafson, D. Holt-Casper, D.W. Grainger, H. Ghandehari, Nanoparticle uptake: the phagocyte problem, Nano Today 10 (2015) 487-510.
[52] Y. Tsubamoto, et al., Dextran sulfate, a competitive inhibitor for scavenger receptor, prevents the progression of atherosclerosis in Watanabe heritable hyperlipidemic rabbits, Atherosclerosis 106 (1994) 43-50.
[53] E.I. Christensen, H. Birn, Megalin and cubilin: synergistic endocytic receptors in renal proximal tubule, Am. J. Physiol. Ren. Physiol. 280 (2001) F562-F573.
[54] E.I. Christensen, H. Birn, P. Verroust, S.K. Moestrup, Membrane receptors for endocytosis in the renal proximal tubule, Int. Rev. Cytol. 180 (1998) 237-284.
[55] A. Wischnjow, et al., Renal targeting: peptide-based drug delivery to proximal tubule cells, Bioconjugate Chem. 27 (2016) 1050-1057.
[56] X.Y. Zhai, et al., Cubilin- and megalin-mediated uptake of albumin in cultured proximal tubule cells of opossum kidney, Kidney Int. 58 (2000) 1523-1533.
[57] S. Gao, et al., Megalin-mediated specific uptake of chitosan/siRNA nanoparticles in mouse kidney proximal tubule epithelial cells enables AQP1 gene silencing, Theranostics 4 (2014) 1039-1051.
[58] N. Platt, S. Gordon, Scavenger receptors: diverse activities and promiscuous binding of polyanionic ligands, Chem. Biol. 5 (1998) R193-R203.

[59] K. Kawabata, Y. Takakura, M. Hashida, The fate of plasmid DNA after intravenous injection in mice: involvement of scavenger receptors in its hepatic uptake, Pharm. Res. (N. Y.) 12 (1995) 825-830.
[60] M. van Oosten, E. van de Bilt, T.J. van Berkel, J. Kuiper, New scavenger receptor-like receptors for the binding of lipopolysaccharide to liver endothelial and Kupffer cells, Infect. Immun. 66 (1998) 5107-5112.
[61] M. Abbate, C. Zoja, G. Remuzzi, How Does Proteinuria Cause Progressive Renal Damage, 2006.
[62] R.P. Miller, R.K. Tadagavadi, G. Ramesh, W.B. Reeves, Mechanisms of cisplatin nephrotoxicity, Toxins 2 (2010) 2490-2518.
[63] J.J. Grantham, Polycystic kidney disease: a predominance of giant nephrons, Am. J. Physiol. 244 (1983) F3-F10.
[64] L. Jia, et al., Reduction-responsive cholesterol-based block copolymer vesicles for drug delivery, Biomacromolecules 15 (2014) 2206-2217.
[65] R.J. Lamm, et al., Peptide valency plays an important role in the activity of a synthetic fibrin-crosslinking polymer, Biomaterials 132 (2017) 96-104.
[66] J. Strohalm, J. Kope_cek, Poly[N-(2-hydroxypropyl)methacrylamide]. IV. Heterogeneous polymerization, Die Angewandte Makromolekulare Chemie 70 (1978) 109-118.
[67] A. Mitra, A. Nan, J.C. Papadimitriou, H. Ghandehari, B.R. Line, Polymer-peptide conjugates for angiogenesis targeted tumor radiotherapy, Nucl. Med. Biol. 33 (2006) 43-52.
[68] V. Omelyanenko, P. Kopeckova, C. Gentry, J. Kopecek, Targetable HPMA copolymer-adriamycin conjugates. Recognition, internalization, and subcellular fate, J. Contr. Release 53 (1998) 25-37.
[69] C.B. Marshall, R.D. Krofft, J.W. Pippin, S.J. Shankland, CDK inhibitor p21 is prosurvival in adriamycin-induced podocyte injury, in vitro and in vivo, Am. J. Physiol. Ren. Physiol. 298 (2010) F1140-

Chapter 3

Targeted delivery of polymer-drug conjugates to tubular epithelia to prevent progression of kidney disease

Alexander N. Prossnitz*, Lucy Yang*, Đình Nguyễn, Diana G. Eng, Stuart J. Shankland, and Suzie H. Pun

Abstract

Incidence of chronic kidney disease is rapidly increasing globally. Current clinical interventions such as steroids or angiotensin receptor blockers, can only slow disease progression, meaning that all patients eventually succumb to kidney failure or end stage renal disease. While it is difficult to prevent acute kidney injury, the initial insult to the architecturally complex glomerulus, studies show that prevention of the resulting inflammatory signal cascade can cause the tissue to enter a regenerative state. We aim to reverse this inflammatory response, specifically the epithelial to mesenchymal transition that occurs in tubular epithelial cells, by directly delivering antifibrotic drugs to the injured cells. Our previous work established that 25 kDa anionic polymers accumulate selectively in these tubule cells. Here we conjugate the antioxidant drug epigallocatechin gallate via a reversible boronic ester bond to these anionic polymers. *In vitro* results show that the antioxidant can prevent the epithelial to mesenchymal transition in human tubule cells. Completion of this

work will require testing of the polymer-drug conjugates both *in vitro*, in human and mouse cell lines, and *in vivo*, in an antibody induced murine kidney disease model.

3.1. Introduction

Focal segmental glomerular sclerosis (FSGS) is the leading cause end stage renal disease (ESRD) globally. Genetic predispositions, infections, medication, or circulating factors can cause acute kidney injury, damaging the functional cell of the glomerulus (the podocyte) (**Figure 3.1**). Podocytes are terminally differentiated cells with an intricate three-dimensional structure, that once damaged, are replaced with nonfunctional extracellular matrix (ECM) proteins in a process called glomerulosclerosis. If the insult to the podocytes cannot be alleviated, as is the case for ESRD or chronic kidney disease (CKD), the buildup of scar tissue in the glomerulus eventual leads to loss of entire nephrons and kidney failure.[1]

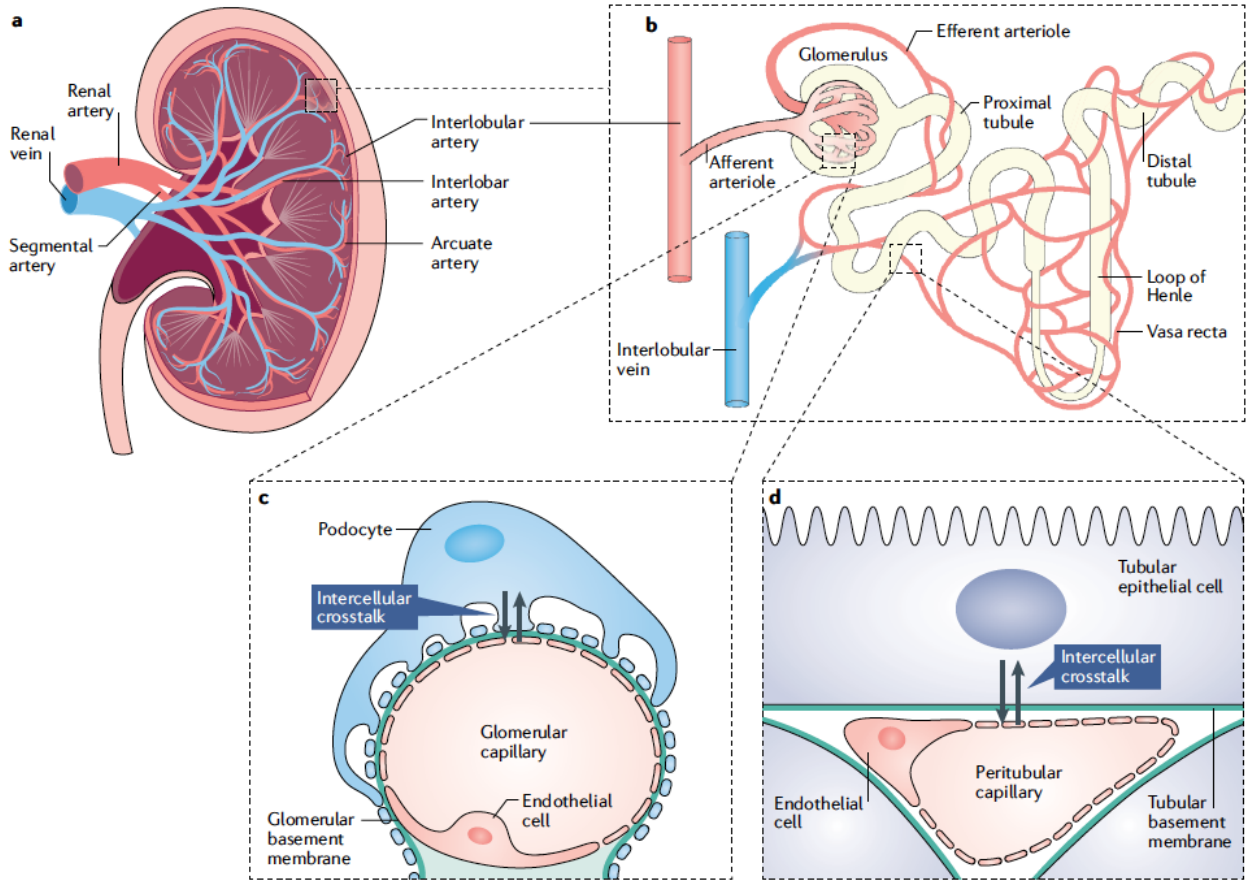

Figure 3.1 Overview of kidney structure and organization. The kidney (a) has over 1 million functional units called nephrons (b). Within the nephron, blood is filtered by the glomerulus (c), consisting of a selective barrier composed of the interdigitating foot processes of podocytes. After filtration, ions and remaining nutrients are reabsorbed in the proximal tubules by tubular epithelial cells (d) prior to excretion. Figure adapted from Tanabe *et al.* [2]

The prevalence of FSGS among adults is increasing and as a result, global prevalence of CKD has increased 30% from 1990 to 2017.[2–4] Since current treatments only slow the progression of CKD, most patients eventually become reliant on dialysis or kidney transplantation. The rise of CKD has corresponded with a similar increase in these procedures. Over the same time period, dialysis and kidney transplantation increased by 43% and 34% respectively.[2] Despite the initial success of these interventions, patients still face high mortality and morbidity rates.[5] Over 1 million people died from CKD in 2017, and even though intervention incidence has increased, mortality has increased by 41% over the past 30 years.[6] Not

only are dialysis and kidney transplantation ineffective, but in 2015 Medicare spending for these procedures exceeded $100 billion.[7]

The main contributing factor to the increasing incidence, mortality, and high cost of CKD is the inability of current clinical practices to halt or reverse disease progression. The most common treatment for CKD is angiotensin-converting enzyme (ACE) inhibitors or angiotensin receptor blockers (ARBs) because most disease is proteinuric and hypertensive in nature. Unfortunately, even when patients respond well to the therapy, CKD progression is only slowed, not halted.[8] For individuals with FSGS induced CKD, glucocorticoid steroids, immunosuppressive drugs, are the frontline therapy and again these treatments only delay disease advancement. Due to serious side effects such as obesity, hypertension, infection, and nephrotoxicity patients will often halt treatment. These breaks result in over 50% of patients relapsing.[9,10] There is currently an unmet clinical need to develop therapeutics for CKD with potential to reverse or at a minimum halt disease progression.

A key part of CKD advancement is the destruction and injury of the tubular epithelial cells (TECs).[11] TECs are highly metabolically active and this high mitochondria content makes them susceptible to damage from hypoxia, proteinuria, and metabolic disorders. Chronic insults to the TECs directly cause cell death and upregulation of pro-inflammatory and pro-fibrotic mediators (**Figure 3.2**).[1,11,12] The resulting infiltration of immune cells and continued upregulation of inflammatory pathways increases kidney scarring and proteinuria.[13] As damage to the tubules accumulates, the TECs undergo an epithelial to mesenchymal transition (EMT) and become α-smooth muscle actin (α-SMA) myofibroblasts. These myofibroblasts not only lose the ability to perform the functions of TECs, but also have aberrant secrotomes, which continue to increase inflammatory signaling. Preserving TEC function by preventing EMT was found to

protect mice from several kidney injury models.[14,15] Specifically, knocking out transcription factors Twist1 or Snai1 reduced kidney fibrosis and rescued TECs resulting in repair of the tubular basement membrane. This discovery presents the EMT pathway as a drugable target for development of new CKD therapeutics.

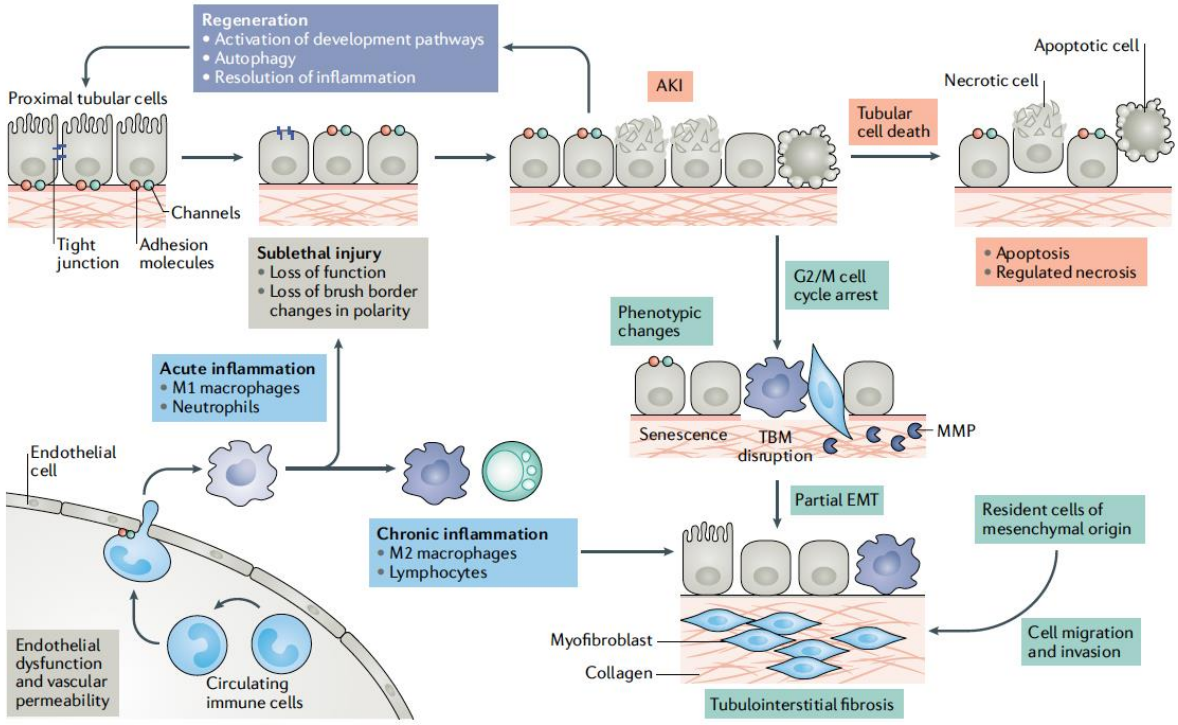

Figure 3.2 Acute kidney injury (AKI) induces tubular cell death and damage. Both reduction in the number of TECs and conversion of remaining TECs into mesenchymal cells dramatically increases inflammation, immune cell infiltration, and scarring. Figure adapted from Ruiz-Ortega *et al.*[1]

Here, we pursued a combination approach using the anionic polymers developed in chapter 2 for passive targeting of TECs and delivering the anti-EMT drug epigallocatechin-3-gallate (EGCG). Anionic polymers with molecular weights of 25 kDa preferentially accumulate in the proximal tubule cells of mice with FSGS.[16] Modifying these polymers with stimuli responsive boronic acid (BA) functional groups enables pH sensitive intracellular drug release of EGCG. Due to the catechol moieties on EGCG, this drug will form strong dynamic covalent boronic esters with the BAs on the polymer.[17] Once the polymer-drug conjugates are

endocytosed, the acidic environment of the endosome will cleave the boronic ester, releasing unaltered EGCG. This drug prevents EMT by reducing oxidative stress, TGF-β1, vimentin, and α-SMA. Importantly, EGCG also increases expression of E-cadherin and antioxidant enzymes that protect TECs from further injury.[18,19] We hypothesize that these polymer-drug conjugates will be able to reduce markers of EMT in TECs both *in vitro* and *in vivo*.

Herein the first half of this work is detailed, validating EGCG activity *in vitro* and synthesizing the EGCG-conjugated anionic polymers. Future work determining the targeting and efficacy of the polymer-drug conjugates for treating FSGS is also proposed.

3.2. Results and Discussion

3.2.1. Efficacy determination of EGCG *in vitro*

To validate the effects of EGCG on EMT in TEC cells, the human derived proximal renal tubule cell line (HK-2) was selected. These cells were cultured in Dulbecco's Modified Eagle's medium (DMEM), supplemented with penicillin-streptomycin 1%, and 10% inactivated fetal bovine serum (FBS), and kept at 37 °C with 5% CO_2. First, the half maximum inhibitor concentration (IC_{50}) of a 48 h EGCG treatment was determined by measuring cell viability (MTS/PMS assay, Promega). Concentrations of EGCG from as low as 50 nm to 300 μM were tested (**Figure 3.3**). We found that doses up to 10 μM were extremely well tolerated and the maximum tolerable dose was 40 μM.

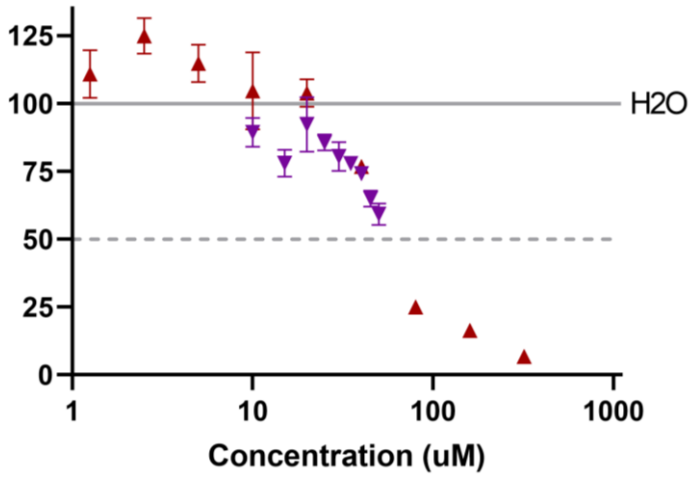

Figure 3.3 Determination of IC_{50} value of EGCG in HK-2 cells after 48 h exposure. Cell viability determined by measuring absorbance at 490 nm after 4 h treatment with MTS/PMS.

Next, we chose to assess the ability of EGCG to prevent EMT in HK-2 cells. As previously mentioned, several changes in protein expression including, vimentin (a filament protein expressed in mesenchymal cells), Twist1 (a transcription factor responsible for EMT), and α-SMA (an isoform of actin present in myofibroblasts) can indicate loss of the TEC phenotype. In tissue culture, EMT induced by supplementation of the cells' media with TGFβ, an immunomodulatory cytokine that is produced during inflammatory reactions. After 48 hours of exposure to TGFβ, increases in vimentin expression can be quantified by measuring the intracellular mRNA levels with reverse transcriptase quantitative PCR (RT-qPCR). Fold changes in expression were quantified relative to housekeeping gene GAPDH (**Figure 3.4**).

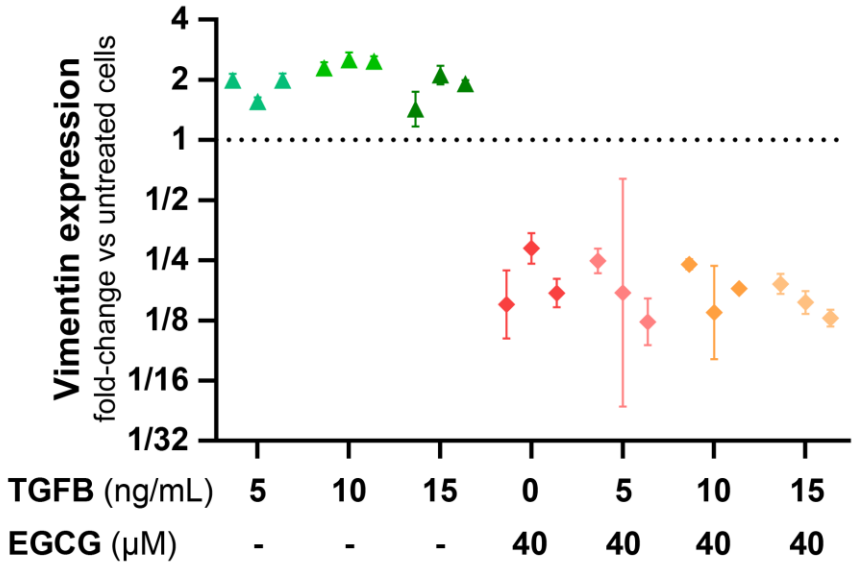

Figure 3.4 Quantification of vimentin expression after induction of EMT with TGFβ. EGCG decreases vimentin expression and prevents TGFβ from increasing expression across all concentrations tested.

A high dose of EGCG, 40 μM, administered 1 h prior to TGFβ dramatically reduced expression of vimentin in HK-2 cells, despite the addition of various concentrations of TGFβ. This preliminary study convinced us that the previously reported effects of EGCG were robust and reproducible.[18,19] This confirmation was particularly important after our first attempt to validate the Twist1 inhibitor, harmol, failed (data not shown).

Expanding on the previous experiment, we chose to explore if EGCG would decrease vimentin expression in a dose dependent manner, and if Twist1 would show similar trends (**Figure 3.5**).

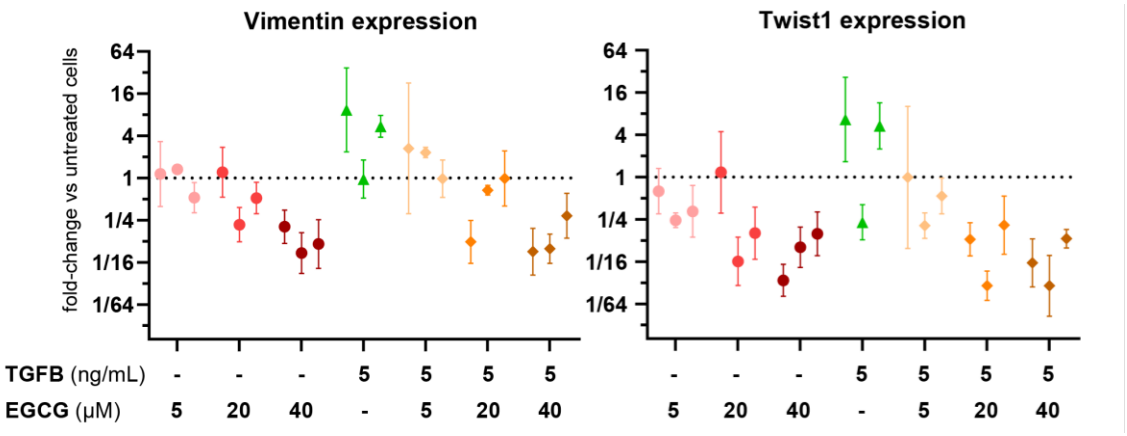

Figure 3.5 Treatment with EGCG decreases vimentin and Twist1 expression in a dose dependent manner. RT-qPCR experiment was performed with 1 biological replicate and 3 technical replicates. Average values determined from 1 RT reaction and error bars represent the standard deviation of technical replicates.

While low doses of EGCG (5 μM) did not decrease expression of vimentin and twist1 below baseline, these treatments did prevent the TGFβ dependent increase in expression. At higher doses, both vimentin and twist1 expression decreased in a dose dependent manner, regardless of TGFβ presence. By downregulating the expression of multiple proteins associated with EMT, EGCG looks to be a promising drug for the prevention and protection of TECs.

3.2.2. Anionic polymer synthesis

To translate these early *in vitro* successes of EGCG to *in vivo* experiments, we needed a polymer platform to both deliver the drug to TECs and increase the drug stability. To this end, we synthesized an anionic polymer capable of targeting TECs both in normal and FSGS mice.[16] For this efficacy focused study, quantitative labeling was unnecessary, but improved polymerization control and large scale synthesis would be key to successful translation. As a result, we chose to switch from ATRP to a RAFT polymerization. RAFT polymerizations of methacrylates are well controlled (often with dispersities lower than 1.1) and can be run to high conversion.[20,21] Due to

the large number of carboxylic acids (>100), we chose to modify this polymer with BAs after polymerization via an activated ester and amine coupling. This approach facilitates easy substitution of the BA moieties to tune the pH sensitivity of the boronic ester bond, and ultimately the drug release kinetics. Additionally, by using the same base polymer and independently changing the drug release kinetics, the effects of specific drug linkers profiles can be directly correlated with disease outcomes.

A trithiocarbonate and ABCVA were selected for this RAFT polymerization due to increased solubility in polar solvents and the high aqueous stability of trithiocarbonates compared to dithiobenzoates (**Figure 3.6**).[22]

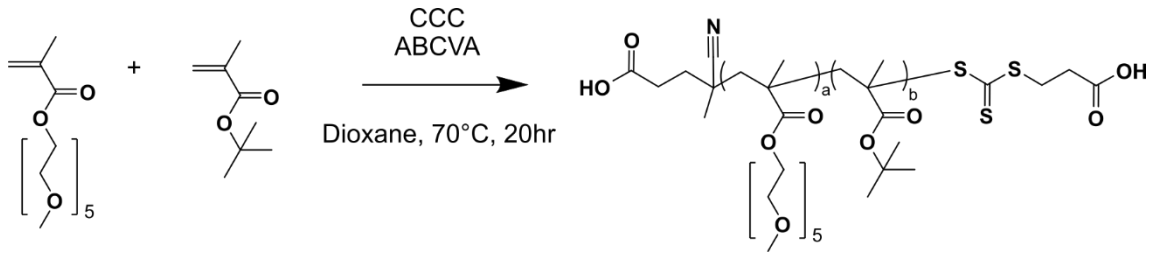

Figure 3.6 Scheme for RAFT polymerization of highly anionic polymer for TEC targeting.

The same monomers as chapter 2, tBuMA and $OEGMA_{300}$, were copolymerized in dioxane at CTA:I:tBuMA:OEGMA ratios of 1:0.2:200:50 (labeled MOB). The conversion, 78%, was determined by ^{1}H NMR after halting the reaction via exposure to air. The theoretical Mw after deprotection of the t-Buyl groups was 23,365 Da and the ratio of tBuMA to OEGMA was 4.70. Since the conjugation with BA will both increase the Mw and decrease the number of anionic charges, (moving both values closer to those previously determined for optimal TEC targeting, 25 kDa and 4 respectively), we decided to move forward. Next the tBuyl protecting groups were removed by dissolving the polymer in neat TFA. Complete deprotection was observed by measuring the disappearance of the ^{1}H NMR peak at 1.4ppm (**Figure 3.7**).

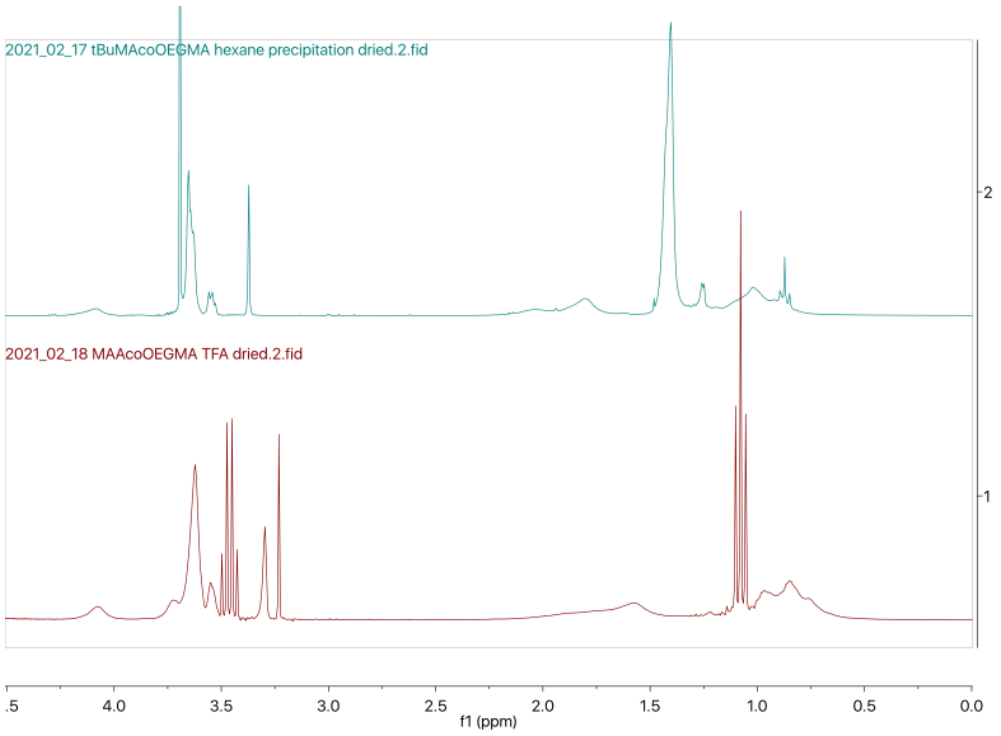

Figure 3.7 ^{1}H NMR spectra showing the complete deprotection of tBuMA via the disappearance of the peak at 1.4 ppm. The triplet at 1.1 is residual diethyl ether from precipitation.

We also synthesized a more hydrophilic anionic polymer by substituting $OEGMA_{300}$ with $OEGMA_{900}$ in a RAFT polymerization otherwise identical to the one above (MOB2). Importantly the ratio of PEG to tBuMA was kept constant, but the relative theoretical number of methacrylate backbone repeats decreased from 189 to 153, increasing the hydrophilicity of the polymer. We found that the absolute molecular weight, determined by size exclusion chromatography (SEC) (**Figure 3.8**), of the $OEGMA_{900}$ polymer before deprotection was 36,500 Da, which corresponded to DPs of the tBuMA and $OEGMA_{900}$ of 170 and 13 respectively at a ratio of 5:1 (where each OEGMA is multiplied by 3 to compare against the previous polymers synthesized with $OEGMA_{300}$). For initial optimization of the post polymerization modification of the anionic polymers with BA, MOB was used. The final preparation of functional materials was all done with MOB2.

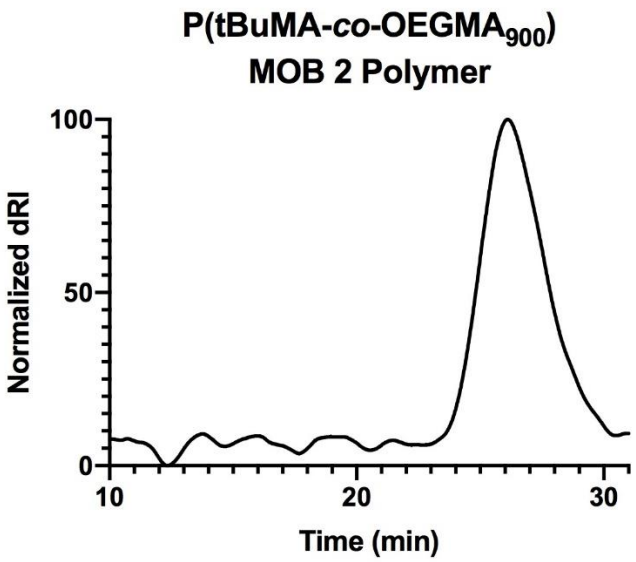

Figure 3.8 SEC chromatogram for MOB 2 polymer, with calculated M_n = 36,050 Da and $Đ$ = 1.05.

3.2.3. Boronic acid conjugation

We have previously demonstrated that post polymerization modification of polymethacrylamides with BA functional groups enabled pH sensitive drug release of catechol drugs.[17] To adapt this approach to anionic (carboxylic acid) polymers, we attempted using EDC/NHS coupling of amine functionalized phenyl boronic acids (PBAs) (**Figure 3.9a**). Compared to the relatively efficient reactions observed in the previous work, minimal conversion was observed after a 24 h reaction of the aniline boronic acid with EDC/NHS (4.4%, **Table 3.1**). We assumed that the overwhelming presence of acidic residues in combination with the poor nucleophilicity of the aniline moiety were resulting in the poor yield. So next we attempted the same reaction with a primary amine BA that was also pinacol protected (**Figure 3.9b**). With a similarly poor yield, we then explored converting the carboxylic acids in the polymer to acid chlorides with oxalyl chloride (**Figure 3.9c**). The extremely harsh nature of this reaction and difficult work up ultimately prevented any BA modified polymer from being recovered. Finally, we resorted to the

most reactive peptide coupling reagent on the market, HATU. Preactivation of the polymer with HATU and DIPEA followed by addition of the primary amine BA achieved a remarkable 80% conjugation efficiency (**Figure 3.9**, and **Table 3.1**). The extent of BA modification was quantified by comparing the ratio of OEGMA (methyl peak, 3H, at 3.4ppm) with the aromatic protons of the BA (benzyl peaks, 4H, at 7-8ppm) (**Figure 3.10**).

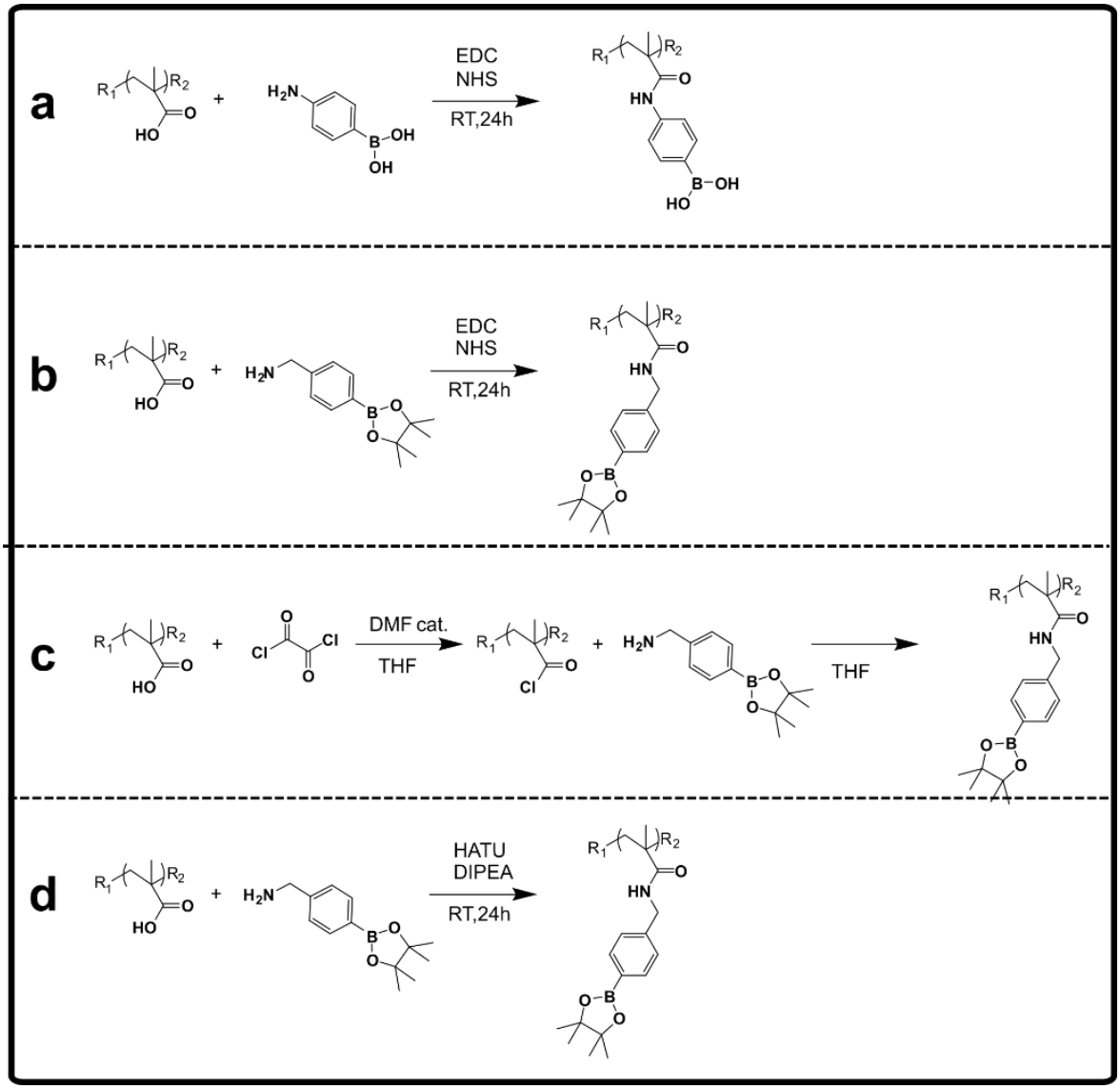

Figure 3.9 Post polymerization modification of methacrylic acid containing anionic polymer with a) EDC/NHS aniline PBA b) EDC/NHS amine PBA c) Oxalyl Chloride d) HATU/DIPEA peptide coupling reaction.

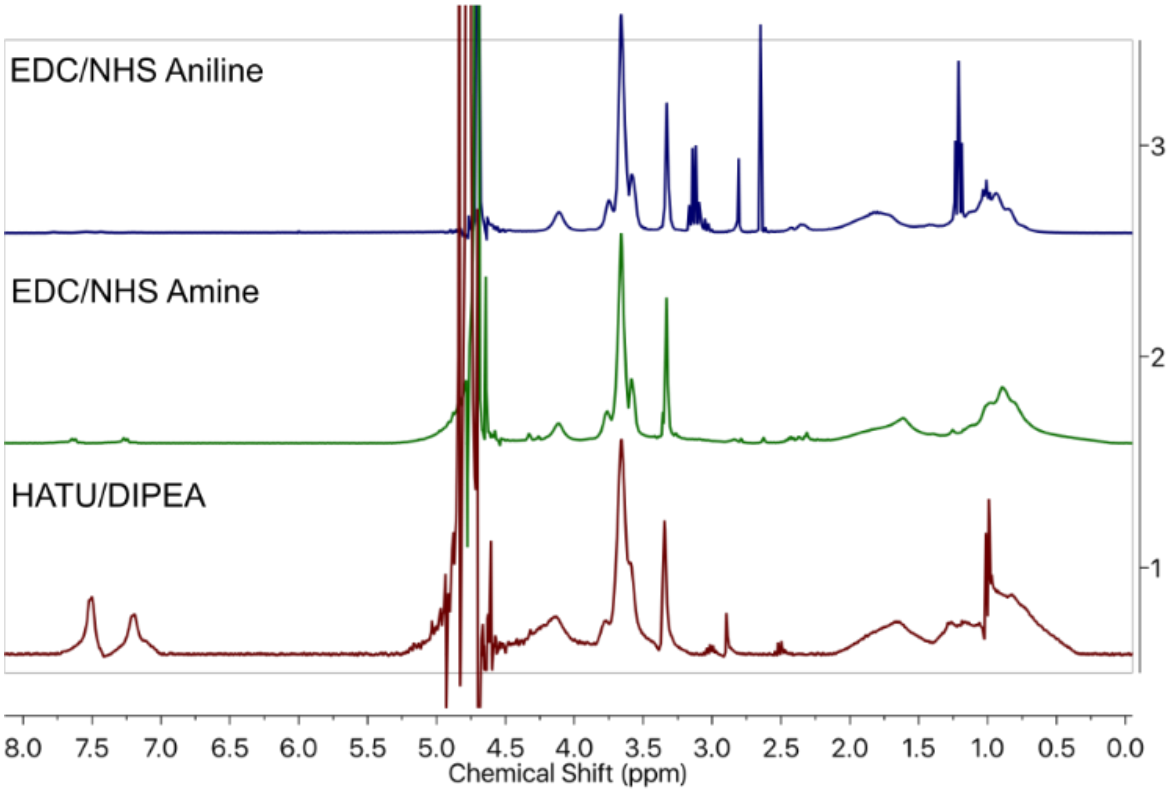

Figure 3.10 ^{1}H NMR spectra of anionic polymers after various conjugation reactions with amino PBAs.

Table 3.1 Efficiency of coupling reactions between amino phenyl boronic acids and carboxylic acid polymers.

Reaction Type	Efficiency
EDC/NHS Aniline	4.4%
EDC/NHS Amine	4.8%
Oxalyl Chloride	N/A
HATU/DIPEA	80.0%

Subsequently, the pinacol protection groups on the BA were removed by adding a 6-fold excess of sodium periodate (relative to BA) in aqueous solution. Importantly, sodium periodate is a potent oxidizing agent, which degrades regenerated cellulose, preventing its removal by

dialysis. However, in the presence of excessive sodium hydroxide sodium periodate and its byproducts precipitate, allowing purification by centrifugation, followed by dialysis to remove NaOH. The final poly(methacrylic acid-*co*-OEGMA900-*co*-phenyl boronic acid methacrylamide) or MOB polymer was obtained after lyophilization. For measuring intracellular uptake and biodistribution, the MOB polymer was also labeled with Cy5-amine (**Figure 3.11**).

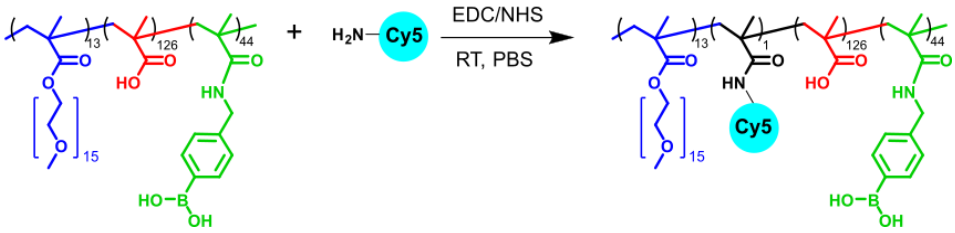

Figure 3.11 Conjugation of fluorescent Cy5 amine to MOB polymer.

As a quick proof of concept, Quercetin, a yellow catechol drug that fluoresces when bound to a BA, was added to a small stock solution of MOB polymer. If residual sodium periodate remained in the sample the catechol would immediately oxidize to a black color, but if quercetin complexed to the boronic acid the solution would turn bright orange. After this optimized purification, the MOB polymer complexed to quercetin, without any detectable traces of sodium periodate.

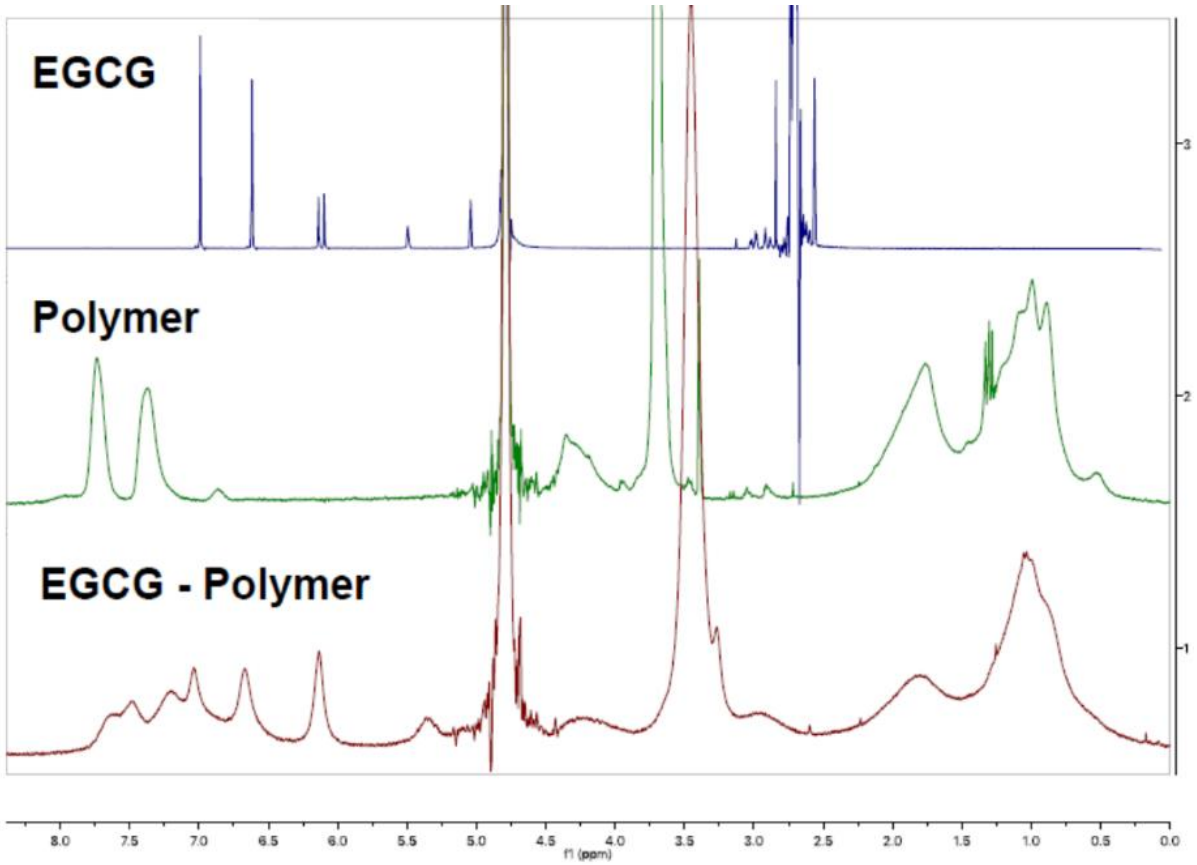

Figure 3.12 ^{1}H NMR spectra of EGCG, MOB polymer, and purified EGCG-MOB polymer-drug conjugate. Additional aromatic peaks of EGCG are clearly visible in addition to the PBA peaks in the polymer.

3.2.4. EGCG conjugation

To prepare EGCG and MOB polymer-drug conjugates, equal masses of drug and polymer were mixed in DI water. The use of excess EGCG to the BA in the polymer ensures a) minimal crosslinking since EGCG has two catechols per drug and b) the maximum amount of drug is loaded. After purification of the conjugate by spin filtration, (this technique is preferable to dialysis because EGCG is unstable in aqueous environments at RT on the time scale of hours) the material was lyophilized, and the drug loading was measured by NMR (**Figure 3.12**). Specifically, the aromatic peaks of EGCG were compared to the aromatic protons of the BA groups and the drug percent by weight was determined (35%) (**Figure 3.13**).

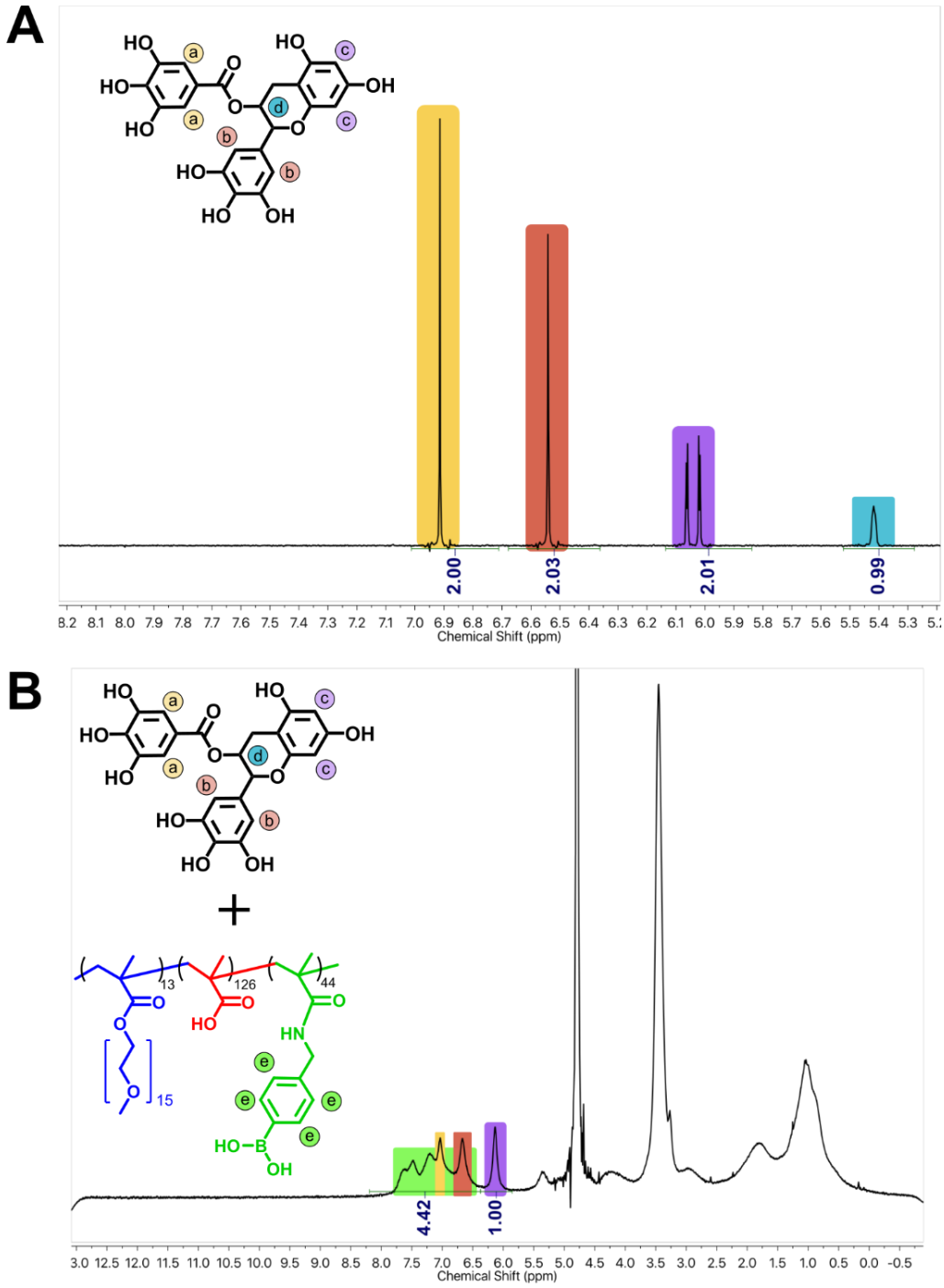

Figure 3.13 A) ^{1}H NMR spectra of the aromatic region of EGCG B) Annotated protons for MOB polymer EGCG conjugate and relative integrations for the calculation of drug percent by weight (35%).

3.3. Conclusions

Here we synthesized a novel polymer-drug conjugate engineered for targeted delivery and specific release of EGCG in TECs. Anionic polymers were synthesized by RAFT polymerization, with a ratio of anionic to neutral monomers of 5:1. These polymers were deprotected, and the conjugation of PBA moieties was optimized with a final efficiency of 80%. These anionic polymers modified with PBA (MOB polymers), complexed to the catechol drug EGCG, resulting in a high maximum drug loading of 35% by weight. This polymer-drug conjugate has the potential to halt the progression of FSGS and CKD by protecting fragile TECs from injury and the resulting EMT.

Our preliminary data shows that free EGCG can decrease the expression of two markers for EMT, even in the presence of an inflammatory signaling molecule, TGFβ. The next steps of this project are to determine efficacy of the anionic polymer EGCG conjugate, which will be validated for both *in vitro* and *in vivo*.

3.4. Future Work

The first part of this project, synthesis of a labeled anionic polymer conjugated to EGCG has been successfully completely. Here an outline for the second half, delivery of EGCG to TECs and improving disease outcomes *in vivo* in models of FSGS, is proposed.

3.4.1. EMT prevention *in vitro*

In similar experiments to those described in section 3.2.1, the activity of the polymer EGCG conjugate will be tested in HK-2 cells. In brief, vimentin and twist1 expression will be measured by RT-qPCR after of treatment with the conjugates and 48 h exposure to TGFβ.

Various concentrations (5, 10, and 40 μM by drug) of the polymer-drug conjugate will be compared against equal concentrations of free EGCG.

Next we will compare the results of this human derived cell line with a murine proximal tubular cell line (MCT).[23] The same RT-qPCR experiment comparing the effects of free drug and polymer-drug conjugate will be conducted. Even though human cell lines are more relevant to translation, it is important to validate the therapeutic in a small animal model which will require activity in murine cells.

Expected Outcomes

We expect that the polymer-drug conjugate will show efficacy, but that the potency might be reduced. The current understanding is that free EGCG enters cells both passively by diffusion and actively as a ligand to the 67 kDa laminin receptor.[19,24] Since the polymer conjugate will only delivery EGCG via endocytosis, which is a slower process, we expect to need a slightly higher drug concentration to achieve the same effect as free drug.

Alternative Approaches

If the polymer-drug conjugate does not perform well at the same concentrations as the free drug, first we will measure a the IC_{50} for the conjugate as previously done for free EGCG. If the IC_{50} of the conjugate is higher than free EGCG, we will try higher concentrations of the conjugate in the EMT prevention assay. Second, we will measure uptake over 48 hours via flow cytometry and confocal microscopy. If the polymer is not internalized, we will try to increase the negative charge by increasing the DP of the tBuMA monomer. Lastly, if we still observe no effect of the

polymers on protein expression, we will stain and image cells for fibronectin, which will be present if the EMT occurs, but will be minimally visible if EMT is prevented.[19]

3.4.2. FSGS rescue *in vivo*

First, we will confirm that the biodistribution of the polymer-drug conjugates is similar to the previously described anionic polymers in both normal and FSGS mice. FSGS will be induced by antibody treatment and the biodistribution of the polymers labeled with a Cy5-amine fluorophore will be tracked to as previously described.[16] Second, analogous to determining the IC_{50} *in vitro*, we will determine the maximum tolerated dose (MTD) of both free EGCG and polymer-drug conjugate. Increasing concentrations of the therapeutics will be injected intravenously, and the animals will be monitored for complications or toxicity by measuring weight and body temperature. Once the MTD is determined, we will evaluate the efficacy of the free drug and polymer in the experimental model of FSGS. Every 3 days the animals will be injected with 25% of the MTD for 18 days. The animals will be left to recover for 10 days until euthanasia. The kidneys from these animals will be collected and studied via flow cytometry and histology. Upon digestion of the kidney into single cells, cells will be labeled with various antibodies (anti-CD45, anti-granzyme, anti-CD3, anti-FoxP3 etc.), and gated to determine the composition of immune cell populations.[15] For histological analysis, kidneys will be fixed, sectioned and stained with H&E, Masson's trichrome, and picrosirius red. By determining both the cell populations in the kidneys and the gross morphology of the tissue we will be able to assess the efficacy of both EGCG and the polymer-drug conjugates.

Expected Outcomes

We expect both the free EGCG and polymer-drug conjugates to decrease progression of FSGS by limiting damage to TECs. Since EGCG is highly unstable in serum (half-life < 30min), we would expect the protection of the drug via conjugation to result in increased activity.[24] Additionally, we expect the accumulation of the polymer-drug conjugates in the proximal tubules to greatly increase the local drug concentration. Overall, we expect the polymer-drug conjugates to outperform the free EGCG *in vivo* due to increased stability and targeted delivery.

Alternative approaches

If the polymers are accumulating in the proximal tubules but we do not see decreased fibrosis we will try to increase drug loading by including additional BA groups and try to increase stability by using boronic acids with lower pKas. If both free EGCG and polymer-drug conjugate do not show any efficacy *in vivo*, we will a try a different catechol drug, quercetin or baicalin, which have both shown efficacy at preventing EMT via multiple pathways.[25,26]

3.5. Experimental

3.5.1. Materials

All reagent grade materials and solvents were purchased from Sigma Aldrich, Tokyo Chemical Industry (TCI), Fisher, Boron Molecular or Cayman Chemical and used as received. Snake skin dialysis tubing (16 mm diameter) was used for all dialysis purification.

3.5.2. Instrumentation

Nuclear Magnetic Resonance (NMR) Spectroscopy

^{1}H NMR spectra were obtained using a Bruker AVance 300 MHz instrument. Solvents used in this study were obtained from Cambridge Isotope Laboratories and included: deuterium oxide, deuterated methanol, deuterated sodium hydroxide, deuterated dimethylsulfoxide, and deuterated chloroform. Data was processed with MestReNova 10.0.

Size exclusion chromatography (SEC)

The molecular weight ($M_{n\ SEC}$) and dispersity were determined using 100% mass recovery and multiangle light scattering (MALS) SEC. The running solvent was N,N-dimethyl formamide (DMF) with 1 g/L LiBr (flow rate: 0.8 mL/min) heated to 60 °C and samples were prepared at 5 mg/mL. Separation was done through three columns Tosoh TSKgel alpha 4000, Tosoh TSKgel alpha 3000 and Phenomenex Phenogel 5 µm 10E3 Å and data was collected by a Wyatt miniDAWN Treos and Wyatt Optilab T-rex. For data analysis, specifically determination of absolute molecular weight and dispersity, Wyatt ASTRA software was used. The RI traces were normalized using Prism 10.

3.5.3. Methods

Anionic polymer synthesis

As an example reaction, a 50 mL round bottom flask (RBF), 4-((((2-carboxyethyl)thio)carbonothioyl)thio)-4-cyanopentanoic acid (CCC) (50 mg, 0.16 mmol), 4,4-Azobis(4-cyanovaleric acid) (ACVA) (9.12 mg, 0.033 mmol), *tert*-butyl methacrylate (t-BuMA) (5.29 mL, 32.57 mmol), oligoethyleneglycol methacrylate-900 ($OEGMA_{900}$) (2.42 g, 2.54

mmol), dioxane (40.0 mL) and a magnetic stir bar were added. Then 150 µL of DMF was added to the reaction, as an internal standard, and the solution was stirred until homogenous. A 50 µL solution aliquot was removed and frozen and the remaining reaction was sparged with argon gas vigorously for 30 minutes. Then the reaction was heated to 70 °C for 18 hours and halted with exposure to atmosphere. The conversion, DP, and $M_{n,theo}$ were determined by comparing the ^1H NMRs in $CDCl_3$ of the initial aliquot and the final reaction mixture. The polymer was purified by 3 sequential precipitations into hexanes and dried under vacuum.

t-BuMA Deprotection

The protected prepolymer (5 g) was dissolved in 15 mL of neat trifluoroacetic acid (TFA) in a 20 mL scintillation vial and stirred until a homogenous liquid was obtained. After deprotecting for 24 h, the TFA/polymer mixture was precipitated into diethyl ether at a volume ratio of 1:10. After redissolving in methanol and precipitating 2 more times, the protonated and deprotected carboxylic polymer was dried under vacuum. It is important to purify this polymer via precipitation and not dialysis to ensure that it remains soluble in polar organic solvents for post polymerization modification.

AminoPBA conjugation reactions

EDC/NHS Aniline PBA

To a 1.5 mL eppendorf tube, polymer (48 mg, 0.29 mmol of carboxylic acid), 1-ethyl-3-(-3-dimethylaminopropyl) carbodiimide hydrochloride (EDC, 42 mg, 0.22 mmol), N-hydroxy-succinimide (NHS, 25 mg, 0.22 mmol), 4-aminophenyl boronic acid, (Aniline PBA, 32 mg, 0.15 mmol) and 0.48 mL of DMSO were added and reacted at RT for 24 h. The polymer PBA conjugate was purified by addition of NaOH to the reaction and dialysis against DI water for 24 h followed by lyophilized. The extent of modification was measured by ^1H NMR in D_2O with

NaOD by comparing the ratio of the methyl protons from the OEGMA (3.4 ppm) to the aromatic protons of the PBA (7-8 ppm).

EDC/NHS Amine PBA

To a 20 mL scintillation vial, polymer (210 mg, 1.35 mmol of carboxylic acid), EDC (388 mg, 2.0 mmol), NHS (233 mg, 2.0 mmol), 4-aminomethyl phenyl boronic acid pinacol ester, (Amine PBA, 182 mg, 0.67 mmol), and 10.5 mL DMSO/THF were added and reacted at RT for 24 h. The polymer PBA conjugate was purified by addition of NaOH to the reaction and dialysis against DI water for 24 h followed by lyophilized. The extent of modification was measured by ^{1}H NMR in D_2O with NaOD by comparing the ratio of the methyl protons from the OEGMA (3.4 ppm) to the aromatic protons of the PBA (7-8 ppm).

Oxalyl Chloride

To a 7 mL scintillation vial, polymer (56 mg, 0.40 mmol of carboxylic acid) was dissolved in 3.38 mL of DMF and after completely dissolving, oxalyl chloride (37 µL, 0.44 mmol) and triethylamine (TEA, 73 µL, 0.52 mmol) were added in a pre-activation step for 30 min. Then 4-aminomethyl phenyl boronic acid pinacol ester, (Amine PBA, 10.4 mg, 0.05 mmol) was added and reacted at RT for 24 h. The polymer PBA conjugate was purified by addition of NaOH to the reaction and dialysis against DI water for 24 h followed by lyophilized. The extent of modification was measured by ^{1}H NMR in D_2O with NaOD, but unfortunately, no polymer was detected, only small molecules.

HATU/DIPEA Amine PBA

To a 7 mL scintillation vial, polymer (186 mg, 1.20 mmol of carboxylic acid) was dissolved in 3.72 mL of DMF and after completely dissolving, 1-[Bis(dimethylamino)methylene]-1H-1,2,3-triazolo[4,5-b]pyridinium 3-oxide hexafluorophosphate (HATU, 408 mg, 1.0 mmol) and *N*,*N*-

diisopropylethylamine (DIPEA, 520 μL, 3.0 mmol) were added in a pre-activation step for 30 min. Then 4-aminomethyl phenyl boronic acid pinacol ester, (Amine PBA, 161 mg, 0.60 mmol) was added and reacted at RT for 24 h. The polymer PBA conjugate was purified by precipitation into ether first, and then addition of NaOH to the reaction and dialysis against DI water for 4 days. The extent of modification was measured by ^{1}H NMR in D_2O with NaOD by comparing the ratio of the methyl protons from the OEGMA (3.4 ppm) to the aromatic protons of the PBA (7-8 ppm).

Pinacol Deprotection

After dialysis of the polymer PBA conjugate, directly to the aqueous polymer solution, 700 mg of $NaIO_4$ (6-fold excess to pinacol protected PBA) was added at RT for 24 h. To precipitate the remaining $NaIO_4$ excessive NaOH (5-10 pellets) as added to the solution and the $NaIO_4$ was removed by centrifugation. The remaining highly concentrated aqueous NaOH and polymer solution was dialyzed against DI water for 3 days and lyophilized. The final deprotected polymer of poly(methacrylic acid-*co*-OEGMA900-*co*-phenyl boronic acid methacrylamide) or MOB polymer stored at RT for further use.

Cy5 Amine Labeling

To MOB polymer (120 mg, 0.65 mmol) in 2.5 mL of DMSO, EDC (250 mg, 1.3 mmol), NHS (150 mg, 1.3 mmol), and Cy5 amine (1.75 mg or 35 μL of a 50 mg/mL stock, 0.006 mmol) were added and reacted for 24 h at RT. The labeled MOB polymer was purified by dialysis for 24 h and lyophilization.

EGCG conjugation and drug loading calculations

To load the MOB polymer with EGCG, 50 mg of polymer and 50 mg of EGCG were mixed in 1 mL of DI water. After complete dissolution of the drug, the mixture was sonicated at

RT for 2-3 h, and then diluted 1:10 in DI water and purified via a 10 kDa MWCO Amicon spin filter. The solution was filtered at 4500 x g for 12 min, 2 times and then reduced to 1 mL of final volume. The 1 mL solution was frozen and lyophilized, and then drug loading was determined via ^{1}H NMR in D_2O by comparing 2 EGCG protons at 6.1 ppm to the entire aromatic region, which encompasses 4 more EGCG protons and 4 PBA protons from the polymer. From these values the ratio of EGCG to PBA was determined and with knowledge of the PBA DP and theoretical polymer molecular weight, the percent by weight EGCG was calculated.

Baicalin Loading

The protocol for loading of the hydrophobic polyphenolic drug, Baicalin, was similar to EGCG. First, 23 mg of baicalin was dissolved in 400 µL of DMSO and added to 200 µL DI water solution containing 20 mg of MOB polymer. After complete dissolution of the drug, the mixture was sonicated at RT for 2-3 h, and then diluted 1:10 in DI water (keeping the DMSO concentration below 10%) and purified via a 30 kDa MWCO Amicon spin filter. The solution was filtered at 4500 x g for 20 min, 2 times and then reduced to 1 mL of final volume. The 1 mL solution was frozen and lyophilized. The resulting drug content of the conjugate was determined using a similar method to EGCG, and found to be 17%.

References:

(1) Ruiz-Ortega, M.; Rayego-Mateos, S.; Lamas, S.; Ortiz, A.; Rodrigues-Diez, R. R. Targeting the Progression of Chronic Kidney Disease. Nat Rev Nephrol 2020, 16 (5), 269–288. https://doi.org/10.1038/s41581-019-0248-y.

(2) Carney, E. F. The Impact of Chronic Kidney Disease on Global Health. Nat Rev Nephrol 2020, 16 (5), 251–251. https://doi.org/10.1038/s41581-020-0268-7.

(3) Rosenberg, A. Z.; Kopp, J. B. Focal Segmental Glomerulosclerosis. CJASN 2017, 12 (3), 502–517. https://doi.org/10.2215/CJN.05960616.

(4) Stevens, L. A.; Li, S.; Wang, C.; Huang, C.; Becker, B. N.; Bomback, A. S.; Brown, W. W.; Burrows, N. R.; Jurkovitz, C. T.; McFarlane, S. I.; Norris, K. C.; Shlipak, M.; Whaley-Connell, A. T.; Chen, S.-C.; Bakris, G. L.; McCullough, P. A. Prevalence of CKD and Comorbid Illness in Elderly Patients in the United States: Results from the Kidney Early Evaluation Program (KEEP). Am J Kidney Dis 2010, 55 (3 Suppl 2), S23-33. https://doi.org/10.1053/j.ajkd.2009.09.035.

(5) Sarnak, M. J.; Jaber, B. L. Mortality Caused by Sepsis in Patients with End-Stage Renal Disease Compared with the General Population. Kidney International 2000, 58 (4), 1758–1764. https://doi.org/10.1111/j.1523-1755.2000.00337.x.

(6) Bikbov, B.; Purcell, C. A.; Levey, A. S.; Smith, M.; Abdoli, A.; Abebe, M.; Adebayo, O. M.; Afarideh, M.; Agarwal, S. K.; Agudelo-Botero, M.; Ahmadian, E.; Al-Aly, Z.; Alipour, V.; Almasi-Hashiani, A.; Al-Raddadi, R. M.; Alvis-Guzman, N.; Amini, S.; Andrei, T.; Andrei, C. L.; Andualem, Z.; Anjomshoa, M.; Arabloo, J.; Ashagre, A. F.; Asmelash, D.; Ataro, Z.; Atout, M. M. W.; Ayanore, M. A.; Badawi, A.; Bakhtiari, A.; Ballew, S. H.; Balouchi, A.; Banach, M.; Barquera, S.; Basu, S.; Bayih, M. T.; Bedi, N.; Bello, A. K.; Bensenor, I. M.; Bijani, A.; Boloor, A.; Borzì, A. M.; Cámera, L. A.; Carrero, J. J.; Carvalho, F.; Castro, F.; Catalá-López, F.; Chang, A. R.; Chin, K. L.; Chung, S.-C.; Cirillo, M.; Cousin, E.; Dandona, L.; Dandona, R.; Daryani, A.; Das Gupta, R.; Demeke, F. M.; Demoz, G. T.; Desta, D. M.; Do, H. P.; Duncan, B. B.; Eftekhari, A.; Esteghamati, A.; Fatima, S. S.; Fernandes, J. C.; Fernandes, E.; Fischer, F.; Freitas, M.; Gad, M. M.; Gebremeskel, G. G.; Gebresillassie, B. M.; Geta, B.; Ghafourifard, M.; Ghajar, A.; Ghith, N.; Gill, P. S.; Ginawi, I. A.; Gupta, R.; Hafezi-Nejad, N.; Haj-Mirzaian, A.; Haj-Mirzaian, A.; Hariyani, N.; Hasan, M.; Hasankhani, M.; Hasanzadeh, A.; Hassen, H. Y.; Hay, S. I.; Heidari, B.; Herteliu, C.; Hoang, C. L.; Hosseini, M.; Hostiuc, M.; Irvani, S. S. N.; Islam, S. M. S.; Jafari Balalami, N.; James, S. L.; Jassal, S. K.; Jha, V.; Jonas, J. B.; Joukar, F.; Jozwiak, J. J.; Kabir, A.; Kahsay, A.; Kasaeian, A.; Kassa, T. D.; Kassaye, H. G.; Khader, Y. S.; Khalilov, R.; Khan, E. A.; Khan, M. S.; Khang, Y.-H.; Kisa, A.; Kovesdy, C. P.; Kuate Defo, B.; Kumar, G. A.; Larsson, A. O.; Lim, L.-L.; Lopez, A. D.; Lotufo, P. A.; Majeed, A.; Malekzadeh, R.; März, W.; Masaka, A.; Meheretu, H. A. A.; Miazgowski, T.; Mirica, A.; Mirrakhimov, E. M.; Mithra, P.; Moazen, B.; Mohammad, D. K.; Mohammadpourhodki, R.; Mohammed, S.; Mokdad, A. H.; Morales, L.; Moreno Velasquez, I.; Mousavi, S. M.; Mukhopadhyay, S.; Nachega, J. B.; Nadkarni, G. N.; Nansseu, J. R.; Natarajan, G.; Nazari, J.; Neal, B.; Negoi, R. I.; Nguyen, C. T.; Nikbakhsh, R.; Noubiap, J. J.; Nowak, C.; Olagunju, A. T.; Ortiz, A.; Owolabi, M. O.; Palladino, R.; Pathak, M.; Poustchi, H.; Prakash, S.; Prasad, N.; Rafiei, A.; Raju, S. B.; Ramezanzadeh, K.; Rawaf, S.; Rawaf, D. L.; Rawal, L.; Reiner, R. C.; Rezapour, A.; Ribeiro, D. C.; Roever, L.; Rothenbacher, D.; Rwegerera, G. M.;

Saadatagah, S.; Safari, S.; Sahle, B. W.; Salem, H.; Sanabria, J.; Santos, I. S.; Sarveazad, A.; Sawhney, M.; Schaeffner, E.; Schmidt, M. I.; Schutte, A. E.; Sepanlou, S. G.; Shaikh, M. A.; Sharafi, Z.; Sharif, M.; Sharifi, A.; Silva, D. A. S.; Singh, J. A.; Singh, N. P.; Sisay, M. M. M.; Soheili, A.; Sutradhar, I.; Teklehaimanot, B. F.; Tesfay, B. etsay; Teshome, G. F.; Thakur, J. S.; Tonelli, M.; Tran, K. B.; Tran, B. X.; Tran Ngoc, C.; Ullah, I.; Valdez, P. R.; Varughese, S.; Vos, T.; Vu, L. G.; Waheed, Y.; Werdecker, A.; Wolde, H. F.; Wondmieneh, A. B.; Wulf Hanson, S.; Yamada, T.; Yeshaw, Y.; Yonemoto, N.; Yusefzadeh, H.; Zaidi, Z.; Zaki, L.; Zaman, S. B.; Zamora, N.; Zarghi, A.; Zewdie, K. A.; Ärnlöv, J.; Coresh, J.; Perico, N.; Remuzzi, G.; Murray, C. J. L.; Vos, T. Global, Regional, and National Burden of Chronic Kidney Disease, 1990–2017: A Systematic Analysis for the Global Burden of Disease Study 2017. The Lancet 2020, 395 (10225), 709–733. https://doi.org/10.1016/S0140-6736(20)30045-3.

(7) Saran, R.; Robinson, B.; Abbott, K. C.; Agodoa, L. Y. C.; Bhave, N.; Bragg-Gresham, J.; Balkrishnan, R.; Dietrich, X.; Eckard, A.; Eggers, P. W.; Gaipov, A.; Gillen, D.; Gipson, D.; Hailpern, S. M.; Hall, Y. N.; Han, Y.; He, K.; Herman, W.; Heung, M.; Hirth, R. A.; Hutton, D.; Jacobsen, S. J.; Jin, Y.; Kalantar-Zadeh, K.; Kapke, A.; Kovesdy, C. P.; Lavallee, D.; Leslie, J.; McCullough, K.; Modi, Z.; Molnar, M. Z.; Montez-Rath, M.; Moradi, H.; Morgenstern, H.; Mukhopadhyay, P.; Nallamothu, B.; Nguyen, D. V.; Norris, K. C.; O'Hare, A. M.; Obi, Y.; Park, C.; Pearson, J.; Pisoni, R.; Potukuchi, P. K.; Rao, P.; Repeck, K.; Rhee, C. M.; Schrager, J.; Schaubel, D. E.; Selewski, D. T.; Shaw, S. F.; Shi, J. M.; Shieu, M.; Sim, J. J.; Soohoo, M.; Steffick, D.; Streja, E.; Sumida, K.; Tamura, M. K.; Tilea, A.; Tong, L.; Wang, D.; Wang, M.; Woodside, K. J.; Xin, X.; Yin, M.; You, A. S.; Zhou, H.; Shahinian, V. US Renal Data System 2017 Annual Data Report: Epidemiology of Kidney Disease in the United States. American Journal of Kidney Diseases 2018, 71 (3, Supplement 1), A7. https://doi.org/10.1053/j.ajkd.2018.01.002.

(8) Sanz, A. B.; Ramos, A. M.; Soler, M. J.; Sanchez-Niño, M. D.; Fernandez-Fernandez, B.; Perez-Gomez, M. V.; Ortega, M. R.; Alvarez-Llamas, G.; Ortiz, A. Advances in Understanding the Role of Angiotensin-Regulated Proteins in Kidney Diseases. Expert Rev Proteomics 2019, 16 (1), 77–92. https://doi.org/10.1080/14789450.2018.1545577.

(9) Ruggenenti, P.; Ruggiero, B.; Cravedi, P.; Vivarelli, M.; Massella, L.; Marasà, M.; Chianca, A.; Rubis, N.; Ene-Iordache, B.; Rudnicki, M.; Pollastro, R. M.; Capasso, G.; Pisani, A.; Pennesi, M.; Emma, F.; Remuzzi, G. Rituximab in Steroid-Dependent or Frequently Relapsing Idiopathic Nephrotic Syndrome. JASN 2014, 25 (4), 850–863. https://doi.org/10.1681/ASN.2013030251.

(10) Liu, Y.; Shi, Y.; Ren, R.; Xie, J.; Wang, W.; Chen, N. Advanced Therapeutics in Focal and Segmental Glomerulosclerosis. Nephrology 2018, 23 (S4), 57–61. https://doi.org/10.1111/nep.13463.

(11) Tubulointerstitial Damage in Glomerular Diseases: Its Role in the Progression of Renal Damage. American Journal of Kidney Diseases 1995, 26 (1), 124–132. https://doi.org/10.1016/0272-6386(95)90165-5.

(12) In Vitro and in Vivo Interleukin-8 Production in Human Renal Cortical Epithelia. Kidney International 1992, 41 (1), 191–198. https://doi.org/10.1038/ki.1992.26.

(13) Grgic, I.; Campanholle, G.; Bijol, V.; Wang, C.; Sabbisetti, V. S.; Ichimura, T.; Humphreys, B. D.; Bonventre, J. V. Targeted Proximal Tubule Injury Triggers Interstitial Fibrosis and Glomerulosclerosis. Kidney Int 2012, 82 (2), 172–183. https://doi.org/10.1038/ki.2012.20.

(14) Lovisa, S.; Zeisberg, M.; Kalluri, R. Partial Epithelial-to-Mesenchymal Transition and Other New Mechanisms of Kidney Fibrosis. Trends in Endocrinology & Metabolism 2016, 27 (10), 681–695. https://doi.org/10.1016/j.tem.2016.06.004.
(15) Lovisa, S.; LeBleu, V. S.; Tampe, B.; Sugimoto, H.; Vadnagara, K.; Carstens, J. L.; Wu, C.-C.; Hagos, Y.; Burckhardt, B. C.; Pentcheva-Hoang, T.; Nischal, H.; Allison, J. P.; Zeisberg, M.; Kalluri, R. Epithelial-to-Mesenchymal Transition Induces Cell Cycle Arrest and Parenchymal Damage in Renal Fibrosis. Nature Medicine 2015, 21 (9), 998–1009. https://doi.org/10.1038/nm.3902.
(16) Liu, G. W.; Prossnitz, A. N.; Eng, D. G.; Cheng, Y.; Subrahmanyam, N.; Pippin, J. W.; Lamm, R. J.; Ngambenjawong, C.; Ghandehari, H.; Shankland, S. J.; Pun, S. H. Glomerular Disease Augments Kidney Accumulation of Synthetic Anionic Polymers. Biomaterials 2018, 178, 317–325. https://doi.org/10.1016/j.biomaterials.2018.06.001.
(17) Cheng, Y.; Liu, G. W.; Jain, R.; Pippin, J. W.; Shankland, S. J.; Pun, S. H. Boronic Acid Copolymers for Direct Loading and Acid-Triggered Release of Bis-T-23 in Cultured Podocytes. ACS Biomater. Sci. Eng. 2018, 4 (12), 3968–3973. https://doi.org/10.1021/acsbiomaterials.8b01163.
(18) Chen, J.; Du, L.; Li, J.; Song, H. Epigallocatechin-3-Gallate Attenuates Cadmium-Induced Chronic Renal Injury and Fibrosis. Food and Chemical Toxicology 2016, 96, 70–78. https://doi.org/10.1016/j.fct.2016.07.030.
(19) Kanlaya, R.; Peerapen, P.; Nilnumkhum, A.; Plumworasawat, S.; Sueksakit, K.; Thongboonkerd, V. Epigallocatechin-3-Gallate Prevents TGF-B1-Induced Epithelial-Mesenchymal Transition and Fibrotic Changes of Renal Cells via GSK-3β/β-Catenin/Snail1 and Nrf2 Pathways. The Journal of Nutritional Biochemistry 2020, 76, 108266. https://doi.org/10.1016/j.jnutbio.2019.108266.
(20) Perrier, S. 50th Anniversary Perspective: RAFT Polymerization - A User Guide. Macromolecules 2017, 50 (19), 7433–7447. https://doi.org/10.1021/acs.macromol.7b00767.
(21) Truong, N. P.; Jones, G. R.; Bradford, K. G. E.; Konkolewicz, D.; Anastasaki, A. A Comparison of RAFT and ATRP Methods for Controlled Radical Polymerization. Nat Rev Chem 2021, 5 (12), 859–869. https://doi.org/10.1038/s41570-021-00328-8.
(22) Thomas, D. B.; Convertine, A. J.; Hester, R. D.; Lowe, A. B.; McCormick, C. L. Hydrolytic Susceptibility of Dithioester Chain Transfer Agents and Implications in Aqueous RAFT Polymerizations. Macromolecules 2004, 37 (5), 1735–1741. https://doi.org/10.1021/ma035572t.
(23) Wolf, G.; Neilson, E. G. Angiotensin II Induces Cellular Hypertrophy in Cultured Murine Proximal Tubular Cells. Am J Physiol 1990, 259 (5 Pt 2), F768-777. https://doi.org/10.1152/ajprenal.1990.259.5.F768.
(24) Hong, J.; Lu, H.; Meng, X.; Ryu, J.-H.; Hara, Y.; Yang, C. S. Stability, Cellular Uptake, Biotransformation, and Efflux of Tea Polyphenol (−)-Epigallocatechin-3-Gallate in HT-29 Human Colon Adenocarcinoma Cells. Cancer Res 2002, 62 (24), 7241–7246.
(25) Liu, X.; Sun, N.; Mo, N.; Lu, S.; Song, E.; Ren, C.; Li, Z. Quercetin Inhibits Kidney Fibrosis and the Epithelial to Mesenchymal Transition of the Renal Tubular System Involving Suppression of the Sonic Hedgehog Signaling Pathway. Food Funct 2019, 10 (6), 3782–3797. https://doi.org/10.1039/c9fo00373h.
(26) Lu, Q.; Ji, X.-J.; Zhou, Y.-X.; Yao, X.-Q.; Liu, Y.-Q.; Zhang, F.; Yin, X.-X. Quercetin Inhibits the MTORC1/P70S6K Signaling-Mediated Renal Tubular Epithelial-

Mesenchymal Transition and Renal Fibrosis in Diabetic Nephropathy. Pharmacol Res 2015, 99, 237–247. https://doi.org/10.1016/j.phrs.2015.06.006.

Chapter 4

Modulating boronic ester stability in block copolymer micelles via the neighbor effect of copolymerized tertiary amines for controlled release of polyphenolic drugs

Alexander N. Prossnitz and Suzie H. Pun

Abstract

Boronic esters have been exploited for a variety of controlled release applications but still suffer from low stability under physiologically relevant conditions and synthetically demanding optimization to tune drug release profiles. The boronic acid functional group is an attractive conjugation chemistry for polymer-drug conjugates because it forms dynamic covalent bonds with catechols at neutral pH, which can then be reversibly cleaved under acidic conditions. We hypothesized that the high c atechol affinity and boronic ester stability of Wulf type boronic acids could be mimicked by copolymerization of phenyl boronic acid with a tertiary amine and subsequent micellization. We found that these copolymer micelles have higher affinity for catechols, such as polyphenolic drugs, than homopolymers, and that this affinity could be tuned to control drug release. These findings demonstrate that copolymerization of boronic acid and tertiary amine monomers is a powerful modular approach to improving boronic ester chemistry for drug delivery applications.

Adapted with permission from **Prossnitz** *et al.* Modulating boronic ester stability in block copolymer micelles via the neighbor effect of copolymerized tertiary amines for controlled release of polyphenolic drugs. *ACS Macro Letters* 11, 276-283 (2022).

4.1 Introduction

Polymer-drug conjugates offer unique opportunities to enhance the biodistribution, pharmacokinetics, and ultimately the efficacy of both small molecule drugs and biologics.[1–4] Key contributors to the success of these hybrid materials are stimuli-responsive linkers that release drug in specific biological contexts.[3,5] For example, the majority of macromolecular carriers are internalized in gradually acidifying (pH 7.4 to 4.5) vesicles via endocytosis.[6–8] The ubiquity of this internalization process has spurred tremendous efforts to develop acid-sensitive linkers for intracellular delivery using hydrazone, acetal, *cis*-aconityl, and Schiff base chemistries.[9–14] These approaches give polymer-drug conjugates stability and acid-triggered burst release at distinct pH values, often at the cost of extensive drug modification and the inability to tune release kinetics.[5] By comparison, the release kinetics of hydrolytic linkers have been extensively engineered to deliver relevant drug doses of chemotherapeutics, antibiotics, and antidiabetics to great *in vivo* success.[4,15,16] Additional pH-sensitive conjugation approaches that are simple, traceless, and tunable are needed to replicate the success of hydrolytic linkers intracellularly.

The use of dynamic covalent bonds, particularly between boronic acids and diols, is a promising drug conjugation approach that is both pH-sensitive and traceless.[17] Polymers with pendant boronic acid functional groups are promising materials for drug delivery due to the highly reversible and tunable stability of boronic ester bonds.[18] For example, Messersmith and coworkers conjugated bortezomib (BTZ) to a catechol-functionalized polyethylene glycol (PEG) and illustrated that BTZ was effectively released at *in vitro* at pH 5.0.[19] Still, instability of boronic ester conjugates at physiologic conditions, due to low binding affinity, has prevented the use of this linker chemistry in drug delivery systems.[19–21] One option for overcoming this obstacle is to utilize the library of modified phenyl boronic acids (PBAs) with pKas ranging from

5-9 to modulate both the catechol affinity and pH sensitivity.[22–24] However, depending on the properties of the specific catechol drug, changes to the substituents on the PBA (even if the pKa changes) may not alter affinity or drug release.[21] The complexity of synthesizing multiple substituted PBA polymers as well as the inability to finely tune the affinity of these polymers for their drug cargo has hindered the adoption of boronic-ester chemistry as a pH-sensitive drug linker.

A common approach to increase the functionality of polymer-drug conjugates is to design block copolymers that self-assemble into micellar nanoparticles (NPs).[25] Sequestration of drug cargo into the hydrophobic micellar core, enables drug release to be controlled by both linker chemistry and micelle disassembly.[26] Consequently, polymeric micelles are a mainstay of modern drug delivery technology for improving circulation time, stability, and specific drug release.[25–28] pH-sensitive micellar systems can also control drug release without the use of linkers.[29–32] For example, transistor-like pH-sensitive nanoparticles (NPs) undergo rapid micelle degradation at a target pH value.[33–36] These pH-sensitive micelles have been utilized to increase tumor penetration, gene delivery, and vaccine potency.[37–40]

To expand the toolbox of pH-sensitive linkers for polymer-drug carriers and leverage the flexibility of micellar NPs, we developed self-assembling block copolymers composed of PBA and tertiary amines to efficiently load and release catechol drugs. While investigating PBAs with high catechol binding constants, the Wulf type caught our attention.[41] This subclass of PBA has high catechol affinity, which is surprising given the absence of electron withdrawing substituents on the phenyl ring.[22,41,42] While the exact mechanism of the phenomenon has been debated, recent work has demonstrated that the presence of tertiary amines increases diol affinity by both decreasing the pKa of PBA and intermolecular acid catalysis of the solvent leaving group.[43] We

hypothesized that micelles with hydrophobic cores composed of PBA and tertiary amines would result in similar intermolecular and intramolecular interactions to the Wulf type BAs and increase the catechol binding affinity in the physiologic range. By comparing catechol affinity, micelle disassembly, and drug release of diblock copolymers with only PBA (BA) to polymers containing PBA and a tertiary amine (DB), we found that the DB polymers and micelles had higher affinity for catechols and increased stability. To the best of our knowledge, this is the first study to elucidate the neighbor effect of tertiary amines on boronic ester stability in micelles and show monomer ratio-dependent drug release kinetics. Herein, we report the synthesis and characterization of tunable PBA and tertiary amine diblock copolymer micelles that efficiently load, stabilize, and release polyphenolic drugs.

4.2 Results and Discussion

4.2.1 Polymer Synthesis and micelle characterization

We utilized the reverse addition fragmentation chain transfer (RAFT) polymerization of dimethylacrylamide (DMA) and acrylamidophenyl boronic acid (APBA) developed by Sumerlin and coworkers to synthesize diblock copolymers with various hydrophobic block lengths (Figure 1A, 1B, and S1).[44,45] Micellization occurred most efficiently when twice as much DMA mass relative to the APBA mass (5.7 kDa and 2.4 kDa respectively) was present (Table S1). For the tertiary amine-functionalized monomer, we chose N,N-dibutylaminoethylacrylamide (DBEAA), which has a sharp transition from hydrophobic to hydrophilic at ~ pH 6.5.[39,46–48] We hypothesized that the hydrophobic nature of DBEAA at neutral pH would facilitate drug encapsulation and that the hydrophilic transition at acidic pH would overcome the hydrophobicity of the APBA, leading to micelle disassembly. We polymerized the APBA and

DBEAA monomers at a ratio of approximately 1:1.5 to ensure Lewis Acid-Base pairing of the two monomers, and that the solubility properties of the DBEAA monomer would dominate. Successful copolymerization of DBEAA and APBA from the DMA macro chain transfer agent (mCTA) was confirmed via ^{1}H NMR (S2) and size exclusion chromatography (SEC) (Figure 1C).[44] BA functional groups must be protected before chromatography (S2), which slightly increases the measured molecular weight over the theoretical value (Table 1).[45] The DMA-block-APBA (BA) and DMA-block-APBAcoDBEAA (DB) polymers were nanoprecipitated into phosphate buffered saline (PBS) to form uniform micelles with diameters of 60 nm (BA) and 55 nm (DB) (Figure 1D).

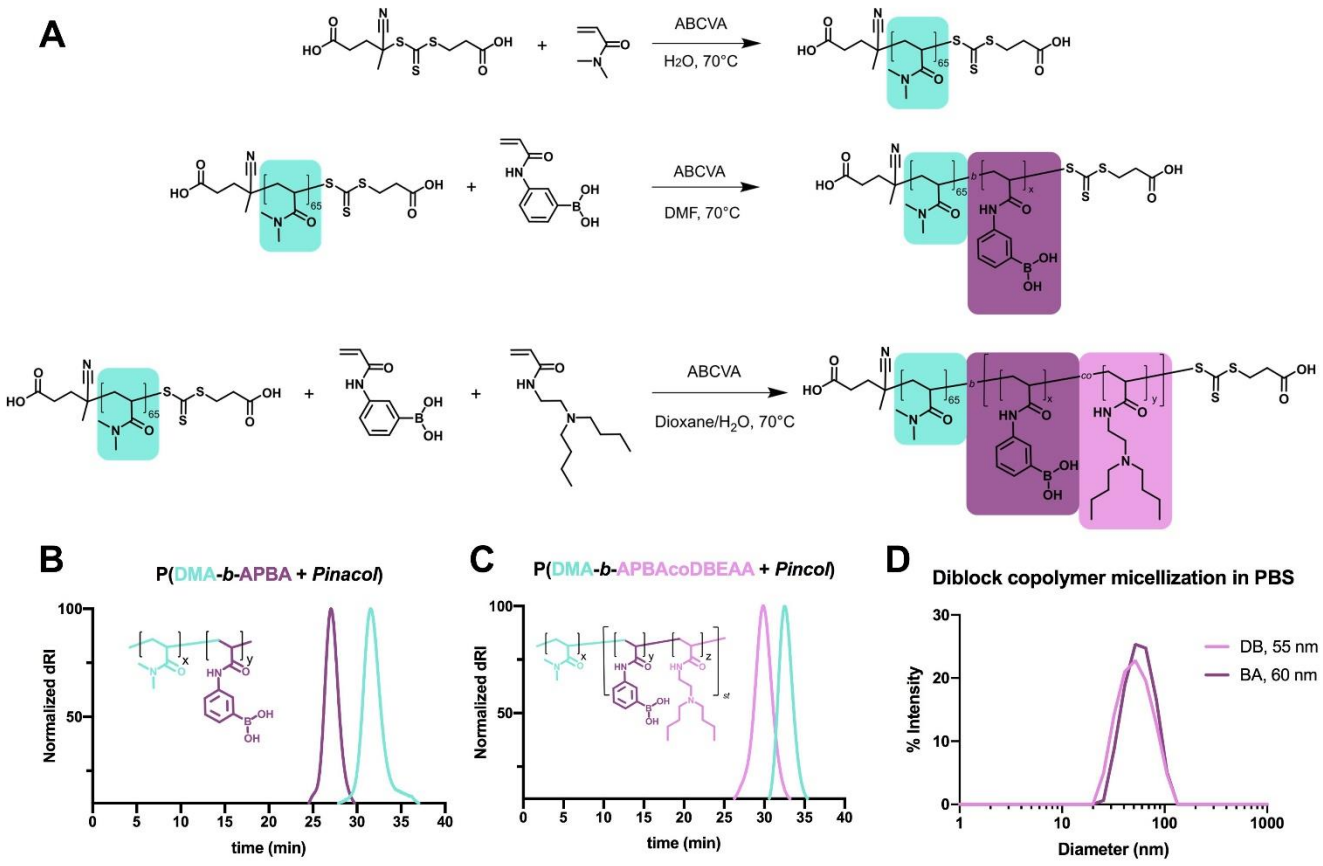

Figure 4.1 A) Synthesis scheme for diblock copolymers BA and DB using sequential RAFT polymerization. B) Comparison of SEC chromatograms of DMA mCTA and chain extended APBA copolymer after pinacol protection of the boronic acid. C) Comparison of SEC

chromatograms of DMA mCTA and chain extended APBAcoDBEAA copolymer after pinacol protection of the boronic acid. D) DLS determination of micelle size after nanoprecipitation of BA and DB diblock copolymers.

Table 4.1 Degree of polymerization and molecular weight of polymers synthesized by RAFT polymerization

Label	Polymer	APBA[a]	DBEAA[a]	$M_{n,\ theory}$ [a]	$M_{n,\ SEC}$ [b]	$Đ$ [b]
MacroCTA	PDMA	N/A	N/A	6,534	6,684	1.01
BA	P(DMA-*b*-APBA)	19	0	10,220	14,870	1.22
DB	P(DMA-*b*-APBA$_{co}$DBEAA)	16	27	15,470	16,710	1.12

[a]Determined via NMR and calculations of conversion after halting the polymerization. [b]Determined with SEC and, in the cases where the polymers contained boronic acid, the polymer was protected with pinacol functional groups.

4.2.2 Determination of catechol affinity of polymeric boronic acids via ^{19}F NMR

Next, we compared the effects of the copolymerization on catechol binding and affinity. The standard assay, quantifying the fluorescence of alizarin red, is not suitable for our polymer systems due to altered fluorescence of the dye in the presence of base and a failure to describe avidity effects in compounds with multiple boronic acids.22,49,50 Recently, 19F NMR measurements of 3-fluorocatechol (F-Cat) in the presence of boronic acids have illustrated exquisite sensitivity, quantitatively differentiating free and bound catechols.50–52 In particular, Larcher et al. illustrated that distinct fluorine peaks could be differentiated for each F-Cat bound to a multi-functional boronic acid and confirmed the identity of these boronic ester species with 11B NMR.50 We investigated boronic ester formation of a model small molecule boronic acid (carboxyphenyl boronic acid, CPBA), and the polymers (BA and DB) in organic solutions to eliminate interference from micellization. CPBA only achieved a 46% conversion of F-Cat to boronic ester, even in the presence of 20-fold molar excess of CPBA (S5A). In contrast to CPBA, the DB polymer showed quantitative conversion of all boronic acids

to boronic esters while the F-Cat remained in excess, and complete conversion of the F-Cat to ester when the boronic acid was in excess (Figure 2A and S4B). To compare the binding affinities of CPBA, DB, and BA, we graphed the percent of F-Cat bound to boronic acid as a function of the ratio of boronic acid to catechol (Figure 2B). We observed low maxima in catechol binding for both the CPBA and BA polymers (49% and 33% respectively), while the DB polymer reached 100%. This data provides strong evidence that copolymerization of a tertiary amine monomer dramatically increases the affinity of boronic acid monomers for catechols.

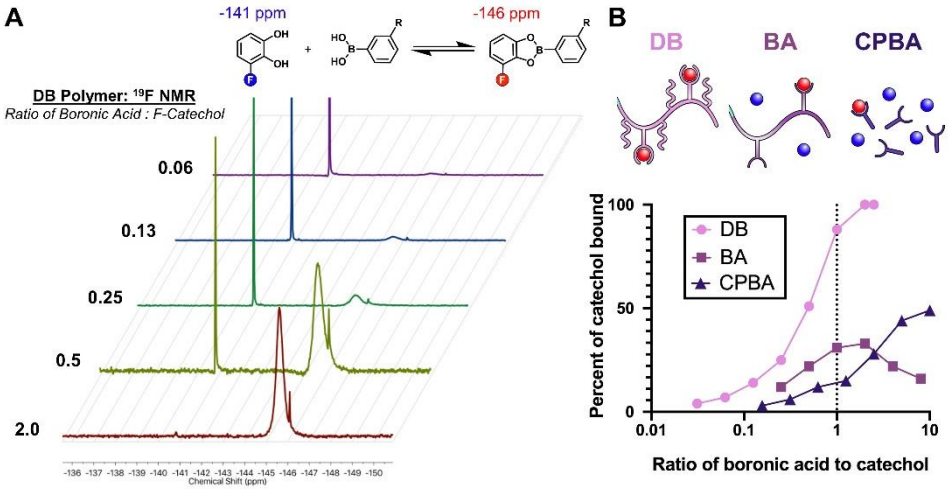

Figure 4.2 A) Equilibrium of F-Cat and DB polymer complex at various boronic acid to catechol ratios measured by ^{19}F NMR and normalized to free F-Cat signal. B) Schematic depicting higher binding affinity and quantitative binding of catechols to DB polymer compared to the mixture of bound and unbound catechols in the presence of BA polymer and CPBA. Percent of F-Cat bound to boronic acid and converted to boronic ester as a function of boronic acid to catechol ratio for DB polymer, BA polymer, and CPBA.

4.2.3 Drug loading optimization of DB micelles with EGCG, Quercetin, and EA

We next loaded the DB polymer with a variety of polyphenolic drugs.[53] Specifically, we selected epigallocatechin gallate (EGCG), quercetin, and ellagic acid (EA) as therapeutic polyphenols of interest.[54–61] These drugs span a range of solubility, from the hydrophilic EGCG to the hydrophobic quercetin, and finally the extremely insoluble EA (aqueous solubility of 10 μg/mL[62]). DB-drug micelles

(~40 nm) were formed by simple mixing, nanoprecipitation, and dialysis (Figures 3A and 3B). The spectroscopic profiles of the drug-loaded micelles revealed increases in absorption upon drug-loading (~400 nm for quercetin and EA, and ~312 nm for EGCG, Figure 3C). We varied the drug weight percent in the formulation and determined the maximum drug loading by quantifying this spectroscopic shift (Figure 3D). Drug concentration did not linearly correlate with drug loading due to drug aggregation at high concentrations, as quantified by monitoring turbidity at 750 nm (Figure 3E). We observed aggregation at loadings as low as 20% weight for EA and 30% weight for quercetin. The hydrophilic EGCG also had a maximum drug loading at 30% weight despite remaining soluble at this concentration. In contrast to the micellar formulations of quercetin or EA, which maintained diameters < 100 nm, the DB-EGCG conjugates more than doubled in diameter at 30% weight (from 93 nm to 217 nm) and continued to increase as more drug was added (Figure 3F). We hypothesize that excess EGCG in the solution caused intramolecular crosslinking of micelles into gels, decreasing the drug loading for the EGCG conjugates at higher weight percentage. To summarize, we determined that EGCG and quercetin could be stably loaded into DB micelles at amounts as high as 20% by weight, and that even the extremely insoluble EA could be loaded effectively at 10% weight. To our knowledge, this approach is the only reported nanoparticle system to covalently load EA.[63]

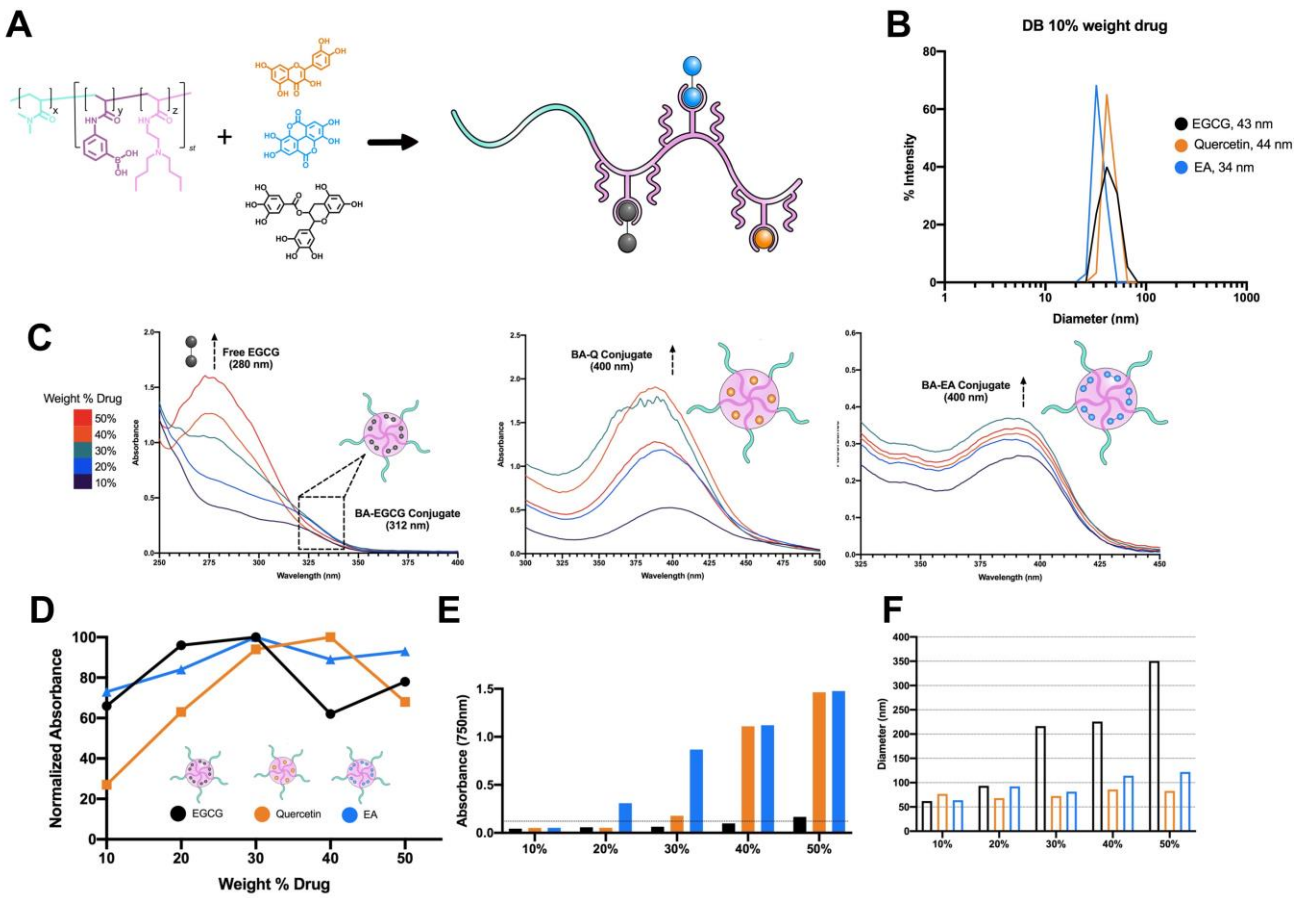

Figure 4.3 A) Representation of complexing polyphenolic drugs Quercetin, EA and EGCG with the boronic acids in the DB polymer. B) Determination of micelle size in PBS after nanoprecipitation of each polymer drug conjugate loaded with 10% weight drug. C) UV-Vis spectra for each polymer drug micelle at 10%, 20%, 30%, 40% and 50% weight drug. D) Comparison of normalized absorbance intensity at the wavelength characteristic to the polymer drug conjugate (EGCG, 312 nm), (Quercetin, 400 nm), and (EA, 400 nm) at various weight percentages. E) Transparency of micelle solutions at various weight percentages. F) Diameter of soluble micelles at various weight percentages.

4.2.4 pH sensitive micelle disassembly

We then compared the pH sensitivity and drug protection of BA and DB micelles. First, we used the solvatochromic dye Nile Red, which is fluorescent inside the lipophilic core of micelles, but not in aqueous solvents.[25] We were particularly interested to learn if protonation of the DBEAA monomer would overcome the hydrophobicity of the APBA monomer and trigger micelle disassembly under acidic conditions (Figure 4A). At neutral pH, both BA and DB micelles had high Nile Red fluorescence reflecting micellar encapsulation, but the fluorescence of the DB micelle decreased with pH, indicative

of micelle disassembly in acidic conditions. In contrast, the BA polymer fluorescence remained relatively constant between pH 5.5 and 7.4 (Figure 4B). Additionally, at the basic pH of 11 (above the pKa for APBA) the BA micelles disassembled into unimers while the DB micelles remained intact, likely due to increased hydrophobicity provided by the DBEAA monomers at this pH.

4.2.5 Optimization of tertiary amine content in DB block copolymers

To optimize the APBA and DBEAA ratio, we synthesized a second polymer with ~50% more DBEAA (DB 2.5). While the DB 2.5 micelles remained pH sensitive (S6), we observed significant decreases in both drug loading and stability for all three drug formulations (S7). We hypothesized that at higher DBEAA to APBA ratios, the increased hydrophobicity of the second block and the presence of drugs caused precipitation. Supporting this hypothesis, we found that increasing the APBA content also led to aggregation and precipitation (Table S2). Given these limitations in addition to those established for the BA polymers, we continued to study the original DB polymer (1.7 DBEAA to APBA).

4.2.6 Prevention of radical scavenging due to high binding affinity DB polymer

Subsequently, we investigated the functional effect of this high drug affinity by comparing the radical scavenging activity and polyphenol stability of both polymer-drug conjugates. The radical scavenging activity of catechol drugs is primarily due to free phenols and is significantly reduced when bound to boronic acid. We hypothesized that the higher affinity of the DB polymers would result in larger decreases in the radical scavenging activity of the bound catechol. We used the 2,2 diphenyl-1-picrylhydrazyl (DPPH) to assess radical scavenging activity, correlating antioxidant activity with decreased absorbance at 517 nm (Figure 4C). [64,65] We found that the DB polymers dramatically reduced the scavenging ability of EA, and even decreased the reactivity of EGCG (Figure 4D and E). The DB polymer is more effective at preventing EA reactivity likely because all the phenols of EA can be complexed to boronic acids. In the EGCG-polymer conjugate, at best, only 50% of the phenol groups

can be protected by esterification. Quercetin conjugates were not tested due to interference from its extremely high absorbance values when complexed to boronic acids (S5).

4.2.7 Increased catechol affinity enhances polyphenol stability

Additionally, we explored the stability of the drug-loaded micelles by monitoring polyphenol oxidation in a forced degradation experiment. Forced degradation experiments determine the stability of drugs or therapeutics under harsh conditions to rapidly compare properties of different formulations.[66] The main pathway for polyphenol degradation is oxidation of the phenols, which occurs quickly, even at neutral pH.[67,68] We exposed EA, selected due to its clear shift in absorbance at 425 upon oxidation, BA-EA, and DB-EA micelles to increasing amounts of NaOH (Figures 4F,G,H). We expected the formation of boronic esters to prevent oxidation of EA in a manner proportional to the binding affinity. The BA micelles slightly increased the EC_{50} value of oxidizing agent (NaOH) from 4.2 mM to 5.3 mM, whereas the DB micelles more than doubled the EC_{50} to 9.4 mM (Figure 4I). Thus, nanocarriers synthesized by copolymerization of APBA and DBEAA can help overcome the inherent instability of polyphenol therapeutics.

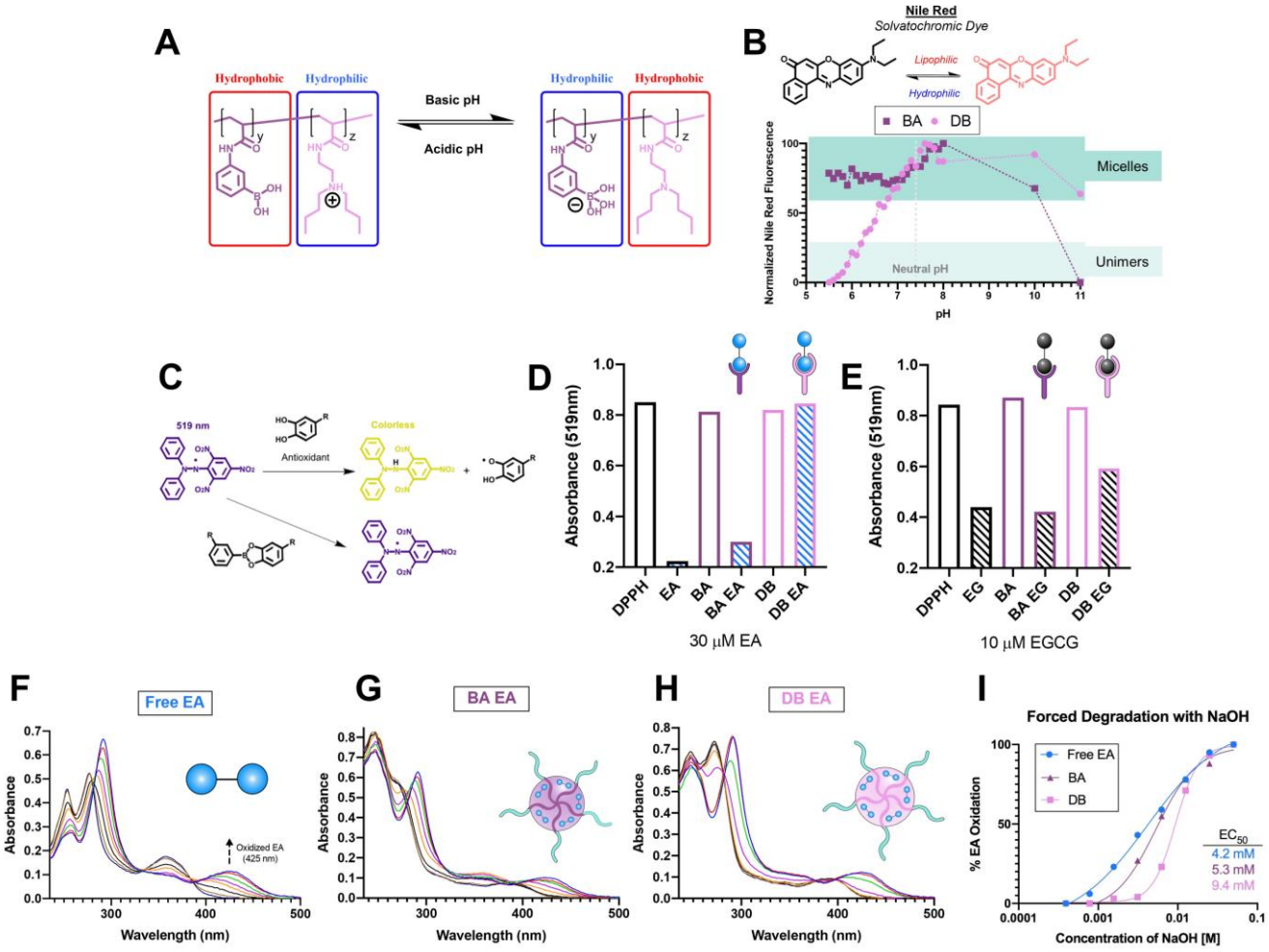

Figure 4.4 A) Scheme of pH dependent transition in ionization state of DB polymer. B) Determination of micelle stability between pH 5.5 and 11 for BA and DB polymers. The increased fluorescence of solvatochromic dye Nile Red indicates the presence of micelles. C) Depiction of DPPH assay for determining antioxidant potential. D) Comparison of radical scavenging activity of EA, polymers, and polymer-drug conjugates at 10% weight drug in methanol. E) Comparison of radical scavenging activity of EGCG, polymers, and polymer-drug conjugates at 10% weight drug in methanol. F) UV-Vis of free EA at 425 nm as a function of increased NaOH concentration and drug oxidation. G) UV-Vis of BA-EA conjugate at 425 nm as a function of increased NaOH concentration and drug oxidation. H) UV-Vis of DB-EA conjugate at 425 nm as a function of increased NaOH concentration and drug oxidation. I) Percent oxidation of EA in solution, BA micelles or DB micelles at various NaOH concentrations. EC_{50} values were determined by normalization and nonlinear curve fitting.

4.2.8 Monomer ratio dependent drug release kinetics

Since the BA and DB copolymers have dramatic differences in catechol affinity, we were interested in exploiting these interactions to tailor drug release profiles. We hypothesized that DB micelles would release minimal drug at physiologic pH (7.4), but that BA micelles would slowly release a substantial amount of drug. To test if the drug release rate was proportional to the tertiary amine content of the micelle, we compared the release rate of 20% weight quercetin loaded BA, DB, and 1:1 DB to BA mixed micelles using the dialysis method at pH 7.4 and 4.5 (Figure 5A).25 We chose quercetin because it had the lowest limit of detection, due to the high absorbance of the free drug at 380 nm. At neutral pH, we found that the BA micelles indeed released a substantial amount of cargo (20%) while both micelles containing the DB polymer released half that amount (~10%) over 24 h (Figure 5B). At pH 4.5, again we saw the BA polymer release the most drug over 24 h at 43%. The 1:1 mixed micelle released up to 34% of the encapsulated drug, which was much greater than the release from the DB micelles of 19% (Figure 5C). Comparatively, the mixed micelles released 3-fold more drug under acidic conditions while both the BA and DB polymers only showed a 2-fold increase. The lower affinity of the mixed micelle for the catechol drugs (compared to the DB micelle) combined with the pH sensitive disassembly (compared to the BA micelle) may cause the increase in pH-dependent drug release. These results illustrate that the drug release rate from boronic acid micelles can be incrementally tuned by titrating a tertiary amine comonomer.

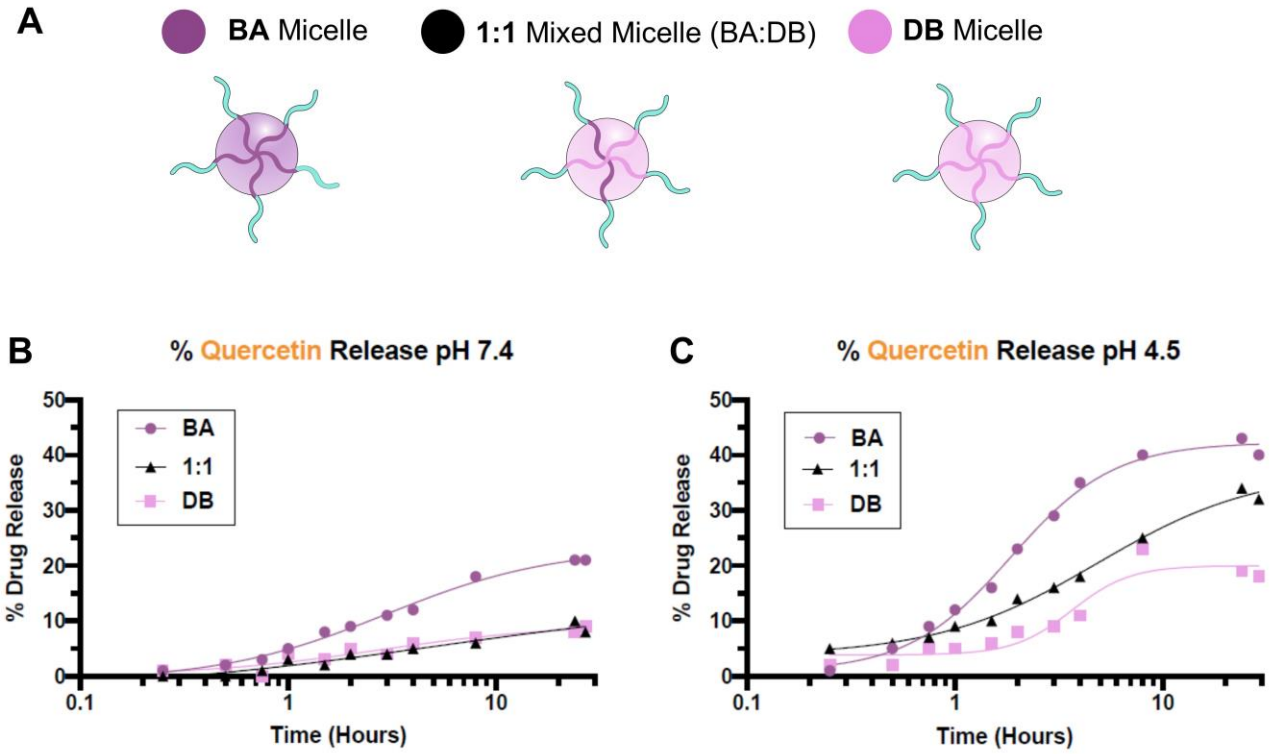

Figure 4.5 A) Formulation of 20% by weight Q micelles with BA polymer, DB polymer or an equal mix of BA and DB polymer. B) Percent drug release determined by dialysis of BA, a 1:1 mix of BA and DB, and DB micelles over 24 hours at pH 7.4. C) Percent drug release determined by dialysis of BA, a 1:1 mix of BA and DB, and DB micelles over 24 hours at pH 4.5.

4.3 Conclusions

We illustrated that boronic acid affinity for catechols in micellar systems can be tuned using the neighbor effect of tertiary amines. We successfully synthesized diblock copolymers that can encapsulate polyphenols, agnostic of solubility, up to 20% by weight. Compared to copolymers without the tertiary amines, these DB polymers showed higher binding affinity to catechols, disassembled at acidic pH, and protected polyphenolic drugs from degradation. Additionally, these drug-loaded DB micelles exhibit higher stability at neutral pH and tunable drug release profiles. These results highlight a paradigm shift in the design of boronic acid

micelles for drug delivery, whereby disassembly and drug release can be modularly controlled simply by varying comonomer ratios. The potential of the DB platform for drug delivery is underscored by the successful loading, stabilization, and release of several polyphenolic drugs. With applications in treating cancer, preventing neurodegeneration, and protecting against oxidative stress, effective polyphenolic delivery vehicles must be designed with release profiles specifically tailored to the drug and target disease.[55,57,58,61,69,70] Future work will explore translation of these tailored and drug-loaded DB micelles to treat cancer and protect cells from oxidative stress *in vitro* and *in vivo.*

ACKNOWLEDGMENTS

This work was supported by DOD W81XWH-20-1-0440 (PR190121) and W81XWH-16-1-0167 (PR151175) and a National Science Foundation Graduate Research Fellowship Grant No. DGE-1762114 to ANP. We thank Shixian Lv, Trey Pichon, and Daniel C. Lee for sharing their time and expertise in the form of thoughtful discussions. We also thank the Institute for Protein Design for the use of their Wyatt DynaPro NanoStar DLS.

4.4 References

(1) Ekladious, I.; Colson, Y. L.; Grinstaff, M. W. Polymer–Drug Conjugate Therapeutics: Advances, Insights and Prospects. *Nat. Rev. Drug Discov.* **2019**, *18* (4), 273–294. https://doi.org/10.1038/s41573-018-0005-0.

(2) Harada, M.; Bobe, I.; Saito, H.; Shibata, N.; Tanaka, R.; Hayashi, T.; Kato, Y. Improved Anti-Tumor Activity of Stabilized Anthracycline Polymeric Micelle Formulation, NC-6300. *Cancer Sci.* **2011**, *102* (1), 192–199. https://doi.org/10.1111/j.1349-7006.2010.01745.x.

(3) Gong, Y.; Leroux, J.-C.; Gauthier, M. A. Releasable Conjugation of Polymers to Proteins. *Bioconjug. Chem.* **2015**, *26* (7), 1172–1181. https://doi.org/10.1021/bc500611k.

(4) Das, D.; Chen, J.; Srinivasan, S.; Kelly, A. M.; Lee, B.; Son, H.-N.; Radella, F.; West, T. E.; Ratner, D. M.; Convertine, A. J.; Skerrett, S. J.; Stayton, P. S. Synthetic Macromolecular Antibiotic Platform for Inhalable Therapy against Aerosolized Intracellular Alveolar Infections. *Mol. Pharm.* **2017**, *14* (6), 1988–1997. https://doi.org/10.1021/acs.molpharmaceut.7b00093.

(5) Ghosal, S.; Walker, J. E.; Alabi, C. A. Predictive Platforms of Bond Cleavage and Drug Release Kinetics for Macromolecule–Drug Conjugates. *Annu. Rev. Chem. Biomol. Eng.* **2021**, *12* (1), 241–261. https://doi.org/10.1146/annurev-chembioeng-091720-030636.

(6) Rennick, J. J.; Johnston, A. P. R.; Parton, R. G. Key Principles and Methods for Studying the Endocytosis of Biological and Nanoparticle Therapeutics. *Nat. Nanotechnol.* **2021**, *16* (3), 266–276. https://doi.org/10.1038/s41565-021-00858-8.

(7) Hu, Y.-B.; Dammer, E. B.; Ren, R.-J.; Wang, G. The Endosomal-Lysosomal System: From Acidification and Cargo Sorting to Neurodegeneration. *Transl. Neurodegener.* **2015**, *4* (1), 18. https://doi.org/10.1186/s40035-015-0041-1.

(8) Olden, B. R.; Cheng, E.; Cheng, Y.; Pun, S. H. Identifying Key Barriers in Cationic Polymer Gene Delivery to Human T Cells. *Biomater. Sci.* **2019**, *7* (3), 789–797. https://doi.org/10.1039/c8bm01262h.

(9) Pang, X.; Jiang, Y.; Xiao, Q.; Leung, A. W.; Hua, H.; Xu, C. PH-Responsive Polymer–Drug Conjugates: Design and Progress. *J. Controlled Release* **2016**, *222*, 116–129. https://doi.org/10.1016/j.jconrel.2015.12.024.

(10) Kakinoki, A.; Kaneo, Y.; Ikeda, Y.; Tanaka, T.; Fujita, K. Synthesis of Poly(Vinyl Alcohol)-Doxorubicin Conjugates Containing Cis-Aconityl Acid-Cleavable Bond and Its Isomer Dependent Doxorubicin Release. *Biol. Pharm. Bull.* **2008**, *31* (1), 103–110. https://doi.org/10.1248/bpb.31.103.

(11) Gillies, E. R.; Goodwin, A. P.; Frechet, J. M. J. Acetals as PH-Sensitive Linkages for Drug Delivery. 10.

(12) Zou, J.; Jafr, G.; Themistou, E.; Yap, Y.; Wintrob, Z. A. P.; Alexandridis, P.; Ceacareanu, A. C.; Cheng, C. PH-Sensitive Brush Polymer-Drug Conjugates by Ring-Opening Metathesis Copolymerization. *Chem. Commun.* **2011**, *47* (15), 4493–4495. https://doi.org/10.1039/C0CC05531J.

(13) Ke, X.; Coady, D. J.; Yang, C.; Engler, A. C.; Hedrick, J. L.; Yang, Y. Y. PH-Sensitive Polycarbonate Micelles for Enhanced Intracellular Release of Anticancer Drugs: A Strategy to Circumvent Multidrug Resistance. *Polym. Chem.* **2014**, *5* (7), 2621. https://doi.org/10.1039/c3py01784b.

(14) Bae, Y.; Nishiyama, N.; Fukushima, S.; Koyama, H.; Yasuhiro, M.; Kataoka, K. Preparation and Biological Characterization of Polymeric Micelle Drug Carriers with Intracellular PH-Triggered Drug Release Property: Tumor Permeability, Controlled Subcellular

Drug Distribution, and Enhanced in Vivo Antitumor Efficacy. *Bioconjug. Chem.* **2005**, *16* (1), 122–130. https://doi.org/10.1021/bc0498166.
(15) Vohidov, F.; Andersen, J. N.; Economides, K. D.; Shipitsin, M. V.; Burenkova, O.; Ackley, J. C.; Vangamudi, B.; Nguyen, H. V.-T.; Gallagher, N. M.; Shieh, P.; Golder, M. R.; Liu, J.; Dahlberg, W. K.; Ehrlich, D. J. C.; Kim, J.; Kristufek, S. L.; Huh, S. J.; Neenan, A. M.; Baddour, J.; Paramasivan, S.; de Stanchina, E.; KC, G.; Turnquist, D. J.; Saucier-Sawyer, J. K.; Kopesky, P. W.; Brady, S. W.; Jessel, M. J.; Reiter, L. A.; Chickering, D. E.; Johnson, J. A.; Blume-Jensen, P. Design of BET Inhibitor Bottlebrush Prodrugs with Superior Efficacy and Devoid of Systemic Toxicities. *J. Am. Chem. Soc.* **2021**, *143* (12), 4714–4724. https://doi.org/10.1021/jacs.1c00312.
(16) Santi, D. V.; Schneider, E. L.; Reid, R.; Robinson, L.; Ashley, G. W. Predictable and Tunable Half-Life Extension of Therapeutic Agents by Controlled Chemical Release from Macromolecular Conjugates. *Proc. Natl. Acad. Sci.* **2012**, *109* (16), 6211–6216. https://doi.org/10.1073/pnas.1117147109.
(17) Stubelius, A.; Lee, S.; Almutairi, A. The Chemistry of Boronic Acids in Nanomaterials for Drug Delivery. *Acc. Chem. Res.* **2019**, *52* (11), 3108–3119. https://doi.org/10.1021/acs.accounts.9b00292.
(18) Brooks, W. L. A.; Sumerlin, B. S. Synthesis and Applications of Boronic Acid-Containing Polymers: From Materials to Medicine. *Chem. Rev.* **2016**, *116* (3), 1375–1397. https://doi.org/10.1021/acs.chemrev.5b00300.
(19) Su, J.; Chen, F.; Cryns, V. L.; Messersmith, P. B. Catechol Polymers for PH-Responsive, Targeted Drug Delivery to Cancer Cells. *J. Am. Chem. Soc.* **2011**, *133* (31), 11850–11853. https://doi.org/10.1021/ja203077x.
(20) Xie, C.; Yang, C.; Zhang, P.; Zhang, J.; Wu, W.; Jiang, X. Synthesis of Drug-Crosslinked Polymer Nanoparticles. *Polym. Chem.* **2015**, *6* (10), 1703–1713. https://doi.org/10.1039/C4PY01722F.
(21) Cheng, Y.; Liu, G. W.; Jain, R.; Pippin, J. W.; Shankland, S. J.; Pun, S. H. Boronic Acid Copolymers for Direct Loading and Acid-Triggered Release of Bis-T-23 in Cultured Podocytes. *ACS Biomater. Sci. Eng.* **2018**, *4* (12), 3968–3973. https://doi.org/10.1021/acsbiomaterials.8b01163.
(22) Brooks, W. L. A.; Deng, C. C.; Sumerlin, B. S. Structure–Reactivity Relationships in Boronic Acid–Diol Complexation. *ACS Omega* **2018**, *3* (12), 17863–17870. https://doi.org/10.1021/acsomega.8b02999.
(23) Suzuki, Y.; Kusuyama, D.; Sugaya, T.; Iwatsuki, S.; Inamo, M.; Takagi, H. D.; Ishihara, K. Reactivity of Boronic Acids toward Catechols in Aqueous Solution. *J. Org. Chem.* **2020**, *85* (8), 5255–5264. https://doi.org/10.1021/acs.joc.9b03326.
(24) Yan, J.; Springsteen, G.; Deeter, S.; Wang, B. The Relationship among PKa, PH, and Binding Constants in the Interactions between Boronic Acids and Diols—It Is Not as Simple as It Appears. *Tetrahedron* **2004**, *60* (49), 11205–11209. https://doi.org/10.1016/j.tet.2004.08.051.
(25) Ghezzi, M.; Pescina, S.; Padula, C.; Santi, P.; Del Favero, E.; Cantù, L.; Nicoli, S. Polymeric Micelles in Drug Delivery: An Insight of the Techniques for Their Characterization and Assessment in Biorelevant Conditions. *J. Controlled Release* **2021**, *332*, 312–336. https://doi.org/10.1016/j.jconrel.2021.02.031.
(26) Mitchell, M. J.; Billingsley, M. M.; Haley, R. M.; Wechsler, M. E.; Peppas, N. A.; Langer, R. Engineering Precision Nanoparticles for Drug Delivery. *Nat. Rev. Drug Discov.* **2021**, *20* (2), 101–124. https://doi.org/10.1038/s41573-020-0090-8.

(27) Kakkar, A.; Traverso, G.; Farokhzad, O. C.; Weissleder, R.; Langer, R. Evolution of Macromolecular Complexity in Drug Delivery Systems. *Nat. Rev. Chem.* **2017**, *1* (8), 0063. https://doi.org/10.1038/s41570-017-0063.
(28) Aguirre-Chagala, Y. E.; Santos, J. L.; Aguilar-Castillo, B. A.; Herrera-Alonso, M. Synthesis of Copolymers from Phenylboronic Acid-Installed Cyclic Carbonates. *ACS Macro Lett.* **2014**, *3* (4), 353–358. https://doi.org/10.1021/mz500047p.
(29) Rozema, D. B.; Ekena, K.; Lewis, D. L.; Loomis, A. G.; Wolff, J. A. Endosomolysis by Masking of a Membrane-Active Agent (EMMA) for Cytoplasmic Release of Macromolecules. *Bioconjug. Chem.* **2003**, *14* (1), 51–57. https://doi.org/10.1021/bc0255945.
(30) Gillies, E. R.; Fréchet, J. M. J. A New Approach towards Acid Sensitive Copolymer Micelles for Drug Delivery. *Chem Commun* **2003**, No. 14, 1640–1641. https://doi.org/10.1039/B304251K.
(31) Heller, J.; Barr, J.; Ng, S. Y.; Abdellauoi, K. S.; Gurny, R. Poly(Ortho Esters): Synthesis, Characterization, Properties and Uses. *Adv. Drug Deliv. Rev.* **2002**, *54* (7), 1015–1039. https://doi.org/10.1016/S0169-409X(02)00055-8.
(32) Heffernan, M. J.; Murthy, N. Polyketal Nanoparticles: A New PH-Sensitive Biodegradable Drug Delivery Vehicle. *Bioconjug. Chem.* **2005**, *16* (6), 1340–1342. https://doi.org/10.1021/bc050176w.
(33) Feng, Q.; Wilhelm, J.; Gao, J. Transistor-like Ultra-PH-Sensitive Polymeric Nanoparticles. *Acc. Chem. Res.* **2019**, *52* (6), 1485–1495. https://doi.org/10.1021/acs.accounts.9b00080.
(34) Li, Y.; Wang, Y.; Huang, G.; Gao, J. Cooperativity Principles in Self-Assembled Nanomedicine. *Chem. Rev.* **2018**, *118* (11), 5359–5391. https://doi.org/10.1021/acs.chemrev.8b00195.
(35) Li, Y.; Wang, Z.; Wei, Q.; Luo, M.; Huang, G.; Sumer, B. D.; Gao, J. Non-Covalent Interactions in Controlling PH-Responsive Behaviors of Self-Assembled Nanosystems. *Polym. Chem.* **2016**, *7* (38), 5949–5956. https://doi.org/10.1039/C6PY01104G.
(36) Bennett, Z. T.; Feng, Q.; Bishop, J. A.; Huang, G.; Sumer, B. D.; Gao, J. Detection of Lymph Node Metastases by Ultra-PH-Sensitive Polymeric Nanoparticles. *Theranostics* **2020**, *10* (7), 3340–3350. https://doi.org/10.7150/thno.41239.
(37) Li, S.; Luo, M.; Wang, Z.; Feng, Q.; Wilhelm, J.; Wang, X.; Li, W.; Wang, J.; Cholka, A.; Fu, Y.; Sumer, B. D.; Yu, H.; Gao, J. Prolonged Activation of Innate Immune Pathways by a Polyvalent STING Agonist. *Nat. Biomed. Eng.* **2021**, *5* (5), 455–466. https://doi.org/10.1038/s41551-020-00675-9.
(38) Li, H.-J.; Du, J.-Z.; Liu, J.; Du, X.-J.; Shen, S.; Zhu, Y.-H.; Wang, X.; Ye, X.; Nie, S.; Wang, J. Smart Superstructures with Ultrahigh PH-Sensitivity for Targeting Acidic Tumor Microenvironment: Instantaneous Size Switching and Improved Tumor Penetration. *ACS Nano* **2016**, *10* (7), 6753–6761. https://doi.org/10.1021/acsnano.6b02326.
(39) Cheng, Y.; Yumul, R. C.; Pun, S. H. Virus-Inspired Polymer for Efficient In Vitro and In Vivo Gene Delivery. *Angew. Chem. Int. Ed.* **2016**, *55* (39), 12013–12017. https://doi.org/10.1002/anie.201605958.
(40) Ulkoski, D.; Munson, M. J.; Jacobson, M. E.; Palmer, C. R.; Carson, C. S.; Sabirsh, A.; Wilson, J. T.; Krishnamurthy, V. R. High-Throughput Automation of Endosomolytic Polymers for MRNA Delivery. *ACS Appl. Bio Mater.* **2021**, *4* (2), 1640–1654. https://doi.org/10.1021/acsabm.0c01463.

(41) Wulff, G.; Lauer, M.; Böhnke, H. Rapid Proton Transfer as Cause of an Unusually Large Neighboring Group Effect. *Angew. Chem. Int. Ed. Engl.* **1984**, *23* (9), 741–742. https://doi.org/10.1002/anie.198407411.
(42) Wiskur, S. L.; Lavigne, J. J.; Ait-Haddou, H.; Lynch, V.; Chiu, Y. H.; Canary, J. W.; Anslyn, E. V. PKa Values and Geometries of Secondary and Tertiary Amines Complexed to Boronic AcidsImplications for Sensor Design. *Org. Lett.* **2001**, *3* (9), 1311–1314. https://doi.org/10.1021/ol0156805.
(43) Sun, X.; Chapin, B. M.; Metola, P.; Collins, B.; Wang, B.; James, T. D.; Anslyn, E. V. The Mechanisms of Boronate Ester Formation and Fluorescent Turn-on in Ortho-Aminomethylphenylboronic Acids. *Nat. Chem.* **2019**, *11* (9), 768–778. https://doi.org/10.1038/s41557-019-0314-x.
(44) Bapat, A. P.; Roy, D.; Ray, J. G.; Savin, D. A.; Sumerlin, B. S. Dynamic-Covalent Macromolecular Stars with Boronic Ester Linkages. *J. Am. Chem. Soc.* **2011**, *133* (49), 19832–19838. https://doi.org/10.1021/ja207005z.
(45) Roy, D.; Cambre, J. N.; Sumerlin, B. S. Sugar-Responsive Block Copolymers by Direct RAFT Polymerization of Unprotected Boronic Acid Monomers. *Chem. Commun.* **2008**, No. 21, 2477. https://doi.org/10.1039/b802293c.
(46) Wang, K.; Song, Z.; Liu, C.; Zhang, W. RAFT Synthesis of Triply Responsive Poly[N-[2-(Dialkylamino)Ethyl]Acrylamide]s and Their N-Substitute Determined Response. *Polym. Chem.* **2016**, *7* (20), 3423–3433. https://doi.org/10.1039/C6PY00526H.
(47) Li, Y.; Wang, Z.; Wei, Q.; Luo, M.; Huang, G.; Sumer, B. D.; Gao, J. Non-Covalent Interactions in Controlling PH-Responsive Behaviors of Self-Assembled Nanosystems. *Polym. Chem.* **2016**, *7* (38), 5949–5956. https://doi.org/10.1039/C6PY01104G.
(48) Kitano, S.; Hisamitsu, I.; Koyama, Y.; Kataoka, K.; Okano, T.; Sakurai, Y. Effect of the Incorporation of Amino Groups in a Glucose-Responsive Polymer Complex Having Phenylboronic Acid Moieties. *Polym. Adv. Technol.* **1991**, *2* (5), 261–264. https://doi.org/10.1002/pat.1991.220020508.
(49) Springsteen, G.; Wang, B. A Detailed Examination of Boronic Acid–Diol Complexation. *Tetrahedron* **2002**, *58* (26), 5291–5300. https://doi.org/10.1016/S0040-4020(02)00489-1.
(50) Larcher, A.; Lebrun, A.; Smietana, M.; Laurencin, D. A Multinuclear NMR Perspective on the Complexation between Bisboronic Acids and Bisbenzoxaboroles with *Cis* -Diols. *New J. Chem.* **2018**, *42* (4), 2815–2823. https://doi.org/10.1039/C7NJ04143H.
(51) Iannazzo, L.; Benedetti, E.; Catala, M.; Etheve-Quelquejeu, M.; Tisné, C.; Micouin, L. Monitoring of Reversible Boronic Acid–Diol Interactions by Fluorine NMR Spectroscopy in Aqueous Media. *Org. Biomol. Chem.* **2015**, *13* (33), 8817–8821. https://doi.org/10.1039/C5OB01362C.
(52) Axthelm, J.; Askes, S. H. C.; Elstner, M.; G, U. R.; Görls, H.; Bellstedt, P.; Schiller, A. Fluorinated Boronic Acid-Appended Pyridinium Salts and 19F NMR Spectroscopy for Diol Sensing. *J. Am. Chem. Soc.* **2017**, *139* (33), 11413–11420. https://doi.org/10.1021/jacs.7b01167.
(53) Huang, Z.; Delparastan, P.; Burch, P.; Cheng, J.; Cao, Y.; Messersmith, P. B. Injectable Dynamic Covalent Hydrogels of Boronic Acid Polymers Cross-Linked by Bioactive Plant-Derived Polyphenols. *Biomater. Sci.* **2018**, *6* (9), 2487–2495. https://doi.org/10.1039/C8BM00453F.
(54) Rady, I.; Mohamed, H.; Rady, M.; Siddiqui, I. A.; Mukhtar, H. Cancer Preventive and Therapeutic Effects of EGCG, the Major Polyphenol in Green Tea. *Egypt. J. Basic Appl. Sci.* **2018**, *5* (1), 1–23. https://doi.org/10.1016/j.ejbas.2017.12.001.

(55) Ramassamy, C. Emerging Role of Polyphenolic Compounds in the Treatment of Neurodegenerative Diseases: A Review of Their Intracellular Targets. *Eur. J. Pharmacol.* **2006**, *545* (1), 51–64. https://doi.org/10.1016/j.ejphar.2006.06.025.
(56) Panche, A. N.; Diwan, A. D.; Chandra, S. R. Flavonoids: An Overview. *J. Nutr. Sci.* **2016**, *5*, e47. https://doi.org/10.1017/jns.2016.41.
(57) Wang, H.; Wang, C.; Zou, Y.; Hu, J.; Li, Y.; Cheng, Y. Natural Polyphenols in Drug Delivery Systems: Current Status and Future Challenges. *Giant* **2020**, *3*, 100022. https://doi.org/10.1016/j.giant.2020.100022.
(58) Zhang, M.; Chen, X.; Radacsi, N. New Tricks of Old Drugs: Repurposing Non-Chemo Drugs and Dietary Phytochemicals as Adjuvants in Anti-Tumor Therapies. *J. Controlled Release* **2021**, *329*, 96–120. https://doi.org/10.1016/j.jconrel.2020.11.047.
(59) Anand David, A.; Arulmoli, R.; Parasuraman, S. Overviews of Biological Importance of Quercetin: A Bioactive Flavonoid. *Pharmacogn. Rev.* **2016**, *10* (20), 84. https://doi.org/10.4103/0973-7847.194044.
(60) Evtyugin, D. D.; Magina, S.; Evtuguin, D. V. Recent Advances in the Production and Applications of Ellagic Acid and Its Derivatives. A Review. *Molecules* **2020**, *25* (12), 2745. https://doi.org/10.3390/molecules25122745.
(61) Zhang, J.; Fu, Y.; Yang, P.; Liu, X.; Li, Y.; Gu, Z. ROS Scavenging Biopolymers for Anti-Inflammatory Diseases: Classification and Formulation. *Adv. Mater. Interfaces* **2020**, *7* (16), 2000632. https://doi.org/10.1002/admi.202000632.
(62) Bala, I.; Bhardwaj, V.; Hariharan, S.; Kumar, M. N. V. R. Analytical Methods for Assay of Ellagic Acid and Its Solubility Studies. *J. Pharm. Biomed. Anal.* **2006**, *40* (1), 206–210. https://doi.org/10.1016/j.jpba.2005.07.006.
(63) Ceci, C.; Graziani, G.; Faraoni, I.; Cacciotti, I. Strategies to Improve Ellagic Acid Bioavailability: From Natural or Semisynthetic Derivatives to Nanotechnological Approaches Based on Innovative Carriers. *Nanotechnology* **2020**, *31* (38), 382001. https://doi.org/10.1088/1361-6528/ab912c.
(64) Apak, R.; Gorinstein, S.; Böhm, V.; Schaich, K. M.; Özyürek, M.; Güçlü, K. Methods of measurement and evaluation of natural antioxidant capacity/activity (IUPAC Technical Report). *Pure Appl. Chem.* **2013**, *85* (5), 957–998. https://doi.org/10.1351/PAC-REP-12-07-15.
(65) Brand-Williams, W.; Cuvelier, M. E.; Berset, C. Use of a Free Radical Method to Evaluate Antioxidant Activity. *LWT - Food Sci. Technol.* **1995**, *28* (1), 25–30. https://doi.org/10.1016/S0023-6438(95)80008-5.
(66) Blessy, M.; Patel, R. D.; Prajapati, P. N.; Agrawal, Y. K. Development of Forced Degradation and Stability Indicating Studies of Drugs—A Review. *J. Pharm. Anal.* **2014**, *4* (3), 159–165. https://doi.org/10.1016/j.jpha.2013.09.003.
(67) Cai, Z.-Y.; Li, X.-M.; Liang, J.-P.; Xiang, L.-P.; Wang, K.-R.; Shi, Y.-L.; Yang, R.; Shi, M.; Ye, J.-H.; Lu, J.-L.; Zheng, X.-Q.; Liang, Y.-R. Bioavailability of Tea Catechins and Its Improvement. *Molecules* **2018**, *23* (9), 2346. https://doi.org/10.3390/molecules23092346.
(68) Li, N.; Taylor, L. S.; Ferruzzi, M. G.; Mauer, L. J. Kinetic Study of Catechin Stability: Effects of PH, Concentration, and Temperature. *J. Agric. Food Chem.* **2012**, *60* (51), 12531–12539. https://doi.org/10.1021/jf304116s.
(69) Shen, Y.; Zhang, N.; Tian, J.; Xin, G.; Liu, L.; Sun, X.; Li, B. Advanced Approaches for Improving Bioavailability and Controlled Release of Anthocyanins. *J. Controlled Release* **2021**, S016836592100626X. https://doi.org/10.1016/j.jconrel.2021.11.031.

(70) Forman, H. J.; Zhang, H. Targeting Oxidative Stress in Disease: Promise and Limitations of Antioxidant Therapy. *Nat. Rev. Drug Discov.* **2021**, *20* (9), 689–709. https://doi.org/10.1038/s41573-021-00233-1.

4.5 Supporting Information

4.5.1 Materials

All reagent grade materials and solvents were purchased from Sigma Aldrich, Tokyo Chemical Industry (TCI), Fisher or Cayman Chemical and used as received. DMF was dried over activated mole sieves twice and under argon atmosphere for 3 days. Snake skin dialysis tubing (16 mm diameter) was used for all dialysis purification and experiments.

4.5.2 Instrumentation

Nuclear Magnetic Resonance (NMR) Spectroscopy

^{1}H NMR spectra were obtained using a Bruker AVance 300 MHz instrument. Solvents used in this study were obtained from Cambridge Isotope Laboratories and included: deuterium oxide, deuterated methanol, deuterated sodium hydroxide, deuterated dimethylsulfoxide, and deuterated chloroform. Data was processed with MestReNova 10.0.

Size exclusion chromatography (SEC)

The molecular weight ($M_{n\ SEC}$) and dispersity were determined using 100% mass recovery and multiangle light scattering (MALS) SEC. The running solvent was N,N-dimethyl formamide (DMF) with 1 g/L LiBr (flow rate: 0.8 mL/min) heated to 60 °C and samples were prepared at 5 mg/mL. Separation was done through three columns Tosoh TSKgel alpha 4000, Tosoh TSKgel alpha 3000 and Phenomenex Phenogel 5 µm 10E3 Å and data was collected by a Wyatt miniDAWN Treos and Wyatt Optilab T-rex. For data analysis, specifically determination of absolute molecular weight and dispersity, Wyatt ASTRA software was used. The RI traces were normalized using Prism 10.

Dynamic Light Scattering (DLS)

The hydrodynamic diameter and dispersity of polymeric micelles were determined with a Wyatt DynaPro NanoStar. Samples between 0.1 – 1 mg/mL in PBS were centrifuged at 10,000 rpm for 2 minutes to remove dust and then 10 measurements were taken and averaged.

UV-Vis Spectroscopy

All UV-Vis spectra were taken on a Thermofisher Scientific NanoDrop, using 2 µL of sample, a 1mm path length and a baseline measurement at 750 nm.

Absorbance and Fluorescence

All absorbance and fluorescence measurements were collected on 200 µL solutions in a 96-well plate using a Tecan Infinite M1000 Pro plate reader, at 25 °C.

4.5.3 Methods

Synthesis

4.5.3.1 DMA macroCTA synthesis

To a 25 mL round bottom flask (RBF), 4-((((2-carboxyethyl)thio)carbonothioyl)thio)-4-cyanopentanoic acid (CCC) (162 mg, 0.53 mmol), 4,4-Azobis(4-cyanovaleric acid) (ABCVA) (14.28 mg, 0.05 mmol), *N*,*N*-dimethaylacrylamide (DMA) (3.62 mL, 35.18 mmol), nanopure water (7.0 mL) and a magnetic stir bar were added. The solution was stirred until it was a homogenous and then sparged with argon gas vigorously for 20 minutes. Then the reaction was heated to 70 °C for 2 hours and halted with exposure to atmosphere. The conversion, DP, and $M_{n,theo}$ were determined by ^{1}H NMR in methanol-d_4 of the reaction mixture. The polymer was dialyzed against DI water for 24 hours with 3.5 kDa molecular weight cutoff (MWCO) dialysis tubing and then lyophilized.

4.5.3.2 DMA chain extension with APBA

These polymers were synthesized according to previous reports.[1] As an example polymerization, DMA MacroCTA (248.5 mg, 3.8×10^{-2} mmol), ABCVA (1.06 mg, 3.8×10^{-3} mmol), 3-acrylamidophenylboronic acid (APBA) (144.5 mg, 0.76 mmol), dioxane (0.95 mL), nanopure water (0.24 mL) and a magnetic stir bar were added to a 5 mL RBF. Once fully dissolved a 50 µL aliquot was removed and frozen. The reaction was sparged vigorously for 10 minutes and then heated to 70 °C. After 2.5 hours, the reaction was stopped by exposing it to air and the conversion, DP, and $M_{n,theo}$ were determined by ^{1}H NMR in methanol-d_4. The copolymer was purified by precipitation into cold diethyl ether. To remove trace amounts of the remaining

APBA monomer, two more precipitations were done by dissolving the precipitate in methanol and reprecipitating into fresh diethyl ether. The weight percent of APBA in the final polymer (42%) was confirmed by using levofloxacin as an NMR standard.

4.5.3.3 DBEAA monomer synthesis

The following method was adapted from a published procedure.[2,3] In brief, N,N-dibutylethylenediamine (DBEDA) (16 g, 93 mmol) was added to 150 mL of chloroform and cooled with an ice bath. Acryloyl chloride (15.01 mL, 186 mmol) in 25 mL of chloroform was added to the DBEDA solution dropwise over 30 minutes. Then the ice bath was removed and the reaction was left at RT for 1.5 hours. The crude reaction was washed with 1N NaOH (3×100 mL), dried with sodium sulfate and concentrated under reduced pressure. To remove any trace amine impurities, a flash column with pure ethyl acetate was run. Final yield of N-(2-(dibutylamino)ethyl)acrylamide (DBEAA) 15 g (71%).

4.5.3.4 DMA chain extension with APBA and DBEAA

As an example polymerization, DMA MacroCTA (307 mg, 4.9×10^{-2} mmol), ABCVA (4.57 mg, 1.6×10^{-2} mol), APBA (398.7 mg, 2.10 mmol), DBEAA (818 mg, 3.62 mmol), dioxane (8.17 mL), nanopure water (0.82 mL) and a magnetic stir bar were added to a 25mL RBF. Once fully dissolved a 50 µL aliquot was removed and frozen. The reaction was sparged vigorously for 20 minutes and then heated to 70 °C for 24 hours. After exposing the reaction to air, the conversion, DP, and $M_{n,theo}$ were determined by comparing the ^{1}H NMR spectra of the aliquot (taken at 0 minutes) and the final reaction. The copolymer was purified by precipitation into cold diethyl ether. To remove trace amounts of the remaining monomers, two more precipitations were done

by dissolving the precipitate in methanol and reprecipitating into fresh diethyl ether. The weight percent of APBA in the final polymer (22%) was confirmed by using levofloxacin as an NMR standard.

Experimental

4.5.3.5 Pinacol protection of APBA containing copolymers

The following method was adapted from a published procedure.[4] In brief, DMA-bl-APBA (124 mg, 1.2×10^{-2} mmol) and pinacol (650 mg, 5.5 mmol) were dissolved in dry DMF (12 mL) and heated to 105 °C for 48 hours. The solution was cooled to RT, precipitated into cold diethyl ether and dried under vacuum overnight.

4.5.3.6 Micelle formulation

First, stock solutions of polymer (50 mg/mL in methanol) and drug (25 mg/mL) were prepared. For EGCG and Quercetin, using DMF as the solvent, whereas EA was only soluble in N-methyl pyrrolidone (NMP). To prepare approximately 1.2 mg of micelles, 1 mg of polymer (20 µL) was mixed with either 10% or 20% drug by weight, 4.4 µL or 10 µL respectively. DMF was added to raise the volume to 100 µL and then the mixture was sonicated for 30 minutes. After sonication, the solutions were nanoprecipitated into 1 mL of PBS (pH 7.4).

4.5.3.7 Drug loading measurements

Micelle samples were used without dilution (1 mg/mL polymer). To remove aggregates and only measure soluble micelle-drug conjugates, all samples were centrifuged at 13,000 rpm prior to

measurement. The UV-Vis spectra were then recorded on the nanodrop for all 15 micelle solutions.

4.5.3.8 Transparency

To determine the extent of micelle aggregation and precipitation, the absorbance of micelle solutions was measured at 750 nm on the plate reader. 200 µL of 1 mg/mL micelles solutions were vortexed and sonicated to suspend particulates and the 1 mg/mL polymer solutions were measured without dilution.

4.5.3.9 Micelle disassembly

Determination of pH dependent micelle dissociation was adapted from a previously published report. [5] In brief, polymers were dissolved at 25 mg/mL in 0.1N NaOH. These stock solutions were diluted to 0.4 mg/mL in 500 µL of DI water and the mixed with 0.2 M sodium phosphate buffer (at various pH values) that contained 1 µM Nile Red. After waiting for 30 minutes for the dye to enter micelles, the fluorescence intensity was measured (ex. 556, em. 625). The results were unchanged over a period of 24 hours, so these short time points were used. Due to variations in the absolute fluorescence intensity across polymer compositions, most likely a result of the structural variation in the hydrophobic core of the different micelles, the values were normalized.

4.5.3.10 Boronic ester equilibrium determination with ^{19}F NMR

Boronic ester formation of CPBA was measured in DMSO-d_6, DMF-d_7, and methanol-d_4. DMSO was found to have the highest conversion, followed by DMF and methanol where no conversion was observed. This finding is corroborated by Larcher et al. who also found higher

affinity in DMSO compared to a buffer mixture.[6] Due to polymer solubility constraints the DB polymer binding affinity was measured in a poor boronic ester forming solvent, methanol-d_4. Interestingly, the BA polymer affinity was so low that no boronic ester formed in pure organic solvents and only in a 60/40 DMSO/buffer (phosphate 7.4) mixture was any complexation observed. For ^{19}F NMR measurements stock solutions of 1 mg/mL F-Cat, 50 mg/mL CPBA, 100 mg/mL DB polymer and 100 mg/mL BA polymer were prepared. The boronic acid solution (CPBA, DB, or BA) was then added to the F-Cat solution at the target molar ratio and serially diluted to obtain concentration dependent binding affinity. Samples were allowed to equilibrate for 1 h prior to taking the ^{19}F NMR spectra. The limit of detection in these studies was 5% boronic ester complex (or 0.05 mg of F-Cat).

To better visualize the ratios of F-Cat (catechol), boronic acid, and boronic ester moieties in the 19 NMR measurements, we graphed the ratio of boronic ester to boronic acid as a function of the ratio of boronic acid to catechol (Figure S4B). When the ratio of boronic ester to boronic acid approaches 1 all the free boronic acid has been converted to the ester. Interestingly, with excess F-Cat in the reaction, the boronic acids in the DB polymer are quantitatively and completely converted to esters. However, for the CPBA only 75% of the boronic acid becomes boronic ester and for the BA polymer only 50% even in the presence of excess F-Cat. The lowest concentration of boronic acid was determined by the limit of detection of the boronic ester complex.

4.5.3.11 Radical scavenging activity

Stock solutions of DPPH (10mg/mL in DMF), polymers (50 mg/mL in methanol) and drug (25 mg/mL in DMF for EGCG and in NMP for EA) were prepared. Polymer-drug conjugates were formulated by mixing 20 µL of polymer with either (10 µL of EGCG or 4.4 µL of EA) and diluted with methanol to 100 µL. Methanol prevents self-assembly of the polymers, isolating the effects of boronic acid affinity without the confounding variable of micellization. After 30 minutes of sonication, free drug, polymer, or polymer drug conjugates were diluted into 1 mL of methanol at approximately the EC_{50}. EA solutions were prepared at 30 µM and EGCG solutions at 10 µM. Polymer only samples were added in equal amounts to the polymer drug conjugates. Once all the solutions were prepared, in quick succession, 6 µL of DPPH was added to every sample. After 10 minutes the absorbance at 517 nm was measured on the plate reader.

4.5.3.12 Forced degradation of EA

Serial dilutions of NaOH at concentrations ranging from 100 mM to 0.78 mM were prepared in DI water. Equal concentrations of 10% EA loaded micelles with either the DMA-bl-APBA or DMA-bl-APBAcoDBEAA, were diluted with a one-to-one volume of the various NaOH solutions. After 10 minutes the UV-Vis spectra of all the samples was collected, and EC_{50} values were determined using the normalized absorbance for degraded drug at 425 nm and the nonlinear fit in Prism 10.

4.5.3.13 Drug release: dialysis method

Concentrated solutions of polymer and drug (20% by weight quercetin) were prepared and nanoprecipitated at 1 mg/mL polymer concentrations, at a scale of 5 mg. After a 30 minute

equilibration of the micelles at room temperature, 5mL from each of the 1 mg/mL micelle solutions was added to a 10 kDa MWCO dialysis membrane. The membranes were then placed in a 30 mL solution of 200 mM sodium acetate buffer (pH 7.4 or 4.5) with 0.1% tween. At every timepoint 1 mL of the sink was removed, frozen, and replaced with 1 mL of fresh buffer. At the end of the study all the timepoints were thawed and the absorbance at 360 nm was measured and compared to a standard curve for quercetin. Total drug release values were adjusted based on the mass of drug removed at each time point. Due to the instability of quercetin in aqueous solutions, we could not measure drug release for longer than 24 hours without significant errors.

4.5.4 Supporting Figures

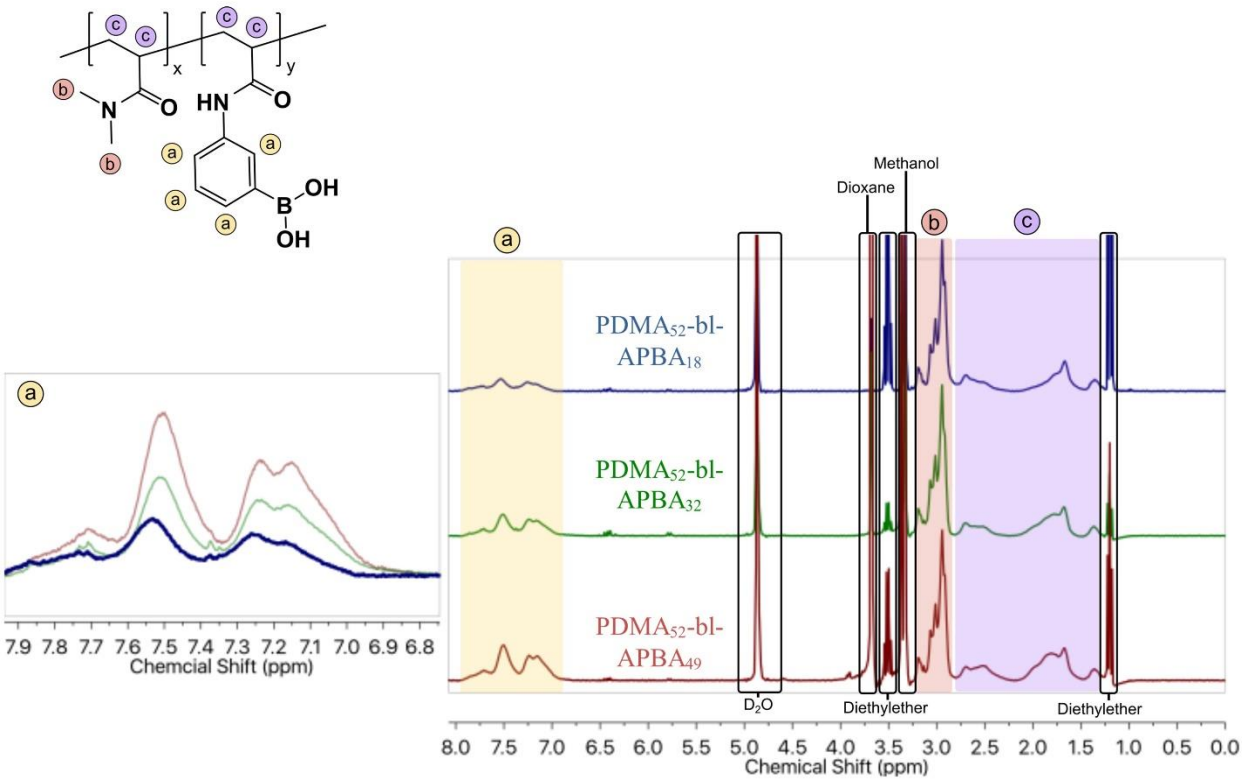

Figure S1. The ^{1}H NMR spectra of BA polymers in basic D_2O. Expanded view of aromatic region illustrates increasing content of APBA. All spectra were normalized to the peaks of the PDMA macroCTA.

Table S1. Characterization of DP, molecular weight, hydrophobicity, and micelle solubility in PBS of BA polymers

Polymer Composition	Conversion	Hydrophobic to Hydrophilic (Mass)	$M_{n,\ theory}$ (Da)	$Đ$	Micelle Solubility
$PDMA_{52}$	70%	N/A	5700	1.2	N/A
$PDMA_{52}$-bl-$APBA_{18}$	24%	0.66	8,100	N/A	✓
$PDMA_{52}$-bl-$APBA_{32}$	55%	1.2	11,500	N/A	×
$PDMA_{52}$-bl-$APBA_{49}$	95%	1.78	16,000	N/A	×

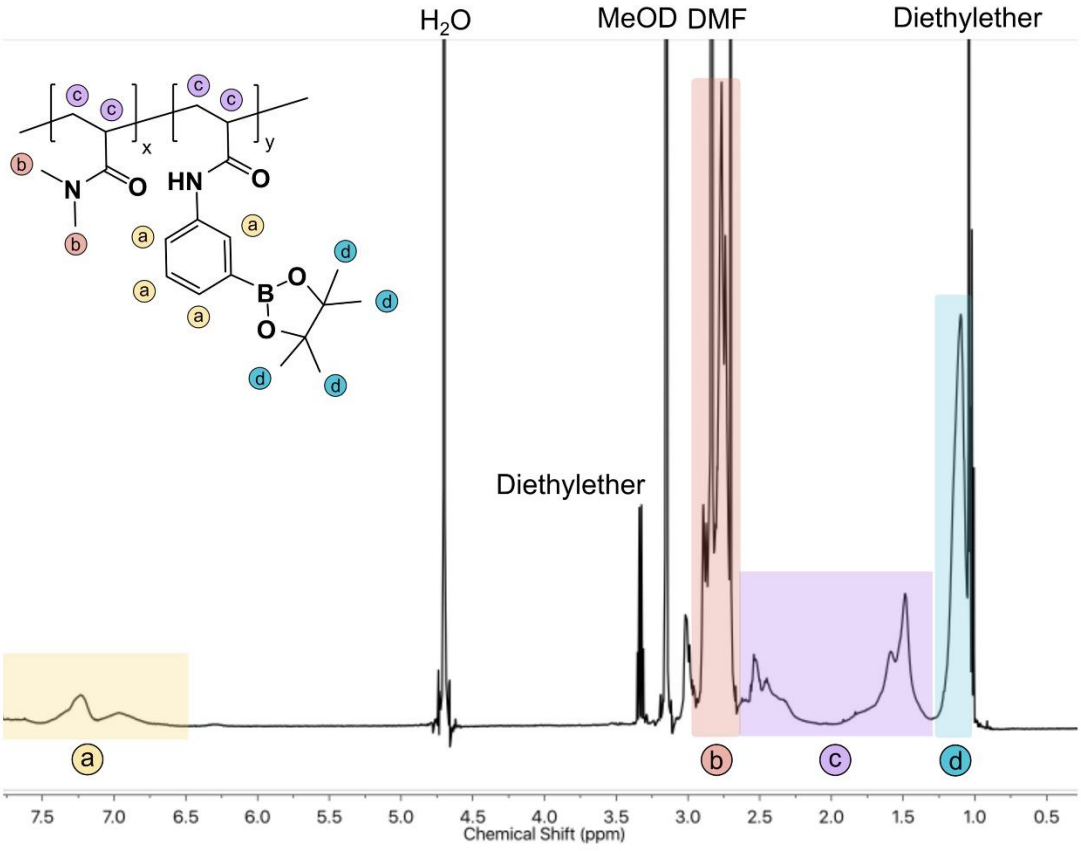

Figure S2. The ^{1}H NMR of pinacol protected BA polymer in methanol-d_4.

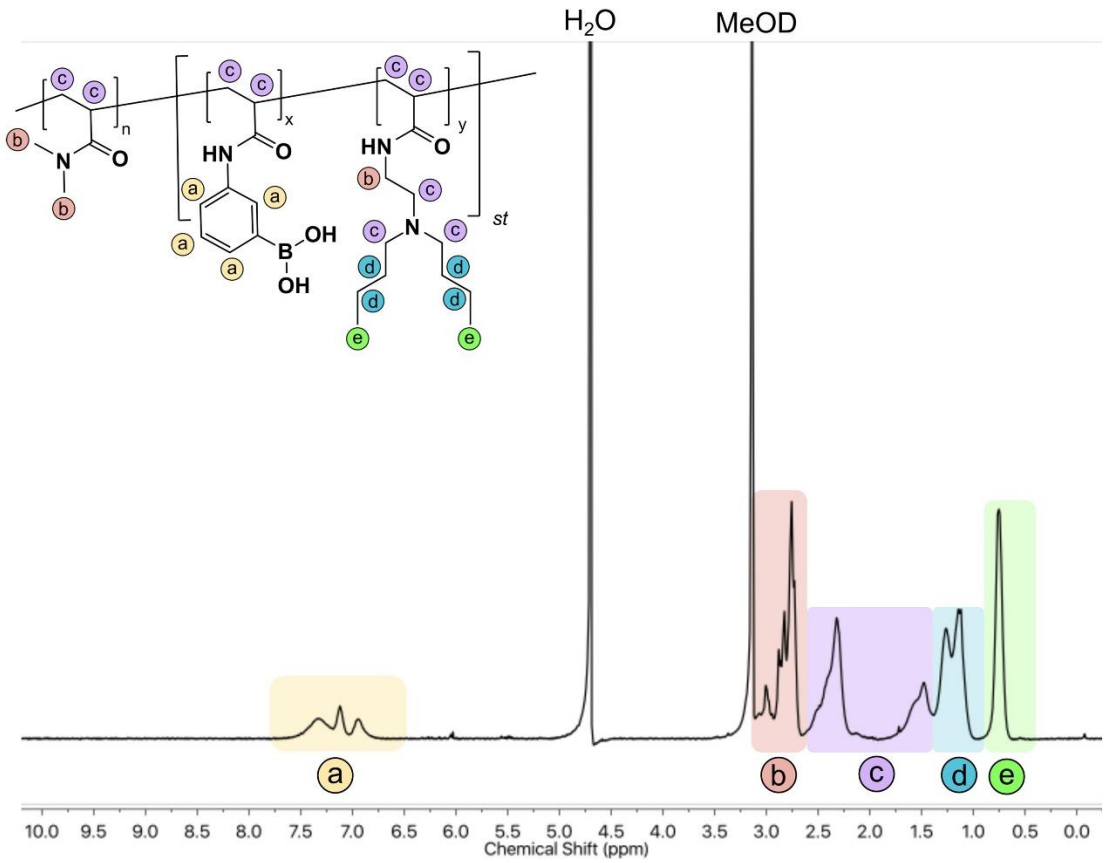

Figure S3. The ^{1}H NMR of DB polymer in methanol-*d*$_4$.

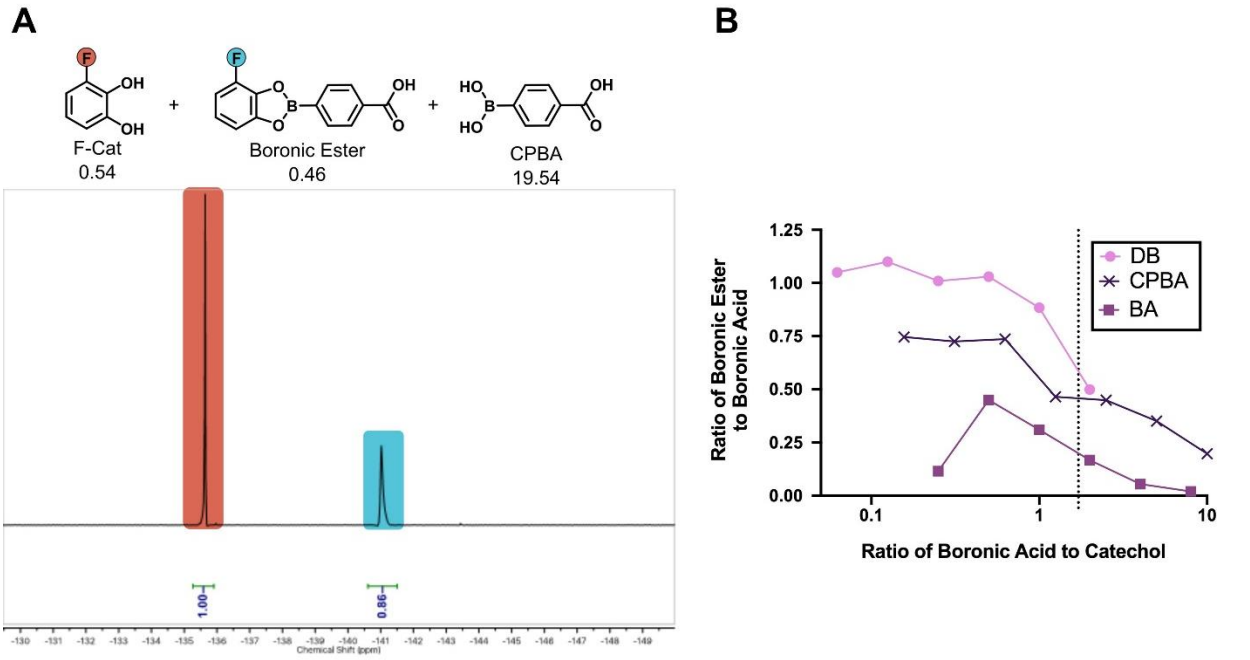

Figure S4. A) Conversion of F-Cat to boronic ester in the presence of 20-fold excess of CPBA in DMSO-d_6 measured by ^{19}F NMR. B) Ratios of boronic acid to boronic ester complex as a function of boronic acid to catechol ratio were plotted. Values near 1 indicate quantitative conversion of boronic acids to boronic esters in the presence of catechol.

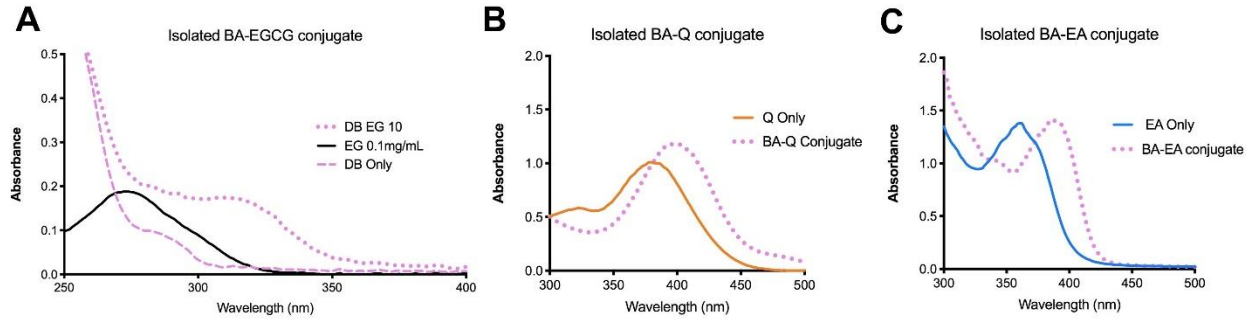

Figure S5. A) Distinct absorbance shift for EGCG when conjugated to boronic acids in DB polymer from 280 to 312 nm. B) Increased absorbance of Quercetin at 400 nm when conjugated to boronic acids in the DB polymer. C) Distinct absorbance shift for EA when conjugated to boronic acids in DB polymer from 360 to 400 nm.

Table S2. Characterization of DP, molecular weight, amine content, and drug loaded micelle stability in PBS of DB polymers. DB 2.5 and DB 0.8 precipitated when complex with EGCG, Quercetin, and EA at 10% weight drug-loading.

Nickname	Polymer	APBA	DBEAA	DB to BA	$M_{n,\ theory}$ (Da)	Drug-loaded Micelle Stability
DB 2.5	$PDMA_{62}$-bl-$APBA_{co}DBEAA$	19	49	2.5	22,721	X
DB 1.7	$PDMA_{62}$-bl-$APBA_{co}DBEAA$	16	27	1.7	15,470	✓
DB 0.8	$PDMA_{62}$-bl-$APBA_{co}DBEAA$	27	24	0.88	16,897	X

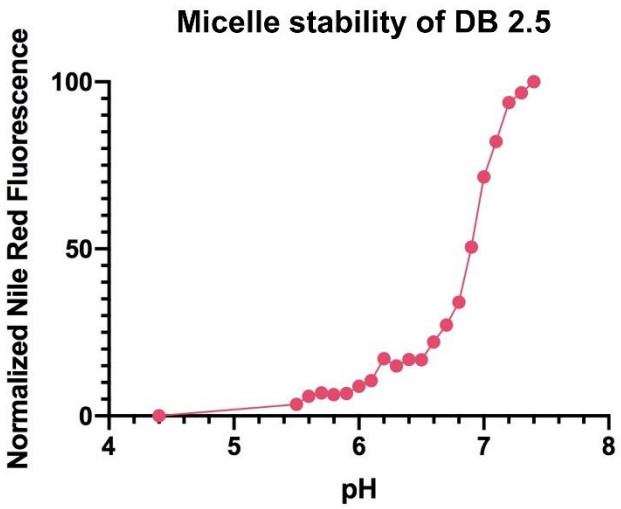

Figure S6. pH responsive micelle disassembly of DB 2.5 as determined by Nile Red fluorescence assay.

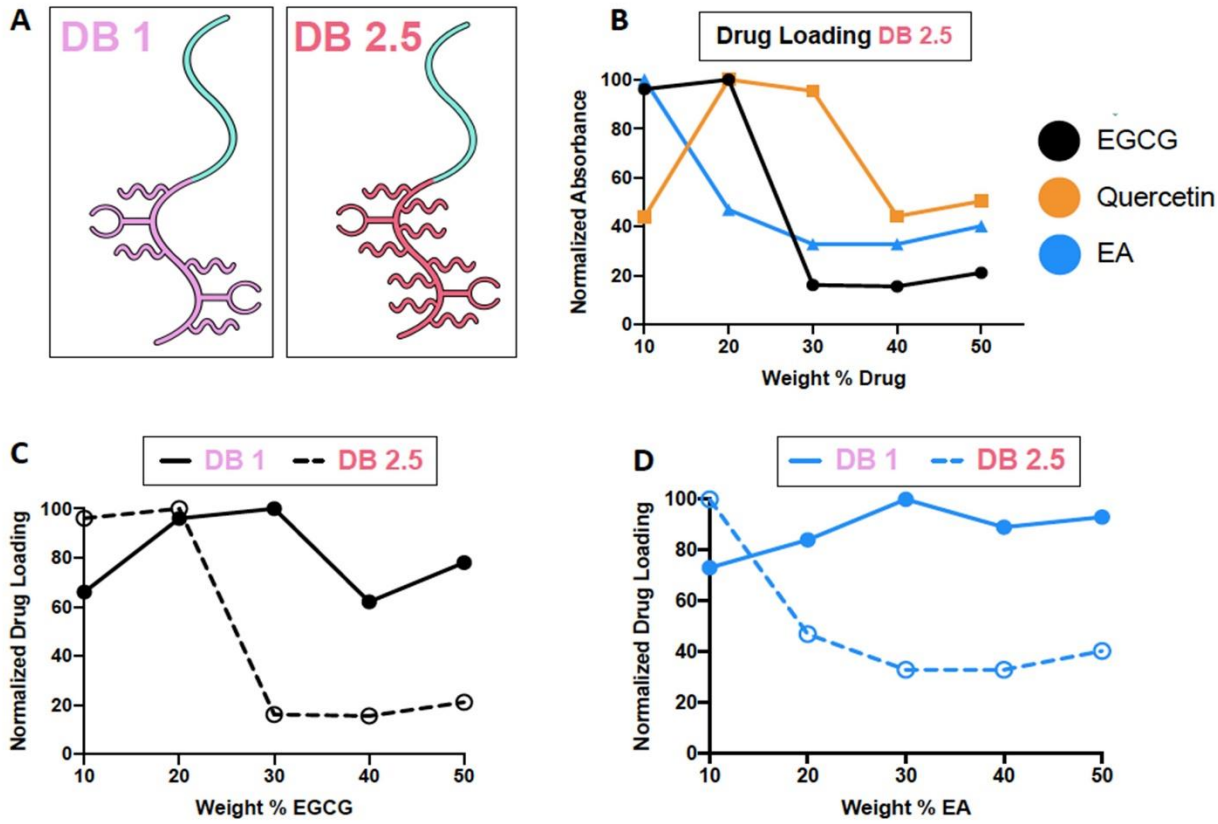

Figure S7. A) Schematic representing increased DBEAA (tertiary amine) content in DB 2.5 polymers compared to DB 1.7 (DB 1). B) Comparison of normalized absorbance intensity at the wavelength characteristic to the polymer drug conjugate (EGCG, 312 nm), (Q, 390), and (EA, 400 nm) at various weight percent after centrifugation. C) Drug loading ability of DB 1 and DB 2.5 compared at various weight % of EGCG. D) Drug loading ability of DB 1 and DB 2.5 compared at various weight % of EA.

References

(1) Bapat, A. P.; Roy, D.; Ray, J. G.; Savin, D. A.; Sumerlin, B. S. Dynamic-Covalent Macromolecular Stars with Boronic Ester Linkages. *J. Am. Chem. Soc.* **2011**, *133* (49), 19832–19838. https://doi.org/10.1021/ja207005z.

(2) Wang, K.; Song, Z.; Liu, C.; Zhang, W. RAFT Synthesis of Triply Responsive Poly[N-[2-(Dialkylamino)Ethyl]Acrylamide]s and Their N-Substitute Determined Response. *Polym. Chem.* **2016**, *7* (20), 3423–3433. https://doi.org/10.1039/C6PY00526H.

(3) Song, Z.; Wang, K.; Gao, C.; Wang, S.; Zhang, W. A New Thermo-, PH-, and CO_2-Responsive Homopolymer of Poly[*N* -[2-(Diethylamino)Ethyl]Acrylamide]: Is the

Diethylamino Group Underestimated? *Macromolecules* **2016**, *49* (1), 162–171. https://doi.org/10.1021/acs.macromol.5b02458.
(4) Roy, D.; Cambre, J. N.; Sumerlin, B. S. Sugar-Responsive Block Copolymers by Direct RAFT Polymerization of Unprotected Boronic Acid Monomers. *Chem. Commun.* **2008**, No. 21, 2477. https://doi.org/10.1039/b802293c.
(5) Cheng, Y.; Yumul, R. C.; Pun, S. H. Virus-Inspired Polymer for Efficient In Vitro and In Vivo Gene Delivery. *Angew. Chem. Int. Ed.* **2016**, *55* (39), 12013–12017. https://doi.org/10.1002/anie.201605958.
(6) Larcher, A.; Lebrun, A.; Smietana, M.; Laurencin, D. A Multinuclear NMR Perspective on the Complexation between Bisboronic Acids and Bisbenzoxaboroles with *Cis* -Diols. *New J. Chem.* **2018**, *42* (4), 2815–2823. https://doi.org/10.1039/C7NJ04143H.

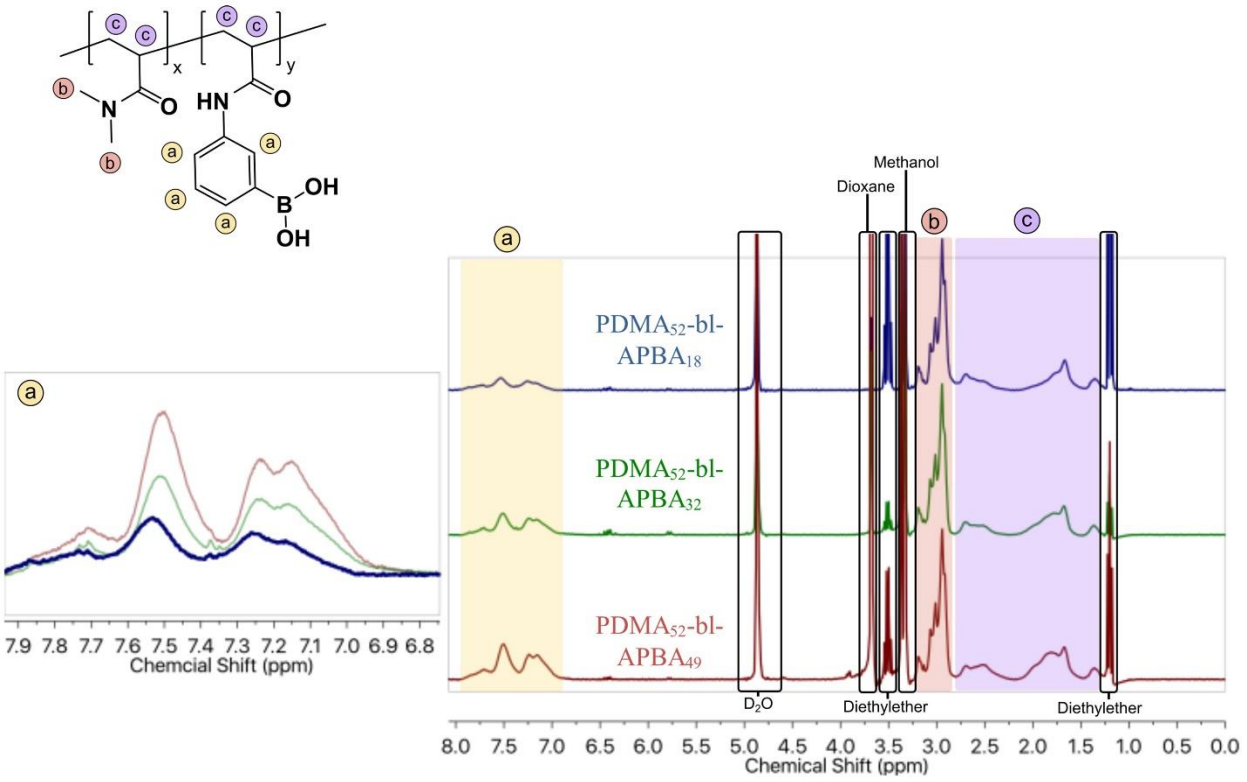

Figure S8. The ^{1}H NMR spectra of BA polymers in basic D_2O. Expanded view of aromatic region illustrates increasing content of APBA. All spectra were normalized to the peaks of the PDMA macroCTA.

Table S3. Characterization of DP, molecular weight, hydrophobicity, and micelle solubility in PBS of BA polymers

Polymer Composition	Conversion	Hydrophobic to Hydrophilic (Mass)	$M_{n,\ theory}$ (Da)	$Đ$	Micelle Solubility
$PDMA_{52}$	70%	N/A	5700	1.2	N/A
$PDMA_{52}$-bl-$APBA_{18}$	24%	0.66	8,100	N/A	✓
$PDMA_{52}$-bl-$APBA_{32}$	55%	1.2	11,500	N/A	×
$PDMA_{52}$-bl-$APBA_{49}$	95%	1.78	16,000	N/A	×

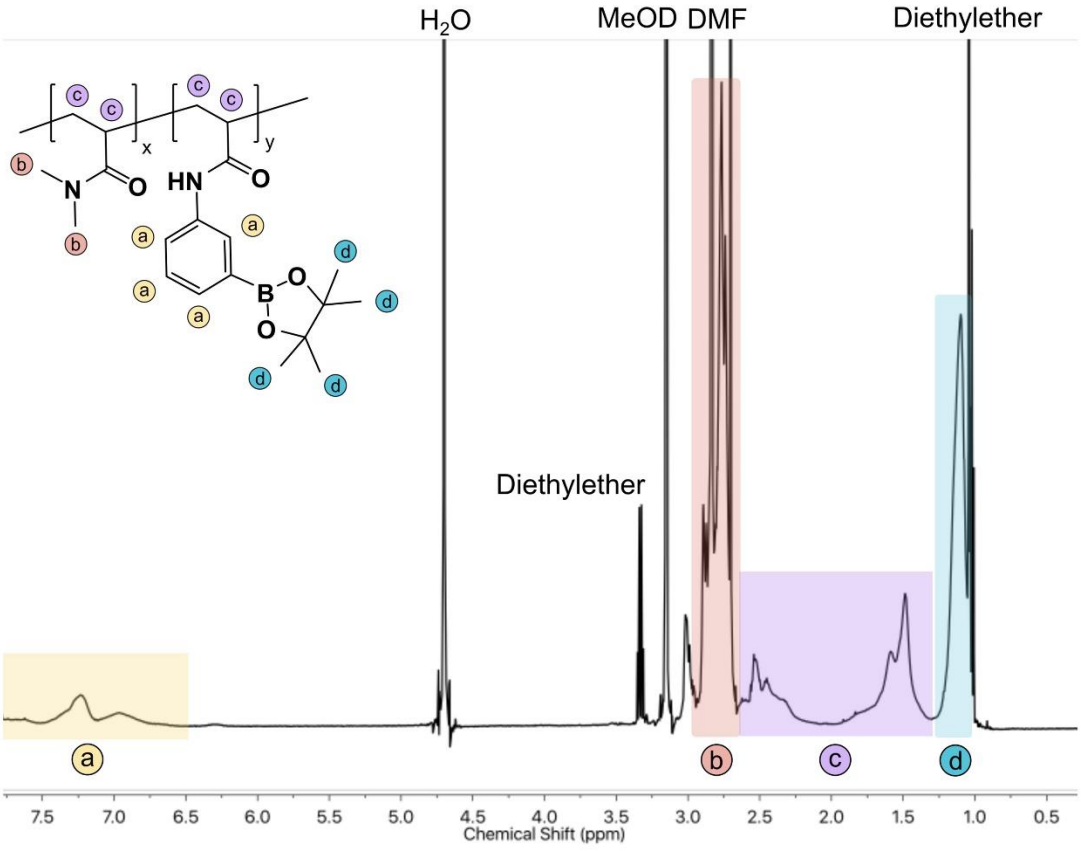

Figure S9. The ^{1}H NMR of pinacol protected BA polymer in methanol-d_4.

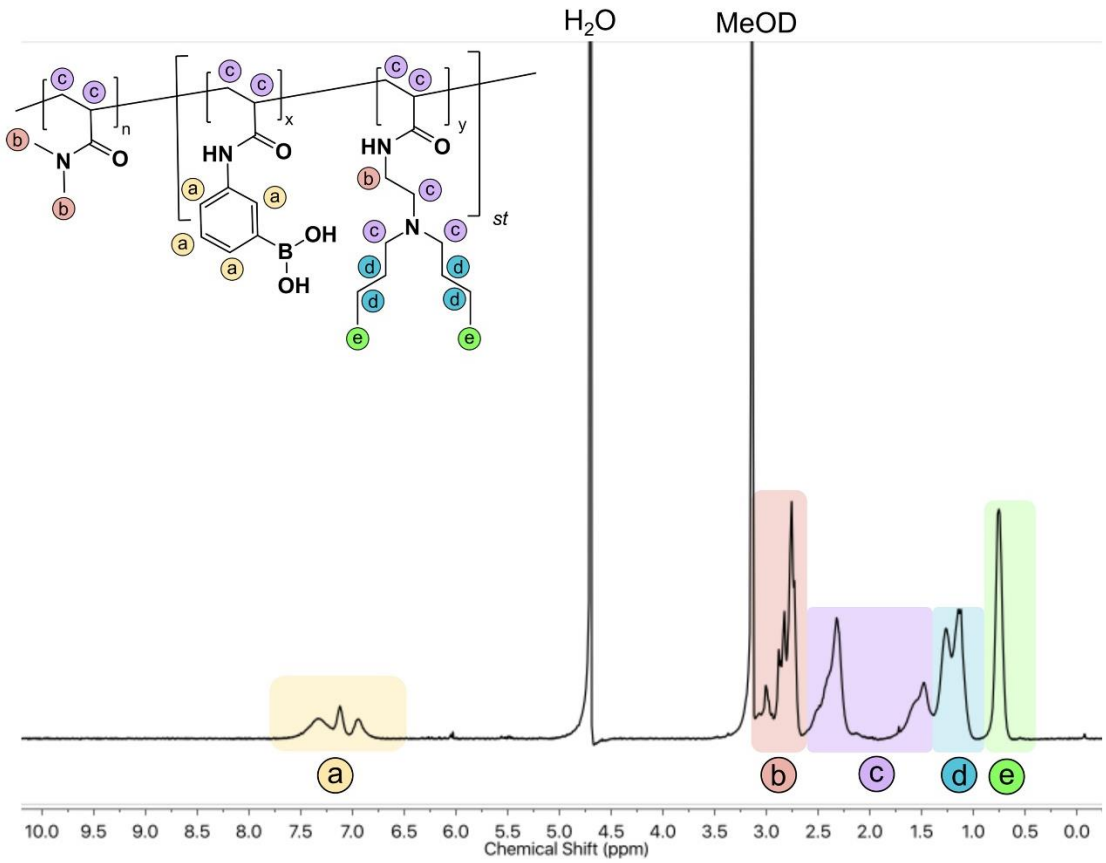

Figure S10. The ^{1}H NMR of DB polymer in methanol-d_4.

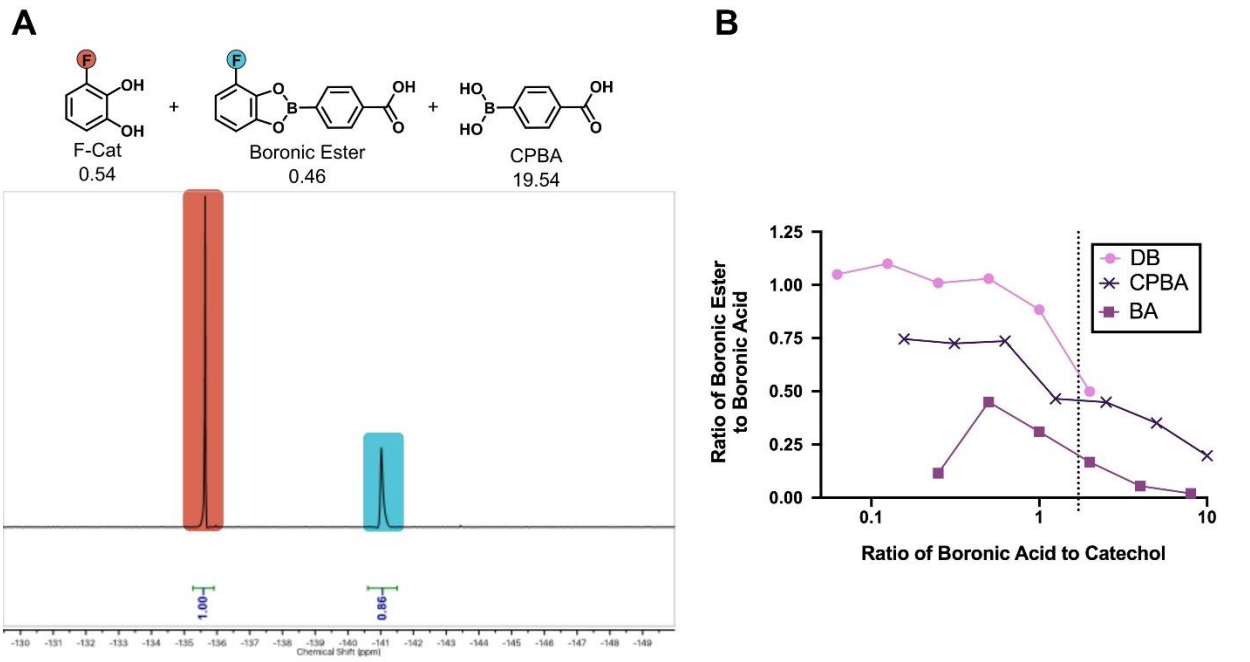

Figure S11. A) Conversion of F-Cat to boronic ester in the presence of 20-fold excess of CPBA in DMSO-d_6 measured by ^{19}F NMR. B) Ratios of boronic acid to boronic ester complex as a function of boronic acid to catechol ratio were plotted. Values near 1 indicate quantitative conversion of boronic acids to boronic esters in the presence of catechol.

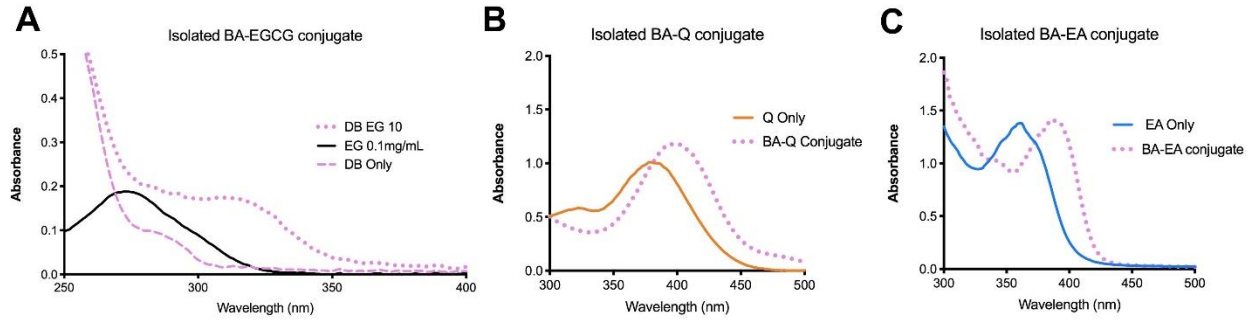

Figure S12. A) Distinct absorbance shift for EGCG when conjugated to boronic acids in DB polymer from 280 to 312 nm. B) Increased absorbance of Quercetin at 400 nm when conjugated to boronic acids in the DB polymer. C) Distinct absorbance shift for EA when conjugated to boronic acids in DB polymer from 360 to 400 nm.

Table S4. Characterization of DP, molecular weight, amine content, and drug loaded micelle stability in PBS of DB polymers. DB 2.5 and DB 0.8 precipitated when complex with EGCG, Quercetin, and EA at 10% weight drug-loading.

Nickname	Polymer	APBA	DBEAA	DB to BA	$M_{n,\ theory}$ (Da)	Drug-loaded Micelle Stability
DB 2.5	$PDMA_{62}$-bl-$APBA_{co}DBEAA$	19	49	2.5	22,721	X
DB 1.7	$PDMA_{62}$-bl-$APBA_{co}DBEAA$	16	27	1.7	15,470	✓
DB 0.8	$PDMA_{62}$-bl-$APBA_{co}DBEAA$	27	24	0.88	16,897	X

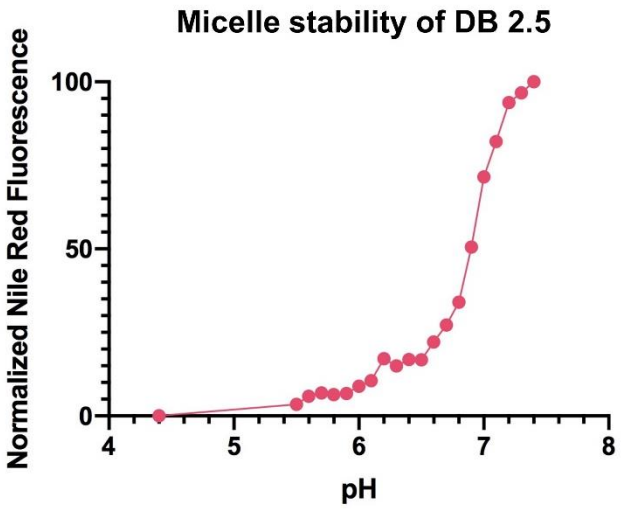

Figure S13. pH responsive micelle disassembly of DB 2.5 as determined by Nile Red fluorescence assay.

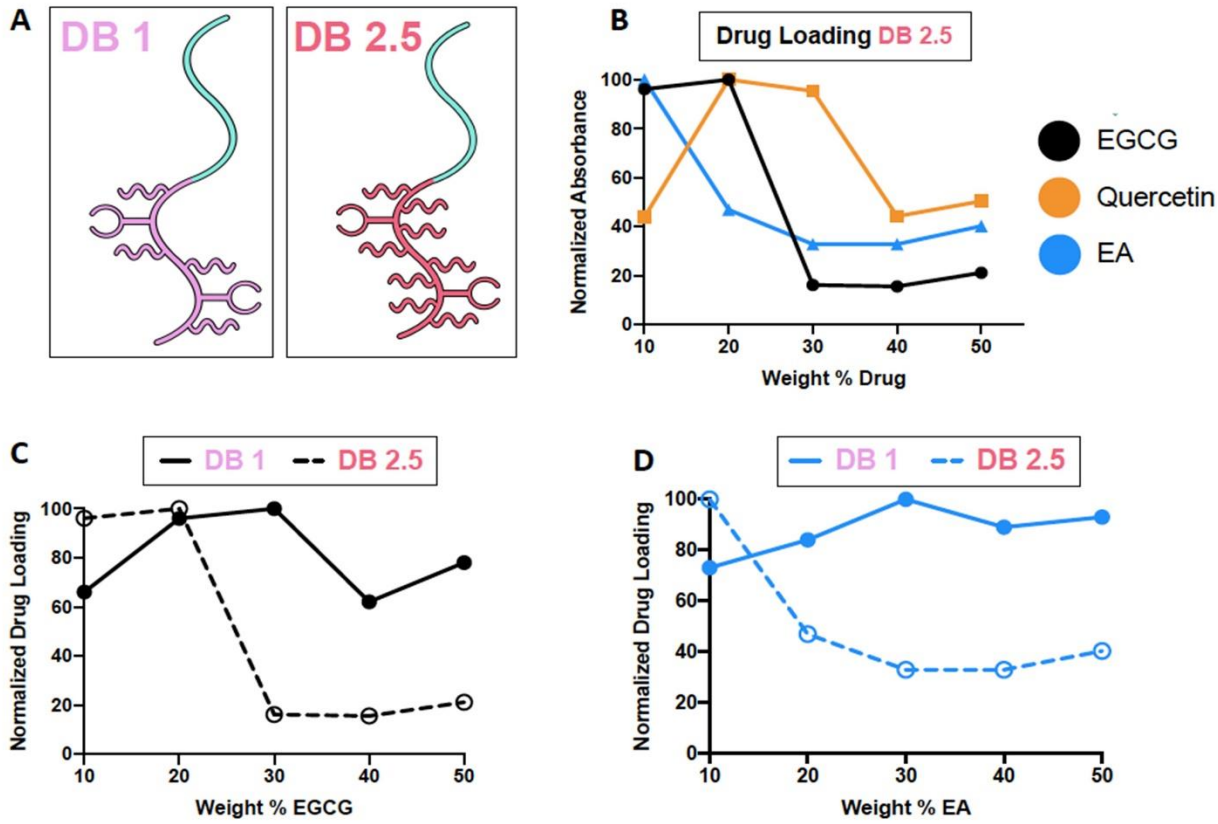

Figure S14. A) Schematic representing increased DBEAA (tertiary amine) content in DB 2.5 polymers compared to DB 1.7 (DB 1). B) Comparison of normalized absorbance intensity at the wavelength characteristic to the polymer drug conjugate (EGCG, 312 nm), (Q, 390), and (EA, 400 nm) at various weight percent after centrifugation. C) Drug loading ability of DB 1 and DB 2.5 compared at various weight % of EGCG. D) Drug loading ability of DB 1 and DB 2.5 compared at various weight % of EA.

References

(1) Bapat, A. P.; Roy, D.; Ray, J. G.; Savin, D. A.; Sumerlin, B. S. Dynamic-Covalent Macromolecular Stars with Boronic Ester Linkages. *J. Am. Chem. Soc.* **2011**, *133* (49), 19832–19838. https://doi.org/10.1021/ja207005z.

(2) Wang, K.; Song, Z.; Liu, C.; Zhang, W. RAFT Synthesis of Triply Responsive Poly[N-[2-(Dialkylamino)Ethyl]Acrylamide]s and Their N-Substitute Determined Response. *Polym. Chem.* **2016**, *7* (20), 3423–3433. https://doi.org/10.1039/C6PY00526H.

(3) Song, Z.; Wang, K.; Gao, C.; Wang, S.; Zhang, W. A New Thermo-, PH-, and CO_2 -Responsive Homopolymer of Poly[*N* -[2-(Diethylamino)Ethyl]Acrylamide]: Is the Diethylamino Group Underestimated? *Macromolecules* **2016**, *49* (1), 162–171. https://doi.org/10.1021/acs.macromol.5b02458.

(4) Roy, D.; Cambre, J. N.; Sumerlin, B. S. Sugar-Responsive Block Copolymers by Direct RAFT Polymerization of Unprotected Boronic Acid Monomers. *Chem. Commun.* **2008**, No. 21, 2477. https://doi.org/10.1039/b802293c.
(5) Cheng, Y.; Yumul, R. C.; Pun, S. H. Virus-Inspired Polymer for Efficient In Vitro and In Vivo Gene Delivery. *Angew. Chem. Int. Ed.* **2016**, *55* (39), 12013–12017. https://doi.org/10.1002/anie.201605958.
(6) Larcher, A.; Lebrun, A.; Smietana, M.; Laurencin, D. A Multinuclear NMR Perspective on the Complexation between Bisboronic Acids and Bisbenzoxaboroles with *Cis* -Diols. *New J. Chem.* **2018**, *42* (4), 2815–2823. https://doi.org/10.1039/C7NJ04143H.

Chapter 5

Boronic acid copolymers for intracellular delivery of proteins, peptides, and nucleic acids

Alexander Prossnitz, Karthikeya Gottimukkala, David Liu, Nataly Kacherovsky, Ian Cardle, and Suzie Pun

Abstract

The therapeutic potential of gene delivery has received a second wind in light of both mRNA based COVID19 vaccines and the continued evolution of CRIPR/Cas9 editing technology. This renewed interest has highlighted the need for new approaches to overcome the major barriers to successful gene therapies, intracellular delivery and endosomal escape. We utilized the affinity boronic acid functional groups for cellular membrane sugars to improve intracellular delivery of proteins and nucleic acids. By synthesizing two distinct copolymers, we were able to encapsulate proteins and peptides with high efficiency (>80%), and complex plasmid DNA. These nanomaterials demonstrated high internalization, despite low cationic surface charge. Future studies will determine the extent to which encapsulated protein retains their structure and function, the ability of encapsulated cargo to escape the endosome, and ultimately the efficiency of these platforms for gene therapy.

5.1 Introduction

5.1.1 Intracellular delivery of biologics for gene therapy

Broadly gene therapeutics can be classified into two distinct groups, nucleic acids (DNA and RNA) and ribonucleoproteins (RNPs, such as CRISPR, prime editing, etc.). A detailed discussion of nucleic acid therapeutics was included in chapter 1 so only a summary will be included here. Non-viral delivery of both DNA and RNA, transiently effects protein expression on the time scales of months and days respectively. The induction or silencing of protein expression can induce potent immune response to novel pathogens, replace a critical missing protein, or endow novel functionality to an *ex vivo* engineered cell.[1–3] On the opposite side of the spectrum, delivery of gene editing RNPs enables permanent changes to cellular protein expression profiles.[4] For example, the CRISPR-Cas9 system, when complexed to a guide RNA (gRNA), can selectively knock out gene expression via non-homologous end joining (NHEJ).[5] The same protein when delivered with gRNA and a donor DNA strand can repair nonfunctional coding DNA, restoring protein expression.[6] While the benefits to creating gene therapeutics that can be directly administered are immense for a host of diseases, the field has been unable to design delivery vehicles that can simultaneously overcome all of the *in vivo* delivery barriers, such as adverse immune responses, the RES, enzymatic degradation, colloidal stability in serum, selective cellular internalization, and endosomal escape.[7–12]

One of the most promising applications of gene delivery is in chimeric antigen receptor (CAR) T cell cancer therapies. In this cancer treatment, T cells from the patient are purified from the blood and genetically engineered *ex vivo* to express a novel cancer targeting T cell receptor (TCR).[13,14] There exist a multitude of approaches to genetically engineer cells *ex vivo*, but current state-of-the-art CAR T cell manufacturing uses viral vectors to deliver plasmids encoding

for CARs. While highly efficient, these vectors are expensive to use both due to manufacturing of the virus itself, but also due to the additional quality control required to remove residual virus from the product cell therapy.[15] As a result of this limited capacity to genetically modify primary T cells, only a few highly specialized centers can even provide CAR T cell therapy, while access to most patients is blocked by cost.[16] Substituting polymeric gene delivery agents for the viral vectors would dramatically reduce production costs and increase the safety of CAR T cell therapy.[3] Unfortunately, T cells are difficult to transfect with polymers due to low nonspecific internalization and less acidic endosomes.[17] While overcoming these T cell specific barriers is not trivial, the reduced complexity of *ex vivo* gene delivery makes this application an impactful and ideal proving ground for novel gene delivery vehicles.

With regards to RNPs, there has been significant research efforts to develop nanomaterial systems capable of delivering proteins intracellularly, but progress has been slow due to the dual challenges of cellular uptake and endosomal escape.[18,19] Current commercially available materials for cytosolic delivery of CRISPR/Cas9 leave much to be desired compared to recent highly engineered dendrimers or cationic polymers.[20–23] Specifically, these BA based polymers for drug delivery showed high protein loading, and endosomal escape.[22,24] Interestingly, the interactions between the phenyl BA and several nitrogen containing protein functional groups (lysine and arginine) caused the formation of stable nanocomplexes under neutral conditions. We sought to leverage the utility of this BA approach to increase RNP delivery to T-cells.

Improving upon these previously published systems, we propose co-loading a lytic peptide, to enhance endosomal escape and ultimately gene editing. Previous studies show lytic peptides such as melittin can facilitate endosomal escape after cellular uptake.[25–27] With the understanding that the protein loading is due to amine interactions with the BA functional

groups, we hypothesized that cationic lytic peptides could also be encapsulated with high efficiency. In a similar approach, the combination of a lytic protein and therapeutic protein was successfully used to deliver active Cre recombinase to perform gene editing *in vitro* and *in vivo*.[28] This study illustrates the viability of this strategy while leaving room for improvement in both cost and utility. By substituting an inexpensive peptide analog for the expensive and toxic protein, the proposed polymeric nanoassembly will be an efficient tool for intracellular protein delivery. We used the diblock copolymers developed in chapter 4, to create a nanocomplex of labeled proteins and peptides with high efficiency and improve delivery of this cargo into a model human cell line. Future work will determine the functionality of protein cargo after cellular internalization, and ultimately the ability enhance genetic engineering of T cells with RNPs.

In a second approach, we explored the use of linear cationic polymers with BA and lipophilic functional groups to augment T cell internalization and endosomal escape to improve delivery of plasmid DNA. In these materials, pendent BA groups will be available to bind proteins and sugars on the cell surface nonspecifically increasing polyplex internalization. Previous reports have highlighted the ability of BA to facility cellular uptake.[29] Additionally, hydrophobicity has been implicated as a tool to increase membrane association of gene delivery vectors.[30] We synthesized a panel of labeled cationic acrylamides with various compositions of BAs and hydrophobic dodecyl chains and have started screening Jurkat cells for transfection. Our preliminary data shows that inclusion of BA increases internalization by two orders of magnitude, validating our hypothesis that the chemical composition of cationic polymers dramatically effects gene delivery.

Herein we first present a comprehensive review of the current polymer systems for peptide delivery, to highlight successful material designs and techniques that can be applied to intracellular delivery and endosomal escape. Polymeric materials for intracellular protein and RNP delivery have been exhaustively reviewed and to date there are still only a few materials that have been studied.[4,18,31–35] The field of polymeric nucleic acid delivery has similarly been reviewed.[36,37] The field of peptide delivery is much broader and the lessons learned from the past two decades of research are directly applicable to protein delivery. Second, the preliminary work developing micelles with BA functionality for intracellular protein delivery will be presented along with the synthesis of cationic linear BA polymers for improved nucleic acid delivery to T cells.

5.2 Results and Discussion

5.2.1 Cytocompatibility of BA and DB micelles

Before expanding the use of the DMA-*co*-APBA micelles to intracellular delivery of proteins and nucleic acids, we investigated the biocompatibility of these materials in a non-cancerous cell line. We chose NIH 3T3 cells because of their availability, rapid doubling time, and immortalized nature. The cells were exposed to micelles for 1 h at 37 ºC in PBS. Then the cells were washed and incubated overnight before viability was determined with an MTS/PMS assay (Figure 5.13). Even the highest dose of 0.5 mg/mL showed no signs of toxicity with both DB and BA micelles maintaining over 90% viability.

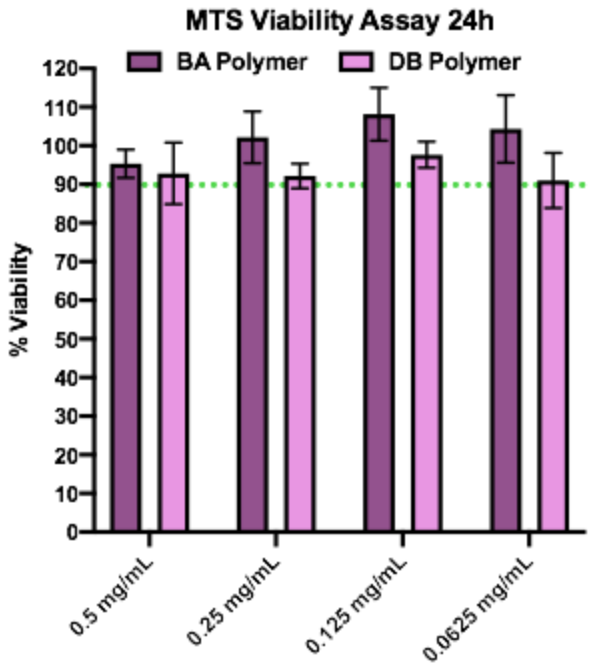

	BA Polymer			DB Polymer		
	Mean	SD	N	Mean	SD	N
0.5 mg/mL	95.333	3.670	6	92.833	7.985	6
0.25 mg/mL	102.167	6.706	6	92.167	3.189	6
0.125 mg/mL	108.167	6.853	6	97.667	3.386	6
0.0625 mg/mL	104.333	8.733	6	91.000	7.127	6

Figure 5.1 MTS viability assay measuring cytotoxicity of micelle doses over 24h.

5.2.2 BA copolymer Synthesis

As previously described in chapter 4 (Experimental) and other references, lableled diblock copolymers of DMA and APBA were prepared by sequential RAFT polymerizations for cellular internalization studies.[38,39] In brief, a 6,200 Da polymer of DMA labeled with RHEA was synthesized by aqueous RAFT. This macroCTA was chain extended with APBA to create a second hydrophobic block with a mass of ~3,000 Da. These diblock copolymers were chosen due to their ability to form stable micelles under dilute nanoprecipitation conditions (50 mg/mL methanol stock solution into neutral PBS at 1 mg/mL) as shown in chapter 4.

5.2.3 Cellular Internalization

While we expected the micelles with outer blocks composed of DMA to be biocompatible, we were unsure how effectively these materials would be internalized. [40–42] We used BA micelles labeled with RHEA to determine the extent of internalization after 1 h of treatment. The same NIH 3T3 cells were used, and the presence of the polymers within cells was detected with flow cytometry. All concentrations were highly internalized into 99% of the cells, while the MFI increased with increasing micelle dose. We were surprised to see rapid and complete internalization of these micelles since the surface is both neutrally charged, and bare of targeting moieties.

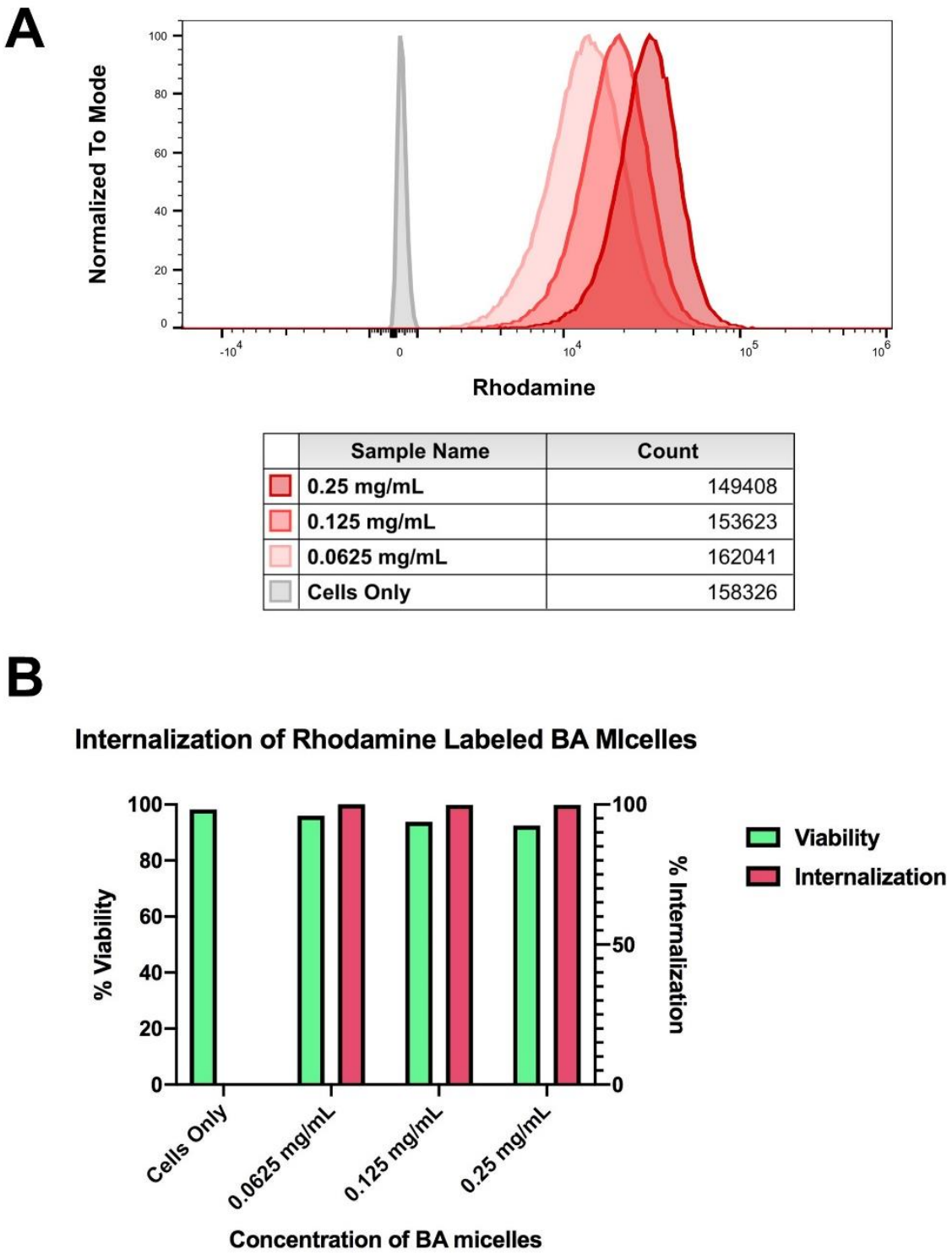

Figure 5.2 A) Fluorescence intensity histograms of cellular internalization of rhodamine labeled BA micelles in NIH 3T3 cells. Cells were treated with micelles at various concentrations 0.5, 0.25, 0.125, and 0.0625 mg/mL for 1 h, stained with zombie violet, and analyzed by flow cytometry. B) Viability and internalization percentages of NIH 3T3 cells treated with rhodamine labeled BA micelles

5.2.4 Effect of micelle surface charge on cellular internalization

Having established the cytocompatibility in a robust cell type (fibroblasts) we evaluated the acute toxicity and internalization of BA micelles with different degrees of cationic surface charge in an extremely sensitive neuronal cell line (PC-12). Two new labeled BA diblock copolymers were synthesized with the cationic monomer DMPA at degrees of polymerization of 5 (DDR5), and 10 (DDR10) (Figure 5.3A). The original labeled BA polymer with no cationic charge, will be referred to as DR0 (Table 5.1). These materials were nanoprecipitated as previously described and formed stable micelles (Figure 5.3B).

Table 5.1 Degrees of polymerization of monomers in the DR polymers and relative fluorescence intensity ratios.

Nickname	DMA	DMPAA	APBA	RHEA	*F.I. Ratio*
DR 0	49	0	17	0.4	2.3
DDR 5	48	4.8	25	0.2	2.6
DDR 10	38.5	8.6	17	0.2	1

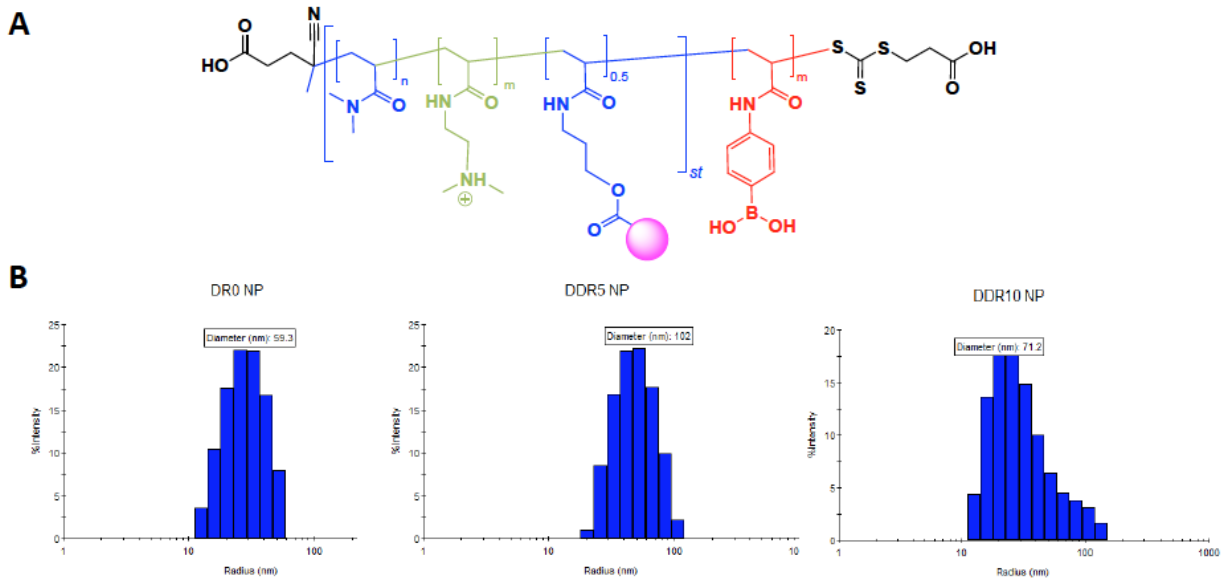

Figure 5.3 A) Structure of DR polymers including DMA, DMPA, RHEA, and APBA. B) DLS histograms of micelle sizes, with diameters for each micelle DR0 (59.3 nm), DDR5 (102 nm), and DDR10 (71.2 nm).

We treated PC-12 cells with 0.25 mg/mL concentrations of DR0, DDR5, and DDR10 for 1 hour, washed the cells extensively, and then measured the intracellular rhodamine fluorescence with flow cytometry (Figure 5.4A and B). Importantly, all the polymers were non-toxic even to this sensitive neuronal cell line with cell viability in each sample exceeding 90% (Figure 5.4C). Interestingly, DR0 and DDR10 were internalized in almost 100% of the cells measured. In contrast, only 76% of cells had internalized DDR5 after the 1 h incubation. Since both the highly cationic DDR10 and neutral DR0 micelles had high uptake, we believe that the reduced internalization of DDR5 was due to its larger diameter (100 nm, Figure 5.3B). Much to our surprise, cationic charge seemed to have little effect on BA micelle uptake, with size potentially being a more important consideration.

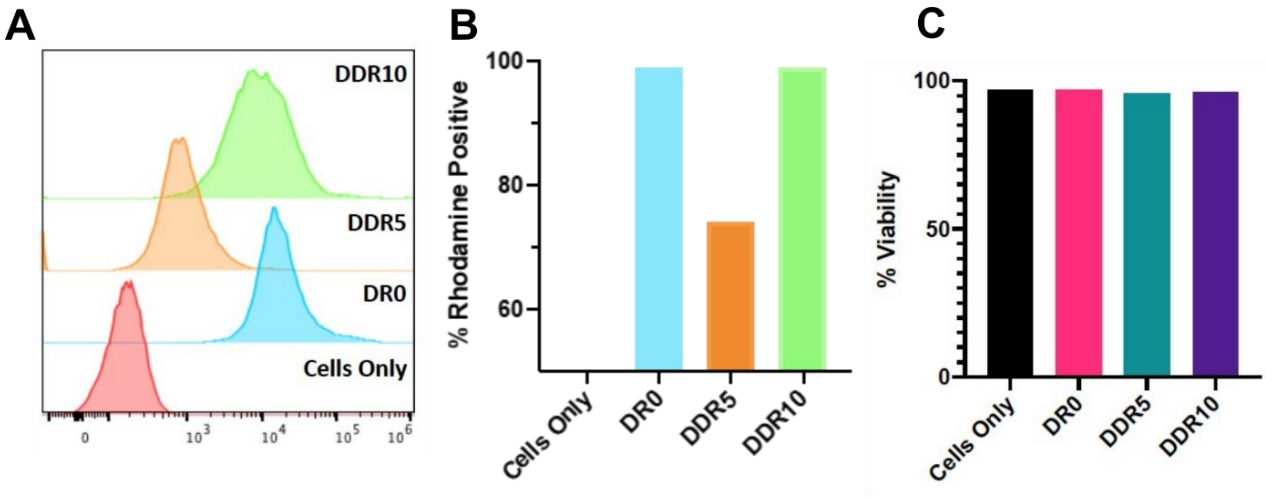

Figure 5.4 A) Fluorescence intensity histograms of PC-12 cells after 1 h incubation with cationic BA micelles. B) Percentages of cells that internalized BA micelles based on rhodamine fluorescence. C) Acute toxicity of cationic BA micelles to neuronal cell line after 1 h exposure, determined by Zombie Violet live/dead staining.

5.2.5 BA – protein nanocomplex formation and characterization

The procedure for the encapsulation of protein cargo in polymeric nanocarriers was similar to the nanoprecipitation described in chapter 4 but has a key distinction. Importantly, the protein cargo is hydrophilic and often charged, precluding it from being loaded into the polymer at high concentrations in organic solution. Instead, the model protein, BSA, was dissolved in neutral PBS at a concentration of 1 mg/mL. To this solution an equal mass of copolymer was added slowly from the 50 mg/mL methanol stock solution (20 µL), with rapid stirring.[28,43,44] The interactions between the BA groups and nitrogen containing amino acids cause the polymers to self-assemble around the BSA forming nanocomplexes. At this equal mass ratio of polymer to protein in PBS, uniform nanoparticles with diameters of 150 nm were formed (Figure 5.5). Since BSA itself is a 67 kDa protein, it has a diameter of ~8-10 nm.[45] The small peak in the DLS around 10 nm indicates that most of the protein was encapsulated by the BA copolymer.

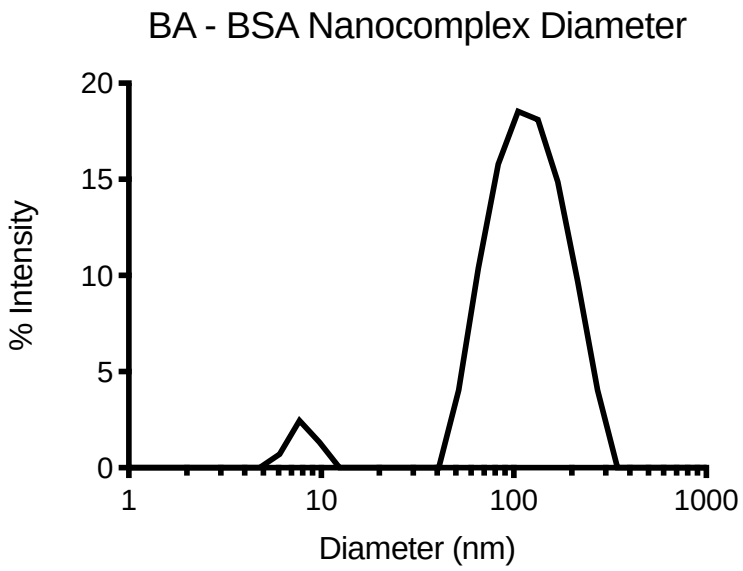

Figure 5.5 Dynamic Light Scattering (DLS) measurement of the nanocomplex composed of BA copolymers and BSA (diameter 150 nm).

5.2.6 Protein and peptide encapsulation efficiency

Next we quantified the efficiency of the BSA encapsulation in the BA copolymer. Particularly, at these high protein to polymer mass ratios (1:1) only a few systems have achieved greater than 50% encapsulation efficiency.[46] The BSA was labeled with an NHS functionalized Cy5 fluorophore at a 1% by mass ratio. The same procedure for complex formation described in the previous section was repeated with the labeled BSA, and after a 30 minute equilibration, the fluorescence of the complex was measured. To determine encapsulation efficiency, free labeled BSA and BA – BSA nanocomplex were separately centrifuged in 100 kDa Amicon spin filters. After normalizing the fluorescence measurements to account for the differences in volume between the flow through and the retained fractions, the percent of the labeled BSA that was either free or encapsulated was calculated (Figure 5.6). The 100 kDa filter does not retain free BSA, however when encapsulated in the BA nanocomplex 76% of the protein is retained. For this formulation strategy the resulting nanocomplexes are roughly 43% protein by weight.

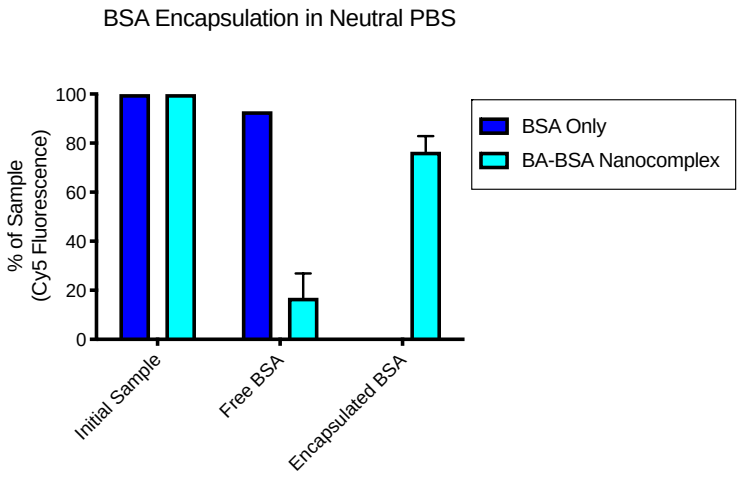

Figure 5.6 Encapsulation efficiency of labeled BSA in BA copolymer nanocomplex at neutral pH, resulting in a nanocomplex with 76% encapsulation efficiency. Free protein and complexed protein were separated by spin filtration with a 100k MWCO filter.

Excited by encapsulating large macromolecules with greater than 50% efficiency, we investigated if the BA-BSA nanocomplexes would release the protein cargo under slightly acidic conditions that mirror early endosomal pH. Using the same filtration technique, BA-BSA nanocomplexes were diluted into either slightly acidic PBS (pH 6.8) or neutral PBS (pH 7.4) and centrifuged to separate free and encapsulated protein. We found that in as little as 15 minutes in acidic buffer, the free BSA in solution more than doubled from 17% to 48% (Figure 5.7).

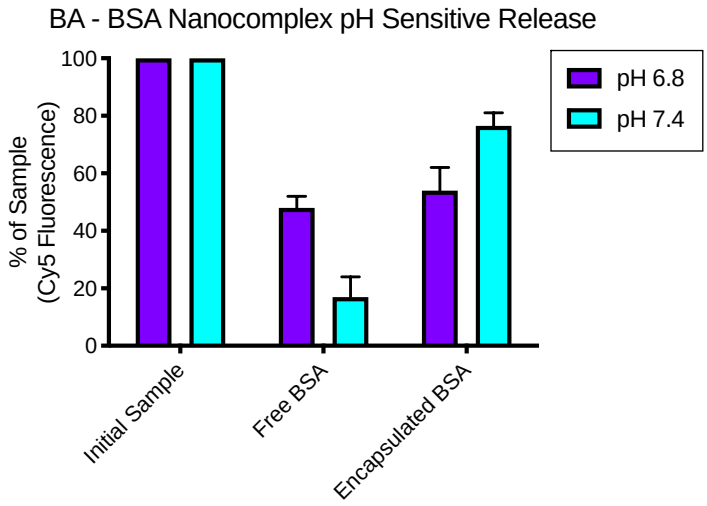

Figure 5.7 Comparison of encapsulated and free labeled BSA in BA-BSA nanocomplex formulations at pH 6.8 and 7.4.

Lastly, with promising results for both encapsulation and release of proteins, we investigated the ability of BA copolymers to encapsulate peptides. The melittin peptide, the active component of honey bee venom, was synthesized on a Liberty Blue microwave peptide synthesizer, and labeled with rhodamine via EDC/NHS conjugation. After removing free rhodamine by dialysis, the peptide was dissolved at 1 mg/mL in PBS. Following the same procedure for BSA nanocomplex formation, 1 mg of BA copolymer from concentrated solution was added dropwise with vigorous stirring. Since the peptide in this study, is 3,300 Da, to determine encapsulation efficiency a 10 kDa amicon filter was used. After centrifugation the fluorescence of the flow through and retained fractions was measured and adjusted for changes in volume to calculate the encapsulation efficiency (Figure 5.8). At this 1:1 weight ratio, 88% of the peptide was encapsulated, for a total weight percent of 46% peptide in the nanocomplex

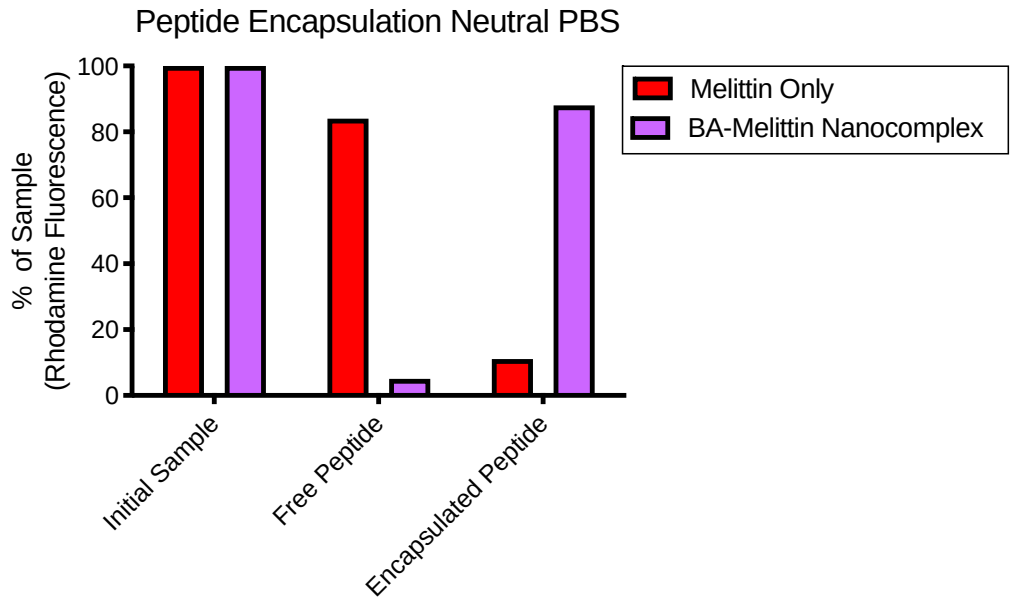

Figure 5.8 Encapsulation efficiency of labeled melittin in BA-melittin nanocomplex at equal mass loading of peptide and polymer.

5.2.7 Intracellular protein delivery

Having assessed the ability of BA copolymers to encapsulate both proteins and peptides, we next evaluated if the protein-polymer nanocomplex could facilitate cellular uptake of labeled BSA. HeLa cells were washed with serum free media, and then treated with nanocomplex in the same media for 4 hours. After the incubation, the cells were washed 3 times with PBS and the extent of internalization was measured using flow cytometry (Figure 5.9). The median fluorescence intensity averaged over ~20,000 live cell events was used to compare the extent of fluorescent internalization of free BSA and BA-BSA nanocomplex. At protein doses of 20 μg and 40 μg, the BA-BSA nanocomplexes increased the internalization of BSA. This preliminary data is promising because the overall charge of the polymers is neutral and the BSA is negative. As a result, these nanocomplexes have high translational potential because of the increased stability of neutral and negatively charged nanomaterials *in vivo*.

.

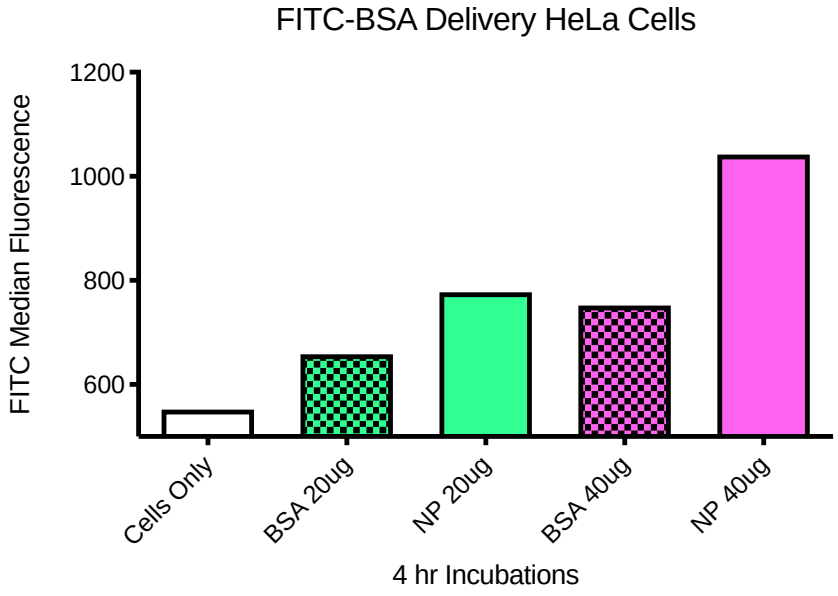

Figure 5.9 Median FITC signal from fluorescently labeled BSA in HeLa cells after 4 hour incubation with either free BSA or BA-BSA nanocomplex.

5.2.8 Linear cationic and lipophilic boronic acid polymers for gene delivery to T-cells

To improve nonviral gene delivery to primary T-cells we pursued a similar strategy to our previously published work, but instead of varying polymer architecture, we explored the effects of polymer composition.[17,47] Specifically, we aimed to leverage the ability of boronic acid functional groups to increase cellular internalization and lipophilic sidechains to increase association with hydrophobic cell membranes. To this end, we designed a library of linear polymers with various cationic charges, boronic acid contents, and lipophilic sidechains. To synthesize these polymers, we used RAFT polymerization, which despite this broad range of monomer properties can yield accurate molecular weights and low dispersities. Importantly for scale up, all the functional monomers (DMA, DMPA, DDA, and APBA) are commercially available, and only the fluorescently labeled monomer had to be synthesized (Figure 5.10).

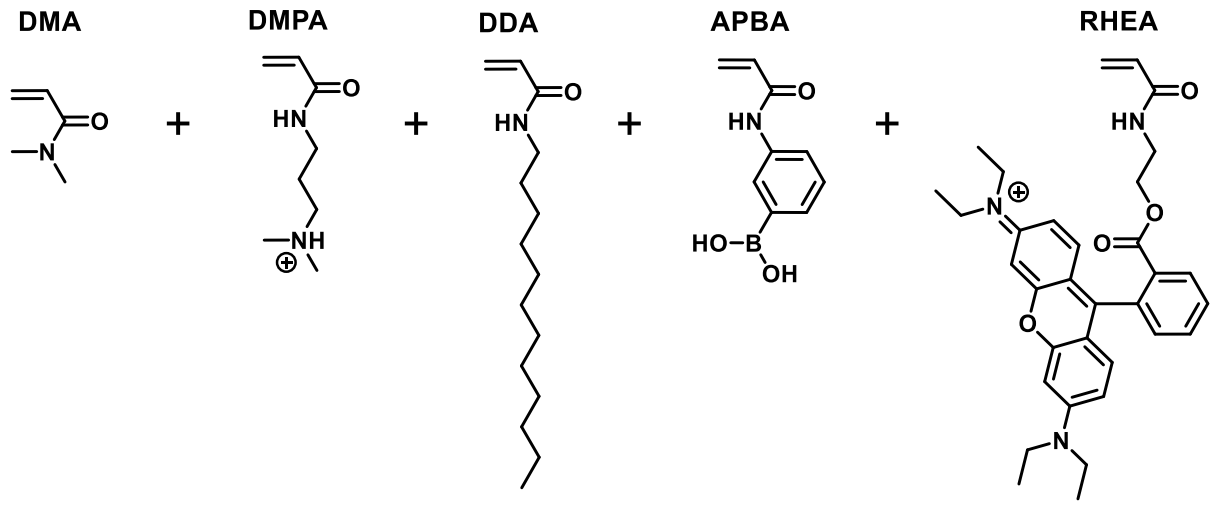

Figure 5.10 Structures of the monomers used for the synthesis of linear cationic boronic acid polymers for nonviral gene delivery.

While it is difficult to achieve high conversion of cationic acrylamides, high concentrations of acidic buffers mixed with polar organic solvents can dramatically increase reaction rates.[48,49] We found that as the cationic monomer content increased conversion decreased, but that mixtures of

1 M Sodium Acetate buffer (pH 5.5) with Dioxane (at 1:2 or 1:1) recovered some of this lost conversion after 20 h (Figure 5.11). Interestingly, reactions without RHEA also polymerized faster than reactions with the monomer.

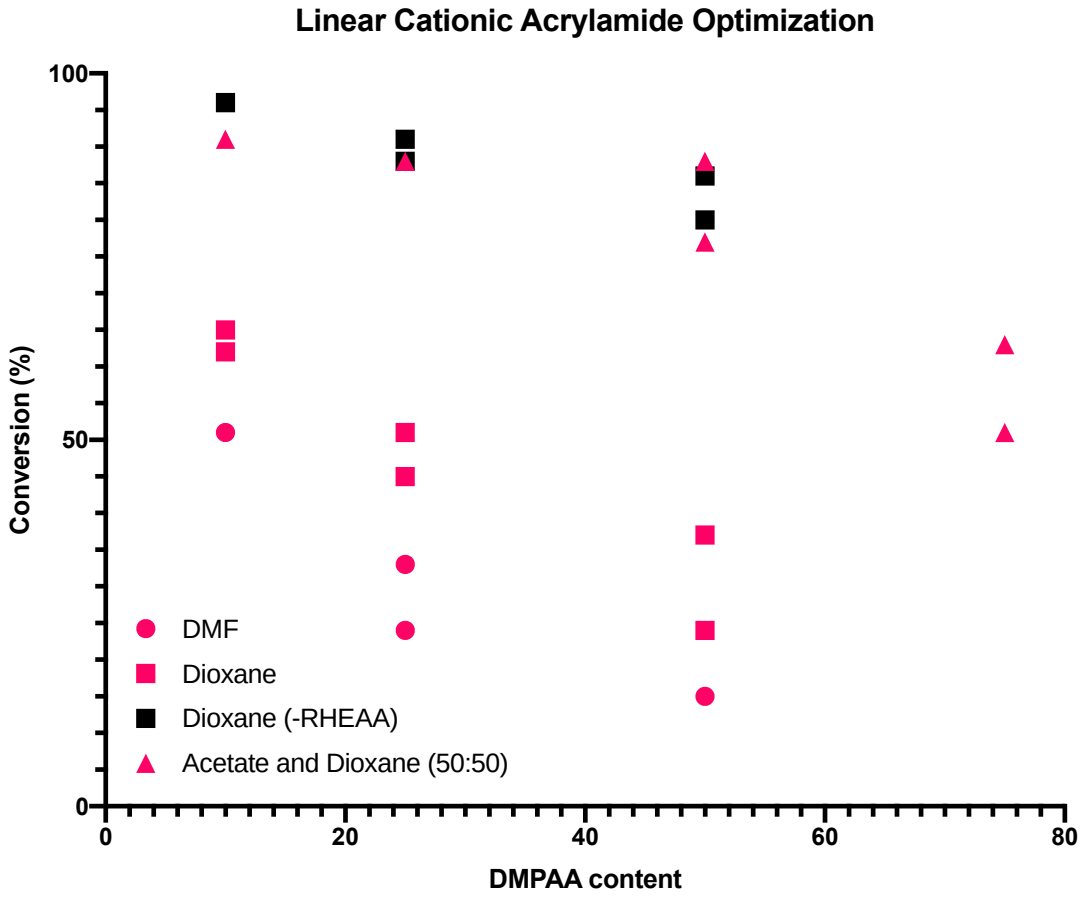

Figure 5.11 Conversion of acrylamide polymerizations with various DMPA content. Increasing the DMPA content reduced conversion as did adding the fluorescently labeled monomer (RHEA).

After optimization of the polymerization conditions, a representative polymer without RHEA, DDA, or APBA was synthesized for SEC characterization (DD50). We chose to synthesize a polymer with only DMA and DMPA because the majority of the mass of these polymers is DMA and DMPA, and all the excluded monomers make SEC characterization difficult or impossible. We used 150 mM Acetate buffer (pH 4.4) as the elutant, and determined the DD50 polymer ($M_{n,theory}$ = 24,960 Da) had an absolute molecular weight of 28,450 Da and dispersity of 1.32

(Figure 5.12). Next, we synthesized a labeled panel of 8, ~20 kDa, polymers varying cationic charge, lipophilicity, and boronic acid content (Table 5.2). We chose to keep all boronic acid content at 10% by weight because we did not want to decrease polymer solubility. Additionally, when we tried to synthesize polymers with cationic content above 50%, we were unable to achieve high enough conversion to hit the target 20 kDa molecular weight.

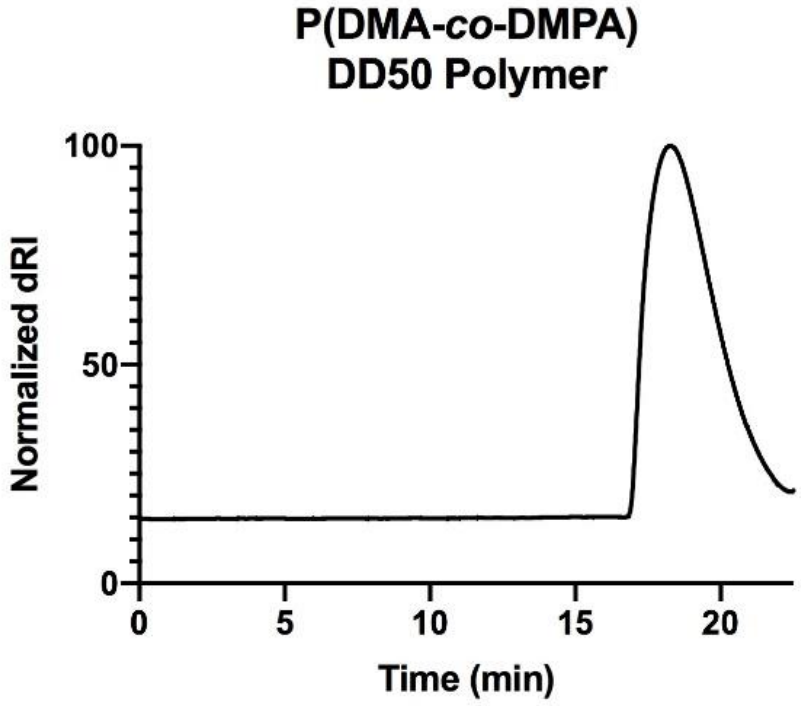

Figure 5.12 SEC of DD50 polymer in 150 mM Acetate buffer (pH 4.4). $M_{n,\ absolute}$ = 28,960 Da and $Đ$ = 1.32.

Table 5.2 Compositions of cationic BA polymers used for nucleic acid delivery to T cells.

Named	Cationic weight %	DMA	DMPA	APBA	DDA	Mw_{th}
DD50B10	50	79	64	11	---	20,000
DD25B10	25	142	35	12	---	22,000
DD10B10	10	182	15	12	---	22,750
DD25	25	140	30	---	---	18,750
DD25L20	25	110	32	---	17	20,250
DD50B10L5	50	64	61	10	5	19,250
DD75B10	*75*	*22*	*75*	*8*	---	*15,750*
DD75B10L5	*75*	*10*	*61*	*7*	*3*	*12,750*

5.2.9 Boronic acid polyplex cellular internalization

We first isolated the effect of the boronic acid functional group on polymer internalization in Jurkat T cells, a suspension cell line. This cell line is more predictive of polyplex transfection in primary T cells than adherent cell lines.[47] Polyplexes with DD25 and DD25B10 were prepared with GFPmax plasmid at N/P ratios of 3, 5, 10 and 15. We compared the transfection of these polyplex against the previously developed comb polymers. For the new polymers, we measured both polymer internalization and transfection efficiency with flow cytometry and obtained promising preliminary results, despite not observing any transfection. Unfortunately, the tested comb polymers were extremely toxic, killing almost 90% of the T cells. The new polymers (DD25 and DD25B10) showed remarkably high viability even at N/P ratios of 15 (>90%). While we could not detect any GFP in the cells treated with the DD25 and DD25B10 polymers, we saw concentration dependent increases in polymer uptake of the DD25B10 polymers. This

observation contrasts with the DD25 polymer, which despite increasing the polymer treatment from 18 to 90 µg was internalized into less than 1% of the Jurkats. Directly comparing polyplexes with N/P ratios of 15, the DD25B10 polymer was present in 100-fold more cells. This preliminary study illustrates that functional groups on cationic linear polymers can dramatically influence internalization into Jurkat cells, and that this approach warrants further study.

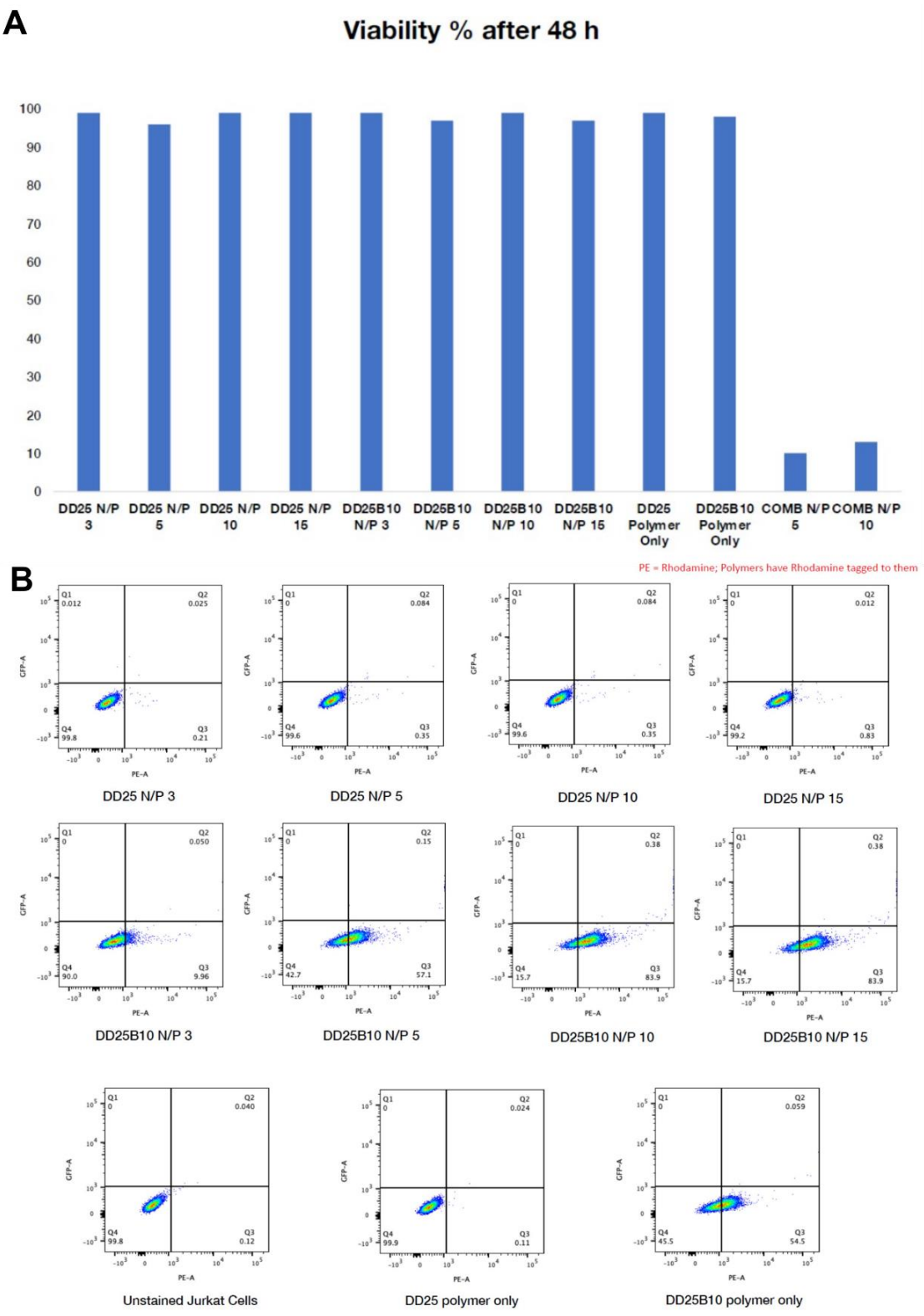

Figure 5.13 Flow cytometry analysis of Jurkat cells treated with polyplexes. A) Cytotoxicity of polyplex at N/P ratios of 3, 5, 10, and 15. B) Measurements of fluorescence intensity of GFP (transfection) and polymer internalization (PE).

5.3 Conclusions

In this chapter, the use of BA copolymers as efficient and highly versatile vehicles for the intracellular delivery biologics is explored. This strategy utilizes BAs to coordinate with amine containing amino acids to load peptides and proteins into micelles and takes advantage of BA binding to membrane bound sugars to increase cellular internalization. Current progress has confirmed the biocompatibility of these polymers and the high loading efficiency of both peptides and proteins into nanocomplexes. Additionally, these nanocomplexes increased the delivery of BSA into HeLa cells, without any cationic charge. Initial experiments also show promising trends for decreased stability of the complex under slightly acidic conditions. While continuing to develop micelles for delivery of RNPs, we explored the potential of cationic BA copolymers to facilitate nucleic acid delivery into notoriously difficult to transfect cells, T cells. We synthesized 8 labeled linear polymers with various cationic charge, BA content, and lipophilicity. Preliminary results show the polymer composition dramatically effects uptake into T cells by up to two orders of magnitude. Overall, BA copolymers have broad utility for the delivery of biologics into various cell types, with minimal toxicity.

Future work will investigate functional protein delivery, in the form of horse radish peroxidase (HRP) for fluorescent detection, or RNPs for gene knock out or repair. If the protein function is retained after intracellular delivery, we will focus efforts on optimizing micelle charge, size, and composition to perform gene editing on primary T cells. While there is some evidence phenyl boronic acid itself can mediate endosomal escape [24], we have observed remarkably high endosomal escape using lytic venom peptides.[50] Since BA copolymers can complex proteins and peptides, if we measure high internalization of nanocomplexes but limited gene editing, we can add the pH sensitive lytic peptide C6M3 to the formulation to facilitate

endosomal escape. Additionally, studies comparing the polymers synthesized for nucleic acid delivery will be used to determine the effect of BA content and lipophilicity on transfection efficiency in primary T cells.

5.4 Experimental

5.4.1 Instruments

Nuclear Magnetic Resonance (NMR) Spectroscopy

^{1}H NMR spectra were obtained using a Bruker AVance 300 MHz instrument. Solvents used in this study were obtained from Cambridge Isotope Laboratories and included: deuterium oxide, deuterated methanol, deuterated sodium hydroxide, deuterated dimethylsulfoxide, and deuterated chloroform. Data was processed with MestReNova 10.0.

Size exclusion chromatography (SEC)

The molecular weight ($M_{n\ SEC}$) and dispersity were determined using 100% mass recovery and multiangle light scattering (MALS) SEC. The running solvent was N,N-dimethyl formamide (DMF) with 1 g/L LiBr (flow rate: 0.8 mL/min) heated to 60 °C and samples were prepared at 5 mg/mL. Separation was done through three columns Tosoh TSKgel alpha 4000, Tosoh TSKgel alpha 3000 and Phenomenex Phenogel 5 µm 10E3 Å. For cationic polymers, the running solvent was 150 mM Sodium Acetate buffer with a pH of 4.4, samples were prepared at 5 mg/mL, and the column used was a Phenomenex GFC-P 4000. Data was collected by a Wyatt miniDAWN Treos and Wyatt Optilab T-rex. For data analysis, specifically determination of absolute molecular weight and dispersity, Wyatt ASTRA software was used. The RI traces were normalized using Prism 10.

Dynamic Light Scattering (DLS)

The hydrodynamic diameter and dispersity of polymeric micelles were determined with a Wyatt DynaPro NanoStar. Samples between 0.1 – 1 mg/mL in PBS were centrifuged at 10,000 rpm for 2 minutes to remove dust and then 10 measurements were taken and averaged.

5.4.2 Methods

5.4.2.1 Viability Assay

For viability studies, NIH 3T3 cells were plated in a 96-well plate at 10,000 cells/well. After overnight incubation, 200 µL solutions of the BA and DB micelles (prepared as previously described) in media were added at 0.5, 0.25, 0.125, 0.0625 mg/mL concentrations. After a 1 h incubation cells were washed with PBS, and fresh media was added. 24 h later viability was determined by MTS/PMS.

5.4.2.2 Rhodamine Acrylamide (RHEAA) synthesis

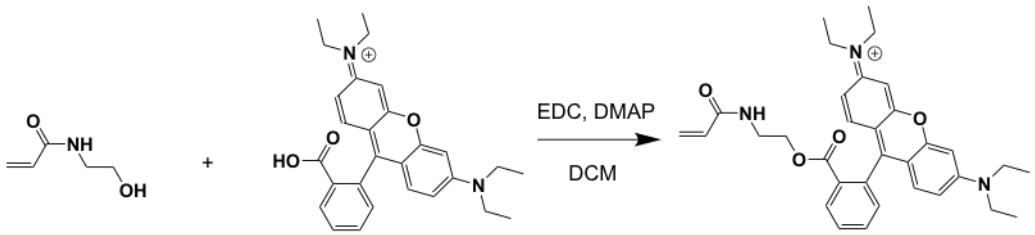

RHEAA synthesis was a adapted from a previous published procedure.[51] In brief, Rhodamine B (1.0 g, 2 mmol), EDC (800 mg, 4 mmol), dimethylaminopyridine (DMAP, 26 mg, 0.2 mmol), hydroxyethyl acrylamide (HEAA, 480 mg, 4 mmol) were added to a 50 mL round bottom flask and dissolved in 15 mL of DCM (0.1 M). The reaction was stirred at RT for 24 h, and then purified via silica plug. The first wash with 5% MeOH/DCM removed the excess HEAA, while

the second wash with 10% MeOH/DCM removed the RHEAA. The remaining impurities remained trapped in the silica.

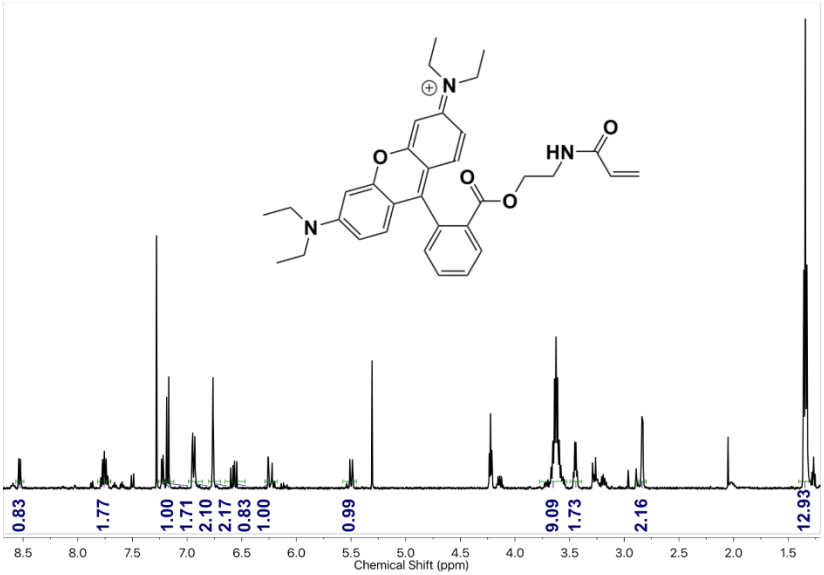

Figure 5.14 ^{1}H NMR Spectrum of RHEAA ($CDCl_3$)

Block copolymer synthesis

5.4.2.3 DMA macroCTA synthesis

To a 25 mL round bottom flask (RBF), 4-((((2-carboxyethyl)thio)carbonothioyl)thio)-4-cyanopentanoic acid (CCC) (162 mg, 0.53 mmol), 4,4-Azobis(4-cyanovaleric acid) (ABCVA) (14.28 mg, 0.05 mmol), *N*,*N*-dimethaylacrylamide (DMA) (3.62 mL, 35.18 mmol), nanopure water (7.0 mL) and a magnetic stir bar were added. For rhodamine labeled polymers, a DP of 0.25 was targeted, by adding 2% RHEAA by mass to the polymerization. For cationic micelles, *N*,*N*-dimethyl amino propyl acrylamide (DMPA) was also added to the reaction solution at target DPs of 5 and 10, and the solvent was switched to 1 M Acetate buffer pH 5.5. The solution was stirred until it was a homogenous and then sparged with argon gas vigorously for 20 minutes. Then the reaction was heated to 70 °C for 2 hours and halted with exposure to atmosphere. The conversion, DP, and $M_{n,theo}$ were determined by ^{1}H NMR in methanol-d_4 of the reaction mixture.

The polymer was dialyzed against DI water for 24 hours with 3.5 kDa molecular weight cutoff (MWCO) dialysis tubing and then lyophilized.

5.4.2.4 DMA chain extension with APBA

These polymers were synthesized according to previous reports.[52] As an example polymerization, DMA MacroCTA (248.5 mg, 3.8×10^{-2} mmol), ABCVA (1.06 mg, 3.8×10^{-3} mmol), 3-acrylamidophenylboronic acid (APBA) (144.5 mg, 0.76 mmol), dioxane (0.95 mL), nanopure water (0.24 mL) and a magnetic stir bar were added to a 5 mL RBF. Once fully dissolved a 50 µL aliquot was removed and frozen. The reaction was sparged vigorously for 10 minutes and then heated to 70 °C. After 2.5 hours, the reaction was stopped by exposing it to air and the conversion, DP, and $M_{n,theo}$ were determined by ^{1}H NMR in methanol-d_4. The copolymer was purified by precipitation into cold diethyl ether. To remove trace amounts of the remaining APBA monomer, two more precipitations were done by dissolving the precipitate in methanol and reprecipitating into fresh diethyl ether. The weight percent of APBA in the final polymer (42%) was confirmed by using levofloxacin as an NMR standard.

5.4.2.5 Cationic Copolymer Synthesis

All polymers were synthesized using RAFT polymerization and conducted similarly to the following example. To a 25 mL round bottom flask (RBF), CCC (3.68 mg, 0.012 mmol), ABCVA (1.12 mg, 0.004 mmol), DMA (103 µL, 1 mmol), APBA (30 mg, 0.158 mmol), DMPA (150 mg, 0.962 mmol), *N*-dodecyl acrylamide (DDA, 18mg, 0.075 mmol), RHEA (3 mg, 0.005 mmol), 1M Acetate buffer (pH 5.5, 367 µL), Dioxane (367 µL) and a magnetic stir bar were added. The solution was stirred until it was a homogenous and then sparged with argon gas

vigorously for 10 minutes. Then the reaction was heated to 70 °C for 20 hours and halted with exposure to atmosphere. The conversion, DP, and $M_{n,theo}$ were determined by ^1H NMR in methanol-d_4 of the reaction mixture. The polymer was dialyzed against DI water for 24 hours with 3.5 kDa molecular weight cutoff (MWCO) dialysis tubing and then lyophilized.

5.4.2.6 Micelle formulation and protein encapsulation

Stock solutions of polymer (50 mg/mL in methanol) were prepared and 1 mg of polymer (20 µL) was nanoprecipitated into 1 mL of PBS (pH 7.4) and dialyzed against PBS for 24 h.

For protein and peptide encapsulation, prior to nanoprecipitation, the biologics were dissolved in the PBS at a concentration of 1 mg/mL and then the organic solution of polymer was added dropwise. These solutions were not sonicated, and were purified with Amicon spin filters (100 kDa MWCO).

5.4.2.7 Polyplex formulation

Polyplexes were formed by adding equal volumes (25 µL) of plasmid DNA (pGFP max, 0.1 mg/mL) and polymer solution (concentration varied depending on N/P ratio). As an example for an N/P ratio of 5 using the DD25B10 polymer, a 20 mg/mL stock solution was diluted to down to 1 mg/mL and added to DNA. Complexes assembled after 5 minutes at RT, and were used to treat cells immediately.

5.4.2.8 Cell Culture

HeLas were cultured in DMEM with 10% fetal bovine serum (FBS) and 1% Pen/Strep. PC-12 cells were cultured in RPMI-1640 with 10% donor equine serum (DHS) and 1% Pen/Strep. NIH

3T3 cells were cultured in DMEM with 10% FBS and 1% Pen/Strep. Jurkat cells were cultured in RPMI-1640 with 10% FBS.

Flow cytometry

5.4.2.9 Neutral polymer internalization

One million NIH 3T3 cells per well were seeded overnight in a 6-well plate. The next day, the media was removed, the cells were washed 2x with PBS and then micelle solutions of 0.5, 0.25, 0.125, and 0.0625 mg/mL in media were added. The cells were incubated with the micelles at 37 ºC for 60 min and then washed 3x with PBS. The cells were lifted with trypsin, spun down at 200 x g for 10 min and then resuspended in PBS. The cells were then stained with the live-dead stain (Zombie Violet) and analyzed by flow cytometry (Attune NxT Flow Cytometer, ThermoFisher Scientific). At least 10 thousand cells were analyzed by FlowJo software after serial gating, and mean fluorescence intensity was used as measure of micelle uptake.

5.4.2.10 Cationic Micelle Toxicity and Uptake

One million PC-12 cells per well were seeded into a round bottom 96-well plate. The same day, the media was removed, the cells were washed 2x with PBS and then micelle solutions of 0.25 mg/mL in media were added. The cells were incubated with the micelles at 37 ºC for 60 min and then washed 3x with PBS by spinning down at 4 ºC and 200 x g. The cells were then stained with the live-dead stain (Zombie Violet) and analyzed by flow cytometry (Attune NxT Flow Cytometer, ThermoFisher Scientific). At least 10 thousand cells were analyzed by FlowJo software after serial gating, and mean fluorescence intensity (of rhodamine dye) was used as measure of micelle uptake.

5.4.2.11 Protein Delivery

One million HeLa cells per well were seeded overnight in a 6-well plate. The next day, the media was removed, the cells were washed 2x with PBS and then protein-polymer complex solutions of 20 μg and 40 μg in media were added. The cells were incubated with the micelles at 37 ºC for 4 h and then washed 3x with PBS. The cells were lifted with trypsin, spun down at 200 x g for 10 min and then resuspended in PBS. The cells were then stained with the live-dead stain (Zombie Violet) and analyzed by flow cytometry (Attune NxT Flow Cytometer, ThermoFisher Scientific). At least 20 thousand cells were analyzed by FlowJo software after serial gating, and mean fluorescence intensity was used as measure of protein delivery.

5.4.2.12 Polyplex Uptake and transfection efficiency

200,000 Jurkat cells per well were seeded into a 24 well plate at a concentration of 1 million cells per mL in Opti-MEM. The same day, the cells were treated with micelle solutions of 0.25 mg/mL in media were added. The cells were incubated with 1 μg of nucleic acid complex to polyplex at 37 ºC for 4 h and then diluted with RPMI with 10% FBS. After 24 h, the cells were then stained with the live-dead stain (Zombie Violet) and analyzed by flow cytometry (Attune NxT Flow Cytometer, ThermoFisher Scientific). At least 10 thousand cells were analyzed by FlowJo software after serial gating, and mean fluorescence intensity (of rhodamine dye) was used as measure of micelle uptake.

References:

(1) Ginn, S. L.; Amaya, A. K.; Alexander, I. E.; Edelstein, M.; Abedi, M. R. Gene Therapy Clinical Trials Worldwide to 2017: An Update. *The Journal of Gene Medicine* **2018**, *20* (5), e3015. https://doi.org/10.1002/jgm.3015.

(2) Jackson, L. A.; Anderson, E. J.; Rouphael, N. G.; Roberts, P. C.; Makhene, M.; Coler, R. N.; McCullough, M. P.; Chappell, J. D.; Denison, M. R.; Stevens, L. J.; Pruijssers, A. J.; McDermott, A.; Flach, B.; Doria-Rose, N. A.; Corbett, K. S.; Morabito, K. M.; O'Dell, S.; Schmidt, S. D.; II, P. A. S.; Padilla, M.; Mascola, J. R.; Neuzil, K. M.; Bennett, H.; Sun, W.; Peters, E.; Makowski, M.; Albert, J.; Cross, K.; Buchanan, W.; Pikaart-Tautges, R.; Ledgerwood, J. E.; Graham, B. S.; Beigel, J. H. An MRNA Vaccine against SARS-CoV-2 — Preliminary Report. *New England Journal of Medicine* **2020**. https://doi.org/10.1056/NEJMoa2022483.

(3) Smith, T. T.; Stephan, S. B.; Moffett, H. F.; McKnight, L. E.; Ji, W.; Reiman, D.; Bonagofski, E.; Wohlfahrt, M. E.; Pillai, S. P. S.; Stephan, M. T. In Situ Programming of Leukaemia-Specific T Cells Using Synthetic DNA Nanocarriers. *Nature Nanotech* **2017**, *12* (8), 813–820. https://doi.org/10.1038/nnano.2017.57.

(4) van Haasteren, J.; Li, J.; Scheideler, O. J.; Murthy, N.; Schaffer, D. V. The Delivery Challenge: Fulfilling the Promise of Therapeutic Genome Editing. *Nat Biotechnol* **2020**, *38* (7), 845–855. https://doi.org/10.1038/s41587-020-0565-5.

(5) Wang, H.-X.; Li, M.; Lee, C. M.; Chakraborty, S.; Kim, H.-W.; Bao, G.; Leong, K. W. CRISPR/Cas9-Based Genome Editing for Disease Modeling and Therapy: Challenges and Opportunities for Nonviral Delivery. *Chem. Rev.* **2017**, *117* (15), 9874–9906. https://doi.org/10.1021/acs.chemrev.6b00799.

(6) Nambiar, T. S.; Billon, P.; Diedenhofen, G.; Hayward, S. B.; Taglialatela, A.; Cai, K.; Huang, J.-W.; Leuzzi, G.; Cuella-Martin, R.; Palacios, A.; Gupta, A.; Egli, D.; Ciccia, A. Stimulation of CRISPR-Mediated Homology-Directed Repair by an Engineered RAD18 Variant. *Nat Commun* **2019**, *10* (1), 3395. https://doi.org/10.1038/s41467-019-11105-z.

(7) Degors, I. M. S.; Wang, C.; Rehman, Z. U.; Zuhorn, I. S. Carriers Break Barriers in Drug Delivery: Endocytosis and Endosomal Escape of Gene Delivery Vectors. *Acc. Chem. Res.* **2019**, *52* (7), 1750–1760. https://doi.org/10.1021/acs.accounts.9b00177.

(8) Zhang, Y.; Satterlee, A.; Huang, L. In Vivo Gene Delivery by Nonviral Vectors: Overcoming Hurdles? *Molecular Therapy* **2012**, *20* (7), 1298–1304. https://doi.org/10.1038/mt.2012.79.

(9) Jones, C. H.; Chen, C.-K.; Ravikrishnan, A.; Rane, S.; Pfeifer, B. A. Overcoming Nonviral Gene Delivery Barriers: Perspective and Future. *Mol. Pharmaceutics* **2013**, *10* (11), 4082–4098. https://doi.org/10.1021/mp400467x.

(10) Rosenblum, D.; Gutkin, A.; Dammes, N.; Peer, D. Progress and Challenges towards CRISPR/Cas Clinical Translation. *Advanced Drug Delivery Reviews* **2020**, *154–155*, 176–186. https://doi.org/10.1016/j.addr.2020.07.004.

(11) Behr, M.; Zhou, J.; Xu, B.; Zhang, H. In Vivo Delivery of CRISPR-Cas9 Therapeutics: Progress and Challenges. *Acta Pharmaceutica Sinica B* **2021**, *11* (8), 2150–2171. https://doi.org/10.1016/j.apsb.2021.05.020.

(12) Wei, T.; Cheng, Q.; Farbiak, L.; Anderson, D. G.; Langer, R.; Siegwart, D. J. Delivery of Tissue-Targeted Scalpels: Opportunities and Challenges for *In Vivo* CRISPR/Cas-Based

Genome Editing. *ACS Nano* **2020**, *14* (8), 9243–9262. https://doi.org/10.1021/acsnano.0c04707.
(13) Rosenberg, S. A.; Restifo, N. P. Adoptive Cell Transfer as Personalized Immunotherapy for Human Cancer. *Science* **2015**, *348* (6230), 62–68. https://doi.org/10.1126/science.aaa4967.
(14) June, C. H.; O'Connor, R. S.; Kawalekar, O. U.; Ghassemi, S.; Milone, M. C. CAR T Cell Immunotherapy for Human Cancer. *Science* **2018**, *359* (6382), 1361–1365. https://doi.org/10.1126/science.aar6711.
(15) Wang, X.; Rivière, I. Clinical Manufacturing of CAR T Cells: Foundation of a Promising Therapy. *Mol Ther Oncolytics* **2016**, *3*, 16015. https://doi.org/10.1038/mto.2016.15.
(16) New Costly Cancer Treatments Face Hurdles Getting to Patients - WSJ https://www.wsj.com/articles/new-costly-cancer-treatments-face-hurdles-getting-to-patients-1412627150 (accessed 2022 -01 -20).
(17) Olden, B. R.; Cheng, E.; Cheng, Y.; Pun, S. H. Identifying Key Barriers in Cationic Polymer Gene Delivery to Human T Cells. *Biomater. Sci.* **2019**, *7* (3), 789–797. https://doi.org/10.1039/C8BM01262H.
(18) Fu, A.; Tang, R.; Hardie, J.; Farkas, M. E.; Rotello, V. M. Promises and Pitfalls of Intracellular Delivery of Proteins. *Bioconjugate Chem.* **2014**, *25* (9), 1602–1608. https://doi.org/10.1021/bc500320j.
(19) Bareford, L. M.; Swaan, P. W. ENDOCYTIC MECHANISMS FOR TARGETED DRUG DELIVERY. *Adv Drug Deliv Rev* **2007**, *59* (8), 748–758. https://doi.org/10.1016/j.addr.2007.06.008.
(20) Chen, G.; Abdeen, A. A.; Wang, Y.; Shahi, P. K.; Robertson, S.; Xie, R.; Suzuki, M.; Pattnaik, B. R.; Saha, K.; Gong, S. A Biodegradable Nanocapsule Delivers a Cas9 Ribonucleoprotein Complex for in Vivo Genome Editing. *Nat. Nanotechnol.* **2019**, *14* (10), 974–980. https://doi.org/10.1038/s41565-019-0539-2.
(21) Tan, Z.; Jiang, Y.; Ganewatta, M. S.; Kumar, R.; Keith, A.; Twaroski, K.; Pengo, T.; Tolar, J.; Lodge, T. P.; Reineke, T. M. Block Polymer Micelles Enable CRISPR/Cas9 Ribonucleoprotein Delivery: Physicochemical Properties Affect Packaging Mechanisms and Gene Editing Efficiency. *Macromolecules* **2019**, *52* (21), 8197–8206. https://doi.org/10.1021/acs.macromol.9b01645.
(22) Liu, C.; Wan, T.; Wang, H.; Zhang, S.; Ping, Y.; Cheng, Y. A Boronic Acid–Rich Dendrimer with Robust and Unprecedented Efficiency for Cytosolic Protein Delivery and CRISPR-Cas9 Gene Editing. *Science Advances* **2019**, *5* (6), eaaw8922. https://doi.org/10.1126/sciadv.aaw8922.
(23) Hango, C. R.; Backlund, C. M.; Davis, H. C.; Posey, N. D.; Minter, L. M.; Tew, G. N. Non-Covalent Carrier Hydrophobicity as a Universal Predictor of Intracellular Protein Activity. *Biomacromolecules* **2021**, *22* (7), 2850–2863. https://doi.org/10.1021/acs.biomac.1c00242.
(24) Wang, R.; Yin, C.; Liu, C.; Sun, Y.; Xiao, P.; Li, J.; Yang, S.; Wu, W.; Jiang, X. Phenylboronic Acid Modification Augments the Lysosome Escape and Antitumor Efficacy of a Cylindrical Polymer Brush-Based Prodrug. *J. Am. Chem. Soc.* **2021**, *143* (49), 20927–20938. https://doi.org/10.1021/jacs.1c09741.
(25) Peeler, D. J.; Thai, S. N.; Cheng, Y.; Horner, P. J.; Sellers, D. L.; Pun, S. H. PH-Sensitive Polymer Micelles Provide Selective and Potentiated Lytic Capacity to Venom Peptides for

Effective Intracellular Delivery. *Biomaterials* **2019**, *192*, 235–244. https://doi.org/10.1016/j.biomaterials.2018.11.004.
(26) Sylvestre, M.; Lv, S.; Yang, L. F.; Luera, N.; Peeler, D. J.; Chen, B.-M.; Roffler, S. R.; Pun, S. H. Replacement of L-Amino Acid Peptides with D-Amino Acid Peptides Mitigates Anti-PEG Antibody Generation against Polymer-Peptide Conjugates in Mice. *Journal of Controlled Release* **2021**, *331*, 142–153. https://doi.org/10.1016/j.jconrel.2021.01.015.
(27) Cheng, Y.; Yumul, R. C.; Pun, S. H. Virus-Inspired Polymer for Efficient in Vitro and in Vivo Gene Delivery. *Angew Chem Int Ed Engl* **2016**, *55* (39), 12013–12017. https://doi.org/10.1002/anie.201605958.
(28) Reinhard, S.; Han, H.; Tuma, J.; Røise, J. J.; Li, I.-C.; Li, J.; Lee, H. Y.; Murthy, N. A PH-Sensitive Eosin-Block Copolymer Delivers Proteins Intracellularly. *Chem. Commun.* **2020**, *56* (91), 14207–14210. https://doi.org/10.1039/D0CC05165A.
(29) Andersen, K. A.; Smith, T. P.; Lomax, J. E.; Raines, R. T. Boronic Acid for the Traceless Delivery of Proteins into Cells. *ACS Chem Biol* **2016**, *11* (2), 319–323. https://doi.org/10.1021/acschembio.5b00966.
(30) Incani, V.; Lavasanifar, A.; Uludağ, H. Lipid and Hydrophobic Modification of Cationic Carriers on Route to Superior Gene Vectors. *Soft Matter* **2010**, *6* (10), 2124. https://doi.org/10.1039/b916362j.
(31) Lv, J.; Fan, Q.; Wang, H.; Cheng, Y. Polymers for Cytosolic Protein Delivery. *Biomaterials* **2019**, *218*, 119358. https://doi.org/10.1016/j.biomaterials.2019.119358.
(32) Lee, Y.-W.; Luther, D. C.; Kretzmann, J. A.; Burden, A.; Jeon, T.; Zhai, S.; Rotello, V. M. Protein Delivery into the Cell Cytosol Using Non-Viral Nanocarriers. *Theranostics* **2019**, *9* (11), 3280–3292. https://doi.org/10.7150/thno.34412.
(33) Lv, J.; He, B.; Yu, J.; Wang, Y.; Wang, C.; Zhang, S.; Wang, H.; Hu, J.; Zhang, Q.; Cheng, Y. Fluoropolymers for Intracellular and in Vivo Protein Delivery. *Biomaterials* **2018**, *182*, 167–175. https://doi.org/10.1016/j.biomaterials.2018.08.023.
(34) Kanduri, V.; LaVigne, D.; Larsen, J. Current Advances Toward the Encapsulation of Cas9. *ACS Macro Lett.* **2021**, *10* (12), 1576–1589. https://doi.org/10.1021/acsmacrolett.1c00538.
(35) Li, J.; Røise, J. J.; He, M.; Das, R.; Murthy, N. Non-Viral Strategies for Delivering Genome Editing Enzymes. *Advanced Drug Delivery Reviews* **2021**, *168*, 99–117. https://doi.org/10.1016/j.addr.2020.09.004.
(36) Kumar, R.; Santa Chalarca, C. F.; Bockman, M. R.; Bruggen, C. V.; Grimme, C. J.; Dalal, R. J.; Hanson, M. G.; Hexum, J. K.; Reineke, T. M. Polymeric Delivery of Therapeutic Nucleic Acids. *Chem. Rev.* **2021**, *121* (18), 11527–11652. https://doi.org/10.1021/acs.chemrev.0c00997.
(37) Ulkoski, D.; Bak, A.; Wilson, J. T.; Krishnamurthy, V. R. Recent Advances in Polymeric Materials for the Delivery of RNA Therapeutics. *Expert Opinion on Drug Delivery* **2019**, *16* (11), 1149–1167. https://doi.org/10.1080/17425247.2019.1663822.
(38) Bapat, A. P.; Roy, D.; Ray, J. G.; Savin, D. A.; Sumerlin, B. S. Dynamic-Covalent Macromolecular Stars with Boronic Ester Linkages. *J. Am. Chem. Soc.* **2011**, *133* (49), 19832–19838. https://doi.org/10.1021/ja207005z.
(39) Roy, D.; Cambre, J. N.; Sumerlin, B. S. Sugar-Responsive Block Copolymers by Direct RAFT Polymerization of Unprotected Boronic Acid Monomers. *Chem. Commun.* **2008**, No. 21, 2477. https://doi.org/10.1039/b802293c.

(40) Liong, C. S.; Smith, A. A. A.; Mann, J. L.; Roth, G. A.; Gale, E. C.; Maikawa, C. L.; Ou, B. S.; Appel, Eric. A. Enhanced Humoral Immune Response by High Density TLR Agonist Presentation on Hyperbranched Polymers. *Adv. Therap.* **2021**, *4* (4), 2000081. https://doi.org/10.1002/adtp.202000081.
(41) Wilson, J. T.; Postma, A.; Keller, S.; Convertine, A. J.; Moad, G.; Rizzardo, E.; Meagher, L.; Chiefari, J.; Stayton, P. S. Enhancement of MHC-I Antigen Presentation via Architectural Control of PH-Responsive, Endosomolytic Polymer Nanoparticles. *AAPS J* **2015**, *17* (2), 358–369. https://doi.org/10.1208/s12248-014-9697-1.
(42) Lane, D. D.; Chiu, D. Y.; Su, F. Y.; Srinivasan, S.; Kern, H. B.; Press, O. W.; Stayton, P. S.; Convertine, A. J. Well-Defined Single Polymer Nanoparticles for the Antibody-Targeted Delivery of Chemotherapeutic Agents. *Polym. Chem.* **2015**, *6* (8), 1286–1299. https://doi.org/10.1039/C4PY01250J.
(43) Liu, C.; Wan, T.; Wang, H.; Zhang, S.; Ping, Y.; Cheng, Y. A Boronic Acid–Rich Dendrimer with Robust and Unprecedented Efficiency for Cytosolic Protein Delivery and CRISPR-Cas9 Gene Editing. *Sci. Adv.* **2019**, *5* (6), eaaw8922. https://doi.org/10.1126/sciadv.aaw8922.
(44) Liu, C.; Shen, W.; Li, B.; Li, T.; Chang, H.; Cheng, Y. Natural Polyphenols Augment Cytosolic Protein Delivery by a Functional Polymer. *Chem. Mater.* **2019**, *31* (6), 1956–1965. https://doi.org/10.1021/acs.chemmater.8b04672.
(45) Jachimska, B.; Wasilewska, M.; Adamczyk, Z. Characterization of Globular Protein Solutions by Dynamic Light Scattering, Electrophoretic Mobility, and Viscosity Measurements. *Langmuir* **2008**, *24* (13), 6866–6872. https://doi.org/10.1021/la800548p.
(46) Du, F.; Qiao, B.; Nguyen, T. D.; Vincent, M. P.; Bobbala, S.; Yi, S.; Lescott, C.; Dravid, V. P.; Olvera de la Cruz, M.; Scott, E. A. Homopolymer Self-Assembly of Poly(Propylene Sulfone) Hydrogels via Dynamic Noncovalent Sulfone–Sulfone Bonding. *Nature Communications* **2020**, *11* (1), 4896. https://doi.org/10.1038/s41467-020-18657-5.
(47) Olden, B. R.; Cheng, Y.; Yu, J. L.; Pun, S. H. Cationic Polymers for Non-Viral Gene Delivery to Human T Cells. *Journal of Controlled Release* **2018**, *282*, 140–147. https://doi.org/10.1016/j.jconrel.2018.02.043.
(48) Huang, T.; Cui, Z.; Ding, Y.; Lu, X.; Cai, Y. The Use of Electrostatic Association for Rapid RAFT Synthesis of Histamine Polyelectrolyte in Aqueous Solutions at and below 25 °C. *Polym. Chem.* **2015**, *7* (1), 176–183. https://doi.org/10.1039/C5PY01524C.
(49) Liu, G.; Shi, H.; Cui, Y.; Tong, J.; Zhao, Y.; Wang, D.; Cai, Y. Toward Rapid Aqueous RAFT Polymerization of Primary Amine Functional Monomer under Visible Light Irradiation at 25 °C. *Polym. Chem.* **2013**, *4* (4), 1176–1182. https://doi.org/10.1039/C2PY20810E.
(50) Peeler, D. J.; Thai, S. N.; Cheng, Y.; Horner, P. J.; Sellers, D. L.; Pun, S. H. PH-Sensitive Polymer Micelles Provide Selective and Potentiated Lytic Capacity to Venom Peptides for Effective Intracellular Delivery. *Biomaterials* **2019**, *192*, 235–244. https://doi.org/10.1016/j.biomaterials.2018.11.004.
(51) Chen, J.; Son, H.-N.; Hill, J. J.; Srinivasan, S.; Su, F.-Y.; Stayton, P. S.; Convertine, A. J.; Ratner, D. M. Nanostructured Glycopolymer Augmented Liposomes to Elucidate Carbohydrate-Mediated Targeting. *Nanomedicine: Nanotechnology, Biology and Medicine* **2016**, *12* (7), 2031–2041. https://doi.org/10.1016/j.nano.2016.05.001.

(52) Bapat, A. P.; Roy, D.; Ray, J. G.; Savin, D. A.; Sumerlin, B. S. Dynamic-Covalent Macromolecular Stars with Boronic Ester Linkages. *J. Am. Chem. Soc.* **2011**, *133* (49), 19832–19838. https://doi.org/10.1021/ja207005z.

Chapter 6

Summary of major findings and suggestions for future work

6.1 Major Findings

6.1.1 Anionic polymers for passive targeting of glomerular disease

Polymer charge and size alter biodistribution and, if optimized, can increase accumulation in the kidneys. Specifically, we synthesized a panel of polymers in chapter 2, with charges ranging from neutral to highly anionic and sizes above and below the renal filtration cut off to determine which properties would enhance passive targeting of the kidneys. Each polymer was singly labeled with a fluorophore allowing quantitative comparison of the biodistribution between groups. Seven days after the injection of the polymers we observed significant accumulation of the low molecular weight and highly negatively charged materials in the proximal tubule cells of the kidneys. Interestingly, when we compared the biodistribution of these low molecular weight polymers and their high molecular weight counterparts, in models of FSGS, where kidney filtration is compromised, we observed increased accumulation of the low molecular weight polymers in diseased animals, but no difference in the accumulation of the high molecular weight materials. Overall, we determined that polymers with molecular weights of approximately 25 kDa and anionic monomer content of 80% passively target kidneys and show preferential accumulation in diseased kidneys.

6.1.2 Anionic boronic ester-based polymer-drug conjugates for reversal of EMT

Building on the platform developed in chapter 2, we developed pH-sensitive polymer-drug conjugates for the targeted delivery of therapeutics to proximal tubule cells. The health of proximal tubule cells is critical to preserving kidney function after acute injury, but current therapeutics only delay EMT causing patients to eventual succumb to complete kidney failure. We sought to improve the therapeutic effect of the polyphenolic drug EGCG, by both actively targeting the small molecule antioxidant to the cells of interest (proximal tubule cells) and triggering drug release specifically after internalization. First, we confirmed the efficacy of EGCG *in vitro*, by measuring expression of genes associated with EMT. Then we utilized an anionic polymer functionalized with phenyl boronic acid to efficiently load EGCG (up to 30% by weight) at neutral conditions. Future work will explore the extent to which the polymer-drug conjugates improve the efficacy of EGCG *in vivo*.

6.1.3 Utilizing the neighbor effect of tertiary amines for control of polyphenolic drug release from boronic esters

The traceless and pH sensitive properties of boronic esters are attractive for the synthesis of polymer-drug conjugates, but current platforms suffer from both low stability under physiologically relevant conditions and synthetically demanding optimization to tune drug release profiles. In chapter 4, we demonstrate the high catechol affinity and stability of Wulff type boronic acids can be mimicked by copolymerization of phenyl boronic acid with a tertiary amine and subsequent micellization. This strategy yielded a versatile platform for preparation of reversible polymer-drug conjugates, which more than doubled the oxidative stability of encapsulated polyphenolic drug cargo at physiologically relevant pH and enabled simple and

incremental tuning of drug release kinetics. Moreover, we validated, with 19F NMR, that these copolymers exhibit uniquely high catechol affinity that could not be replicated by combinations of similarly functionalized small molecules. Overall, this report demonstrates that copolymerization of boronic acid and tertiary amine monomers is a powerful and modular approach to improving boronic ester chemistry for drug delivery applications.[1]

6.1.4 Boronic acid copolymers for intracellular delivery of proteins, peptides and nucleic acids

As the clinical relevance of cellular therapies grows, nonviral gene delivery vectors that can deliver both nucleic acids and RNPs can dramatically decrease cost and increase safety. We evaluated boronic acid copolymers in both diblock and statistical architectures and found that micelles could encapsulate protein cargo at upwards of 80% efficiency and almost 50% by weight and that polyplexes had increased cellular internalization by orders of magnitude. The ability of boronic acid copolymers to efficiently complex both protein and gene cargo, while simultaneously increasing cellular uptake makes these materials extremely promising for nonviral gene delivery.

6.2 Recommendations for Future Work

6.2.1 Exploring architecture effects of polycations for gene delivery to T cells

Our previous studies have identified polymer architecture as a key feature of polycations for effective gene delivery to primary human T cells.[2] Particularly, comb polymers with high densities of positive charge and high molecular weights resulted in significantly more gene expression, than linear and sunflower analogs. Unfortunately, synthesizing polymers with these sophisticated architectures is synthetically challenging resulting in materials with high

dispersities (> 1.5) and limited functional group compatibility.[2] The importance of developing new synthesis techniques to finely tune polymer composition and size is underscored by the recent work of Reineke and coworkers, were DMAEMA copolymers with brush architecture were synthesized by graft through polymerization resulting in low dispersities (< 1.4). [3] This report not only confirmed the value of brush/comb polymers for improving gene delivery, but clearly illustrated correlations between polymer molecular weight and gene transfection. To continue advancing our understanding of polymer architecture mediated gene delivery, two alternative synthetic approaches are proposed: self-condensing polymerization of CTA-monomers and initiation of photo-RAFT from alkyl bromide functionalized multimacroinitators (MMIs) via the heterogeneous catalyst bismuth oxide.

Self-condensing polymerization of vinyl functionalized trithiocarbonates is a facile technique to synthesized highly branched polymers with low dispersities.[4] By polymerizing these inimers first, highly branched multimacro chain transfer agents can be synthesized with molecular weights of ~10 kDa. From these branched cores, a second block containing cationic monomers can be synthesized by chain extension with extremely high molecular weights (~ 1,000 kDa) and dispersities as low as 1.3.[5] The resulting hyper-branched structures have arm numbers that are easily tunable based on the polymerization time of the first block. Importantly, based on our previous results, the larger the number of arms the greater the T cell transfection. Additionally, by utilizing RAFT instead of ATRP, this approach facilitates the comparison of different chemical functionalities (such as boronic acids, or lipophilic monomers). Overall, the use of star polymers synthesized by RAFT polymerization for gene delivery would enable chemical diversity as well as detailed exploration of arm number effects.

Recent progress in developing light driven photopolymerizations using bismuth oxide has enabled exciting opportunities to leverage ATRP initiators for RAFT polymerization. Upon exposing heterogeneous solutions of bismuth oxide to compact fluorescent light (CFL), the generated radicals initiate vinyl polymerizations.[6,7] The most noteworthy application of this catalyst system was the quantitative initiation of RAFT polymerization from alkyl bromide species.[8] Specifically, the photoreduction of the ATRP initiator with bismuth oxide initiates a free radical polymerization of the vinyl monomers that is quickly halted by the CTA precursor (Bis-trithiocarbonate). From that point, the continuous generation of radicals causes the polymerization to proceed similarly to normal RAFT. For the synthesis of comb polymers, this approached enables the use of MMIs previously for ATRP to be used as initiators for RAFT. One clear advantage of this approach is that unprotected boronic acid monomers can only be synthesized by RAFT, not ATRP. The facile functionalization of both small molecules and macromolecules with alkyl bromide species has long been one of the advantages of ATRP over RAFT, but with the development of this bismuth mediated photoreduction technique these functional initiators can be leveraged for RAFT of highly diverse monomers.

6.2.2 Effects of polymer dispersity on gene delivery

While initial efforts to optimize RDRP techniques focused on minimizing polymer dispersity, there is a growing appreciation for tuning disperity to improve polymer performance for a given application.[9] Specifically by mixing two different CTAs with various Z group, polymers with similar molecular weight can be synthesized with dispersities varying from 1.09 to 2.1. Previous reports (including ours), often vary molecular weight or polymer composition and as a side effect dispersity values of the various polymers change.[2] Using the approached developed by Anastasaki and coworkers, the dispersity of polycations can be controlled independently of

molecular weight and composition. Of particular note, for gene delivery applications, polymer internalization and transfection efficiency are not directly correlated.[3,10] As a result, some materials with less internalization exhibit higher gene expression. These observations imply that particular polymers have better internalization while others that are seldom internalized have higher endosomal escape, and the data begs the question: can formulations composed of multiple types of polymers achieve both high internalization and endosomal escape? One method to achieve these heterogenous polyplex formulations would be to use dispersity-controlled RAFT to synthesize polycations. Linear polymers have consistently performed poorly at gene delivery in vitro compared to brush or comb architectures, but besides the architectural differences the linear analogs have much lower dispersity than complex counterparts. To date, no studies have explored the effect of dispersity on cellular internalization or gene delivery.

6.2.3 DNA-Aptamer modification in organic solvents

The Pun lab has been extremely successful developing multiple DNA-Aptamers for binding of T cells and SARS-COV2, but *in vivo* translation of these binders has been limited by rapid degradation and clearance. A common approach to improve biodistribution and endow additional functionality to targeting ligands is to conjugate these biomacromolecules to polymers.[11] Unfortunately, most approaches to conjugate DNA to polymers are inefficient due to the insoluble nature of DNA in organic solvents, and the limited effectiveness of aqueous coupling chemistry.[12] While some mixed solvent conjugation approaches have been able to achieve efficiencies of ~40% (tetrazine and norbornene) for short DNA sequences (~20 nucleotides), the large size of aptamers (~50) increases the steric hindrance, dramatically decreasing this efficiency. A promising approach for DNA functionalization was developed by Herrmann and coworkers, where DNA strands were complexed with cationic surfactants in water. These DNA-

complexes precipitate in aqueous solutions, but dissolve readily in organic solvents.[13] These DNA strands could be coupled to polymers or small molecules under anhydrous conditions, and, in the case of the extremely reactive and aqueous incompatible acid chloride coupling, up to 90% efficiency was observed. In a similar vein, Ruff *et al.* developed a cationic PEG resin to electrostatically immobilize DNA strands allowing for the removal of water and swelling of the resin in organic solvents.[14] This solid support enabled completely anhydrous modification of DNA in organic solutions and simple purification by removal of the organic solvent and subsequent swelling of the resin in concentrated salt solutions. While neither organic phase approach mentioned has been tested on DNA strands as long as the Pun Lab's aptamers, the opportunity to perform anhydrous coupling reactions would enable NHS conjugation and even the recently developed pentafluorophenyl-thiol ligation.[15,16]

References:

(1) Prossnitz, A. N.; Pun, S. H. Modulating Boronic Ester Stability in Block Copolymer Micelles via the Neighbor Effect of Copolymerized Tertiary Amines for Controlled Release of Polyphenolic Drugs. *ACS Macro Lett.* **2022**, 276–283. https://doi.org/10.1021/acsmacrolett.1c00751.

(2) Olden, B. R.; Cheng, Y.; Yu, J. L.; Pun, S. H. Cationic Polymers for Non-Viral Gene Delivery to Human T Cells. *Journal of Controlled Release* **2018**, *282*, 140–147. https://doi.org/10.1016/j.jconrel.2018.02.043.

(3) Dalal, R. J.; Kumar, R.; Ohnsorg, M.; Brown, M.; Reineke, T. M. Cationic Bottlebrush Polymers Outperform Linear Polycation Analogues for PDNA Delivery and Gene Expression. *ACS Macro Lett.* **2021**, *10* (7), 886–893. https://doi.org/10.1021/acsmacrolett.1c00335.

(4) Floyd, T. G.; Häkkinen, S.; Hartlieb, M.; Kerr, A.; Perrier, S. Complex Polymeric Architectures Synthesized through RAFT Polymerization. In *RAFT Polymerization*; Moad, G., Rizzardo, E., Eds.; Wiley, 2021; pp 933–981. https://doi.org/10.1002/9783527821358.ch20.

(5) Das, D.; Srinivasan, S.; Brown, F. D.; Su, F. Y.; Burrell, A. L.; Kollman, J. M.; Postma, A.; Ratner, D. M.; Stayton, P. S.; Convertine, A. J. Radiant Star Nanoparticle Prodrugs for the Treatment of Intracellular Alveolar Infections. *Polym. Chem.* **2018**, *9* (16), 2134–2146. https://doi.org/10.1039/C8PY00202A.

(6) Riente, P.; Pericàs, M. A. Visible Light-Driven Atom Transfer Radical Addition to Olefins Using Bi_2O_3 as Photocatalyst. *ChemSusChem* **2015**, *8* (11), 1841–1844. https://doi.org/10.1002/cssc.201403466.

(7) Hakobyan, K.; Gegenhuber, T.; McErlean, C. S. P.; Müllner, M. Visible-Light-Driven MADIX Polymerisation via a Reusable, Low-Cost, and Non-Toxic Bismuth Oxide Photocatalyst. *Angewandte Chemie International Edition* **2019**, *58* (6), 1828–1832. https://doi.org/10.1002/anie.201811721.

(8) Hakobyan, K.; McErlean, C. S. P.; Müllner, M. Activating ATRP Initiators to Incorporate End-Group Modularity into Photo-RAFT Polymerization. *Macromolecules* **2020**, *53* (23), 10357–10365. https://doi.org/10.1021/acs.macromol.0c01697.

(9) Whitfield, R.; Parkatzidis, K.; Truong, N. P.; Junkers, T.; Anastasaki, A. Tailoring Polymer Dispersity by RAFT Polymerization: A Versatile Approach. *Chem* **2020**, *6* (6), 1340–1352. https://doi.org/10.1016/j.chempr.2020.04.020.

(10) Hango, C. R.; Backlund, C. M.; Davis, H. C.; Posey, N. D.; Minter, L. M.; Tew, G. N. Non-Covalent Carrier Hydrophobicity as a Universal Predictor of Intracellular Protein Activity. *Biomacromolecules* **2021**, *22* (7), 2850–2863. https://doi.org/10.1021/acs.biomac.1c00242.

(11) Whitfield, C. J.; Zhang, M.; Winterwerber, P.; Wu, Y.; Ng, D. Y. W.; Weil, T. Functional DNA–Polymer Conjugates. *Chem. Rev.* **2021**, *121* (18), 11030–11084. https://doi.org/10.1021/acs.chemrev.0c01074.

(12) Wilks, T. R.; O'Reilly, R. K. Efficient DNA–Polymer Coupling in Organic Solvents: A Survey of Amide Coupling, Thiol-Ene and Tetrazine–Norbornene Chemistries Applied to Conjugation of Poly(N-Isopropylacrylamide). *Sci Rep* **2016**, *6* (1), 39192. https://doi.org/10.1038/srep39192.

(13) Liu, K.; Zheng, L.; Liu, Q.; de Vries, J. W.; Gerasimov, J. Y.; Herrmann, A. Nucleic Acid Chemistry in the Organic Phase: From Functionalized Oligonucleotides to DNA Side Chain Polymers. *J. Am. Chem. Soc.* **2014**, *136* (40), 14255–14262. https://doi.org/10.1021/ja5080486.

(14) Ruff, Y.; Martinez, R.; Pellé, X.; Nimsgern, P.; Fille, P.; Ratnikov, M.; Berst, F. An Amphiphilic Polymer-Supported Strategy Enables Chemical Transformations under Anhydrous Conditions for DNA-Encoded Library Synthesis. *ACS Comb. Sci.* **2020**, *22* (3), 120–128. https://doi.org/10.1021/acscombsci.9b00164.

(15) Noy, J.-M.; Friedrich, A.-K.; Batten, K.; Bhebhe, M. N.; Busatto, N.; Batchelor, R. R.; Kristanti, A.; Pei, Y.; Roth, P. J. Para-Fluoro Postpolymerization Chemistry of Poly(Pentafluorobenzyl Methacrylate): Modification with Amines, Thiols, and Carbonylthiolates. *Macromolecules* **2017**, *50* (18), 7028–7040. https://doi.org/10.1021/acs.macromol.7b01603.

(16) Chan, L. W.; Wang, X.; Wei, H.; Pozzo, L. D.; White, N. J.; Pun, S. H. A Synthetic Fibrin Cross-Linking Polymer for Modulating Clot Properties and Inducing Hemostasis. *Science Translational Medicine* **2015**, *7* (277), 277ra29-277ra29. https://doi.org/10.1126/scitranslmed.3010383.